Lawrence Berkeley National Laboratory
LBL Publications

Title

Chemistry Division Annual Report, 1961

Permalink

https://escholarship.org/uc/item/93t3w5gv

Authors

Hollander, J M

Reynolds, F L

Wallmann, J C

Publication Date

1962

5/1/63

University of California

Ernest O. Lawrence Radiation Laboratory

CHEMISTRY DIVISION ANNUAL REPORT, 1961

Berkeley, California

DISCLAIMER

UNIVERSITY OF CALIFORNIA

Lawrence Radiation Laboratory
Berkeley, California

Contract No. W-7405-eng-48

CHEMISTRY DIVISION ANNUAL REPORT, 1961

January 1962

I. Perlman, Director, Chemistry Division

Editors: J. M. Hollander, F. L. Reynolds, and J. C. Wallmann

CHEMISTRY DIVISION ANNUAL REPORT, 1961

Contents

CHEMISTRY DIVISION ANNUAL REPORT, 1961

Lawrence Radiation Laboratory
University of California
Berkeley, California

January 1962

INTRODUCTION

This report presents a review of the research progress made during the 1961 calendar year by the Nuclear Chemistry Division of the Lawrence Radiation Laboratory. Though the report is not exhaustive, an effort has been made to give a balanced view of the widely ranging research interests and problems of the Division. Contributors to this report include staff members of the Radiation Laboratory, graduate students, and visiting postdoctoral chemists and physicists from many laboratories, domestic and foreign.

Fourteen Ph. D. theses were awarded during 1961 to graduate students who did their research work in this Division, and one Master's thesis was given. Abstracts of these theses are included in this report.

A. RADIOACTIVITY AND NUCLEAR SPECTROSCOPY

1. PREFERENTIAL POLAR EMISSION IN THE ALPHA DECAY OF DEFORMED Cf^{249} and E^{253} (*)

Q. O. Navarro, J. O. Rasmussen,[†] and D. A. Shirley

In 1953 Hill and Wheeler predicted that prolately deformed alpha-emitting nuclei should exhibit enhanced emission from the polar regions, or "tips," because of the lower Coulomb barrier in these regions.[1] Dabbs and co-workers have observed anisotropic angular distributions of α particles from oriented uranium and neptunium nuclei.[2] For Np^{237} they determined the sign of the quadrupole coupling constant in neptunyl ion and showed that α particles are indeed emitted preferentially along the direction of the angular momentum vector, confirming the prediction of Hill and Wheeler. Pryce[3] has suggested that the quadrupole moment of Np^{237} is negative, which would require a different interpretation of the orientation experiments, but this seems unlikely on the basis of the collective nuclear model. In this letter we described orientation experiments on Cf^{249} and E^{253} which provide independent confirmation of the predictions of Hill and Wheeler, that is to say, the L=2 component in the main alpha group is appreciable and is in phase ($\delta > 0$) with the dominant L=0 wave.

Neodymium ethylsulfate was chosen as the crystal most suitable for these experiments. The ions Cf^{+3} and E^{+3} are chemically analogous to Dy^{+3} and Ho^{+3}, nuclei of which have been aligned in this lattice.[4,5] This salt can easily be cooled to 0.02°K, at which fairly complete alignment of these nuclei could be expected. The alpha counters used in this experiment were similar to those described by Walter, Dabbs, and Roberts.[6] In each

_____

[*]Submitted to Phys. Rev. Letters.

[†]Presently on leave at the Institute for Theoretical Physics, Copenhagen, Denmark.

[1] D. L. Hill and J. A. Wheeler, Phys. Rev. 89, 1102 (1953).

[2] J. W. T. Dabbs, L. D. Roberts, and G. W. Parker, Bull. Am. Phys. Soc. II, 2, 31 (1937); Physica 24, 69 (1958); F. J. Walter, J. W. T. Dabbs, L. D. Roberts, and H. W. Wright, Bull. Am. Phys. Soc. II, 3, 304 (1958); S. H. Hanauer, J. W. T. Dabbs, L. D. Roberts, and G. W. Parker, Phys. Rev. 124, 1512 (1961).

[3] M. H. L. Pryce, Phys. Rev. Letters 3, 375 (1959).

[4] Q. O. Navarro and D. A. Shirley, Phys. Rev. 123, 186 (1961).

[5] H. Postma, A. R. Miedema, and Miss M. C. Eversdijk Smulders, Physica 25, 671 (1959).

[6] F. J. Walter, J. W. T. Dabbs, and L. D. Roberts, Rev. Sci. Instr. 31, 756 (1960).

experiment care was taken to grow the radioactive ions only in a thin surface layer on a small spot on the crystal. Low temperatures were obtained by standard adiabatic demagnetization techniques, and the temperature was measured with mutual inductance coils.

At the lowest temperatures the angular distributions of α particles from both isotopes were highly anisotropic. In E^{253}, as in Ho^{166},[5] it could be ascertained by the temperature dependence of the anisotropy that the alignment was nearly complete even at temperatures as high as $0.1^{\circ}K$. Every aspect of the sign, magnitude, and temperature dependence of the nuclear orientation parameters of these two isotopes is consistent with Cf^{+3} and E^{+3} having the same electronic ground states as Dy^{+3} and Ho^{+3}, respectively, in this lattice. For E^{253} the temperature dependence of the α-particle intensity along the crystalline c axis is shown in Fig. A.1-1. Data were also taken at 90° to the c axis. These showed a change in counting rate, on orientation of the E^{253} nuclei, of opposite sign and approximately half the magnitude of that along the c axis, indicating an angular dependence proportional to $P_2(\cos\theta)$. Because of the large solid angle corrections (13% of the coefficient of the P_2 term), we cannot determine with any precision the contributions of higher-order terms in the angular distribution.

In the ethylsulfate lattice the dominant spin-Hamiltonian term affecting nuclear orientation is expected to be of the form $AS_Z I_Z$ for both E^{+3} and Cf^{+3}, and this alone would require "axial" nuclear alignment (states with $I_Z = \pm I$ would lie lowest). Combining this with the observed enhancement of α-particle intensity along the c axis on orientation, we find preferential alpha emission along the nuclear spin direction in both cases. Since the ground states of both Cf^{249} and E^{253} have spins greater than $1/2$ and spin projections K equal to the spin, so that the nuclear spin is along the prolate axis,[7,8,9] alpha emission must take place preferentially from the tips of these prolately deformed nuclei. In both cases the direction of orientation can also be established completely unambiguously from experiment, for E^{253} from the magnitude and temperature dependence of the anisotropy, and in Cf^{249} from the sign of the anisotropy of the (following) 394-kev γ-ray and knowledge of its dipole character with $I \rightarrow I-1$ spin sequence.

The E^{253} decay scheme has been given by Asaro et al.,[8] who estimate an L=2 to L=0 intensity ratio of 1:8 in the main alpha group. The estimate is based on the decay intensity to the first excited state together with the approximate branching relations of Bohr, Fröman, and Mottelson.[10] A 25%

[7] F. S. Stephens, F. Asaro, S. G. Thompson, and I. Perlman, Bull. Am. Phys. Soc. Series II, 2, 394 (1957).

[8] F. Asaro, S. G. Thompson, F. S. Stephens, and I. Perlman, in Proceedings of the Kingston Conference on Nuclear Structure (University of Toronto Press, 1960), p. 581.

[9] S. G. Nilsson, Kgl. Danske Videnskab. Selskab Mat.-fys. Medd. 29, No. 16 (1955).

[10] A. Bohr, P. O. Fröman, and B. R. Mottelson, Kgl. Danske Videnskab. Selskab. Mat.-fys. Medd. 29, No. 10 (1955).
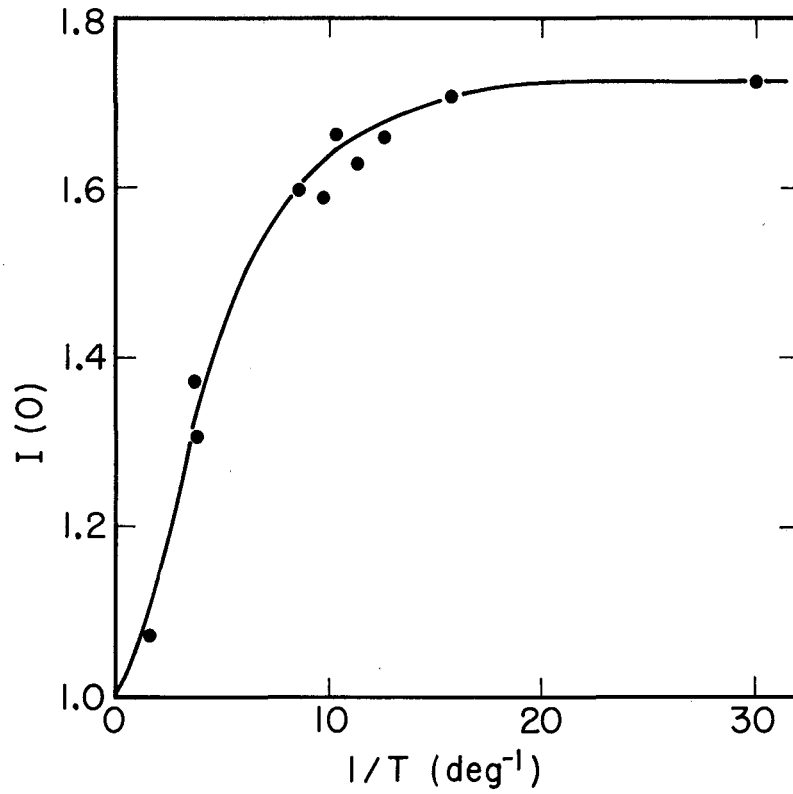
Fig. A.1-1. Normalized total α-particle intensity along the c axis from E^{253} oriented in neodymium ethylsulfate at low temperatures. The upper curve is the best fit using the theoretical temperature dependence for the spin Hamiltonian AS_ZI_Z, with both A and the low-temperature limiting asymptote adjustable.

enhancement of the d-wave admixture has been predicted for U^{233} by taking into account effects due to the quadrupole moment and Coriolis forces.[11,12] A similar enhancement is expected for E^{253}. Using the 1:8 d- to s-wave ratio, assuming them to be in phase, ignoring the small L=4 components, and assuming an isotropic average contribution from the 4% alpha intensity to other groups, we calculate a limiting (T→0) angular distribution for E^{253} of $1 + 0.98 P_2 (\cos \theta)$. There is also predicted a small negative $P_4 (\cos \theta)$ term of magnitude more dependent on L=4 intensity assumptions. Our experimental limiting anisotropy is 25% less than theoretical, probably indicating that not all the E^{253} atoms have gone into crystalline sites equivalent to the Nd atoms of the bulk crystal. The Cf^{249} data are not yet accurate enough to permit a quantitative interpretation, although it is clear that the hyperfine splitting is considerably less than for E^{253}.

It is a pleasure to thank Dr. S. G. Thompson, who participated in early stages of this research, Ray Gatti and Llad Phillips, for providing carrier-free E^{253}, and Professor B. B. Cunningham and Dr. J. C. Wallmann, who lent us their entire supply of Cf^{249}.

_____

[11] R. R. Chasman and J. O. Rasmussen, Phys. Rev. 115, 1257 (1959).

[12] J. O. Rasmussen, Bull. Am. Phys. Soc. II, 6, 232 (1961).

2. THE GROUND STATE OF ODD-ODD Tb^{156} (*)

D. A. Shirley and C. A. Lovejoy

Nuclei of Tb^{158} were oriented in an ethylsulfate lattice, and the angular distribution of gamma radiation from the daughter Gd^{156} was studied as a function of temperature, magnetic environment, and external magnetic field. The anisotropies of these gamma rays showed the same unusual temperature dependence observed for Tb^{160}, which was described with the spin Hamiltonian[1]

$$H = g_{\parallel} \beta H_z S_z + A S_z I_z + \Delta_x S_x + \Delta_y S_y + P [I_z^2 - 1/3 I(I+1)] + C S_z T_z ,$$

where the last term accounts for spin-spin interactions with neighboring ions. The experimental data for the 535-kev γ ray are shown in Fig. A.2-1, along with curves calculated by using the above Hamiltonian.

Curves A-E represent cases in which the total average magnetic field on a terbium ion is 0, approx 100, 200, approx 400, and approx 600 gauss, respectively. This total average field is given by the sum of the external

_____

[1] C. E. Johnson, J. F. Schooley, and D. A. Shirley, Phys. Rev. 120, 2108 (1960).
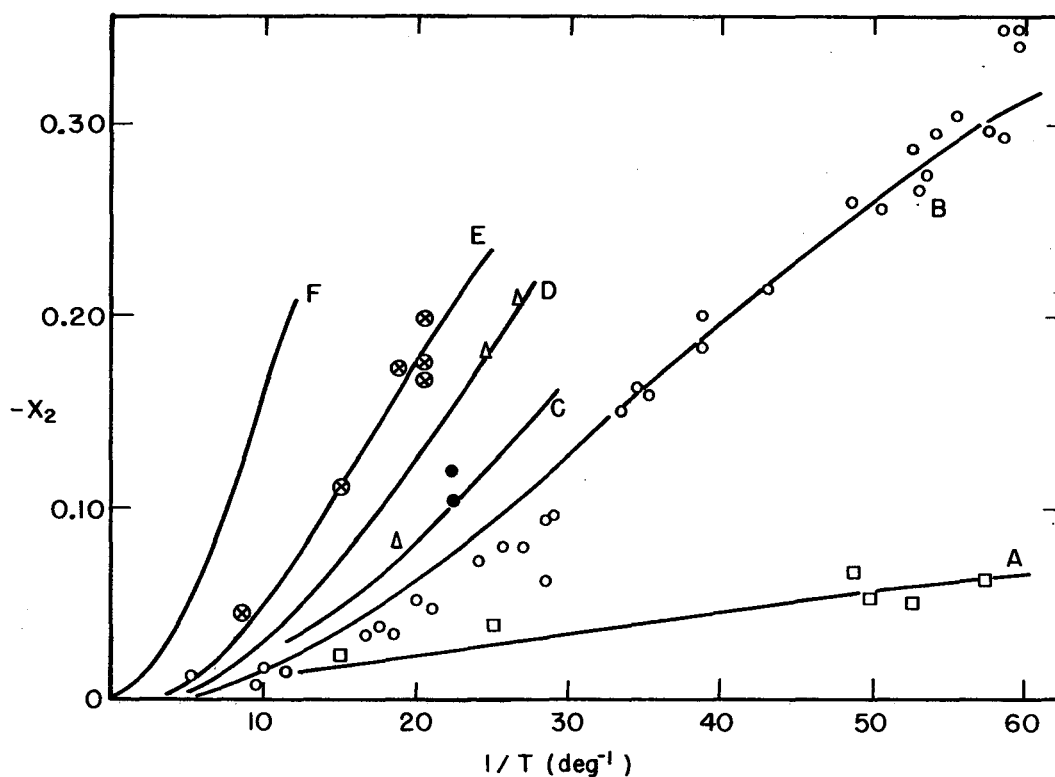
Fig. A.2-1. Temperature dependence of X_2 for the 535-kev γ ray in Gd^{156} following the decay of Tb^{156} oriented in the ethylsulfate lattice, under several experimental conditions. The parameter X_2 is the coefficient of $P_2 (\cos \theta)$ in the angular distribution function $W (\theta) = 1 + X_2 P_2 (\cos \theta)$.

and internal (dipole-dipole) fields,

$$\vec{H} = \vec{H}_e + \vec{H}_i .$$

In neodymium ethylsulfate $|H_i|$ takes the values 0 and 180 with equal probability, depending on whether $|T_z|$ is 0 or 1, in the absence of an external field. When a field is applied along the c axis the states with $H_i = 180$ are much more heavily populated. In a nonmagnetic crystal H_i is always zero. Thus as the local field is increased the anisotropy increases monotonically because the effect of the off-diagonal elements is lessened. In the high-field limit only the terms in A and P in the Hamiltonian should affect nuclear orientation. Curve F was calculated for the infinite-field limit. The anisotropies of all the γ rays in the high-energy portion of the spectrum are shown in Fig. A.2-2. This represents one of the first uses of multichannel analysis in conjunction with a nuclear orientation experiment, and illustrates the power of the method.

A partial level scheme for Gd^{156} is shown in Fig. A.2-3. Detailed analysis indicated a new 3- state at 2091 kev in Gd^{156}, and confirmed the spins of the states at 1620 kev (5+) and 2042 kev (4-) as well as several others which were less in doubt. The electron-capture transitions to the states at 1943 and 2091 kev were shown to be mainly Gamow-Teller. The spin of Tb^{156} was established as 3 from the experimental angular distributions. A ground-state spin and parity of 3- for Tb^{156} is easily explained on the collective model. This state can be formed by combining the proton state 3/2+[411] with the neutron state 3/2-[521] according to the Gallagher-Moszkowski rules.[2] A 4- state cannot be formed, by using these rules, from close-lying Nilsson orbitals.[3] Terbium-159 has a measured spin of 3/2,[4] and a 3/2-[521] neutron state is found in Dy^{161} at 75 kev. The spin of Tb^{160} is 3,[1,6,7,8] and spin 3 is consistent with the available data on Tb^{158}.[9]

---

[2] C. J. Gallagher and S. A. Moszkowski, Phys. Rev. 111, 1282 (1958).

[3] S. G. Nilsson, Kgl. Danske, Videnskab. Selskab, Mat.-fys. Medd. 29, No. 16 (1955).

[4] J. M. Baker and B. Bleaney, Proc. Roy. Soc. (London) A245, 156 (1958).

[5] B. R. Mottelson and S. G. Nilsson, Kgl. Danske Videnskab. Selskab, Mat-fys. Skrifter 1, No. 8 (1959).

[6] H. Postma, Miss M. C Eversdijk Smulders, W. J. Huiskamp, Physica 27, 245 (1961).

[7] Amado Y. Cabezas, Ingvar Lindgren, and Richard Marrus, Phys. Rev. 122, 1796 (1961).

[8] G. Bäckstrom, J. Lindskog, O. Bergman, E. Bashandy, and A. Bäcklin, Arkiv Fysik 15, 121 (1959).

[9] H. R. Lewis, Jr., R. A. Naumann, and J. L. Power, Bull. Am. Phys. Soc, 6, II 238 (1961).
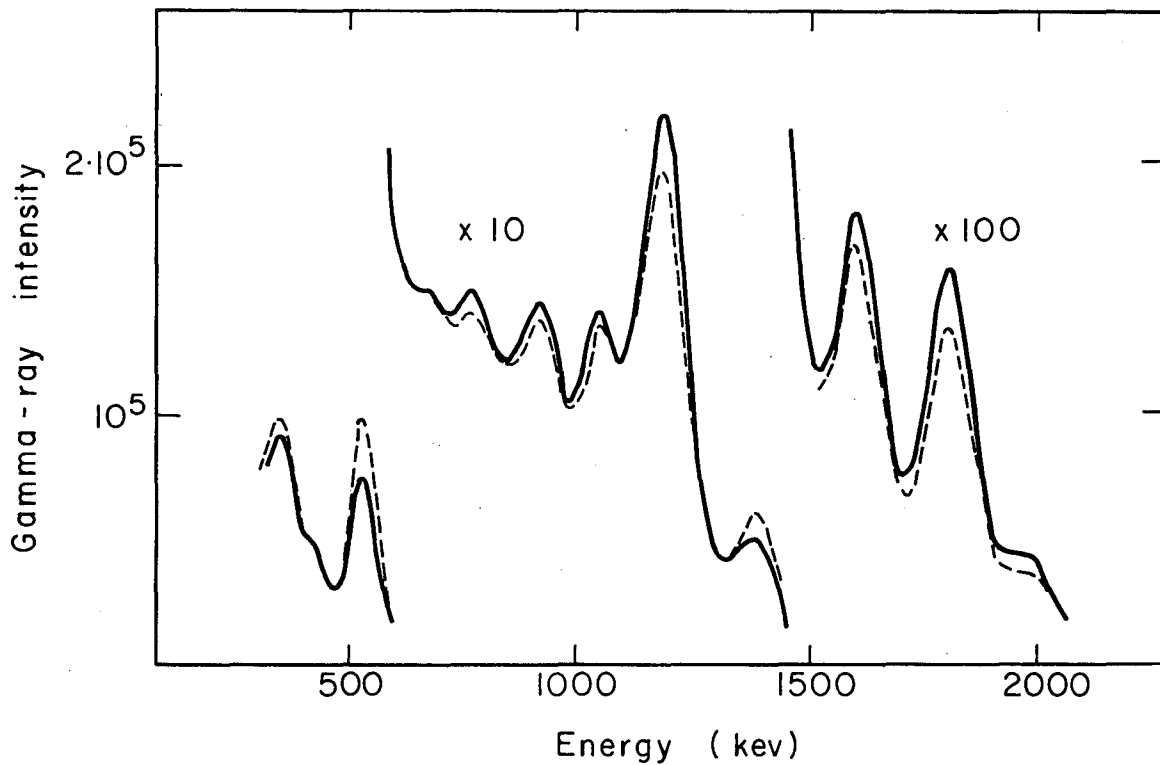
Fig. A. 2-2. High-energy portion of the γ-ray spectrum of Tb^{156} taken along the crystalline c axis. The solid line represents intensities at 0.02°K, and the dashed line represents intensities at 1.1°K.

3 —— Tb^{156}

I π   E
             kev
(3 –)   2091
4 –   2042
3 –   1931

422
534

5 +   1620
4 +   1507

3 +   1246
2 +   1152

924   1643
1330   1841
1038   1220
1417   2002

6 +   584

4 +   288

2 +   89
       89
0 +   0
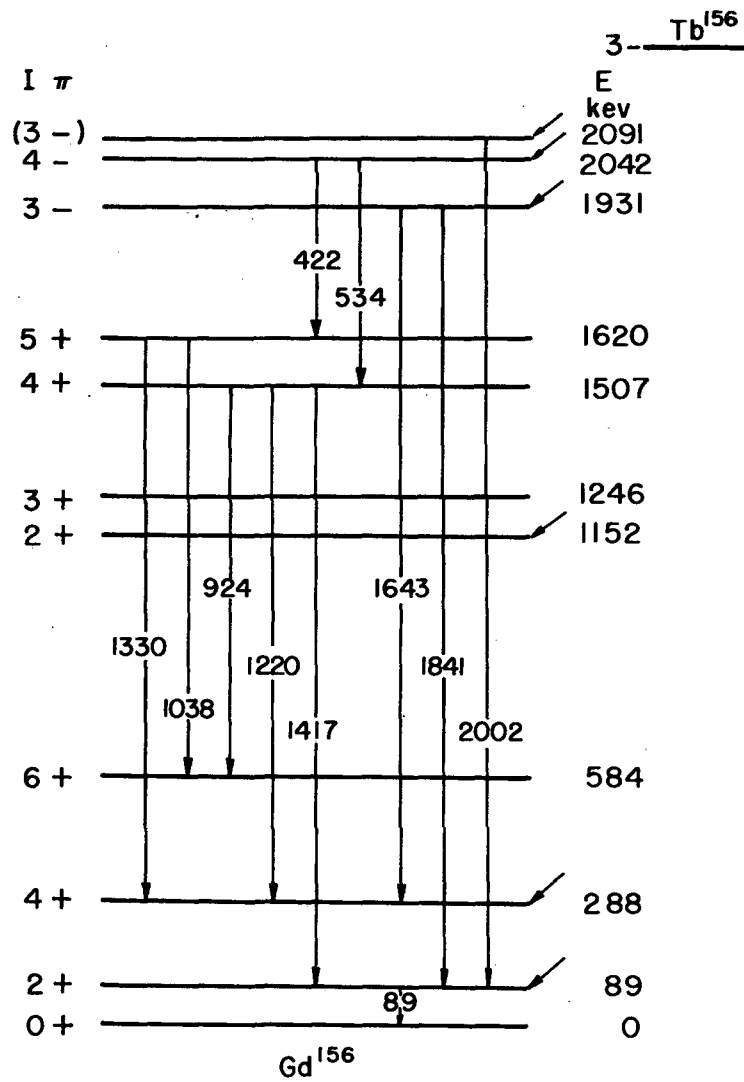
Gd^{156}

MU–24170

Fig. A.2-3. Level scheme of Gd^{156} with transitions relevant to this work. The spins of the top five levels were studied in this work.

Fitting the data to the spin Hamiltonian yielded both magnetic and electric hyperfine-structure constants, from which the magnetic and electric (quadrupole) moments $|\mu_{156}| = 1.45 \pm .18$ nm and $Q_{156} = +1.4 \pm .5$ barns were determined.

Using Nilsson wave functions (with $\eta = +6$) for the $3/2+$ [411] proton state and the $3/2-$ [521] neutron state,[3] and assuming no correlation between the odd particles, we obtain a theoretical magnetic moment of 2.0 nm, in fair agreement with experiment.

A useful empirical comparison is obtained by calculating the magnetic moments of Tb^{156} and Tb^{160},[1] from the measured magnetic moments of odd nucleons in the two states involved, in neighboring nuclei. The measured moment of $+1.92 \pm 0.10$ for Tb^{159} [1,4] provides the value for the $3/2+$ [411] proton state, while the $3/2-$ [521] neutron magnetic moment is obtained from the measured moment of -0.30 for Gd^{155}, and $(-)$ 0.32 ± 0.02 for Dy^{157}. Thus we would calculate $\mu = +1.61 \pm 0.12$ for both Tb^{156} and Tb^{160} (neglecting slight differences in nuclear deformation), in good agreement with the experimental values of 1.45 ± 0.18 for Tb^{156} and 1.60 ± 0.25 for Tb^{160}. From this we may conclude that odd-particle correlations do not significantly affect the magnetic moments of these odd-odd deformed nuclei.

3. NUCLEAR ORIENTATION OF PROMETHIUM-143 (*)

C. A. Lovejoy, J. O. Rasmussen,† and D. A. Shirley

The nuclear energy levels of Nd^{143} and its parents (Fig. A.3-1) pose some interesting problems for nuclear shell-model theory. The ground states of Nd^{143} and Pr^{143} can be identified as the shell-model states $f_{7/2}$ and $d_{5/2}$, respectively. The very low beta branching ratio in the decay of Pr^{143} to the excited state of Nd^{143} (log ft ≥ 10.5),[1] together with the M1-E2 multipolarity[2] of the γ de-excitation of this state, presumably characterizes this beta branch as first forbidden and unique, and the excited state as $9/2-$.

Promethium-143 has a closed shell of 82 neutrons. With 61 protons the ground state is expected to be either $d_{5/2}$ or $g_{7/2}$, by analogy with neighboring nuclei and from the shell model. In fact, with its single closed shell, Pm^{143} is susceptible of theoretical treatment on the "pairing plus p^2 force" model of Kisslinger and Sorensen, who predict that the $d_{5/2}$ state should be the ground state.[3]

*Phys. Rev. 123, 954 (1961).

†Presently on leave at the Institute for Theoretical Physics, Copenhagen, Denmark.

[1] R. W. Grant (Lawrence Radiation Laboratory, Berkeley), unpublished data.

[2] S. Ofer, Phys. Rev. 113, 895 (1959). Actually the data in this reference indicate pure M1 multipolarity, with considerable uncertainty. The present work establishes an E2 mixture of at least 5%.

[3] L. F. Kisslinger and R. Sorensen, Kgl. Danske Videnskab. Selskab, Mat.-fys. Skrifter 32, No. 9 (1960).
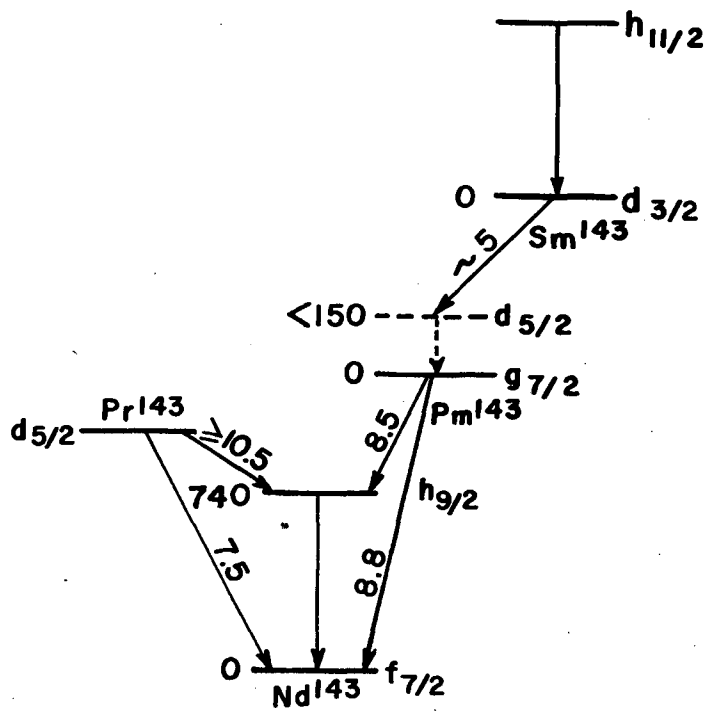
MU – 22708

Fig. A.3-1. Proposed level for several nuclei with A = 143. Numbers on
arrows denote log-ft values. Only indirect evidence is available for
the excited state of Pm^{143}.

The nuclear alignment data are consistent with a spin of $7/2$ for Pm^{143}, and nearly rule out the combination of spin $5/2$ and a magnetic moment near 5 nm (the Schmidt limit, which might be expected on some theoretical grounds, and especially by analogy with Pr^{141}). Further evidence in favor of a spin assignment of $7/2$ for Pm^{143} is the near equality of log ft values of the two electron-capture decay branches. Were the spin $5/2$, electron-capture decay to the excited state would be unique and probably highly attenuated, as in Pr^{143}.

Thus the spin assignment is at present uncertain, and further work is under way to decide it unambiguously. Confirmation of the tentative assignment of $7/2$ would pose a serious problem for the pairing model.

4. THEORY OF THE ISOMERIC CHEMICAL SHIFTS IN Au^{197} (*)

D. A. Shirley

Unusually large chemical shifts have been observed in the Mössbauer spectrum of Au^{197}, exceeding the largest shifts observed in other isotopes by an order of magnitude.[1] We have found that these shifts can be explained by means of a very straightforward model, with results which are in essentially quantitative agreement with experiment.

Previous chemical shifts (in Fe^{57}) had been interpreted as a rather crude model carried over from the theory of isotope shifts, and involving such simplifications as uniform electron density and a uniformly charged spherical nucleus.[2,3] Using this theory one could derive $\Delta \langle r^2 \rangle$, the charge in average-square charge radius between the excited and ground states, from Mössbauer absorption data. Unfortunately there is no straightforward way to compare this derived quantity with theory, Fe^{57} being an odd-N nucleus.

In Au^{197}, an odd-proton nucleus, the outlook is considerably brighter. If we make the approximation that the isomeric transition involves predominantly the odd proton, it is possible to calculate the change in radial moments between the two states using the radial wave functions of the odd proton. We have assumed that the 77-kev and ground states of Au^{197} differ only in that the former has a hole in the $3s_{1/2}$ proton shell which becomes in the latter a hole in the $2d_{3/2}$ shell. The signs of the experimental shifts require this choice rather than that the excited state should contain an unpaired $3s_{1/2}$ proton which becomes an unpaired $2d_{3/2}$ proton in the ground state.

*Phys. Rev. 124, 354 (1961).

[1] D. A. Shirley, M. Kaplan, and P. Axel, Phys. Rev. 123, 816 (1961).

[2] S. DeBenedetti, G. Lang, and R. Ingalls, Phys. Rev. Letters 6, 60 (1961).

[3] L. R. Walker, G. K. Wertheim, V. Jaccarino, Phys. Rev. Letters 6, 98 (1961).

The conduction (6s) electron density within the nucleus was calculated with experimental data from double-resonance experiments[4,5] and the appropriate (relativistic) wave functions given by Bohr and Weisskopf,[6] Racah,[7] and Meligy.[8] The electron density was integrated to yield a Coulomb potential within the nucleus, and this potential was used as a first-order perturbation to assess the effect of conduction-electron transfer on the nuclear level spacing. It was found that this spacing was altered by about 1 part in 10^{11} on transferring one conduction electron, in good accord in the experiment. The electron and odd-proton densities are shown in Fig. A.4-1.

A more quantitative comparison with experiment is given in Table I, where we have tabulated the expected number of conduction electrons gained by a gold atom in several host metals. Here the number of electrons gained is calculated from the above model together with experimental shifts by using proton wave functions derived from several nuclear potentials. The calculated shifts are quite sensitive to the diffuseness of the nuclear potential chosen, and the harmonic-oscillator results are clearly not in agreement with experiment. The other, much less diffuse, potentials yield very reasonable values for the number of conduction electrons transferred to gold atoms, in several hosts. The only datum with which we can compare these results is a value of approx 0.6 for the number of electrons transferred to a gold atom in iron, obtained by Blatt and Eliott,[9] which is in good agreement with our values of 0.5 and 1.9.

Table I. Experimental chemical shifts and derived changes in 6s electron density on a gold atom in several hosts, relative to a gold lattice, using several nuclear potentials.

Host	Observed[6] shift $(ev \times 10^{-6})$	Number of 6s electrons gained by gold atom		
		Harmonic-oscillator potential	Finite square-well potential	Woods-Saxon potential
Pt	0.26±0.06	4	0.09	0.3
Fe	1.42±0.09	20	0.52	1.9
Co	1.23±0.08	18	0.45	1.6
Ni	1.11±0.08	16	0.40	1.5

[4] H. H. Woodbury and G. W. Ludwig, Phys. Rev. 117, 1287 (1960).

[5] G. Fricke, S. Penselm, and E. Recknagel, Naturwiss. 48, 129 (1960).

[6] A. Bohr and V. F. Weisskopf, Phys. Rev. 77, 94 (1950).

[7] G. Racah, Nature 139, 723 (1932).

[8] A. S. Meligy, Nuclear Phys. 14, 248 (1959/60).

[9] R. J. Elliott (Oxford University), private communication, March 1961.
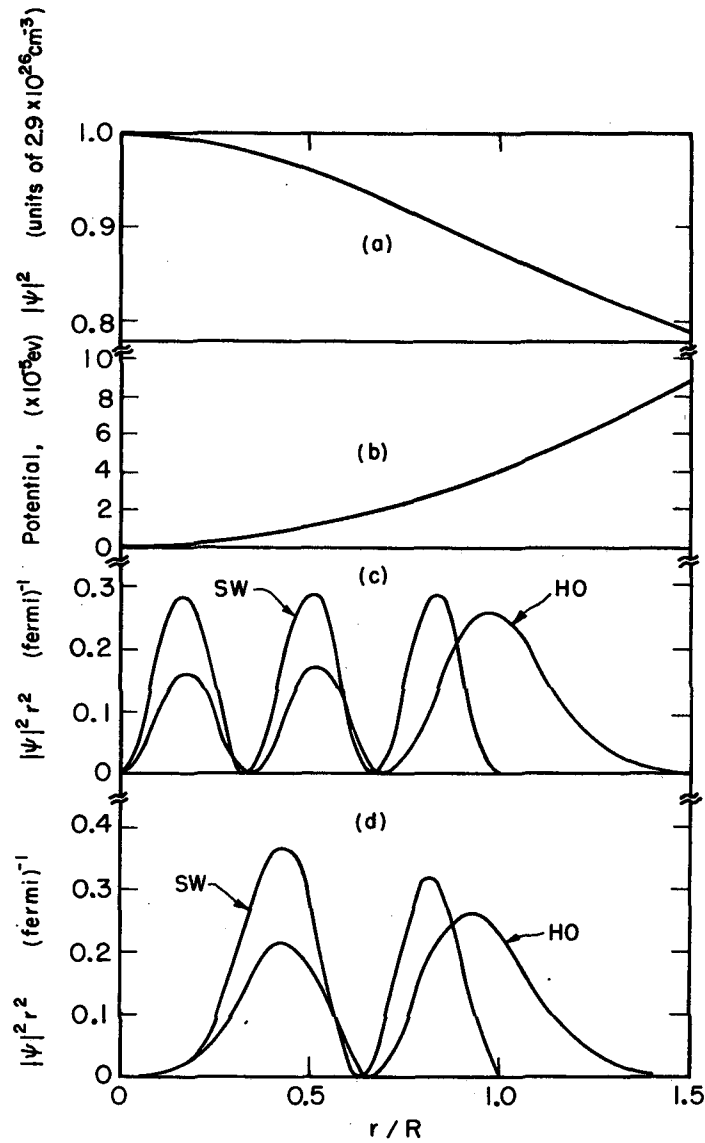
MU-23587

Fig. A.4-1. Plots for Au^{197} of (a) the 6s electron density, (b) the Coulombic potential created by the 6s electron, and (c) and (d) the proton distribution for the $3s_{1/2}$ and $2d_{3/2}$ states, respectively, using harmonic-oscillator and infinite square-well wave functions.

In summary the chemical shift in Au^{197} can be explained at least semi-quantitatively on the basis of the interaction of the odd proton with the 6s electron. The differences among the theoretical results obtained by using nuclear wave functions derived from three different nuclear potentials suggests that this type of data could possibly be a useful criterion for deciding among nuclear potentials.

The interpretation of chemical-shift data on heavy nuclei in terms of radial moments is complicated somewhat by relativistic effects. These effects render the s-electron density near the nucleus nonuniform, thereby producing finite contributions from higher radial moments. The internal expansion of the Coulomb potential due to the 6s electron is sufficiently accurate for some distance outside the nucleus that radial moments of the proton distribution may be evaluated by using only the internal potential and integrating to infinity, even for proton distributions obtained from a harmonic-oscillator nuclear potential.

This shift shows promise of providing useful solid-state information, i.e., the conduction-electron density at impurity sites. In particular, this analysis establishes the signs and approximate magnitudes of differences in the conduction-electron density at a gold atom in several lattices.

Finally, the sign of the shifts indicates that the ground state of Au^{197} is "smaller" or, more exactly, has more $3s_{1/2}$ protons than the 77-kev state. This supports Zeldes' conclusion[10] that the $3s_{1/2}$ subshell is filled in the ground state, which is then best approximated by the shell-model configuration $(h_{11/2})^{10}(3s_{1/2})^2(2d_{3/2})^3$ or $(h_{11/2})^{12}(3s_{1/2})^2(2d_{3/2})^1$.

___

[10] N. Zeldes, Nuclear Phys. 2, 1 (1956/57).

5. THE NUCLEAR SPIN OF NEODYMIUM-141 (*)

S. S. Alpert, B. Budick, E. Lipworth, and R. Marrus

The spin of 2.5-hr neodymium-141 was directly measured by the method of atomic beams and found to be 3/2. This is a verification of the spin assignment first made by Polak et al.,[1] who investigated the positron decay of Nd^{141} and the associated γ rays.

In total, six resolved "flop-in" transitions were observed.

___

(*) Short resumé of UCRL-9774, July 1961.

[1] H. L. Polak, W. Schoo, B. L. Scram, R. K. Girgis, and R. Vanlieshout, Nuclear Phys. 5, 271 (1958).

These are given in Table I.

Table I   Resolved resonances in Nd^{141}. The Zeeman frequency is calculated
on the assumption $I = 3/2$, $J = 4$, and $g_J = -0.6031$.[2]

No.	Resonance type	Field (gauss)	Calculated Zeeman frequency (Mc/sec)	Observed frequency (Mc/sec)	Compound uncertainty
1	α	12.264	7.529	7.545	0.045
2	α	19.566	12.012	12.025	0.052
3	α	36.198	22.223	22.215	0.068
4	β	6.915	4.835	4.838	0.057
5	β	19.566	13.680	13.665	0.062
6	β	36.198	25.310	25.325	0.113

The symbol α refers to transitions of the type $(F = 11/2,\ M_F = -1/2 \leftrightarrow F = 11/2\ \ M_F = -5/2)$ and the symbol β refers to transitions of the type $(F = 9/2,\ M_F = 1/2 \leftrightarrow F = 9/2,\ M_F = -3/2)$.

The radioactive sample was produced in the Berkeley 60-inch cyclotron
by the reaction $Pr^{141}(p, n)Nd^{141}$. The target material, praseodymium, was
machined into discs 0.025 in. thick and bombarded with 12-Mev protons for
5 to 8 hours. The total integrated flux was generally about 175 μa-hr. Usually
less than 2 hr elapsed between the completion of the cyclotron bombardment
and the beginning of an experimental run.

Identification of the observed material as Nd^{141} is assured in
several ways. The target material is known to be more than 99% Pr^{141} by
weight, from spectroscopic analysis. The method of production, the observed
electronic g factor, the half-integral spin, and a half-life of 2.5 hr observed
in the decay of several resonance foils serve to establish unambiguously that
the observed material is Nd^{141}.

The observed data make possible the setting of a lower limit to the zero-
field hyperfine-structure separation between the $F = 11/2$ and $F = 9/2$ states,
$\Delta\nu(11/2,\ 9/2)$. From second-order perturbation theory the deviation of an
α resonance from the Zeeman frequency, δ_α, should be related to $\Delta\nu(11/2,\ 9/2)$ according to

$$\delta_\alpha = 0.1190\ (g_J\ \frac{\mu_0}{h}\ H)^2 / \Delta\nu(11/2,\ 9/2).$$

Assuming the value of δ_α to be equal to or less than the compounded un-
certainty at the highest observed field, we obtain

---

[2] K. F. Smith and Spalding (Cavendish Laboratory, Cambridge, England)
private communication.

$$\Delta\nu(11/2, 9/2) \geq 1630 \text{ Mc/sec}$$

as a lower limit to the hyperfine separation.

6. THE NUCLEAR MOMENTS
AND HYPERFINE STRUCTURE OF 13-YEAR Eu[152]

Seymour S. Alpert

The magnetic dipole interaction constant, a, and the electric quadrupole interaction constant, b, for Eu[152] (13-yr) were measured by the method of atomic beams. These values are a = ± 9.345±.004 Mc/sec and b = ∓ 1.930±.117 Mc/sec. By comparison with the known moment of Eu[153], the nuclear dipole moment of Eu[151] was found to be $|\mu|$ = 1.912±.003 nm. The sign of this moment cannot be inferred from the experimental results. Comparison is made with the nuclear collective model which predicts a dipole moment of μ = +1.73 nm. The zero-field hyperfine separations of levels of different total angular momentum were measured. The results of atomic-beam experiments on Eu[151], Eu[152], Eu[153], and Eu[154] are compared with those results relating to the divalent ions as determined by paramagnetic resonance techniques. A significant discrepancy is noted.

- - - - - - - - - - - - - - - - - - - -

The theory[1] of the atomic beam method and the apparatus[2,3] used have been adequately covered in the literature. No attempt is made in this brief report to expand upon these topics.

In this experiment the source material, 13-year Eu[152], was produced by irradiation with thermal neutrons by the reaction Eu[151](n, γ)Eu[152](13-yr).

A total of eleven resolved resonances was observed, representing eight different types of transitions. The results are displayed in Table I. Under the heading "transition type" in Table I the subheadings F_1, M_1 and F_2, M_2, indicate the levels between which the observed transition occurs.

The eleven observed resonances listed in Table I were used as input data along with the accurately known value of the atomic splitting factor, g_J = -1.9935±.0003,[4] for a least-squares-fit IBM program.

[1] N. F. Ramsey, Molecular Beams (Oxford University Press, New York, 1956).

[2] G. O. Brink, Nuclear Spins of Thallium-197, Thallium-198m, Thallium-199, and Thallium-204 (Thesis), UCRL-3642, June 1957.

[3] J. C. Hubbs, R. Marrus, W. A. Nierenberg, and J. L. Worcester, Phys. Rev. 109, 390 (1958).

[4] P. G. H. Sandars and G. K. Woodgate, Proc. Roy. Soc. (London) A 257, 269 (1960).

Table I. Observed resolved resonances in Eu^{152}; $I = 3$, $J = 7/2$.

No.	Transition Type				Magnetic field (gauss)	Observed resonance frequency (Mc/sec)	$(f_{obs} - f_{calc})$ (Mc/sec)	Compounded uncertainty (Mc/sec)
	F_1	M_1	F_2	M_2				
1	13/2	-5/2	11/2	-5/2	1.000	59.950	+0.006	0.075
2	11/2	-3/2	9/2	-3/2	1.000	51.325	-0.002	0.035
3	9/2	-1/2	7/2	-1/2	1.000	42.350	+0.005	0.063
4	7/2	5/2	5/2	3/2	10.001	49.400	+0.051	0.175
5	7/2	3/2	5/2	5/2	10.001	48.350	-0.107	0.214
6		α			8.248	13.570	+0.035	0.083
7		α			16.001	28.485	-0.079	0.244
8		α			26.001	51.360	+0.074	0.185
9		α			42.007	92.430	+0.003	0.179
10		β			8.248	14.400	+0.008	0.150
11		γ			32.004	83.875	+0.139	0.239

Symbols α, β, and γ denote the transitions of the type

α: $(F = 13/2, M_F = -5/2 \longleftrightarrow F = 13/2, M_F = -7/2)$

β: $(F = 11/2, M_F = -3/2 \longleftrightarrow F = 11/2, M_F = -5/2)$

γ: $(F = 9/2, M_F = -1/2 \longleftrightarrow F = 9/2, M_F = -3/2)$

The magnetic dipole moment was calculated from the results of this experiment and the data of Pichanick et al.[5] and Sandars.[4] The value is $|\mu_I^{152}| = 1.912 \pm .003$ nm. This value is diamagnetically corrected. Using the collective model[6,7] in the limit of strong deformations and the Gallagher-Moszkowski[8] rules, one finds the theoretical value for the nuclear dipole moment μ_I^{152} (theo) $= +1.73$ nm. This compares favorably in magnitude with the experimentally observed value.

[5] F. M. Pichanick, P. G. H. Sandars, and G. K. Woodgate, Proc. Roy. Soc. (London) A 257, 277 (1960).

[6] S. G. Nilsson, Kgl. Danske Videnskab. Selskab, Mat-fys. Medd. 29, No. 16 (1955).

[7] B. R. Mottelson and S. G. Nilsson, Kgl. Danske Videnskab. Selskab, Mat.-fys. Skrifter 1, No. 8 (1959).

[8] C. J. Gallagher, Jr., and S. A. Moszkowski, Phys. Rev. 111, 1282 (1958).

The directly measured values of the hyperfine structures are

$$\Delta\nu_{13/2,\,11/2} = 59.848\pm0.060 \text{ Mc/sec,}$$

$$\Delta\nu_{11/2,\,9/2} = 51.246\pm0.022 \text{ Mc/sec,}$$

$$\Delta\nu_{9/2,\,7/2} = 42,343\pm0.025 \text{ Mc/sec,}$$

$$\Delta\nu_{7/2,\,5/2} = 33.191\pm0.032 \text{ Mc/sec,}$$

where $\Delta\nu_{13/2,\,11/2}$ is the zero-magnetic-field separation between the $F=13/2$ and $F = 11/2$ levels, and similarly for the other separations.

The atomic beam technique is based on the nuclear interaction with the electronic charge in the free atom, whereas the paramagnetic resonance technique is based on nuclear interaction with electronic charge in the Eu^{++} ion bound in a KCl crystal. Abraham, Kedzie, and Jeffries[9] measured the spin of Eu^{152} and Eu^{154} in a paramagnetic resonance experiment and also the magnetic dipole interaction constants of Eu^{151}, Eu^{152}, and Eu^{153} in the doubly ionized form bound in a crystal of KCl. These results, converted to units of Mc/sec, are indicated in Table II along with our results and those of Sandars and Woodgate.[4]

Table II. Values of the magnetic dipole interaction constant.

Isotope	Value from paramagnetic resonance, $\lvert a_{PR} \rvert$ (Mc/sec)	Value from atomic beams, $\lvert a_{ab} \rvert$ (Mc/sec)	Ratio of paramag. resonance value to atomic beam value $\lvert a_{PR}/a_{ab} \rvert$
Eu^{152}	97.61(18)	20.0523(2)	4.868(9)
Eu^{153}	45.33(4)	9.345(4)	4.851(5)
Eu^{154}	43.11(9)	8.8532(2)	4.869(9)

It is seen that the magnetic dipole interaction constant is 4.86 times as large in the crystal-bound Eu^{++} ion as in the free atom.

The theoretical explanation for this large discrepancy is not apparent; both s-electron exchange and s-electron promotion are possible mechanisms that might give rise to this effect. An explanation of the effect would result in a clearer knowledge of the electronic wave function for the Eu^{++} ion.

---

[9] M. Abraham, R. Kedzie, and C. D. Jeffries, Phys. Rev. 108, 58 (1957).

7. NUCLEAR ORIENTATION OF PARAMAGNETIC IMPURITY IONS [*]

Morton Kaplan and D. A. Shirley

The well-known Gorter-Rose method of nuclear orientation has been used with considerable success in recent years.[1-4] The method as used consists in cooling, by adiabatic demagnetization, a paramagnetic salt into which ions containing radioactive nuclei have been incorporated in lattice positions. These ions are polarized by a small applied magnetic field, and they in turn polarize their nuclei. A limitation of the method is that only nuclei of elements which form paramagnetic ions isomorphous with those of certain "good" cooling salts can be studied.

A substantial extension of this technique would result if nuclei of all elements that form paramagnetic ions could be oriented in this way. We believe that this extension may be made possible by incorporating the ions of interest as impurities into single crystals of cerium magnesium nitrate (CMN). The impurity ions may be interstitial or they may be trapped in tiny "brine holes." At any rate, they should be in thermal equilibrium with the lattice after demagnetization and can be polarized in fields of several hundred oersteds at temperatures below 0.01°K. To test this hypothesis, we have carried out nuclear-orientation experiments with Cr^{51} in CMN and have detected nuclear orientation by measuring the anisotropy of the 325-kev γ rays.

The specimen consisted of a 5-g single crystal of CMN grown from a solution containing small amounts of Cr^{51} along with about 1 mg of Cr^{+++} carrier. It was mounted in a demagnetization cryostat described elsewhere,[5] and cooled by adiabatic demagnetization to $\sim 0.003^\circ$K. A polarizing field was applied along the trigonal axis of the crystal, and the γ-ray counting rates were measured along and perpendicular to the field direction. The magnetic temperature of the crystal was monitored continuously during the counting period. The results for two polarizing fields are shown in Fig. A.7-1. The experiments were repeated with a second, independently grown crystal, and the data were found to be reproducible. Nuclear-orientation experiments in zero applied magnetic field show that the γ-ray emission from Cr^{51} is still anisotropic, the normalized intensities being about 1.03 along the axis and 0.98 perpendicular to the axis, at the lowest temperatures reached.

Although the main object of this experiment was to test the above-mentioned nuclear-orientation mechanism, some nuclear information was obtained from a preliminary analysis of the results. Using our data for a

---

[*] Phys. Rev. Letters 6 361 (1961).

[1] C. J. Gorter, Physica 14, 504 (1948).

[2] M. E. Rose, Phys. Rev. 75, 213 (1949).

[3] R. J. Blin-Stoyle and M. A. Grace, Handbuch der Physik, edited by S. Flügge (Springer-Verlag, Berlin, 1957), Vol. 42, p. 555.

[4] E. Ambler, in Progress in Cryogenics (Heywood and Company, Ltd., London, 1960). Vol. 2, p. 235.

[5] C. E. Johnson, J. F. Schooley, and D. A. Shirley, Phys. Rev. 120, 2108 (1960).
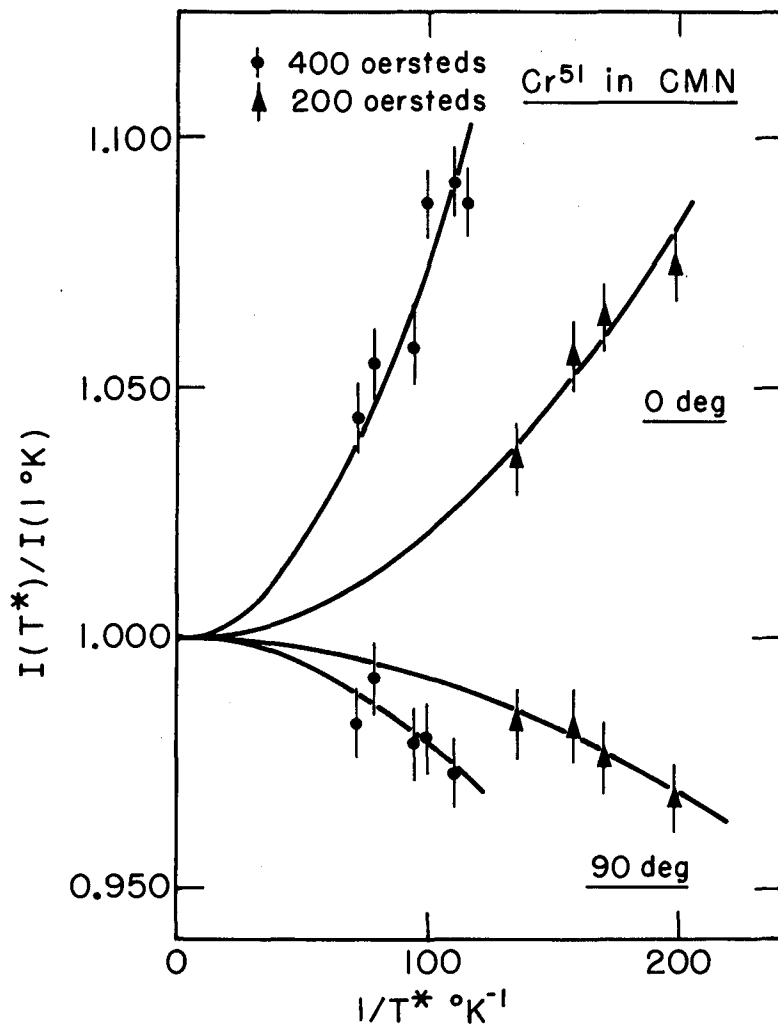
MU-22603

Fig. A. 7-1. Experimental results for nuclear orientation of Cr^{51} in
cerium magnesium nitrate as a function of the reciprocal magnetic
temperature, $1/T^*$. The ordinate is the ratio of the intensity of
325-kev gamma rays at temperature T^* to the intensity at 1^oK.
Data shown are from measurements at 0 to 90 deg to the crystal
trigonal axis, for two values of the magnetic field applied along the
axis. The uncertainties indicated are statistical standard devia-
tions. The curves drawn through the points are proportional to
$(1/T^*)^2$.

polarizing field of 400 oersteds, where nondiagonal interactions should be
least important, together with the measured partial E2 and total lifetimes[6,7]
of the 325-kev state in V^{51}, we find: (a) The E2-M1 mixing ratio of the 325-
kev γ ray of V^{51} has the value $\delta(E2/M1) = +0.37\pm0.04$; (b) a spin assignment
of 7/2 - is absolutely ruled out for this state; and (c) a lower limit of $|\mu| \gtrsim 0.8$
nm can be set for the magnetic moment of Cr^{51}.

The evidence that Cr^{+++} does not go into lattice sites in CMN is derived
from experiments in which we attempted to grow several percent chromium into
cerium magnesium nitrate and lanthanum magnesium nitrate. In these ex-
periments, the double nitrate crystals were grown from solutions containing
relatively high concentrations of Cr^{+++}. The crystals obtained were analyzed
spectroscopically for chromium, with the result that portions of crystals that
were cloudy and slightly blue contained small amounts (approx 0.1%) of chro-
mium. However, those portions of crystals which were optically clear and
colorless contained no detectable traces of chromium. We conclude that
Cr^{+++} does not substitute in lattice positions, but is probably incorporated
into the crystal in "brine holes" as growth proceeds.

Considerable development may be necessary before this technique can
be used to obtain reliable values of nuclear moments. It should be immedi-
ately useful, however, for investigating other nuclear properties. In partic-
ular, nuclei of elements in the 4d, 5d, and 5f transition series should be with-
in the scope of the method.

We thank George Shalimoff for performing the analyses of the double
nitrate crystals.

---

[6] G. M. Temmer and N. P. Heydenburg, Phys. Rev. 104, 967 (1956).

[7] A. W. Sunyar and M. Deutsch, private communication quoted by D. Strominger,
J. M. Hollander, and G. T. Seaborg, Revs. Modern Phys. 30, 585 (1958).

8. THE ALPHA-DECAY SCHEME OF 152-YEAR Am^{242m} (*)

F. Asaro, M. C. Michel, S. G. Thompson, and I. Perlman

A preliminary investigation[1] of the alpha decay of Am^{242m} indicated
further detailed studies could contribute substantially to the understanding
of the energy levels of strongly deformed odd-odd nuclei. The most highly
enriched samples of Am^{242m} made by conventional neutron bombardment of
Am^{241}, however, contain only about $1.5\times10^{-2}\%$ Am^{242m} by alpha activity,
and the predominant Am^{241} activity masks to a large extent the Am^{242m}
alpha-decay radiations. Therefore suitable samples for alpha, electron, and

---

[1] F. Asaro, M. C. Michel, S. G. Thompson, and I. Perlman, reported by
I. Perlman in Proceedings of the International Conference on Nuclear
Structure at Kingston, Canada, (University of Toronto Press, Toronto, 1960),
page 559.

γ-ray spectroscopic measurements were prepared with the aid of the excellent mass separator at the Institute for Theoretical Physics in Copenhagen, Denmark.

The alpha spectra measurements showed groups of 5.404 ($\approx 1.6\%$), 5.360 ($\approx 1.6\%$), 5.308 (0.8%), 5.28(0.4%)(?), 5.244(0.6%), 5.201(88%), 5.136(5.7± .2%), 5.082 (0.30± .06%) and 5.061 Mev (0.25± 0.6%). The main group of Am^{241} at 5.482 Mev was used as an energy standard for these measurements.

The electron spectra indicated only an 87-kev M1 transition which could be assigned to the Am^{242m} alpha decay.

The main γ-ray studies consisted of delay measurements and coincidence studies of the L x-ray and γ-ray spectra occurring before and after two metastable states. The results of these experiments are shown in the decay scheme in Fig. A.8-1. The dashed quantities, those in parentheses, and the relative positions of the 48- and 87-kev γ-rays are considered somewhat uncertain.

The assignment of spins and parities to the various Np^{238} levels depends considerably on the values assigned to the 337-kev level. The partial alpha half-life for the decay of this level is essentially unhindered. In the even-even and odd-mass nuclides the unhindered (or favored) type of decay populates states in the daughter nucleus having the same configuration as the parent. As K, π, and I had been assigned 5-5 for Am^{242m},[2] we calculated the expected relative alpha intensities[3] to the rotational members of a similar 5-5 band in Np^{238}. As is seen in Table I, the agreement is very good--even with respect to the energy spacings, which will be discussed later.

Table I. Am^{242m} favored alpha decay to 5- band

K π I	Energy spacings (kev)		Calculated abundances (%)				Experimental abundances (%)
	Calc.	Exp.	L = 0	L = 2	L = 4	Sum	
5 - 5	----	----	65.2	22.8	0.023	88.0	88
5 - 6	66.0	65.7	----	5.6	0.021	5.6	5.66(± 0.17)
5 - 7	143.0	142	----	0.33	0.006	0.34	0.25(± 0.06)

In Fig. A.8-1 the assigned rotational bands of Np^{238} are classified in terms of the adjacent odd-mass Nilsson orbitals. These orbitals are listed as A, B, etc. according to their increasing excited-state energy in the appropriate odd-mass nuclides. All the observed alpha and γ-ray transitions shown in Fig. A.8-1 can be interpreted as taking place between levels having at least one common Nilsson orbital. In five instances in which comparisons could be made, the reduced γ-ray and alpha-particle transition probabilities were

[2] F. Asaro, I. Perlman, J. O. Rasmussen, and S. G. Thompson, Phys. Rev. 120, 934 (1960).

[3] P. O. Fröman, Kgl. Danske Videnskab. Selskab, Mat.-fys. Skrifter 1, No. 3 (1957).
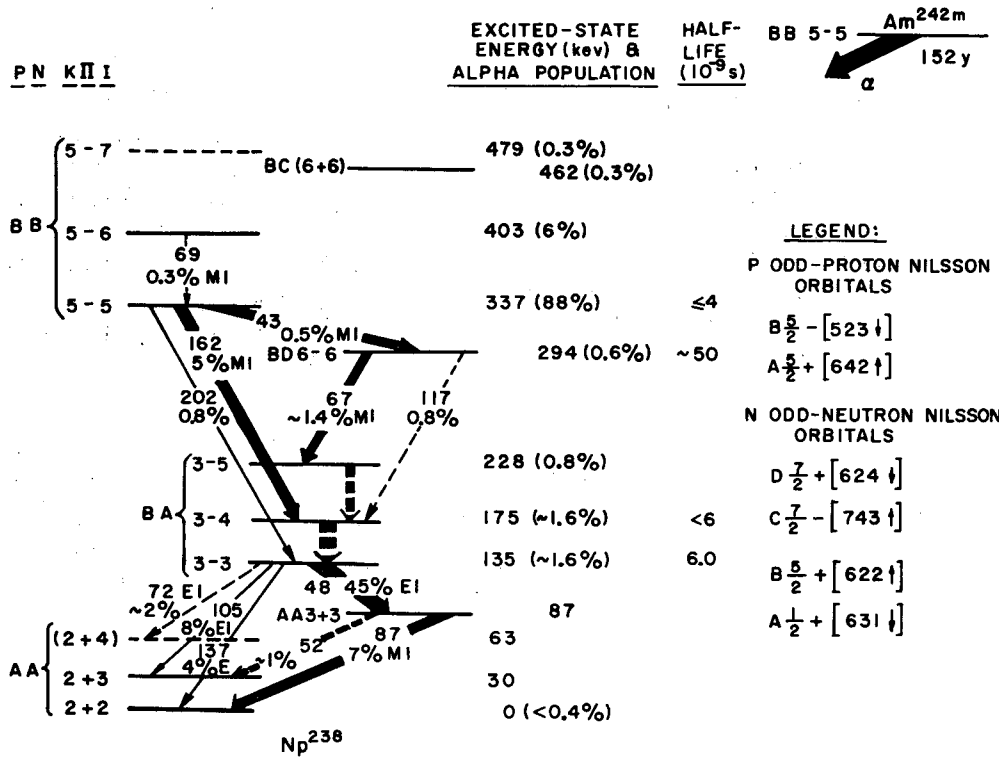
Fig. A.8-1. The alpha-decay scheme of Am^{242m}.

within a factor of four of the values for the corresponding odd-mass trans-
itions in Cm^{243} and Am^{243} alpha decay. This served as a basis for the
assignment made to the 462-kev level.

The rotational energy spacings were calculated from the moments of
inertia of the corresponding levels in Np^{237} modified by the difference be-
tween the even-even and the corresponding odd-neutron moments of inertia.
The agreement was good for the bands BB(5-) and BA(3 -), but the calculated
spacings for the AA(2+) band were about 15% too small.

A peculiar ratio of intensities for the El γ rays populating the AA(2+)
band can be explained qualitatively by a Coriolis interaction between AA(2+),
and AA(3+), and BA(3-), and BA(2-) (unobserved).

9. THE DECAY OF $_{72}Hf^{173}$ (*)

J. Valentin,[†] D. J. Horen, and J. M. Hollander

We have investigated the decay of Hf^{173}, which populates levels in Lu^{173}.
Hf^{173} was prepared via, the (a, 3n) reaction, by irradiation of the "separated
isotope" Yb^{172} [‡] with 38-Mev helium ions from the Crocker 60-inch cyclotron.
The internal-conversion spectrum was measured with 180° permanent-magnet
photographic recording spectrographs having field strengths of 50, 100, 150,
and 340 gauss and momentum resolution $\approx$ 0.1%.[1] In these measurements, the
relative intensities of the lines were determined by a visual comparison
method that has been described by Albridge et al.[2] A 25-cm double-focusing
spectrometer was used to measure the intensities and conversion coefficients
of some of the stronger transitions. Photon spectra were examined under a
variety of conditions with 5×5-cm and 7.6×7.6-cm NaI(Tl) crystals coupled
to either a Penco or a TMC analyzer. Gamma-gamma coincidence measure-
ments were made both with a conventional fast-slow system and with a two-
dimensional[3] coincidence analyzer which utilizes paper-tape data output.

The half life of Hf^{173} was determined as 24.4±1.0 hr by following its
decay for a period of 11 days in a flowing methane proportional counter. In
all, 75 electron lines representing 32 transitions were assigned to the decay
of Hf^{173}. Photons from additional transitions were observed in the scintilla-
tion spectra. Table I gives the relative photon intensities, and Table II lists
the transition energies, relative electron intensities, relative photon intensities,

---

[1] W. G. Smith and J. M. Hollander, Phys. Rev. 101, 746 (1956).

[2] R. G. Albridge, J. M. H llander, C. J. Gallagher, and J. H. Hamilton,
J. Nuclear Phys. 27, 529 (1961).

[3] J. O. Rasmussen and M. Nakamura, in Chemistry Division Semiannual
Report, UCRL-8867, July 1959, p. 56.

experimental K-conversion coefficients, transition multipole orders, and total transition intensities of those transitions that we have been able to place in the decay scheme (see Fig. A.9-1). The level scheme shown in Fig.A.9-1 is based upon energy sums, intensity sums, and gamma-gamma coincidence experiments, both prompt and delayed.

Table I. Hf^{173} relative photon intensities

$E_\gamma{}^a$ (kev)	Relative intensity[b]	E_γ (kev)	Relative intensity
K x-ray	13,500±2000	1032.1 ⎫	
123.6 ⎫		1037.0 ⎬	124±13
134.9 ⎬	11,800±1200	1069.2 ⎭	
139.6 ⎭		1204.6 ⎫	
161.8	653±130	1209.7 ⎭	56±6
296.7 ⎫		1350±10	3.2±1.2
306.4 ⎬	6360±640	1480±10	1.4±0.7
311.2 ⎭		1570±15	~0.8
356.8	64±25	1700±15	~0.5
422.3	563±18	1800±20	~0.5
539.3 ⎫		1910±40	~0.3
549.1 ⎪		2000±40	~0.2
555.4 ⎬	140±21	2120±50	~0.1
567.2 ⎪		~2260	<0.05
576.8 ⎭			
617.0 ⎫	20±10		
624.3 ⎭			
717.4	27±9		
759.4 ⎫	42±9		
764.3 ⎭			
852.6 ⎫			
857.4 ⎪	46±16		
873.3 ⎪			
878.4 ⎭			
897.7	230±35		

[a] When applicable, the photon energies are those determined in electron-spectrographic measurements.

[b] These intensities are normalized in the manner adapted in Table II.

Table II. Experimental K-conversion coefficients and total transition Intensities

Transition energy (kev)	Relative Electron intensity (arbitrary units)		Relative photon intensity		$(e/\gamma)_k$	Multipole order	Total transition intensity (% EC decays)
	K	ΣL,M...					
K - X				13,500±2000			
4.64	M_II/M_III	~0.6				E2	
77.8	.....	10				M1	0.08
123.6	1800	410	9970 }a		0.18	E1	98.5
134.9	460	320	610 }	11800±1200	0.75	M1-E2 (74±4% E2)	11.2
139.6	1950	500	1220 }		1.6	M1-E2 (15±3% E2)	29.7
161.8	63	15		653±130	0.096	E1	5.9
296.7	72	25	4500 }		[0.016]b	E1	37.2
306.4	11.2	3	700c }	6360±640	0.016c	E1	5.8
311.1	18.5	4	1160c }		0.016c	E1	9.55
356.8	6.8	1.5		64±25	0.11	M1-E2	0.5
422.3	0.8	.....		56±18	0.014	E1 or E2	0.46
539.3	1.7	0.5					
549.1	2.0	0.5					
555.4	0.46	0.1		140±21			1.2
567.2	0.40	......					
576.8	0.10	......					
617.0	0.04	......		20±10	0.005±0.004	E1 or E2	0.16
624.3	0.05	......					
717.4	0.10	......		27±9	0.004±0.003	E1 or E2	0.22
759.4	0.18	......		42±9	0.006±0.004	E2	0.34
764.3	0.05						
852.6	0.14	......					
857.4	0.05	......		46±16			0.38
873.7	0.05	......					
878.4	0.10	......					
897.7	1.0	0.2		230±35	0.0043±0.001	E2	1.9
1032.1	0.32	......					
1037.0	0.26	......		124±13			1.0
1069.2	0.052	......					
1204.6	0.17	......		56.6	0.004±0.001	E2	0.46
1209.0	0.07	......					

aExperimental composite photon intensity divided according to the known, independently determined, conversion coefficients of these transitions.

bPhoton relative intensity scale normalized to the theoretical E1 conversion coefficient of the 296.7-kev transition, 0.016.

cThese conversion coefficients were determined, relative to that of the 296.7-kev transition, by internal-external conversion measurements.
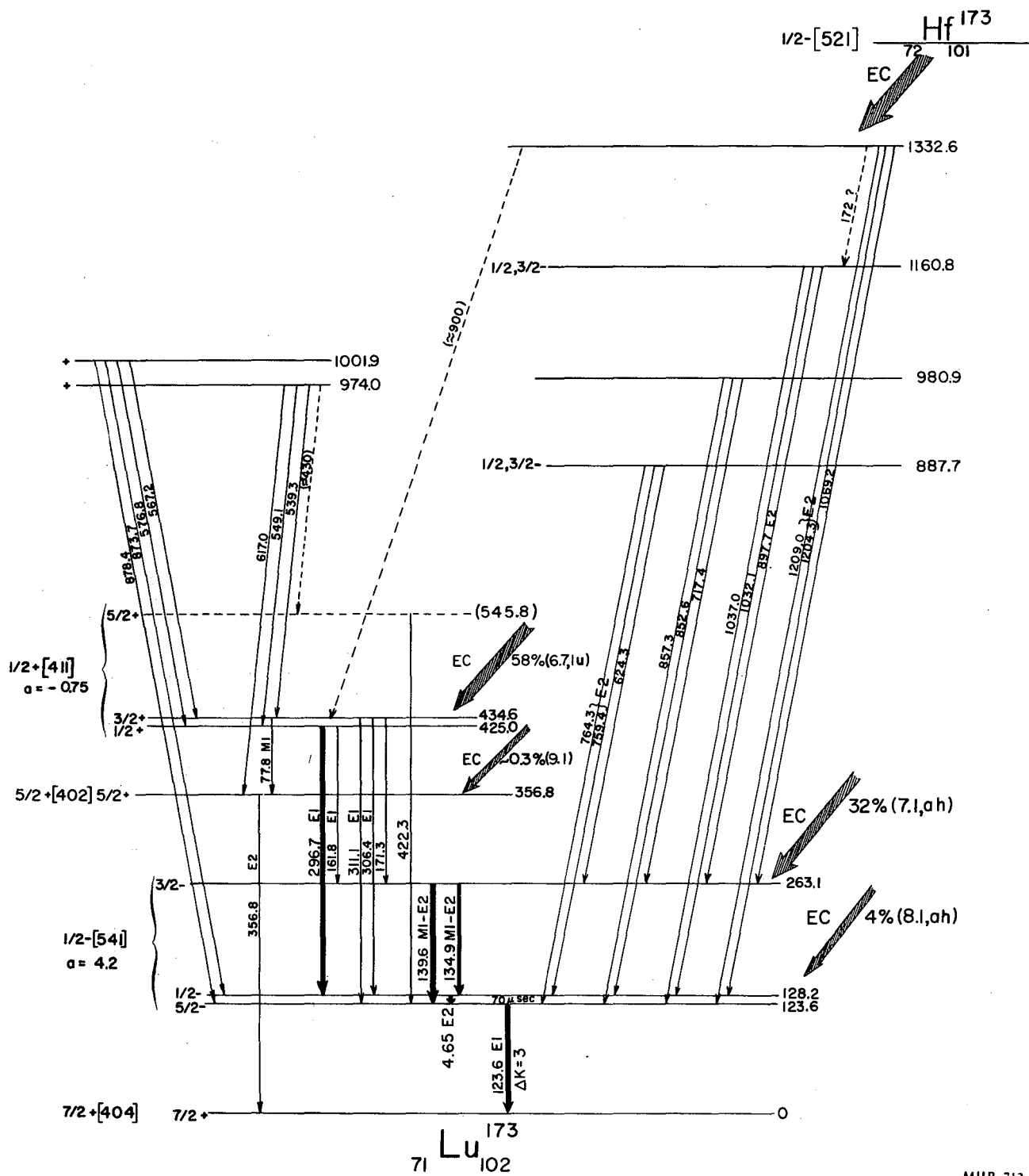
Fig. A. 9-1. Decay scheme of Hf^{173}.

MUB-713

The ground state of Lu^{173} has been assigned by Dzhelepov et al.[4] as the Nilsson state 7/2+ [404]. Although in a separate experiment we did not confirm the excess of x rays from Lu^{173} decay upon which Dzhelepov et al. base this assignement--i.e., evidence of direct ground-to-ground electron capture transition--we feel nevertheless that the assignment is correct. The experimentally determined conversion coefficient of the 123.6-kev transition indicated that it is of E1 character, and its 10^9-fold photon retardation indicates that it is strongly K-forbidden. Hence, we interpret the 123.6-kev state as K = 1/2-, I = 5/2. The 134.9- and 139.6-kev transitions, mixed M1-E2 multipoles, are in all likelihood intraband rotational transitions. Thus, the states at 123.6 and 263.2 kev are interpreted as rotational states of a single K = 1/2 band, with spin I = 5/2, 1/2, and 3/2, respectively. This interpretation is consistent with the measured E2 character of the 4.6-kev transition between the 5/2 and 1/2 states, as well as the calculated value of the decoupling parameter, a = +4.2

In the Nilsson diagram there is no intrinsic state with K = 1/2- in the latter part of the 50-to-82-proton shell. However, the first asymptotic state beyond the 82-proton shell is 1/2- [541], and it is not unreasonable to find, at the large deformation characteristic of the lutetium nuclei ($4 < \eta < 6$), that the energy of this state has become sufficiently low to be competitive with the 7/2- [404] and 9/2- [514] states. By use of the Nilsson[5] wave functions for the 1/2- [541] proton state, we obtain the values a = +4.3 and +3.5 for deformation parameters $\eta = 4$ and 6, respectively. The agreement with the experimental value noted above is quite good.

Additional support for the assignment of these levels as a K = 1/2 band was obtained from the good agreement between the experimental and theoretical values for the ratios of the relative reduced transition probabilities of the M1 and E2 components of the 134.9- and 139.6-kev transitions.

The manner in which the 425.0- and 434.8-kev levels de-excite (i.e., by E1 transitions to levels in the K = 1/2-band) suggests that those states are members of a K = 1/2+ band based upon the proton state, 1/2+ [411]. We have tenuous evidence from the γ-γ coincidence data that a third member of this band with spin 5/2 lies at 545.8 kev. The level at 356.8 kev has the characteristics expected for a 5/2+ [402] proton state.

Since the electron-capture decay of Hf^{173} populates the low-spin members of K = 1/2 bands, we conclude that in the Hf^{173} ground state the 101st neutron occupies the 1/2- [521] orbital. Little can be said about the levels above the 548.6-kev state, except that they are probably of spin 1/2 or 3/2.

---

[4] B. S. Dzhelepov, B. K. Preobrazhenskii, and V. A. Sergienko, Izvestiya Akademii Nauk S.S.S.R. (Seriya fizicheskaya) 22, 795 (1958); Columbia Technical Translations, p. 789.

[5] B. R. Mottelson and S. G. Nilsson, Kgl. Danske Videnskab. Selskab, Mat.-fys Skrifter 1, No. 8 (1959).

10. ENERGY LEVELS OF $_{71}Lu^{172}_{101}$ (*)

J. Valentin,[†] D. J. Horen, and J. M. Hollander

The energy levels of $_{71}Lu^{172}_{101}$ are of interest because of the lack of information about odd-odd deformed nuclei. Hf^{172} has been synthesized by intensive irradiation both of natural ytterbium and of the "separated isotope" Yb^{172}*‡ with 48-Mev helium ions from the 60-inch Crocker cyclotron. The internal-conversion spectrum of Hf^{172} was examined with 180° photographic recording permanent-field spectrographs of field strengths 50, 100, 150, 215, and 340 gauss and also a 50-gauss spectrograph employing a 10.8-kv "pre-accelera-tion" voltage applied to the source.[1] A 25-cm double-focusing spectrometer was used to measure the relative intensities of some of the conversion lines. Gamma-ray spectra were measured with 2.5×0.3-, 5.1×5.1- and 7.6×7.6- cm NaI(Tl) crystals coupled to Penco or TMC analyzers; gamma-gamma coincidence experiments were done with conventional "fast-slow" apparatus with fast resolving time $2\tau \approx 6 \times 10^{-8}$ sec.

Analysis of the internal-conversion data revealed that the Hf^{172} spectrum contains only seven transitions, all with energies less than 130 kev. At these low energies, L-conversion subshell ratios are known to depend sensitively on the multipole order, and this allowed the unambiguous assignment of transition multipole orders, in most cases. The scintillation spectrum of a sample of Hf^{172}, containing a small amount of 70-day Hf^{175}, taken with a 2.5×0.3-cm crystal covered with a thin beryllium window, is shown in Fig. A. 10-1. The fraction of the peak at 24 kev, which is partially composed of the escape peak from the K x ray, attributable to a 24-kev photon, was determined by an absorption experiment. Table I lists the transition energies and multipolarities and relative electron, photon, and total transition intensities.

Because the theoretical single-proton estimate for the half life of a 41.8-kev M3 transition is approx 10 seconds, and M3 transitions have hindrance factors ranging from 1 to 100, a rapid chemical separation of this isomer was attempted.[2] After extensive purification of the hafnium fraction, lutetium was allowed to grow in for periods of 30 seconds, 1 minute, etc., after which it was quickly separated and transferred to a scintillation system capable of recording the pulse-height spectrum, and counting pulses corresponding to Lu L x rays. In this manner, a decay period of 3.7± .5 min was readily observed (see Fig. A. 10-2). Since the photon spectrum of the 3.7-min Lu^{172m} contained only L x rays, the isomeric transition must lie at the bottom of the level scheme.

*Shortened form of a paper submitted to Nuclear Phys.

†On leave from Laboratoire de Physique Nucléaire, Orsay, France.

‡The separated isotopes were purchased from the Stable Isotopes Division, Oak Ridge National Laboratory, Oak Ridge, Tenn.

1. R. G. Albridge, Nuclear Spectroscopic Studies in the Heaviest Element Region (Thesis), UCRL-8642, April 1960.

2. A. H. Wapstra, G. J. Nijgh, and R. Van Lieshout, Nuclear Spectroscopy Tables, (North-Holland Publishing Company, Amsterdam, and Interscience Publishers, Inc., New York, 1959.
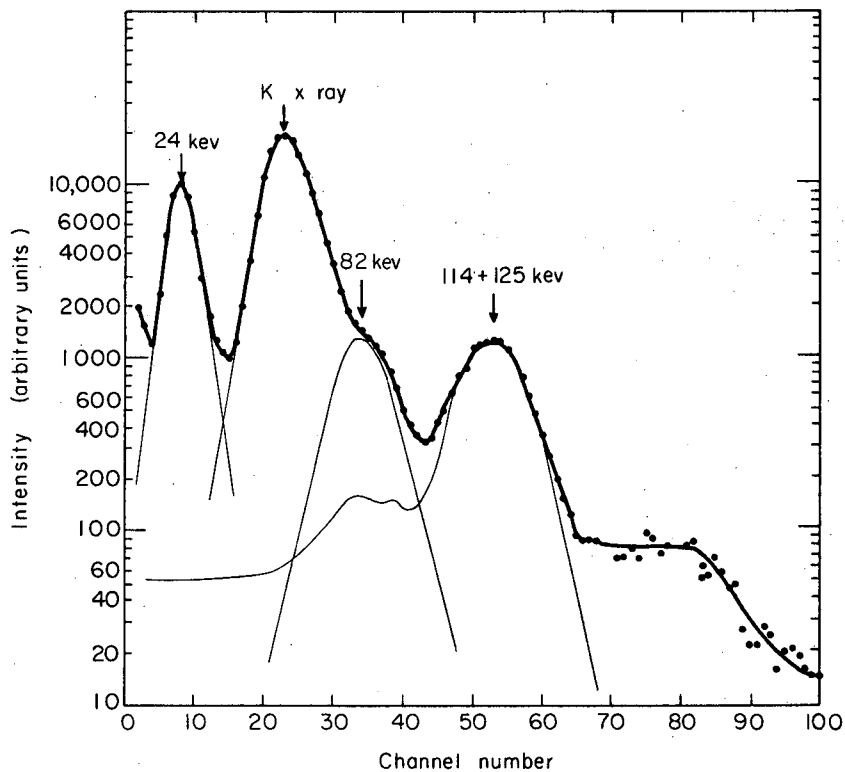
Fig. A. 10-1. Photon spectrum of Hf^{172}. The counts above channel 70
    are due to Compton-scattered photons from the strong 343-kev γ ray
    in Hf^{175}, present in small amounts in the source.

Table I.   Hf^{172} transition intensities and multipolarities.

Transition energy (kev)	Multipole order	Total electron intensity[a]	Photon intensity[a]		Total Relative transition intensity[c]
			Calculated	Experimental	
24.0	E1	2280	700	600	3000
41.8	M3	2410	~ 0.1	- - -	2400
44.1	E2 (M1-E2)	1250	~11	- - -	1250
70.0 (?)	- - -	- - -	- - -	- - -	- - -
81.8	M1	1210	200	265	1400
114.0	E1, M1	195	80 ⎫	[580][b]	~300
125.8	M1	770	500 ⎭		1300
K x rays	- - -	- - -	3700	3760	3700

[a] Same scale

[b] Experimental and calculated values normalized here.

[c] The experimental error of the relative transition intensities is estimated to be ±20%.

        Unfortunately, the data are not sufficient to conclude a unique level scheme for Lu^{172}. However, after consideration of the information pertaining to single-particle states in neighboring nuclei plus general beta-decay selection rules, we select the scheme shown in Fig. A.10-3 as the most probable. The ground state of the 71st proton has in all known cases been reported in the Nilsson designation[3,4] to be 7/2+ [404], while the 101st neutron is 1/2- [521].[3,5] On the assumption that the ground state of Lu^{172} is composed of these two configurations, the Gallagher-Moszkowski coupling rules predict the lowest level to have spin and pairty 4-. With this assumption, the 41.9-kev level must be 1-, because of the M3 character of this transition. This level can be interpreted as arising from the promotion of the neutron to

[3] J. Valentin, D. J. Horen, and J. M. Hollander, The Decay of $_{72}$Hf^{173} (UCRL-9731, June 1961) (to be submitted to Nuclear Phys.).

[4] B. R. Mottelson and S. G. Nilsson, Kgl. Danske Videnskab. Selskab, Mat.-fys. Skrifter 1, No. 8 (1959).

[5] B. Harmatz, T. H. Handley, and J. W. Mihelich, Phys. Rev. 119, 1345 (1960).
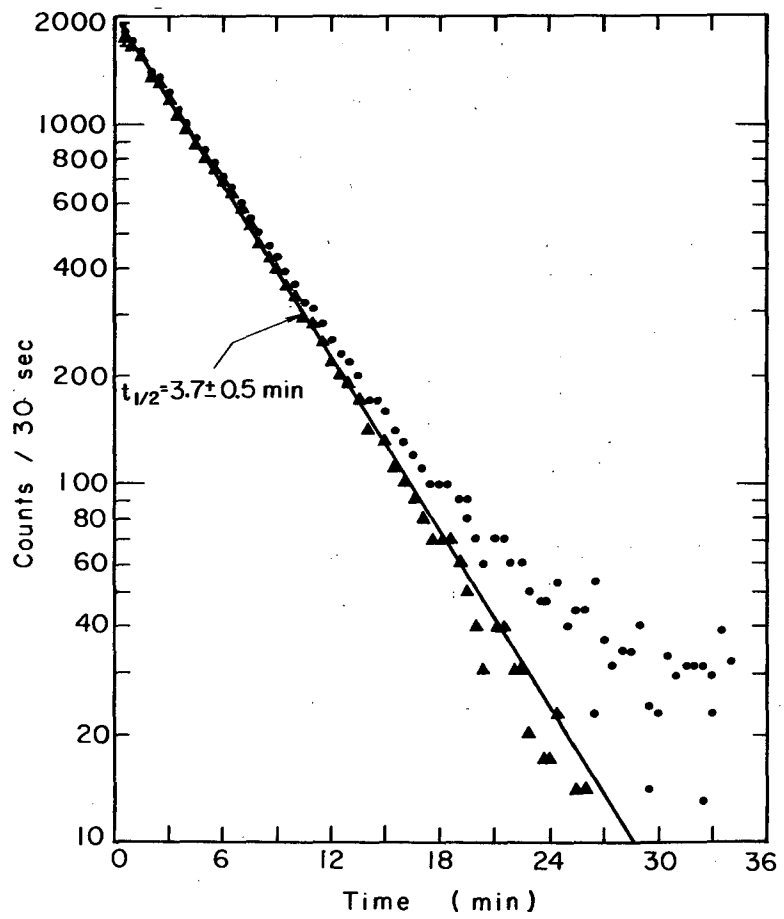
Fig. A. 10-2.   Decay curve of L x rays from Lu^{172m}.
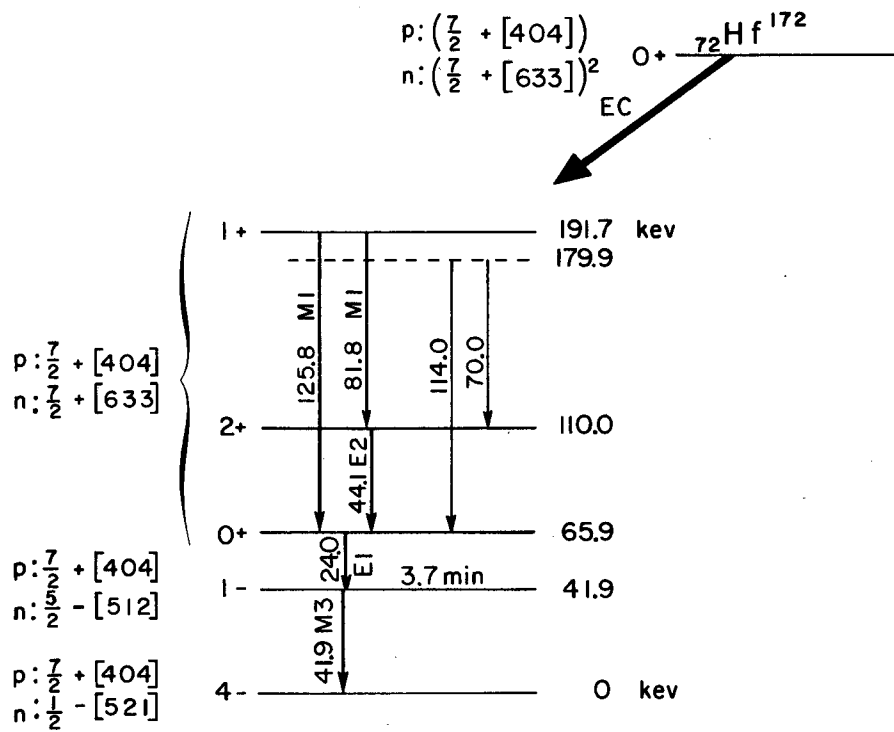
Fig. A.10-3. Proposed level scheme for Lu^{172}.

MU-24567

the $5/2-[512]$ state. One interprets the 65.9-kev (0+), 110.0-kev (2+), and 191.7-kev (1+) levels in terms of a single $K = 0$ rotational band in which the levels of odd spin are displaced relative to those of even spin. (Newby has discussed such displacements, which arise when $K_p = K_n$.[6]) In support of this interpretation is the experimental reduced photon-transition probability ratio, $B_{M1}(81.8)/B_{M1}(125.8) = 1.8 \pm 0.4$, which agrees within the error with the value expected from the branching-ratio rules,[7] 2.0, if all three states have $K = 0$. As a further check on the assignment of the 110.0-kev level as a 2+ rotational state, we have estimated the inertial parameter $3\hbar/\mathcal{J}$ of this band on the basis of that of the even Yb^{170} core plus those of the odd proton and odd neutron, in the relevant Nilsson orbitals. The resulting calculated value, $(3\hbar^2/\mathcal{J})_{71}Lu_{101}^{172} = 53.3$ kev, is to be compared with the experimental value, 44.1 kev. That most of the electron capture decay of Hf^{172} populates the 197.7-kev (1+) state, with little if any population of the 65.9-kev (0+) level, might be caused by the necessity of a pure Fermi transition (0+ → 0+) to the latter state, whereas the transition (0+ → 1+) to the 197.7-kev level can also proceed via the Gamow-Teller interaction.

---

[6]N. D. Newby, Scattering in the K=0 Band of Odd-Odd Deformed Nucleii (UCRL-9764, July 1961)(to be submitted to Phys. Rev.)

[7]G. Alaga, K. Alder, A. Bohr, and B. R. Mottelson, Kgl. Danske Videnskab. Selskab, Mat.-fys. Medd 29, No. 9 (1955).

11. ISOMERIC STATE IN Y^{86} (*)

Y. E. Kim, D. J. Horen, and J. M. Hollander

In the course of an investigation of neutron-deficient yttrium isotopes, we have detected an isomeric state of Y^{86}. The Y^{86m} was produced by irradiations of RbCl (natural or enriched in Rb^{85}) with helium ions and of $Sr(NO_3)_2$ (natural or enriched in Sr^{86}) with deuterons, in the Crocker 60-inch cyclotron.

The sources, radiochemically pure and in most cases carrier-free, were studied with 7.6×7.6-cm NaI(Tl) crystals and with a 100-gauss $180°$ spectrograph and a 25-cm double-focusing spectrograph.

The experiments established that the half life of Y^{86m} is 48 ± 1 minutes. Its radiations, as characterized by a number of cross-bombardments of natural Rb, Rb^{85}, and Sr^{86} with deuterons and α particles, are summarized in Table I.

The absolute K-conversion coefficient of the 208.0-kev transition was measured in a 25-cm double-focusing spectrometer, by use of the internal-external conversion method due to Hultberg and Stockendal.[1] The experimental

---

(*)Brief version of paper to be published in Nuclear Phys.

[1]S. Hultberg and R. Stockendal, Arkiv Fysik 14, 565 (1959).

value $\epsilon_K = 0.04 \pm 0.01$ corresponds to a mixed M1-E2 transition (approx 40% E2).[2,3]

Table I. Internal-conversion data of Y^{86m}

Electron energy (kev)	Shell	Binding energy (Y)	Transition energy (kev)	Intensity ratios
7.98	L_{II}	2.17	10.15	$L_{III}/L_{II} = 1.5 \pm 0.5$
8.06	L_{III}	2.10	10.16	
190.9	K	17.1	208.0	$K/L_I/M_I = 100/8.3/1.7$
205.6	L_I	2.39	208.0	
207.5	M_I	0.41	207.9	

If the reasonable assumption is made that the 10.15-kev transition is responsible for the 48-minute half life, it follows that the transition must be of multipole order E3 or M3.[4] These two alternatives are readily distinguishable by an examination of the L-subshell conversion pattern. A straight-line extrapolation to 10 kev on log-log paper of Rose's theoretical L-shell conversion coefficients[3] indicates for M3 radiation the subshell pattern $L_I/L_{II}/L_{III} = 24/2.6/100$ and for E3 radiation the ratios $L_I/L_{II}/L_{III} = 0.9/49/100$. The experimental observation of only L_{II} and L_{III} conversion, with the ratio $L_{III}/L_{II} = 1.5 \pm .5$, is compatible only with an E3 assignment.

Our interpretation of the data is that the 48-minute isomeric state of Y^{86} decays by a 10.15-kev E3 transition followed by a 208.0-kev E2 transition. It is interesting to speculate briefly on the possible nature of the levels in Y^{86} from which these transitions arise.

Y_1^{86}, with 39 protons and 47 neutrons, has a ground-state configuration $(p_{1/2})_P^1 (g_{9/2})_N^{-3}$, and hence, according to Nordheim's "strong" rule, spin and parity 4-. This assignment is consistent also with the recent results of Yamazaki, Ikegami, and Sakai[5] on the decay of 14.6-hr Y^{86}.

[2] L. A. Sliv and I. M. Band, Coefficients of the Internal Conversion of Gamma Radiation, Part I, K-Shell (U.S.S.R. Academy of Sciences, Leningrad, (1956).

[3] M. E. Rose, Internal Conversion Coefficients (North-Holland Publishing Co., Amsterdam, and Interscience Publishers Inc., N. Y., 1958).

[4] A. H. Wapstra, G. J. Nijgh and R. Van Lieshout, Nuclear Spectroscopy Tables (North-Holland Publishing Co., Amsterdam, and Interscience Publishers Inc., N. Y., 1959).

[5] T. Yamazaki, H. Ikegami, and M. Sakai, University of Tokyo Institute for Nuclear Study Report INS-32, May 1961.

The excited states of this odd-odd nucleus are expected to arise as combinations of the neutron states found in $_{38}Sr^{85}_{47}$ and proton states in $_{39}Y^{85}_{46}$ or $_{39}Y^{87}_{48}$. These are shown in Table II.

Table II   Expected configurations of Y^{86}

Proton state (Y^{87})	Neutron state (Sr^{85})	Resultant spins	Resultant parity
$p_{1/2}$	$g_{9/2}$	4, 5	-
$p_{1/2}$	7/2+	3, 4	-
$p_{1/2}$	$p_{1/2}$	0, 1	+
$g_{9/2}$	$g_{9/2}$	0, 1, 2. . . . 9	+
$g_{9/2}$	7/2+	1, 2, 3. . . . 8	+
$g_{9/2}$	$p_{1/2}$	4, 5	-

Preliminary results of a study of decay of $_{40}Zr^{86}_{46}$ being carried on at this Laboratory indicate that the 48-min isomeric state of Y^{86} is not populated in Zr^{86} decay. This suggests that the spin of the isomer is higher than the ground-state spin 4-. Of those states shown in Table II, a most likely choice for Y^{86m} is the 8+ state arising from $(g_{9/2})_P (7/2+)_N$. Thus, the levels of the isomer might be as shown in Fig. A.11-1.

12. EXPERIMENTAL OBSERVATION OF A NEW REGION OF NUCLEAR DEFORMATION (*)

Raymond K. Sheline,[†] Torbjørn Sikkeland, and Richard N. Chanda

The nuclear periodic table has three or possibly four regions where nuclei have been shown experimentally to be deformed, namely $A \approx$ 19 to 28 and 150 to 190 $A \geqslant 222$, and possibly $A \approx$ 8. The work presented here gives experimental evidence for an additional region of deformation. This new region is located in the neutron-deficient rare earths, where the neutron and proton numbers are in the 50-to-82 group.

In order to study the energy levels of nuclei in this region it was nec-essary to discover a number of new La and Pr nuclides. We report here
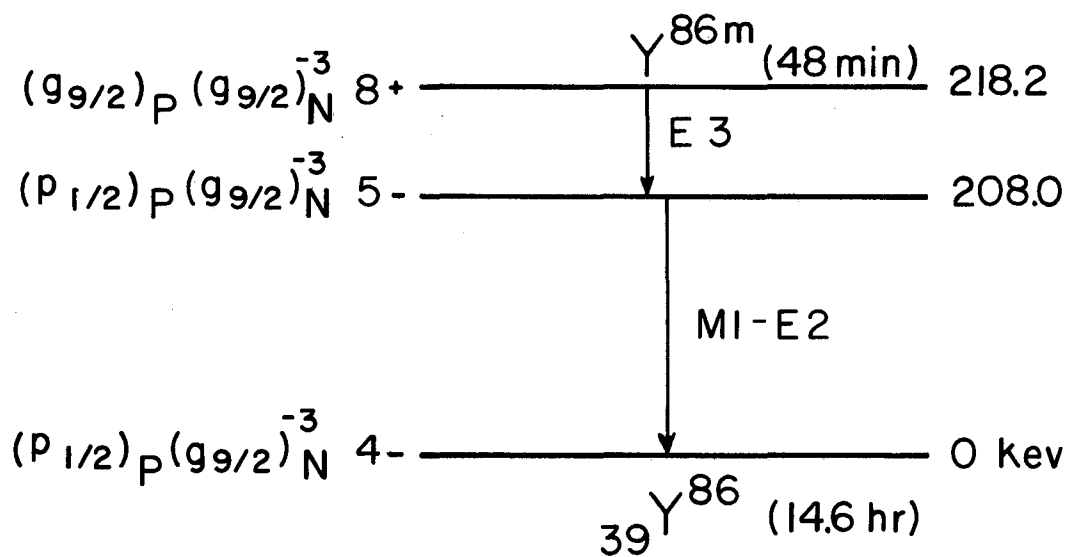
Fig. A.11-1. Suggested level scheme of Y86m.

only on those new nuclides whose mass number, half life, and first excited state are relatively certain.

The simplest available method of proving that nuclei are deformed involves the production of odd-odd nuclei whose decay into daughter even-even nuclei gives a characteristic low energy for the first excited state and, if possible, a rotational band built on the ground state with spins 0^+, 2^+, 4^+, $\cdots$, and ratios of energies to the first excited state of $1.0{:}3.33{:}7.0{:}\cdots$. Accordingly, we have produced the nuclei La^{126}, La^{128}, and La^{130} with half lives of $1.0 \pm .3$, 6.5 ± 1.0, and 9.0 ± 1.0 min, respectively.

By use of the Hilac these La activities were produced from the reactions of C^{12} on nautral Sb and of O^{16} on In. The reaction products recoiling out of approx 1 mg/cm^2 self-supporting targets of Sb and In were caught in 1.8 mg/cm^2 Pd foil which was then dissolved in hot aqua regia. With Ba as holdback carrier, the La activities were precipitated in LaF_3. The mass assignments of the new nuclides were verified by determining the excitation functions. In addition, the nuclide La^{126} was shown to decay into a species that has a spectrum identical[1] with that of Ba^{126}. Further, La^{130} emits a very strong 356 ± 4-kev γ ray. A 359-kev γ ray is observed[2] in the Coulomb excitation of Ba^{130}.

Since coincidence data are not yet complete, the energies of the first excited states are used to verify the existence of a new region of deformation. There are at least three ways to use the first-excited-state energy as a criterion for deformation. These are (a) a direct comparison between the energy of the first excited state and an $(E_{2+})_{crit}$, suggested by Alder et al.,[3] (b) a determination of an empirical deformation, β_{emp}, from a relationship between $\mathfrak{I}/\mathfrak{I}_{rig}$ and β,[4] and (c) a comparison of β_{Mig} from the relationship of Migdal.[5] These three methods are utilized in Table I, where comparisons are made with other nuclei with similar deformations but from other regions of deformation. A comparison of Ba^{126}, Ba^{128}, and Ba^{130} with other deformed nuclei indicates that Ba^{126} is like W^{186}, Os^{186}, and Ra^{224}. Thus all these nuclei have a first-excited-state energy less than $(E_{2+})_{crit}$ and have very similar β_{emp} (0.19 to 0.21) and β_{Mig} (0.15 to 0.18).

Similar statements apply to a comparison of Ba^{128} to Os^{188} and Ra^{222}. On the other hand, both Ba^{130} and Os^{190} seem to be in a transition region. Their first-excited-state energies are each higher than the $(E_{2+})_{crit}$, and each has $\beta_{emp} = 0.16$ and $\beta_{Mig} = 0.12$. Osmium-190 has a rotational band which cannot be fitted well with the simple $I(I+1)$ relationship, but is fitted by

[1] M. I. Kalkstein and J. M. Hollander, Phys. Rev. 96, 730 (1954).

[2] L. W. Fagg, Phys. Rev. 109, 100 (1958).

[3] K. Alder, A. Bohr, T. Huus, B. Mottelson, and A. Winther, Revs. Modern Phys. 28, 432 (1956).

[4] B. Elbek, in Proceedings of the International Conference on Nuclear Structure, Kingston, Canada, 1960, p. 601; N. K. Glendenning and J. Sawicki, UCRL-9178, May 1960. The parameter β_{emp} is an empirical relationship between $\mathfrak{I}/\mathfrak{I}_{rig}$ and β.

[5] A. B. Migdal, Nuclear Phys. 13, 655 (1959).

Table I. Comparisons between the nuclei Ba^{126}, Ba^{128}, and Ba^{130} and nuclei from other regions of deformation.

Nucleus	E_{2+}[a] (kev)	(E_{2+})crit.[b] (kev)	$\mathcal{J}/\mathcal{J}_{rig.}$[c]	$\beta_{emp.}$[d]	$\beta_{Mig.}$[e]	$\beta_{exp.}$[f]	Ratios of energies in the rotational band
Ba^{126}	256	279	0.251	0.20	0.16		
Ba^{128}	279	272	0.225	0.18	0.15		
Ba^{130}	356	265	0.172	0.16	0.12		
Gd^{154}	123	200	0.462	0.29	0.25	0.30	1.0:3.02:5.84
Dy^{156}	138	196	0.333	0.23	0.19		1.0:2.93:5.59
W^{186}	124	147	0.273	0.20	0.17	0.24	1.0:3.28
Os^{186}	137	147	0.247	0.19	0.15	0.20	1.0:3.19:6.33
Os^{188}	155	144	0.215	0.18	0.14	0.18	1.0:3.09
Os^{190}	188	142	0.174	0.16	0.12		1.0:2.93:5.60:8.89
Ra^{222}	111	110	0.228	0.19	0.15		1.0:2.79:5.78
Ra^{224}	84.5	108	0.295	0.21	0.18		1.0:2.98
Th^{226}	72.1	106	0.341	0.23	0.20		1.0:3.14:6.33

a. Throughout the table, energy values are taken from R. K. Sheline, Revs. Modern Phys. 32. 1 (1960) except the values for Ba^{126}, Ba^{128}, and Ba^{130} (reported herein) and Dy^{156} [see E. P. Gregorev and B. S. Dzhelepov, Doklady Akad. Nauk S.S.S.R. 135, 564 (1960)].

b. Values of $(E_{2+})_{crit} = 13 \hbar^2/\mathcal{J}_{rig}$ are given (see Ref.3). This $(E_{2+})_{crit}$ is the criterion by which nuclei may be assumed to be spherical [for $E_{2+} > (E_{2+})_{crit}$] or deformed [for $E_{2+} < (E_{2+})_{crit}$]. Often the transition is not as abrupt as indicated by the single value.

c. Ratio of $\mathcal{J} = 3\hbar/E_{2+}$ to $\mathcal{J}_{rig} = 2\ MAR_0^2/5(1+0.31\beta+\cdots)$ where $R_0 = 1.2 A^{1/3} \times 10^{-13}$ cm, $\beta = 1.08/A^{1/3}$, and MA is the mass of the nucleus.

d. See Ref. 4.

e. Values of β_{Mig} are determined from $\mathcal{J} = 2\ MAR_0^2/5(2.33\beta_{Mig} - 0.1)$ (see Ref. 5).

f. Experimental deformations calculated from the available values of the transition probabilities for Coulomb excitation.

the nonaxially symmetric rotator model of Davydov and Fillipov.[6] It seems probable that Ba^{130} would be similar in this regard.

Although the coincidence data are fragmentary, coincidences were found in each of the La nuclides. The ratio of the supposed second excited state varied from 2.55 in Ba^{130} to 3.13 in Ba^{126}. This agrees very well with the ratios of energies for the first to second excited states of the rotational band built on the ground state, which are given in Table I for similarly deformed nuclei. The coincidence data thus far available, then, strongly favor a rotational-band interpretation and seem inconsistent with a vibrational interpretation. However, none of the second-excited-state spins have been measured and proof of the existence of a rotational band must await a more detailed analysis of the decay schemes.

A characteristic low energy for the first excited states of even-even Ce nuclei has also been observed. However, in this case mass assignments and half lives of the Pr nuclides are not nearly as certain. This evidence does tend to indicate the existence of an extended region of deformation, however.

---

[6] A. S. Davydov and G. F. Fillipov, Nuclear Phys. **8**, 237 (1959).

13. AN ALPHA-EMITTING ISOMERIC STATE OF Tb^{149} (*)

Ronald D. Macfarlane

Bombardment of La^{139} targets with 80- to 140-Mev O^{16} ions has resulted in the identification of a new alpha activity decaying with a half life of $4.3 \pm .2$ min and having an α-particle energy of $3.99 \pm .03$ Mev. The activity was was assigned to an isotope of Tb on the basis of results obtained with $Ba + O^{16}$ bombardments. A recoil-milking experiment using the apparatus shown in Fig. A.13-1 showed that the 4.1-hr Tb^{149} was a daughter of the 4-min activity, indicating that it was due to an isomeric state of Tb^{149}. An alpha decay scheme summarizing the experimental results and possible single-particle states involved is shown in Fig. A.13-2.

Excitation functions for the isomer pair (Fig. A.13-3) showed an "isomer shift" of 18 Mev. This large shift may be related to the large amount of vibration-rotational energy associated with compound nuclei of high angular momentum in this region.[1]

---

[1] James F. Mollenauer, Effects of Angular Momentum on Gamma-Ray Production in Compound-Nucleus Reactions (Thesis), UCRL-9724, June 1961.
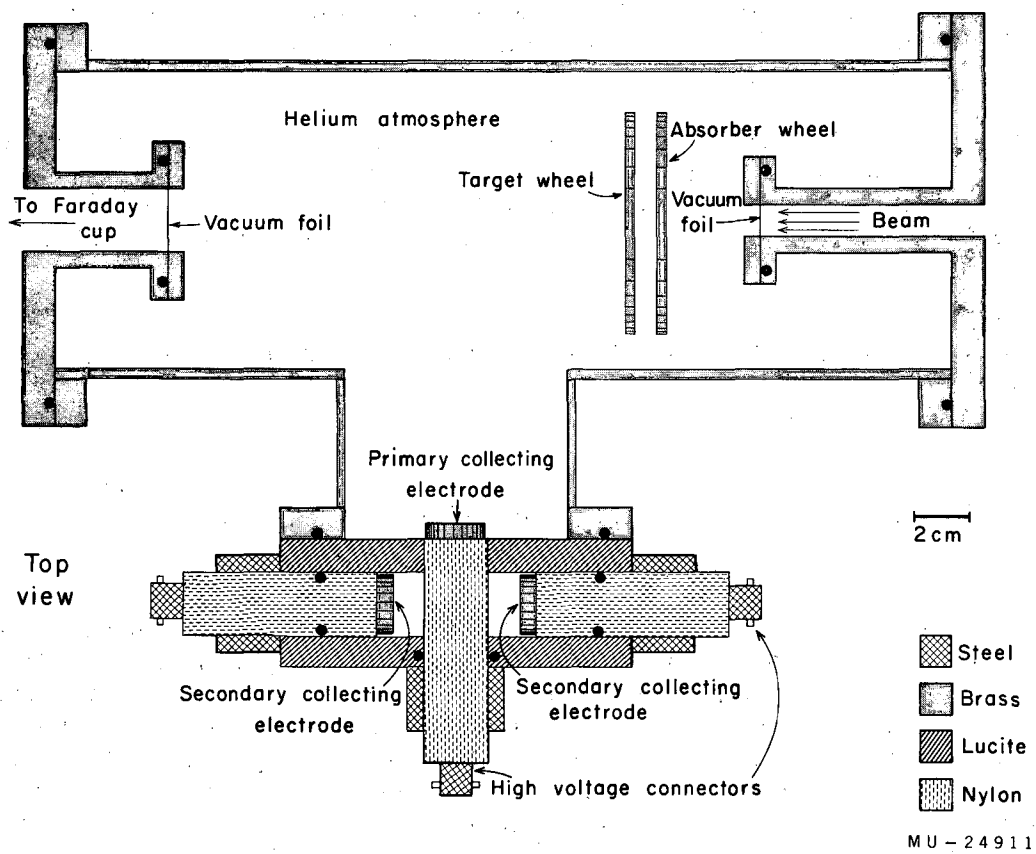
Fig.A.13-1.　Target chamber and "recoil-milking" apparatus.
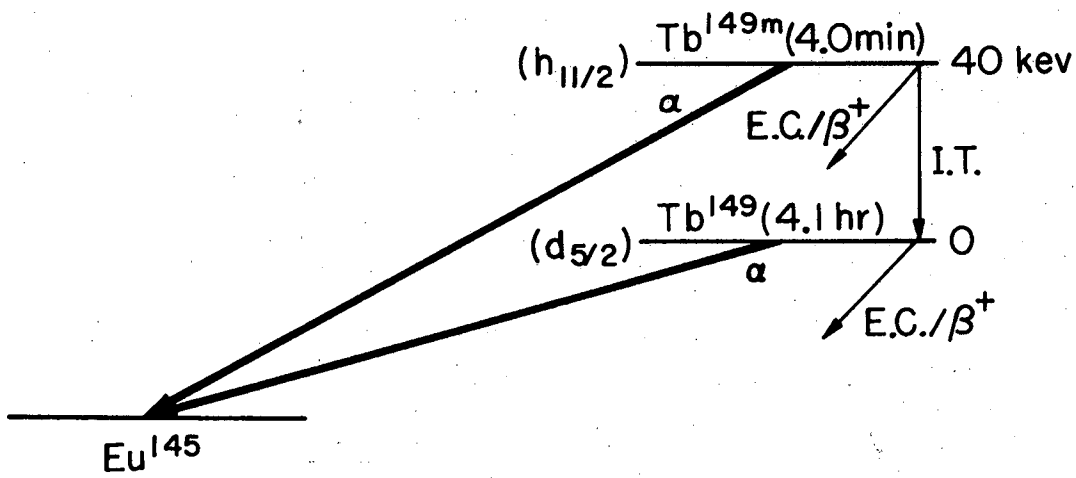
Fig. A. 13-2. Proposed alpha decay scheme of Tb^{149}.
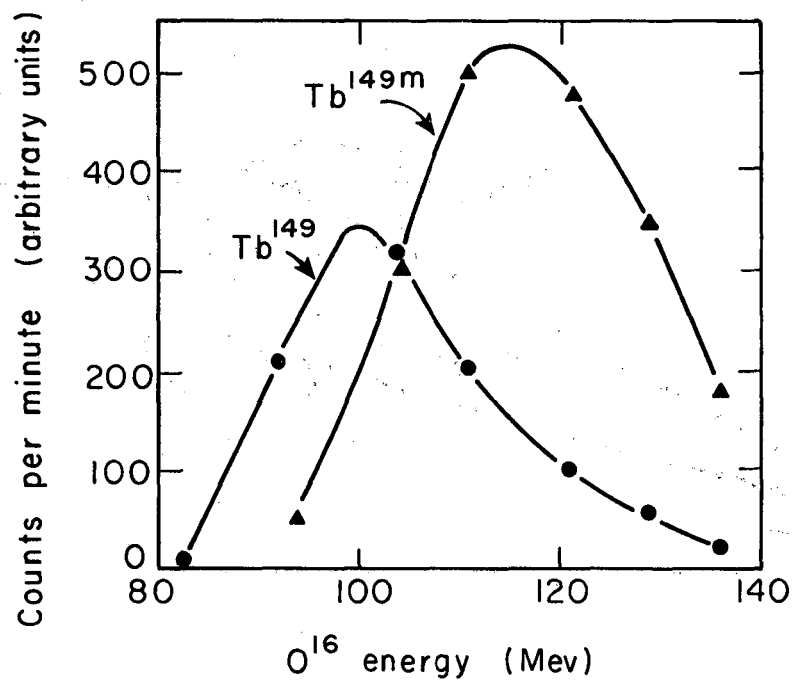
Fig. A.13-3. Excitation functions for Tb^{149} (●) and Tb^{149m} (▲).

14. NEUTRON-DEFICIENT ALPHA EMITTERS OF HOLMIUM

Ronald D. Macfarlane and Roger D. Griffioen

The alpha emitters of holmium previously reported[1] were re-investi-gated for the purpose of searching for alpha-emitting isomers which were found to occur in this region.[2] Analysis of the experimental results has resulted in identification of three new holmium alpha activities and a reinter-pretation of some of the previous results. Isomer pairs were identified for Ho^{151}, Ho^{152}, and Ho^{153}. Their alpha-decay properties are listed in the table. Excitation functions for the isomer pairs showed the same "isomer shift" as observed with the Tb^{149} isomer pair.

Alpha-decay properties of Ho^{151}, Ho^{152}, and Ho^{153}.

Isotope	E_α (Mev)	$t_{1/2}$ (total)	Remarks
Ho^{151}	4.58 ± .03	50 ± 5 sec	low spin
Ho^{151}	4.48 ± .03	36.7 ± .3 sec	high spin
Ho^{152}	4.41 ± .03	52.0 ± .5 sec	high spin
Ho^{152}	4.34 ± .03	142 ± 5 sec	low spin
Ho^{153}	4.00 ± .03	6.5 ± .5 min	high spin
Ho^{153}	3.90 ± .03	9 ± 1 min	low spin

[1] R. D. Macfarlane and R. D. Griffioen, Bull. Am. Phys. Soc. Ser II, 6, No. 3, 287 (1961).

[2] R. D. Macfarlane, Alpha-Emitting Isomeric State of Tb^{149} (UCRL-9870-Rev, Nov. 1961), submitted to Phys. Rev.

15. NEUTRON-DEFICIENT ALPHA EMITTERS OF ERBIUM [*]

Ronald D. Macfarlane and Roger D. Griffioen

By use of a new technique to facilitate the study of short-lived activities, three new alpha emitters of erbium were observed with $Nd^{142} + O^{16}$ bombard-ments using the Berkeley heavy-ion linear accelerator. The apparatus is shown in Fig. A.15-1. Activity is collected in helium in back of the target

[*] Bull. Am. Phys. Soc. Ser. II, 6, 451 (1961).
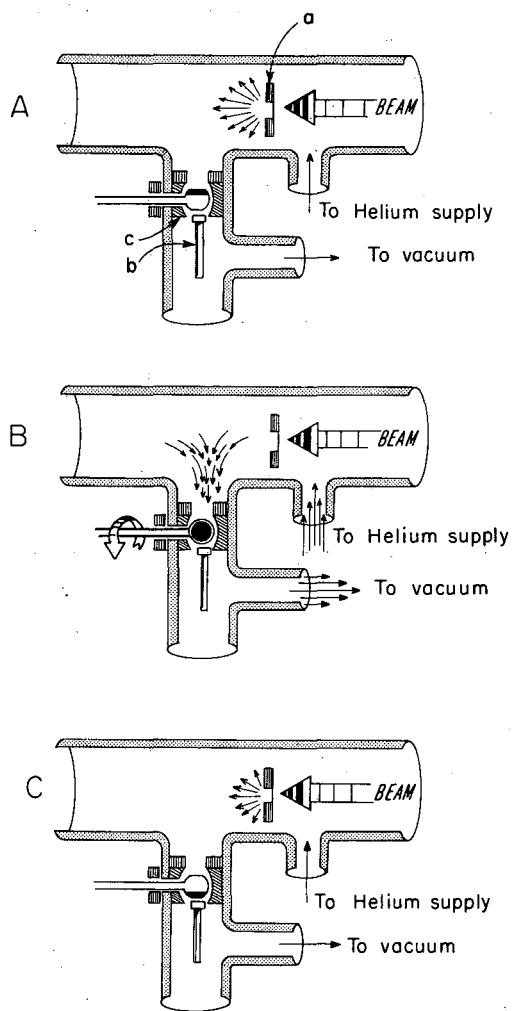
Fig. A. 15-1.   Target and recoil collection assembly for studying short-
    lived alpha emitters.   a = target, b = surface-barrier solid-state
    a-particle detector, c = collecting plate.

and pumped through a collimator onto a collection plate. The plate is then rotated a half-turn to a position in front of a surface-barrier α-particle detector in vacuum. Two of the activities were assigned to Er^{153} and Er^{154} from the identification of the alpha decay daughters Dy^{150} and Dy^{149}, and the third to Er^{152} from excitation function data. The results are summarized in the table.

Alpha decay properties of Er^{152}, Er^{153}, and Er^{154}

Isotope	E_α (Mev)	$t_{1/2}$
Er^{152}	4.78 ± .03	10.5 ± .2 sec
Er^{153}	4.68 ± .03	36.0 ± .3 sec
Er^{154}	4.15 ± .03	5.3 ± .5 min

16. ALPHA-DECAY STUDIES IN THE TRANSLEAD REGION [*]

Roger D. Griffioen and Ronald D. Macfarlane

By use of the apparatus described in the previous report on the erbium alpha activities, several new alpha-emitting isotopes of francium, radium, and actinium were observed in bombardments of Au, Hg, Tl, and Pb targets with B^{11}, C^{12}, N^{14}, and O^{16} ions from the Berkeley heavy-ion linear accelerator (Hilac). Mass assignments were made by identification of the alpha-decay daughter in many cases, and also by comparison of excitation functions with those of previously reported nuclides in this region. The results are summarized in the table below. Alpha decay energy systematics of the Fr alpha emitters show the same trend as has been observed with the corresponding Em isotopes (Fig. A.16-1.) Reduced width alpha decay probabilities for the Fr isotopes were calculated using the method of Rasmussen[1] and are shown in Fig. A.16-2 together with results for the corresponding Po isotopes which were calculated by Rasmussen.[1]

---

[*] Bull. Am. Phys. Soc. Ser II, 6, 451 (1961).

[1] J. O. Rasmussen, Phys. Rev. 113, 1593 (1959).
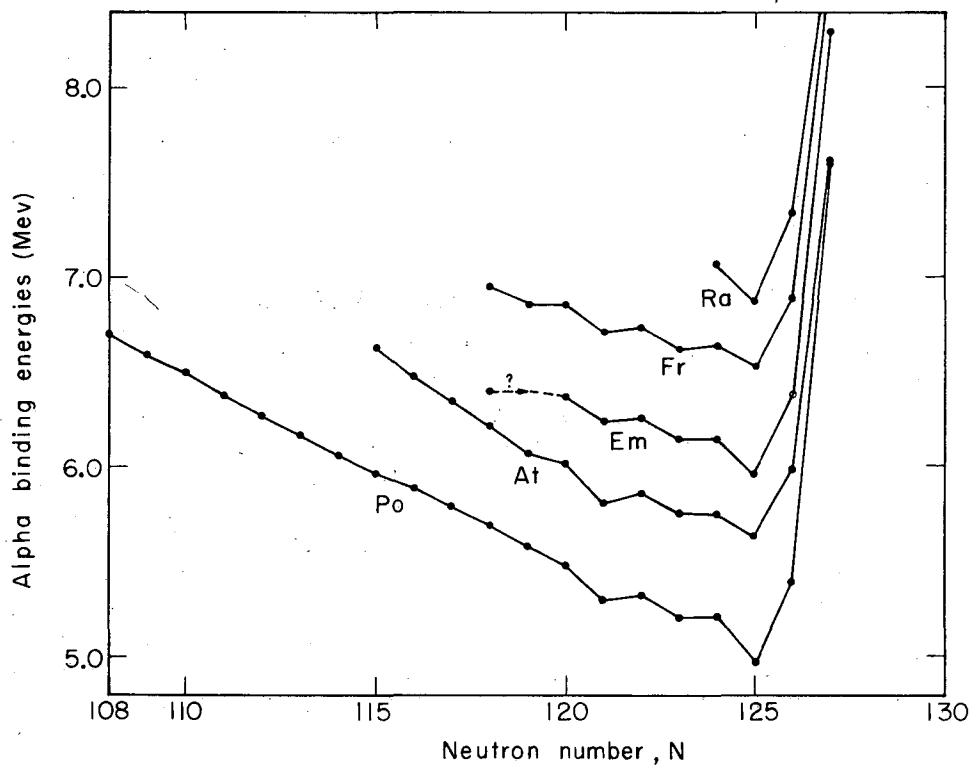
Fig. A.16-1. Alpha-decay systematics in the trans-lead region near the
    closed neutron shell of 126.

10^1

Reduced width, δ^2 (Mev)

10^2

10^3

10^4

• Francium
□ Polonium

118   120   122   124   126   128   130   132
Neutron number, N
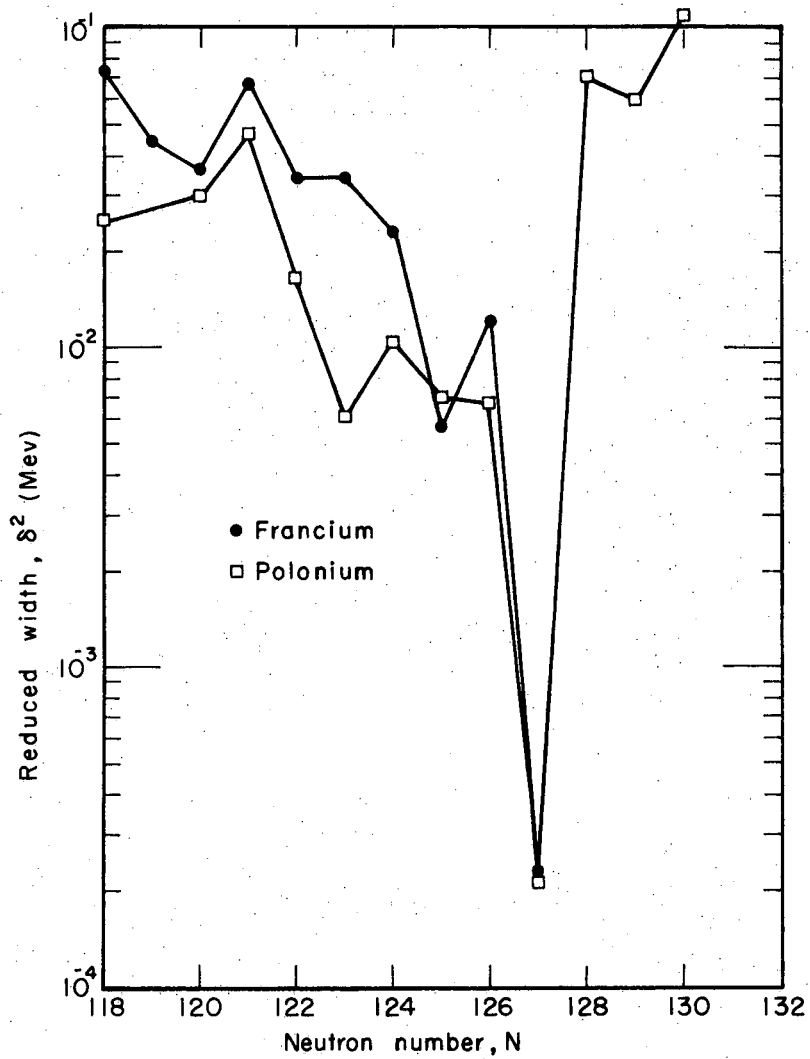
MU–24283

Fig. A. 16-2. Reduced-width alpha emission probabilities vs neutron
number for Fr and Po isotopes.

Alpha-decay properties of new Fr, Ra, and Ac isotopes

Isotope	E_α (Mev)	$t_{1/2}$ (sec)
Fr^{213}	6.77	34
Fr^{211}	6.52	186
Fr^{210}	6.50	159
Fr^{209}	6.62	54.7
Fr^{208}	6.59	37.5
Fr^{207}	6.74	18.7
Fr^{206}	6.74	15.8
Fr^{205} ?	6.83	≈ 4
Ra^{214}	7.17	2.6
Ra^{213}	6.74, 6.61	163
Ra^{212}	6.90	18
Ac^{214}	7.12, 7.18, 7.24	12
Ac^{213}	7.42	≈ 1

17. STUDY OF VERY-SHORT-LIVED ALPHA EMITTERS IN THE TRANSLEAD REGION

Roger D. Griffioen and Ronald D. Macfarlane

A technique was developed which allows for the study of alpha activities with half lives down to 0.1 msec and, at considerably reduced beam levels, down to half lives as short as approx 0.01 μsec. A target is bombarded with heavy ions in vacuum and recoils are collected on a thin Al foil (100 μg/cm^2) situated in back of the target. A surface-barrier solid-state α-particle detector measures the alpha activity of the recoils collected. At full beam intensity (≈ 400 mμa), measurements are made between beam bursts (approx 15/sec and approx 2 msec duration) because the detector is saturated during the time of the beam burst. At reduced beam levels (approx 5 mμa), the detector gives satisfactory α-particle analysis during the beam burst and is capable of detecting alpha activities whose half lives are in the vicinity of the flight time of the recoils from the target to the catcher.

With this technique, some new alpha emitters of Fr and Ra, were observed. The results are summarized in the table below.

Alpha-decay data of some short-lived translead nuclides

Isotope	E_α (Mev)	$t_{1/2}$
Fr^{214}	8.55	3.9 msec
Fr^{215}	~ 9.4	<< 1 msec
Ra^{217}	9.0	<< 1 msec
Ra^{216}	9.3	<< 1 msec
Ra^{215}	8.7	1.6 msec
Em^{213}	8.13	19 msec
At^{212}	7.47	0.22 sec

18. NEW ELEMENT, LAWRENCIUM, ATOMIC NUMBER 103 [*]

Albert Ghiorso, Torbjørn Sikkeland, Almon E. Larsh, and Robert M. Latimer

Bombardment of californium with boron ions have produced α-particle activity which can only be ascribed to decay of a new element with atomic number 103. This activity at best amounts to only a few alpha counts per hour ($\sigma \approx 1$ μb), so it has not yet been possible to detect the mendelevium decay product to prove further the atomic number of the new activity. For the present, attribution of this activity to element number 103 must rest entirely on nuclear rather then chemical evidence.

The method used to produce and identify radiations from element 103 decay is shown schematically in Fig. A.18-1 and is based on the one used for the element 102 experiment. [1] The 3-μg californium target has an isotopic composition at present of 3.3% 249, 32.8% 250, 12.3% 251, and 50.8% 252. [2] It was electroplated in an area 1.10 in. in diameter onto nickel foil 50 micro-inches thick. The purification of the target, crucially important for the success of the experiment, consisted in careful use of ion-exchange columns with specially purified reagents. The last step in the purging of undesirable lead and bismuth impurities was accomplished by heating the final target in vacuo by electron bombardment. Lead and bismuth impurities must be reduced because heavy-ion bombardment of these elements produces in high yield an alpha activity with an 8.8-Mev α-particle energy and a 25-sec half life which can obscure the lower-energy alpha activity of element 103. The heavy-ion beam of either B^{10} of B^{11} was collimated so as to pass through the tiny target, and typically was limited to 0.5 μa dc to avoid melting the target

---

[*] Phys. Rev. Letters 6, 473 (1961).

[1] A. Ghiorso, T. Sikkeland, J. R. Walton, and G. T. Seaborg, Phys. Rev. Letters 1, 18 (1958).

[2] We are indebted to M. C. Michel for the mass analysis.

DEGRADER FOILS

COLLIMATOR

FARADAY CUP

TARGET
-400 VOLTS

BEAM
ENERGY
MEASURING
SILICON
DETECTOR

MULTIPLE DETECTOR
SYSTEM
FOR SHORT-LIVED
ALPHA EMITTERS

HEAVY   ION   BEAM

DEGRADER FOILS

SILICON- GOLD ALPHA
DETECTORS

VACUUM

-150 VOLTS

PULLER

BRAKE NO. 2

HELIUM
ATMOSPHERIC
PRESSURE

SUPPLY REEL
COPPER TAPE
1" WIDE x 0.5 MIL " THICK

SUCTION

SUCTION

TAKE-UP REEL

BRAKE NO. 1
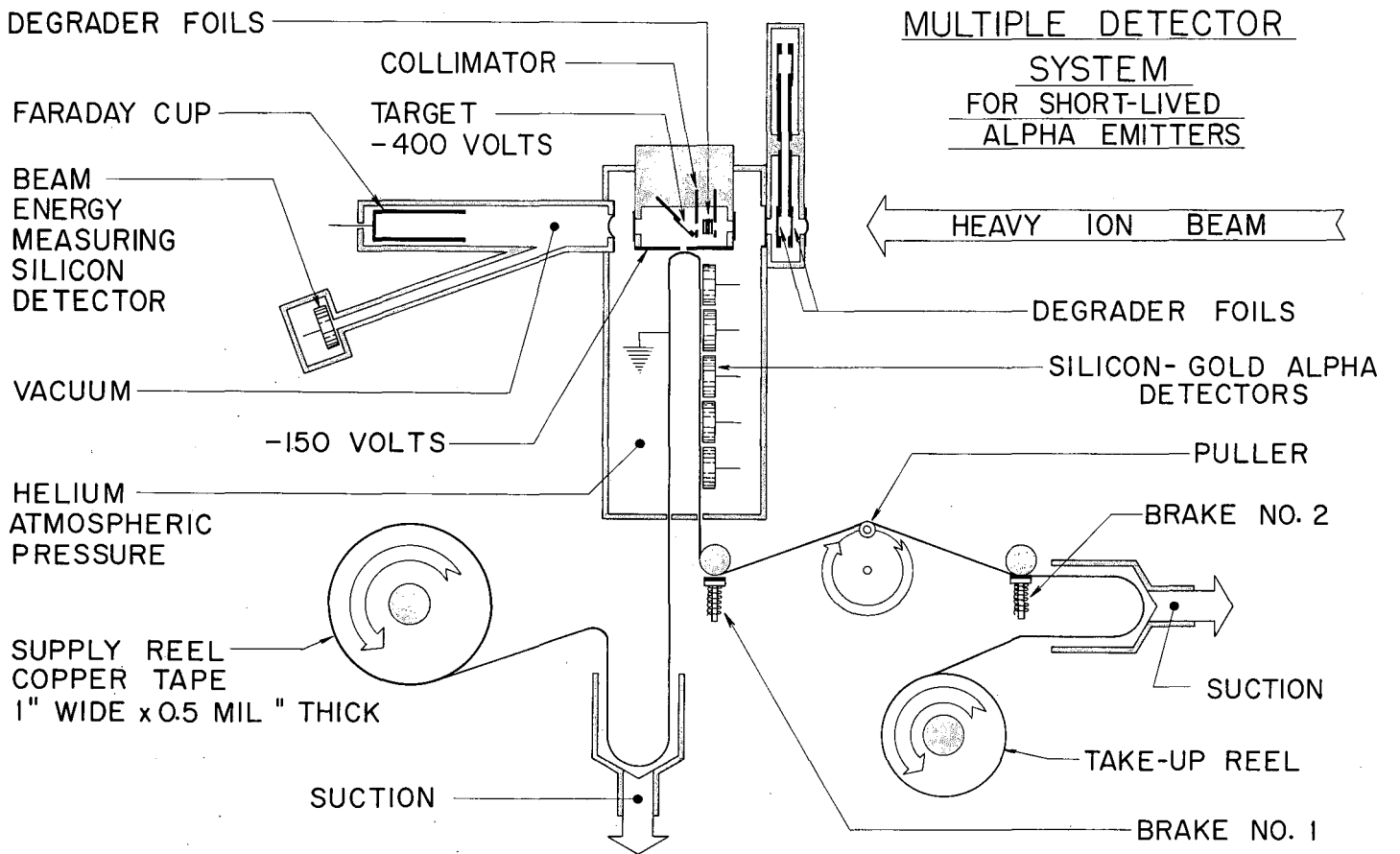
MUB-637

Fig. A. 18-1. Schematic diagram of apparatus.

foil. The transmuted atoms recoiled from the target into an atmosphere of helium. This gas flowed slowly through a nearby 0.050-in. orifice and carried the electrically charged transmutation products to a thin copper conveyor tape. This tape was periodically pulled a short distance to place the groups of collected atoms to positions successively in front of each of five solid-state Au-Si surface-barrier detectors. The pulses caused by passage of α particles into each detector were amplified, except for a few milliseconds during the beam bursts, by separate preamplifiers in the shielded bombardment area, and then sent to a main counting area to be further amplified and analyzed. In the counting area, the pulses were passed through separate window amplifiers and then analyzed by two separate electronic systems. One system consisted of five separate 100-channel pulse analyzers, and the other consisted of a multiplex unit using five punched paper tape storage units. With the multiplex unit, it was possible to determine the time when each event occurred, since the conveyor tape was last advanced.

The silicon crystal detectors vitally necessary for the experiment were brought to the authors' attention by C. J. Borkowski and J. L. Blankenship of the Oak Ridge National Laboratory. With their very kind help, it has been possible in our Laboratory to make silicon detectors suitable for these experiments. The present detectors are made of 800-1800 ohm-cm silicon, 6×10 mm, suitably etched and mounted, and are covered with a layer of gold about $20\,\mu g/cm^2$ thick. Initially, it was found that operation of these detectors was very erratic because of the helium atmosphere and the very intense beta radiation fields. The use of charge-sensitive preamplifiers reduced this effect, but it is still found that because of the circumstances of the experiment it is necessary to replace the crystal detectors occasionally.

The energy of the boron ions was changed by degradation of the 10.3-Mev/nucleon beam in aluminum absorbers. Because the beam is so intensely concentrated, it was found that the amount of energy loss in a given absorber could change with time. To monitor the energy of the ions striking the target, another Si detector was calibrated against nuclear emulsions, and used at a small solid angle to measure the energy of those ions scattered forward at $20°$ by the Faraday cup window.

Calibration and study of the total system without beam was accomplished with either U^{230} recoil products collected onto the tape or with Po^{212} α particles from samples held in front of the detector assembly. Studies of the method with heavy-ion reactions were made by bombarding Sm^{147} to produce short-lived holmium alpha emitters or Pb and Bi to produce various alpha emitters with energy between 7 and 9 Mev.

In the bombardment of Cf with B ions, the activity attributed to element 103 consists of α particles with an energy of 8.6 Mev decaying with a half life of 8 ± 2 sec. Also observed are α particles of 8.4 and 8.2 Mev with similar half lives of about 15 sec, which are probably due to element 102. Figure A.18-2 shows and α-particle spectrum from the first detector obtained during the most recent set of runs. These activities have been observed repeatedly during many weeks of bombardment of the californium target with both B^{10} and B^{11} ions. Similar bombardments of Pb, Bi, Pu^{240}, and Am^{241} do not produce the new activities.
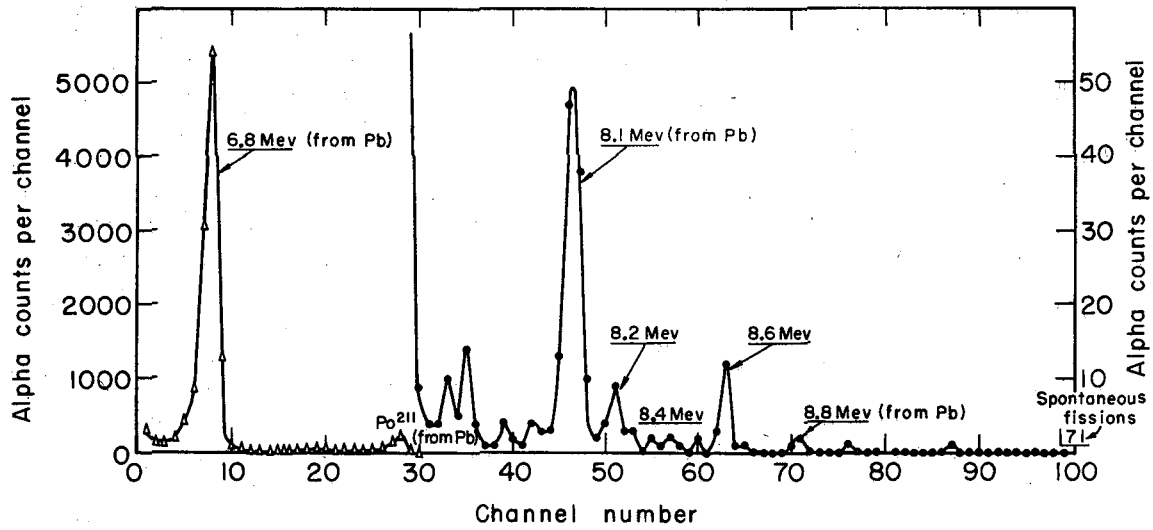
Fig. A.18-2. Cf + B^{11}. Alpha spectrum from first detector. Summation
of Runs Nos. 139-148. Total bombardment = 5.0 μa hr. Cycle time =
15 seconds.

The mass number of the element 103 isotope is thought to be 257 for the following reasons. B^{11} bombardments of Cf^{250}, Cf^{251}, and Cf^{252} cause compound-nucleus reactions which lead to 103^{257} by the emission of four, five, or six neutrons, while with B^{10} this same result is accomplished with three, four, or five neutrons. These are known from other experiments to be the most prominent neutron-out reactions of boron with the transuranium elements. Excitation functions with B^{11} and B^{10} ions for production of the 8.6-Mev alpha activity are consistent with the above deduction.

These excitation functions were, of necessity, very broad because the same activity could be produced by several reactions; consequently, these data could not rule out conclusively (B, pxn) reactions which would produce light isotopes of element 102. The final proof was then accomplished by accentuating the element 102 production by bombarding the californium target with C^{12} ions. It was found that the 8.6-Mev activity was decreased by a factor of more than 2, and the 8.2-Mev activity (thought to be mostly 102^{255}) was increased by a factor of about 20. This was to be expected for the element assignments given. Experiments with Pu^{240} had shown that the (C^{12}, axn) cross sections would be larger, while the (C^{12}, pxn) cross sections would be smaller, than in the boron bombardments of californium. Possible light isotopes of mendelevium that could be produced and conceivably might emit α particles in the 8.2- to 8.6-Mev region were ruled out by bombardments of Am^{243} with C^{12} ions.

In honor of the late Ernest O. Lawrence, we respectfully suggest that the new element be named lawrencium with the symbol Lw.

B. FISSION

1. STUDIES OF THE DISINTEGRATION OF U^{238} BY Gev PROTONS

John M. Alexander, C. Baltzinger, and M. F. Gazdik

Nuclear fission is not very well understood, even for fissile nuclei of very low excitation energy. Quite a large body of experimental data is available for these very low excitation energies. However, very little information is available concerning breakup of very highly excited nuclei. Photographic emulsion studies have sketched out some of the recoil properties of high-energy fission, and radiochemical studies have elucidated some of the yield patterns.[1,2] Recently radiochemical recoil techniques have proved very useful in probing the nature of the disintegrations induced by high-energy irradiation.[3,4]

We have made a number of cross section and recoil measurements for U^{238} breakup by 0.7- to 6.2-Bev protons. An interesting feature of the cross-section data is shown in Fig. B.1-1. The yield pattern for the isotopes of iodine seems to show a twofold grouping for the Gev energies. This suggests that possibly two rather different processes may be operative.

Further information has been obtained by integral recoil range measurements. In order to analyze the recoil experiments we have assumed a two-step process: (a) a fast cascade stage resulting in a component of velocity v along the beam direction, (b) a slow process resulting in an isotropic velocity component, V. The velocity v has been used to infer the average deposition energy in step (a).[5] The velocity V has been converted to kinetic energy, E and compared with the Coulomb energy from two charged spheres, E_{coul}.

Figure B.1-2 shows a summary of these properties for several of the products studied. For the neutron-rich products Mo^{99}, Ag^{111}, and I^{133} the average deposition energy and kinetic energy are relatively insensitive to bombarding energy. Thus the fission process is not strongly affected by bombarding energy. However, for neutron-deficient I^{123} the value of E/E_{coul} changes markedly between 0.7 and 3 Gev. Evidently the nature of these

[1] J. M. Miller and J. Hudis, Ann. Rev. Nuclear Sci. 9, 159 (1959).

[2] N. A. Perfilov, O. V. Lozhkin, and V. P. Shamor, Soviet Phys. Uspekhi 3(60), 1 (1960).

[3] N. Sugarman, M. Campos, and K. Wielgoz, Phys. Rev. 101, 388 (1956).

[4] V. Crespo, Ejection of Large Fragments in High-Energy Nuclear Reactions, UCRL-9683, Sept. 1961.

[5] N. T. Porile, Phys. Rev. 120, 572 (1960).
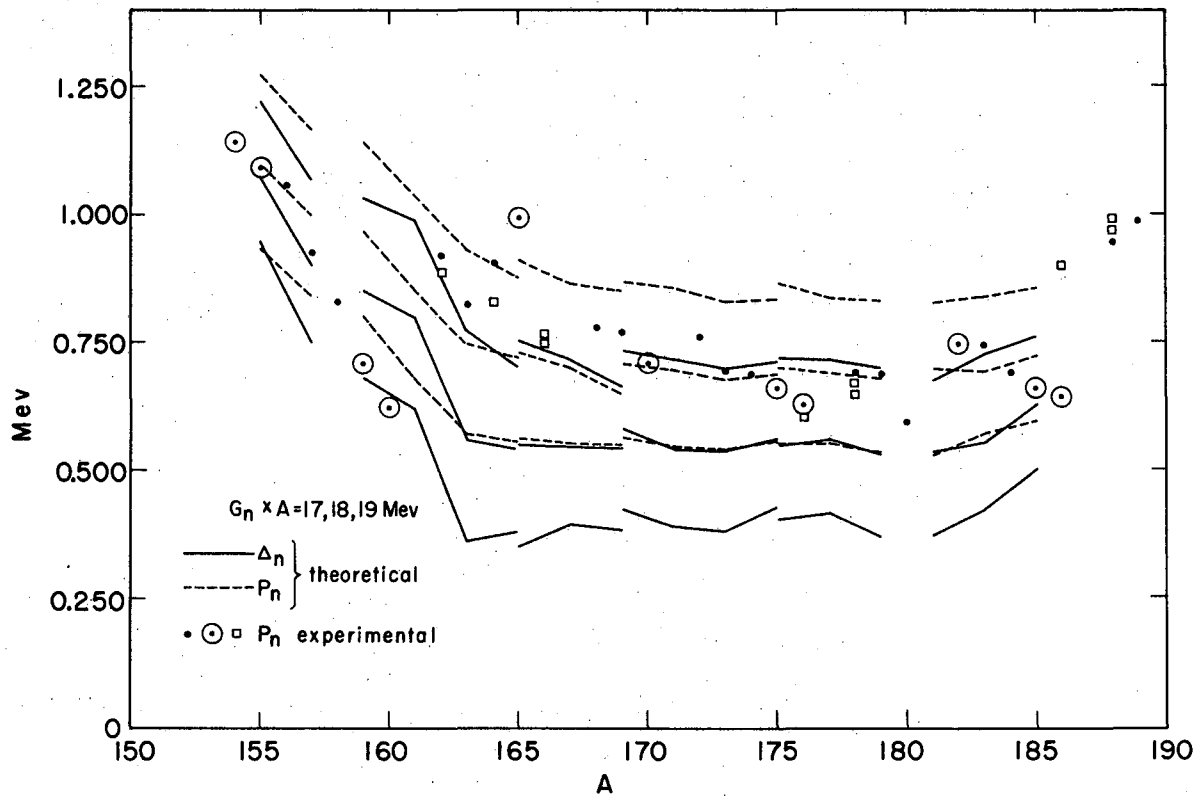
Fig. B. 1-1. Independent cross section versus mass number for iodine
    products.

MU-23280
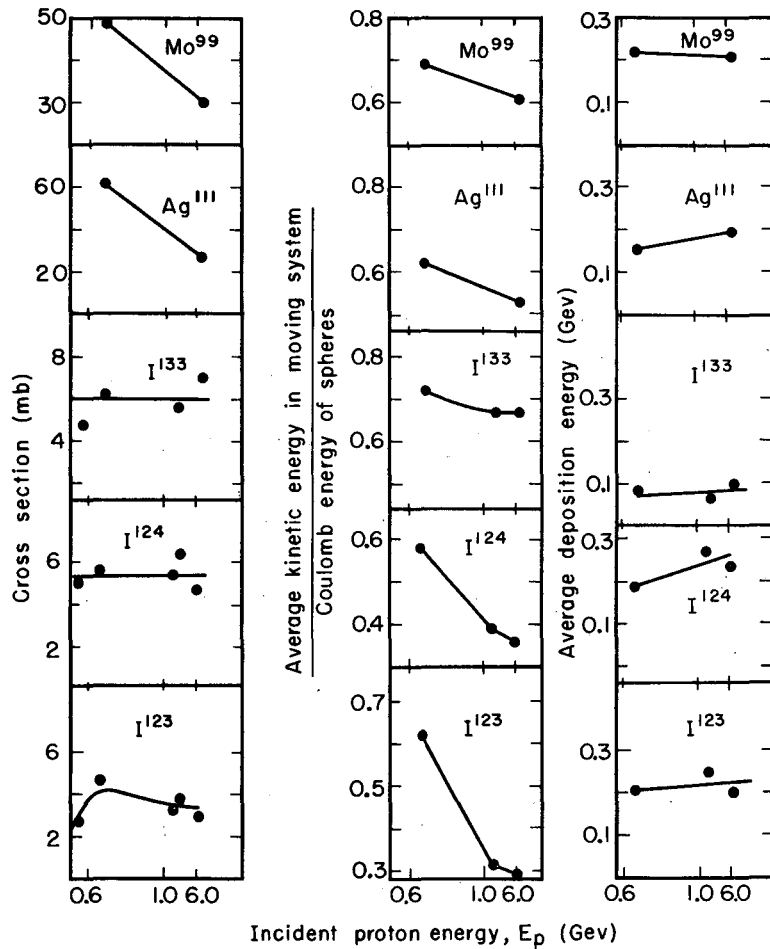
Fig. B. 1-2. Cross section, reduced kinetic energy, and average deposition energy for various products from reactions of protons with U^{238}.

disintegrations is very dependent on incident energy. It is interesting that the apparent deposition energy for I^{123} and I^{124} is only about 200 Mev, and that it is rather insensitive to bombarding energy. We find it difficult to reconcile the apparent constancy of deposition energy with the marked change in kinetic energy. This suggests a major breakdown of the concept of a two-stage reaction.

2. THE DECAY OF THE HEAVIEST NUCLEI

Sven Johansson

In previous work and attempt was made to correlate the spontaneous fission rates with the properties of the single-particle levels in a deformed potential.[1] It turned out that it was possible to account fairly well for the variations in spontaneous fission rates. An attempt has now been made to predict the spontaneous fission rates for heavy, unknown nuclei in this way. In one sense the heavy nuclei are better suited for a calculation of this type since the saddle-point shapes are less elongated than for lighter nuclei. Hence it is not necessary to extrapolate the level diagram to great deformations. On the other hand, there will arise an uncertainty in the position of the levels, since the experimental information about the decay of the heaviest nuclei is very meager. Recently, however, workers at this Laboratory have gained information about the neutron levels above $N = 152$.[2]

The simplest case is the odd-neutron nuclei. It is well known that the hindrance for this type of nuclei compared to neighboring even-even nuclei can be accounted for by the fact that the odd neutron has to stay in its original level in order to conserve spin and parity. If one knows what level the odd neutron occupies, the hindrance factor can be calculated without taking into account the rest of the level diagram. The hindrance factor has been calculated for several odd Cf and Fm isotopes. It has a mean value of about 3.5 but the spread is considerable. An experimental verification was possible for Fm^{255}, for which the half life recently was determined[3] as 1.2×10^4 years. The calculated value is 2×10^4 years.

The odd-proton nuclei should in the first approximation behave in the same way as the odd-neutron nuclei. A comparison with experimental values shows, however, that the hindrance factor is somewhat larger than calculated. This might be explained by the fact that the charge distribution of the extra proton is not in general the same as the distribution of the whole nucleus. A study of the wave function of the odd proton in the few cases for which a comparison is possible shows that this effect goes in the right direction to explain the deviation from the experimental values. However, more experimental data are needed in order to settle this question.

[1] Sven A. E. Johansson, Nuclear Phys. 12, 449 (1959).

[2] Frank Asaro (Lawrence Radiation Laboratory) private communication.

[3] Reinhard Brandt (Lawrence Radiation Laboratory), private communication.

The situation for the even-even nuclei is more complicated, since the properties of many levels enter into the calculation. For the addition of two neutrons it is known that just above N = 152 the half life drops sharply, contrary to what one should expect from the drop model. A study of the level diagram shows, however, that this trend cannot continue. Already for N = 158 to 160 the half lives are expected to stop decreasing. The calculated values are rather uncertain, since they depend on the position of the levels from the N = 8 shell and they are not known experimentally. The fact that a major neutron shell is closed at N = 184 indicates also that the addition of two neutrons eventually will result in an increase of the spontaneous fission half-life, since the fission barrier is known to be high for nuclei in the neighborhood of magic numbers.

The effect of adding two protons depends critically on the position of the steeply sloping levels from the N = 6 and 7 shells, and these positions are not known experimentally for the proton-level diagram. A straightforward calculation using the theoretical position gave the interesting result that the spontaneous fission half-life for nuclei with $Z \geqslant 102$ is quite short. It is very important that the half life for 102^{254} recently has been experimentally determined at this Laboratory to be 6 sec.[4] The calculated value is 10 sec. Even if the close agreement is fortuitous, the calculation seems to give values of the right order of magnitude. For 104^{256} the calculated value is 10^{-4} sec. The situation for nuclei with Z just above 100 is quite analogous to the situation for nuclei with N just above 152.

Finally odd-odd nuclei have been studied. The only nucleus for which an experimental value is known is E^{254}. The calculated hindrance factor is much too large. This indicates that it is necessary to take into account the possibility that the coupling between the odd neutron and the odd proton makes it possible for the two nucleons to jump in the level diagram with the total spin and parity conserved. This is important, since it is often assumed that the odd-odd nuclei have a large hindrance factor. This is not necessarily the case, but for a study of this special problem more experimental data are needed.

In summary, it can be predicted that for A = 102 the longest-lived isotopes will be the ones having A = 251, 253, 254, and 255. It is uncertain if there are any more having half lives longer than 1 to 10 sec. For A = 103 several isotopes should have half lives long enough to be produced. For Z = 104 only the isotopes with A = 255 and 257 are expected to have half lives longer than 1 sec. For Z = 105 the longest-lived isotopes are expected to occur around A = 257, but it is rather uncertain if the half lives will exceed 1 sec. For elements with $Z \geqslant 106$ the spontaneous fission half life is expected to be considerably below 1 sec for all isotopes. It must be kept in mind that all these predictions are based on a theoretical extrapolation of the level diagram to high nucleon numbers and that any deviation from the theoretical values might influence the decay rate considerably. The general trend should not be changed, however.

---

[4] Torbjørn Sikkeland (Lawrence Radiation Laboratory), private communication.

A study has also been made of the masses of the heaviest elements. Previously a correlation was found between the nuclear mass and deformation.[5] This makes it possible to develop a mass formula for deformed nuclei which can be used to predict the mass if the deformation is known. The mean error is about 200 kev. The heavy elements (Z > 94) are probably deformed, but the value of the deformation parameter is not known experimentally. It can be calculated with fairly good accuracy. By use of these values the masses, α-decay energies, β-decay energies, and neutron and proton binding energies have been calculated for a great number of nuclei with Z values up to and including 106. The mass values obtained here are somewhat lower than in previous predictions.[6] The α energies are also lower. This should make the α half lives longer than previously estimated.

---

[5] Sven A. E. Johansson, to be published.

[6] B. M. Foreman and G. T. Seaborg, J. Inorg. Nucl. Chem. 7, 305 (1958).

3. MOMENTS OF INERTIA OF SADDLE-POINT SHAPES OF UNIFORMLY CHARGED LIQUID DROPS

F. Plasil

Recent developments in the liquid-drop theory of nuclear fission indicate the existence of two distinct families of equilibrium shapes. The first family describes the region of elements lighter than radium and has physical shapes resembling those of a dumbell connected by a relatively narrow neck, while the second, representing elements heavier than radium, has shapes resembling more those of a distorted cigar. This difference in physical shapes was expected to be reflected in the moments of inertia of the saddle-point configurations. It was further expected that the calculations would indicate which of the experiments that are in one way or another dependent upon the moment of inertia of saddle-point shape would prove useful for comparison with the liquid-drop theory.

Calculations

The shapes of axially symmetric distorted drops are conveniently represented in polar coordinates by a radius vector $R(\theta)$ given in terms of a polynomial expansion of the type

$$R(\theta) = \frac{R_0}{\lambda} \left[1 + \sum_{n=1} a_n P_n (\cos \theta) \right] ,$$

where R_0 = radius of undistorted sphere,

$P_n (\cos \theta)$ = Legendre polynomial of order n,

λ = normalization constant maintaining constancy of volume upon distortion.

Thus a set of the coefficients a_n specifies the shape of the distorted drop (Fig. B.3-1). Swiatecki and Cohen[1,2] have calculated values of a_n (where n = 2, 4, 6, 8, 10) corresponding to symmetric saddle-point shapes. These a values were used in the moment-of-inertia calculations.
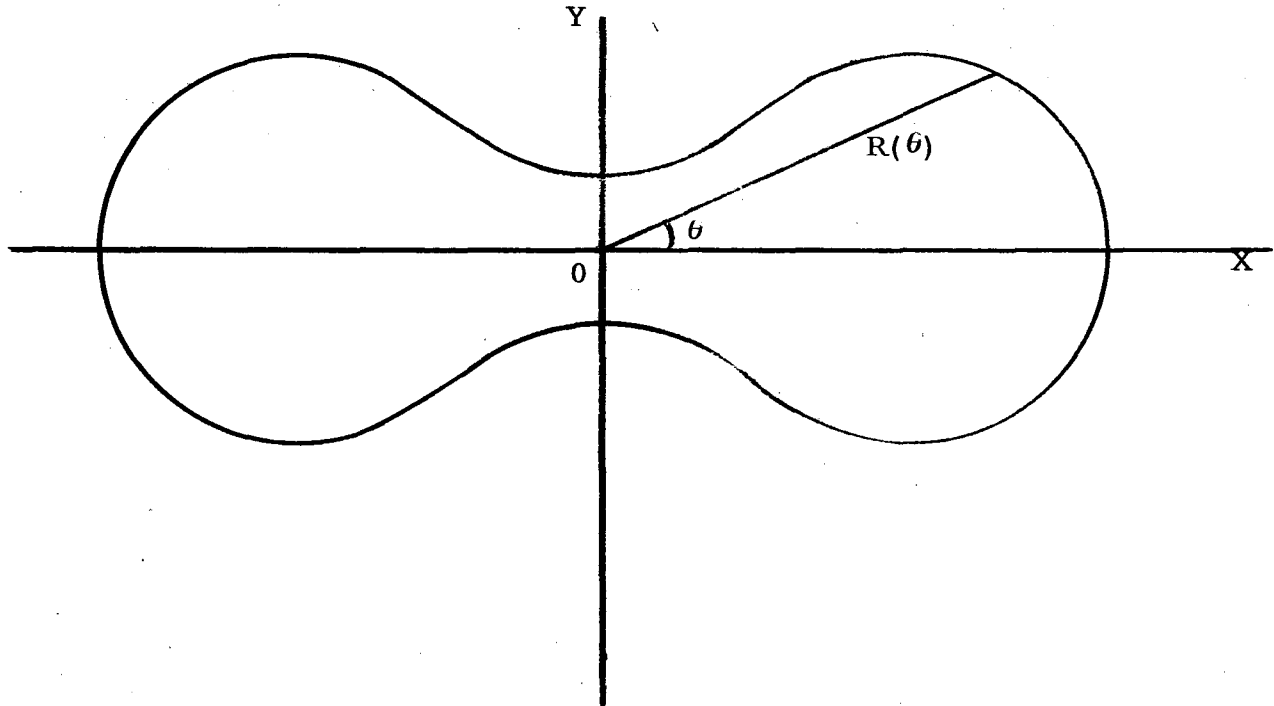
Fig. B.3-1. Distorted liquid drop, cylindrically symmetric about OX axis.

A volume element within the figure is given in polar coordinates by $dV = r^2 \sin\theta\, d\theta\, d\phi\, dr$. Thus the volume of the figure is

$$V_s = \int_0^{\pi} \int_0^{2\pi} \int_0^{R(\theta)} r^2 \sin\theta\, d\theta\, d\phi\, dr$$

$$= \frac{2\pi}{3} \int_0^{\pi} \left[R(\theta) \right]^3 \sin\theta\, d\theta,$$

where

$$R(\theta) = R_0 \left[1 + \sum_{n=1} a_n P_n(\cos\theta) \right].$$

---

[1] W. J. Swiatecki and S. Cohen, Report of Det fysiske institut, Aarhus Universitet, Jan. 1961.

[2] W. J. Swiatecki and S. Cohen, unpublished results.

The normalization constant λ is therefore given by $\lambda = (V_s/V_0)^{1/3}$, where V_0 is the volume of the undistorted sphere; λ is thus available upon the numerical integration of V_s.

The distance of an arbitrary volume element from the OY axis is given by $r(\cos^2\theta + \sin^2\theta \sin^2\phi)^{1/2}$, and upon performing the integrals over ϕ and r, the moment of inertia about the OY axis is given by

$$\mathcal{J}_\perp = \frac{2\pi}{5} \int_0^\pi \left[R(\theta)\right]^5 \sin\theta(1 + \cos^2\theta)\, d\theta \quad.$$

Similarly, moment of inertia about OX axis is given by

$$\mathcal{J}_{||} = \frac{2\pi}{5} \int_0^\pi \left[R(\theta)\right]^5 \sin^3\theta\, d\theta.$$

In cases of asymmetric saddle shapes, the moment of inertia about the center of mass, $\mathcal{J}_{c.m.}$, is of greater interest than $\mathcal{J}_\perp$, which is that about an axis through the origin of the polynomial expansion. $\mathcal{J}_{c.m.}$ is evaluated from the parallel-axis theorem

$$\mathcal{J}_{c.m.} = \mathcal{J}_\perp - D^2 V_0 \quad,$$

where D^2 is the distance of the center of mass from the origin, and is given by

$$V_0 D = \frac{\pi}{2} \int_0^\pi \left[R(\theta)\right]^4 \cos\theta \sin\theta\, d\theta.$$

Owing to the complexity of the $r(\theta)$ expression, numerical integration was used to evaluate the integrals V_s, $\mathcal{J}_\perp$, $\mathcal{J}_{||}$, and D. An IBM 709 program was developed to carry out the integrations for any variable number of a's, and for any number of grid points. The program also gives $\mathcal{J}_{eff}$ defined by

$$\frac{1}{\mathcal{J}_{eff}} = \frac{1}{\mathcal{J}_{||}} - \frac{1}{\mathcal{J}_\perp} \quad.$$

Results are given as a dimensionless ratio of the moment of inertia of a distorted drop to the moment of inertia, $\mathcal{J}_0$, of a sphere of equal volume. The results for even a_n (for $n = 2$, 4, 6, 8, 10) are shown in Fig. B.3-2 as a function of X. $X = (Z^2/A)/(Z^2/A)_0$, where $(Z^2/A)_0$ is a limiting value at which the spherical nucleus loses stability against a small deformation. Accuracy of numerical integration was checked by using analytical expressions such as spheroids and tangent spheres. Integration was accurate to more than one part in 10^4 for a grid of 75 points. There is, however, still a little uncertainty for values of X below 0.7 because the a values of Swiatecki and Cohen may not be final.
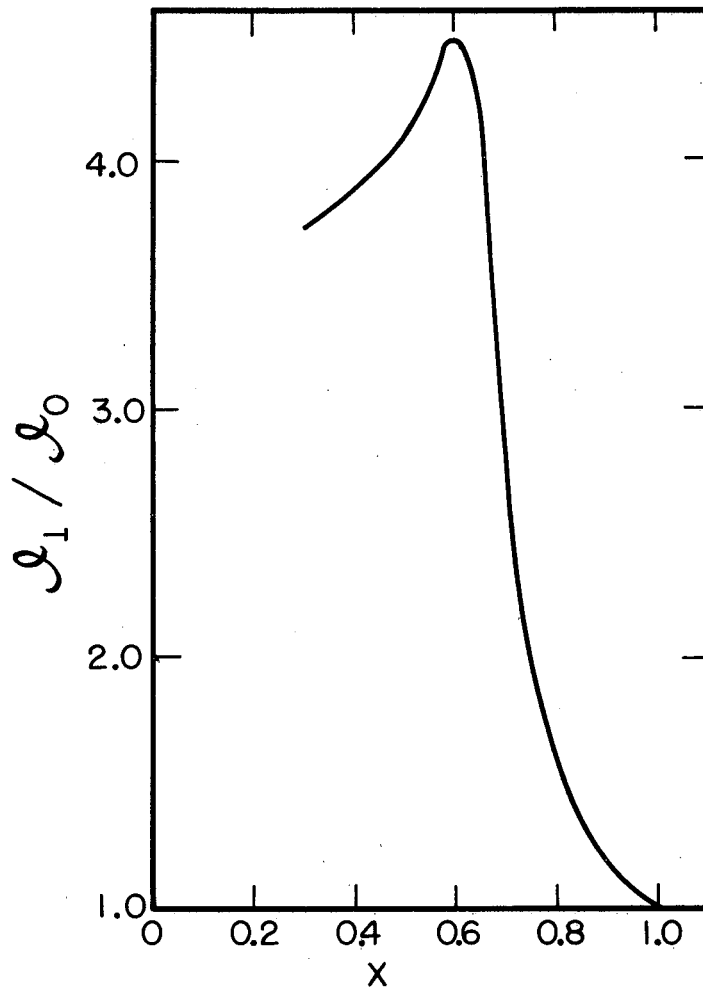
MU-25983

Fig. B.3-2. Moments of inertia of symmetric saddle-point shapes of
uniformly charged liquid drops as a function of X.

Discussion

The peak in Fig. B.3-2 represents the transition from one family of equilibrium shapes to another, and corresponds to about the region of gold. The rapid decrease in the moment of inertia is in accordance with the physical shapes of the two distinct families. This is easily seen upon comparison of the moment of inertia of a dumbbell with that of a spheroid of equal volume. The fact that in the region of elements lighter than gold the saddle-point shapes resemble two fragments connected by a relatively narrow neck would seem to indicate that the body of experimental data in this region would lend itself to easier theoretical interpretation. This follows from the fact that the saddle-point shape closely resembles the fissioning shape. Thus it would be of value to confirm the sudden drop in the moment of inertia experimentally. Among the experiments involving moments of inertia of nuclei at the saddle point are heavy-ion reactions, in which a large amount of angular momentum is brought in by the projectile. In particular, angular distributions of fission fragments and cross-section measurements could be sufficiently sensitive and dependent on the moments of inertia to show up this rapid variation with X.

For angular distributions the experimental results, according to Halpern and Strutinski,[3] are dependent upon $\mathscr{I}_{eff}$, i.e., upon $\mathscr{I}_\perp$ and $\mathscr{I}_\parallel$. With a change in $\mathscr{I}_\perp$ there is associated a corresponding change in $\mathscr{I}_\parallel$. Calculations indicate that these two effects work in opposite directions and tend to cancel. Thus $\mathscr{I}_{eff}$ does not seem to vary rapidly enough with X to enable experimental determination.

The case of cross sections is, however, more encouraging. The effect of the large angular momentum, for example, is such as to make a certain amount of excitation energy take the form of rotational energy of the nucleus at the saddle.[4] The magnitude of this rotational energy, to the first approximation, depends only upon $\mathscr{I}_\perp$. Re-examination of existing data[5] on heavy-ion reactions may prove of value.

---

[3] Halpern and Strutinski, in Proceedings of the Second International Conference on the Peaceful Uses of Atomic Energy, Geneva, 1958 (United Nations, New York, 1959), Vol. 15, Paper P/1513.

[4] Halpern, Ann. Rev. Nuclear Sci. 9, 245 (1959).

[5] John Gilmore, The Effects of Angular Momentum on Fission Probability (Thesis), UCRL-9304, July 1960.

4. SPONTANEOUS FISSION OF CERTAIN CALIFORNIUM, EINSTEINIUM, AND FERMIUM ISOTOPES

R. Brandt, R. C. Gatti, L. Phillips, and S. G. Thompson

Summary

Relatively large amounts of short-lived fermium, einsteinium, and californium isotopes were made available by the recent chemical processing of the curium isotopes re-irradiated at the MTR. This has made it possible to measure the energies of fission fragments for the isotopes Fm^{254}, E^{253}, and Cf^{254}. The energies of the two fragments of each fission event are measured in coincidence by using two solid-state detectors. The fragment energy spectra of these isotopes are reported in this paper. Data processing on the IBM 709 computer is in progress to obtain the mass-yield curve and the distribution of the total kinetic energy release for each isotope.

In addition, the spontaneous fission half life of Fm^{255} was measured and the electron-capture branching ratio of metastable E^{254} has been re-measured.

Experimental Procedures

The isotopes were purified by using standard chemical procedures.[1] Very thin samples of the isotopes were prepared by electroplating on thin nickel foils (110 $\mu g/cm^2$). A small drop of saturated NH_4Cl containing the heavy isotopes in solution was placed on the thin nickel foil, which was held between two steel rings. A 25-mil platinum wire was used for the anode. After electroplating for 15 minutes at a potential difference of 3.4 volts, a small droplet of concentrated NH_4OH was added to the plating solution to prevent the dissolution of the deposit. The thin nickel foil was washed by dipping it into a beaker containing a very weak ammonia solution. The electroplating yields varied between 50% and 90%.

The thin source was mounted in vacuo between two thin-phosphorus-diffused silicon guard-ring detectors,[2] which were used to measure the energies of the fission fragments. The electronic instrumentation was essentially standard equipment which records the energies of the two coincident fission fragments on paper tape. The isotope Cf^{252} was used for energy calibration.[3] In the reported fission-fragment energy spectra there is a

---

[1] S. G. Thompson and M. L. Muga, in Proceedings of the Second International Conference on the Peaceful Uses of Atomic Energy, Geneva, 1958 (United Nations, New York, 1959), Paper P/825.

[2] Fred S. Goulding and William L. Hansen, Leakage Current in Semiconductor Junction Radiation Detectors and Its Influence on Energy-Resolution Characteristics, UCRL-9436, Nov. 18, 1961.

[3] J. C. D. Milton and J. S. Fraser, Phys. Rev. 111, 877 (1958).

Cf^{252} contamination of less than 1% which was caused by contamination of the crystal surface during calibration measurements due to the self-transfer of Cf^{252}.[4] The production of the isotopes is

$$E^{255} \xrightarrow{\;\beta^-\;} Fm^{255} \qquad \text{(milking)}, \tag{1}$$

$$Cf^{253} \xrightarrow{\;\beta^-\;} E^{253} \qquad \text{(milking)}, \tag{2}$$

$$E^{253}(n,\gamma)E^{254\,m} \quad \text{(MTR with a flux of } 3\times10^{14}\text{) (units)}, \tag{3}$$

$$E^{254} \Big\langle \begin{array}{l} \xrightarrow{\;\beta^-\;} Fm^{254} \\[4pt] \xrightarrow[\text{E.C.}]{} Cf^{254} \end{array} \qquad \text{(milking)}. \tag{4}$$
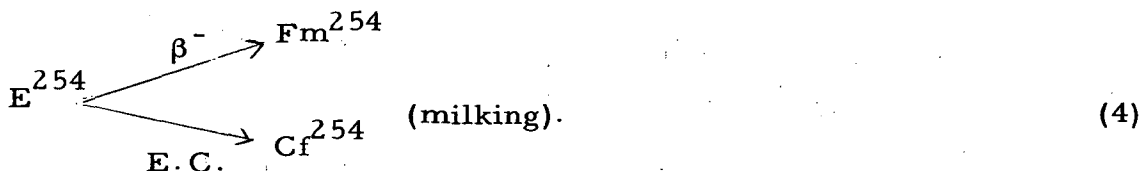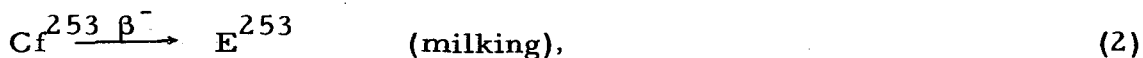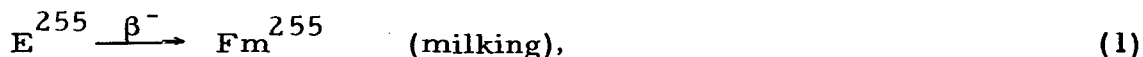
Results

1. The fission-fragment energy spectra of Fm^{254}, E^{253}, and Cf^{254} are shown in Fig. B.4-1. The Cf^{252} standard is included for comparison.
2. The new value for the EC/β^- decay branching ratio is $(0.078 \pm .006)\%$.[5]
3. The Spontaneous fission half life of Fm^{255} on the basis of 38 ± 12 observed fission events is $1.2^{+0.6}_{-0.3} \times 10^4$ years. This half life was calculated by using a value of 21.5 hours for the alpha-decay half life.[6] The fission activity was observed to decay with approximately a 21.5-hour half life.

---

[4] Raymond C. Gatti, Llad Phillips, Harry R. Bowman, and Stanley G. Thompson, in Chemistry Division Annual Report, UCRL-9566, Feb. 1960, p. 184.

[5] B. G. Harvey, S. G. Thompson, G. R. Choppin, and A. Ghiorso, Phys. Rev. 99, 337 (1955).

[6] M. Jones, R. P. Schumann, J. P. Butler, G. Cowper, T. A. Eastwood, and H. G. Jackson, Phys. Rev. 102, 203 (1956).

5. TOTAL FISSION CROSS SECTIONS FOR U^{238}

Torbjørn Sikkeland and Vic Viola, Jr.

The fission excitation functions for bombardment of U^{238} with He^4, B^{11}, C^{12}, N^{14}, O^{16}, and Ne^{20} ions have been measured at energies of 10.4 Mev/nucleon and below. Because of the extremely low fission barriers for the compound nuclei formed in these reactions, nearly all reactions proceeding by both compound-nucleus and direct-interaction mechanisms lead to fission. Studies of spallation products from such reactions[1,2] have shown that these

---

[1] T. Sikkeland, S. G. Thompson, and A. Ghiorso, Phys. 112, 543 (1958).

[2] A. Ghiorso and T. Sikkeland, in Proceedings of the Second Conference on the Peaceful Uses of Atomic Energy, Geneva, 1958 (United Nations, New York, 1958), Vol. 14, p. 158.
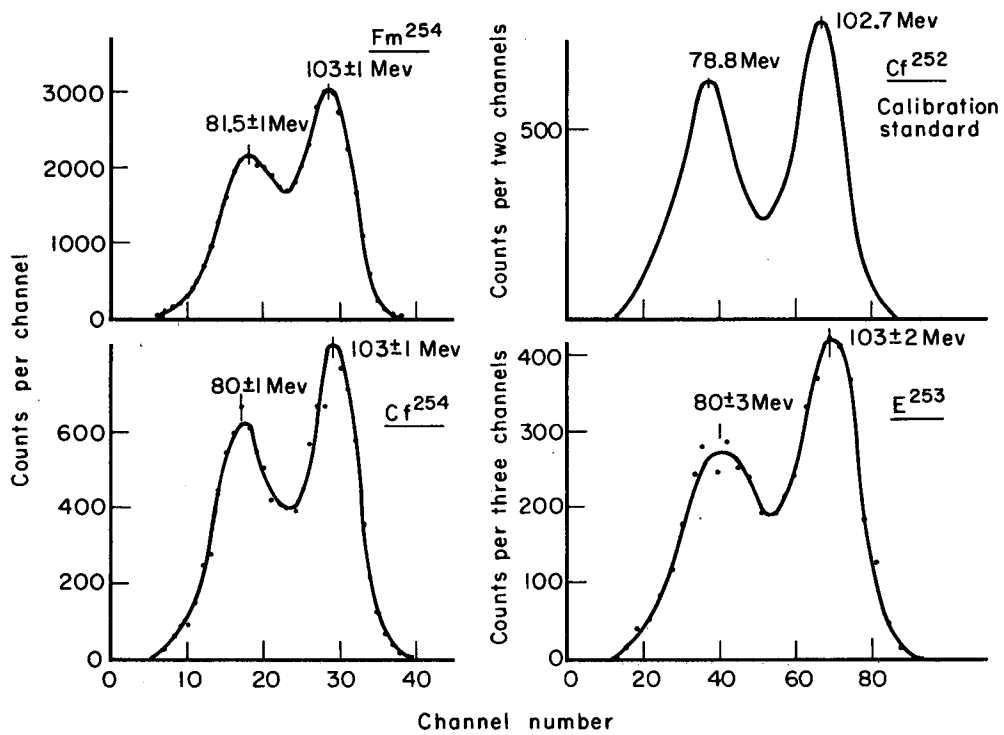
Fig. B.4-1. Energy distributions of both fission fragments in coincidence.

MU-25984

cross sections are negligible with respect to the fission cross section, except for the system $He^4 + U^{238}$.[3] Furthermore, for heavy ions at these bombarding energies, the inelastic and compound elastic scattering cross sections should be quite small. Hence, the total fission cross section also represents the total reaction cross section to a very good approximation. Here we exclude shape elastic scattering reactions from our definition of total reaction cross section.

The fission fragments were detected with a silicon detector placed at 90° to the intersection of the beam axis and the target. The target orientation was 45° with respect to the beam. The cross section for fission can be expressed as

$$\sigma_f = 2\pi \left(\frac{d\sigma}{d\omega} \right)_{90°} \int_0^\pi \frac{(d\sigma/d\omega)_\theta}{(d\sigma/d\omega)_{90°}} \sin\theta \, d\theta \ . \tag{1}$$

The integral factor in Eq. (1) accounts for the anisotropic angular distribution of the fission fragments from these reactions. For each system, the angular distributions were measured at the appropriate energies. The absolute value of $(d\sigma/d\omega)_{90°}$ was obtained by relating the fission cross section to the shape elastic scattering cross section at angles at which the Rutherford scattering relationship is valid. As a check on the absolute value of the energies and the energy spread of the beam, emulsions were exposed to each ion at the maximum and minimum energies studied.

Figure B.5-1 shows the excitation function for $U^{238} + O^{16}$, and is representative of the results obtained for the other ions. Also shown are theoretical predictions for the behavior of this excitation function for two nuclear models, assuming (a) a square-well nuclear potential, and (b) a parabolic nuclear potential. These calculations have been performed by Thomas.[4] The radius parameter r_0 was adjusted to reproduce the cross section at the maximum bombarding energy. For the square-well model $r_0 = 1.5f$, and for the parabolic potential $r_0 = 1.23f$ gave the best fit to the data.

Above 95 Mev bombarding energy both models agree with the data, although the square-well model seems to be somewhat better. As the Coulomb barrier is approached, the parabolic well appears to be the more reasonable, although there is considerable discrepancy between the experimental results and theory. Varying the shape and depth of the parabolic well may provide a better fit to the data. Also it is planned to perform these calculations by using an optical potential.

The experimental results at 10.4 Mev/nucleon bombarding energy are summarized in the Table below. It is observed that the cross section increases regularly with the size of the bombarding ion , as would be expected.

[3] R. Vanenbosch et al., Phys. Rev. 111, 1358 (1958).

[4] T. D. Thomas, Phys. Rev. 116, 703 (1959).
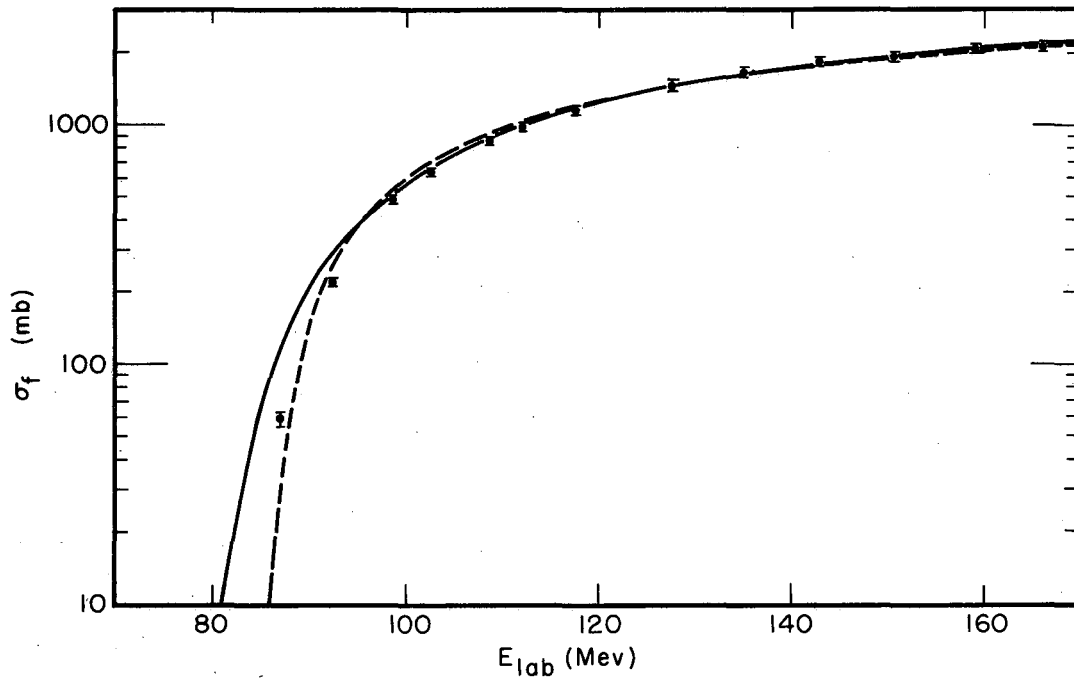
Fig. B.5-1. Fission excitation function for $U^{238} + O^{16}$.
—— theoretical curve for a square-well nuclear potential, $r_0 = 1.5$ f;
--- theoretical curve for a parabolic potential, $r_0 = 1.23$ f.

Table I. Fission cross sections at 10.4 Mev per nucleon as a function of projectile mass.

Projectile	Energy (Mev)	Cross section (mb)
He^4	41.6	1602
B^{11}	114.4	2340
C^{12}	124.6	2070
N^{14}	145.4	2094
O^{16}	166.1	2120
Ne^{20}	207.6	2340

B^{11} is an exception to this behavior. The higher cross section for B^{11} is related to the extra neutron of this nucleus. This is predicted theoretically by the parabolic potential model. Using $r_0 = 1.23f$ as was done above, the predicted cross section for $B^{11} + U^{238}$ at 114.4 Mev is 2325 mb whereas a value of 2340 ± 100 mb is observed. The $He^4 + U^{238}$ cross sections at the maximum energy are in excellent agreement with the radiochemical data of Vandenbosch et al.,[3] and the counter results of Britt and Quinton.[5]

[5] H. C. Britt and A. R. Quinton, Phys. Rev. 120, 1768 (1960).

6. LINEAR MOMENTUM TRANSFER IN HEAVY-ION-INDUCED FISSION[*]

Torbjørn Sikkeland, Eldon L. Haines, and Vic Viola, Jr.

The forward linear momentum transfer in reactions leading to fission between the heavy ions C^{12}, N^{14}, O^{16}, and Ne^{20} and the target Nuclei Ho, Au, Bi, and U^{238} has been investigated by measuring the angular correlation of coincident pairs of fission fragments.

Two solid-state detectors of the surface barrier type were used to detect the fission fragments. The collimation system for the beam and the fission fragments gave a total angular resolution of 2°. Each detector angle was known to an accuracy of $\pm 1/4^o$. The targets (usually about 200 μg/cm² in thickness) were either self-supporting or supported by 100 μg/cm² nickel foil. In order to detect coincidence events between the two detectors, a triple coincidence was required between two linear pulses (approx 1 μsec width) and a fast coincidence pulse (4 μsec width).

*Shortened version of paper to be published in Phys. Rev. (UCRL-9751, July 1961).

The angular deviation from 180° of a binary fission event observed in the laboratory system (lab) is related to the velocity of the compound nucleus according to the vector diagram.
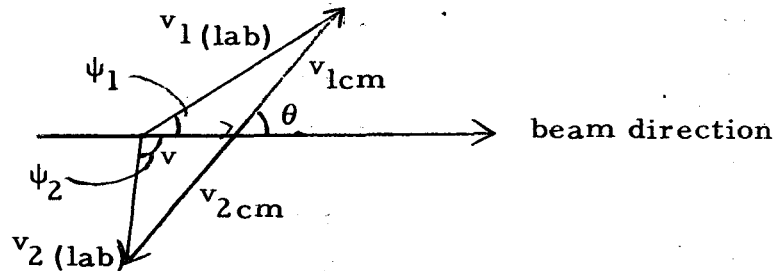
Here v_{lab} and $v_{c.m.}$ are the respective lab and center-of-mass (c.m.) velocities of the fragment, ψ and θ are respective lab and c.m. angles, and V is the velocity of the compound nucleus. The transformation from lab to c.m. system involves the parameter $x^2 = (V/v_{c.m.})^2$. From simple trigonometric relationships, the conditions for coincidence can be written

$$\tan \psi_1 = \sin\theta_{c.m.}/(x_1 + \cos\theta_{c.m.}) \tag{1}$$

$$\tan \psi_2 = \sin\theta_{c.m.}/(x_2 - \cos\theta_{c.m.}). \tag{2}$$

For the simplified case of $\psi_2 = 90^\circ$ and symmetric fission in which $x_1 = x_2 = x_{mp}$, we can write

$$\psi^2_{mp}(\psi_2 = 90^\circ) = \frac{1 - \sin^2\psi_{1mp}}{1 + 3\sin^2\psi_{2mp}}. \tag{3}$$

Hence, the measurement of the most probable angle for coincidence permits us to determine x^2_{mp}, which can then be compared with the calculated value for the average x^2 assuming complete momentum transfer, $\overline{x^2_{CN}}$.

Experimentally, the results of these angular correlation measurements fall into two groups. Group I is characterized by symmetric curves of coincidence rate as a function of angle. To this group belong the Ho, Au, and Bi targets when bombarded by C^{12}, N^{14}, and O^{16}, and the system $U^{238}+75$-Mev C^{12} ions. Group II features an asymmetric angular correlation curve composed of one dominant peak and a second peak (or shoulder) at angles nearer 180° to the fixed detector. This behavior, shown in Fig.B.6-1, and occurs for all ions incident on U^{238} targets at moderate energies and for Ne^{20} on U^{238}, Bi, and Au. Increasing the masses of the target and projectile causes these angular correlations to become more distorted. The measured values for x^2_{mp} for both these groups are given in Table I.
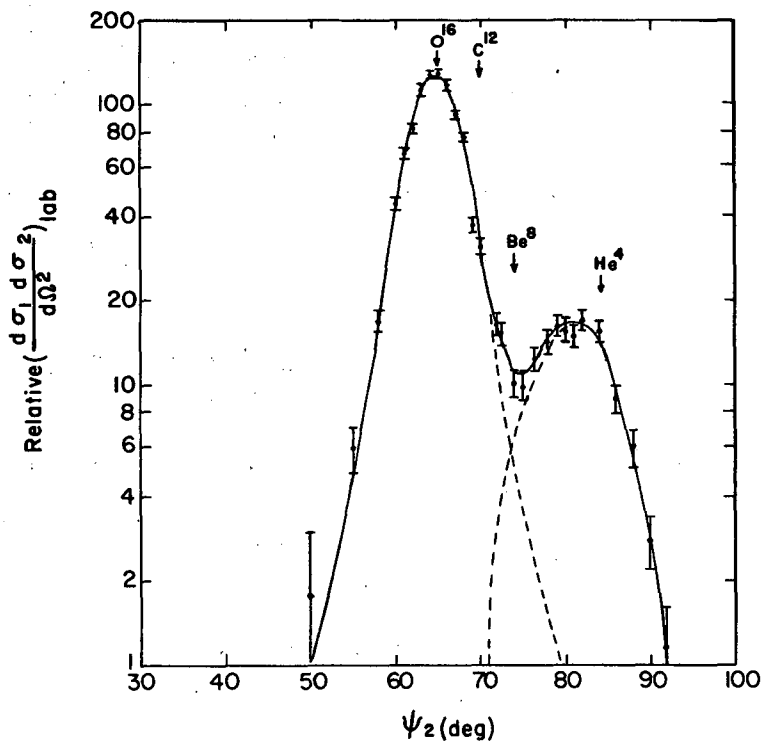
Fig. B.6-1. Fission-fragment angular correlation for the system 166-Mev $O^{16} + U^{238}$. ψ_1 at 90 deg. Each arrow represents the estimated peak position for the capture of the indicated fragment at an energy of 10.4 Mev/nucleon from the incident heavy ion.

Table I. Measured and calculated properties of each fissioning system studied in this work. $W_{1/2}$ is the angular width at half maximum for the angular correlation. Other symbols are defined in the text.

Heavy ion	Target	Heavy-ion energy (Mev)	ψ_1 (deg)	ψ_{2mp} (deg)	$W_{1/2}$ (deg)	X_{mp}^2	NCN (%)	$E_{c.m.}$ (Mev)	A_{ff} (amu)	$\bar{X}_{CN}^2$
C^{12}	Ho^{165}	125	90	61.6	6.5	0.068	0	63[a]	82.2	0.062
	Au^{197}	125	90	66.8	7.3	0.044	0	73[b]	98.5	0.046
	Bi^{209}	125	90	68.0	6.6	0.039	0	78[a]	105.3	0.041
	U^{238}	125	90	70.2	7.0	0.031	11.9%	91[c]	117.6	0.031
	U^{238}	93.7	90	72.4	6.8	0.025	1.8%	91[c]	119.3	0.024
	U^{238}	74.8	90	74.3	6.2	0.019	0	91[c]	120.4	0.019
N^{14}	Au^{197}	145	90	64.4	7.9	0.054	≈ 0	74[a]	98.4	0.061
	Bi^{209}	145	90	65.9	7.7	0.052	≈ 0	79[a]	105.2	0.055
	U^{238}	145	90	68.2	7.1	0.039	16.9%	92[a]	117.4	0.041
	U^{238}	145	40	122.5	8.0	0.042	8.7%	92[a]	117.4	0.041
	U^{238}	103	90	71.2	6.7	0.028	4.8%	92[a]	119.1	0.028
O^{16}	Ho^{165}	166	90	54.7	7.8	0.111	0	65[b]	81.8	0.102
	Au^{197}	166	90	60.5	7.8	0.074	$\approx 1\%$	75[d]	99.0	0.077
	Bi^{209}	166	90	62.1	6.2	0.066	≈ 0	80[d]	104.8	0.069
	U^{238}	166	90	64.6	7.1	0.053	15.7%	93[b]	117.8	0.052
	U^{238}	166	40	120.4	8.6	0.052	8.4%	93[b]	117.8	0.052
	U^{238}	140	90	66.6	7.6	0.045	10.2%	93[b]	119.3	0.045
	U^{238}	110	90	68.8	6.2	0.036	3.2%	93[b]	121.0	0.035
Ne^{20}	Au^{197}	207	90	55.3	9.5	0.107	5.1%	77[a]	99.8	0.111
	Bi^{209}	207	90	57.0	9.0	0.095	8.6%	82[a]	106.1	0.095
	U^{238}	207	90	60.8	7.9	0.072	16.4%	95	118.3	0.078

a. Estimated
b. This work
c. Ref 1
d. Ref 2

To compare the experimental x^2_{mp} values with $\bar{x}^2_{CN}$, one can write, from the definition of x^2,

$$\bar{x}^2_{CN} = A_I E_I A_{ff}/A^2_{CN} E_{c.m.} ,$$

where A_I is the mass and E_I the lab kinetic energy of the heavy ion; A_{CN} is the mass of the compound nucleus, and A_{ff} is the mass and $E_{c.m.}$ the c.m. kinetic energy of the most probable fission fragment. Values for $E_{c.m.}$ in Table I were taken from previous results[1,2] or were measured when necessary. If symmetric fission is assumed, $A_{ff} = 1/2(A_{CN}-\bar{\nu})$, where $\bar{\nu}$ is the number of neutrons emitted in the fission process. According to Leachman,[3]

$$\bar{\nu} = \bar{\nu}_0 + 0.12E , \tag{4}$$

where E is the excitation energy of the compound nucleus and $\bar{\nu}_0$ is the mean number of neutrons emitted in the spontaneous fission of the same nucleus.[4] Values for A_{ff} calculated in this way agree well with the results of Blann.[5] The agreement between x^2_{mp} and $\bar{x}^2_{CN}$ shown in Table I establishes that compound-nucleus formation precedes fission in the most probable fission event.

If one assumes that the compound-nucleus (CN) reactions in Group II give symmetric angular correlation curves, one can estimate the amount of non-compound-nucleus (NCN) reactions by subtracting the CN curve from the total coincidence curve. This method is demonstrated in Fig. B.6-1 by the dashed lines. Values for % NCN reactions leading to fission given in Table I should be minimum values only, because of broadening of the most probable peak from transfer of fragments with masses near that of the projectile.

With respect to the NCN reactions, we have made the following observations:

(1) The dominant NCN reaction appears to be the transfer of an α particle to the target nucleus (see arrows in Fig. B.6-1). Energy measurements requiring coincidences show the most probable energy of the fission fragments from the most probable peak to be 93 Mev (c.m.), whereas from the most probable NCN peak it is 85.5 Mev. This is consistent with the compound nuclei expected in such an interpretation.

---

[1] T. Sikkeland, A. E. Laash, and G. E. Gordon, Fission of Uranium-238 with Carbon Ions, Phys. Rev. 123, 2112 (1960).

[2] H. C. Britt and A. R. Quinton, Phys. Rev. 120, 1768 (1960).

[3] R. B. Leachman, in Proceedings of the Second International Conference on the Peaceful Uses of Atomic Energy, Geneva, 1958 (United Nations, New York, 1958), Vol. 15, p. 229.

[4] J. R. Huizenga and R. Vandenbosch, Nuclear Fission, to be published in Nuclear Reactions, Vol. 2 (North Holland Publishing Co., Amsterdam, Netherlands).

[5] H. Marshall Blann, Fission of Gold with 112-Mev C^{12} Ions: A Yield-Mass and Charge-Distribution Study (Thesis), UCRL-9190 May 23, 1960.

(2) For Ne^{20} + Au and Bi no fission is observed corresponding to a-particle transfer, although NCN reactions involving heavier masses appear. This effect is explained by the large fission barriers for a-particle fission of Au and Bi.

(3) The % NCN fission is lower when ψ_2 is fixed at 40° than at 90°. For the NCN reactions it is known that the fragments are less strongly peaked along the beam axis than the CN events; hence, the NCN/CN fission ratio should become smaller at angles nearer 0° and 180°.

(4) The most probable peak for a-particle transfer (Fig. B.6-1) indicates that about 30% of the momentum of the heavy ion is transferred to the compound nucleus. Apparently the stripped projectile also interacts with the target nucleus in the transfer reaction process.

(5) The % NCN fission decreases with bombarding energy. This result may be due to a lower probability for direct interaction with decreasing energy. However, the angular spread of the correlation is less at reduced energies, so that the % NCN values are subject to greater error.

7. ANGULAR DISTRIBUTIONS FROM HEAVY-ION-INDUCED FISSION REACTIONS (*)

Vic Viola, Jr., and T. Darrah Thomas[†]

Fission-fragment anisotropies from bombardment of Au and Bi with B^{11}, C^{12}, N^{14}, and O^{16} ions at energies up to 10.4 Mev/nucleon have been measured. Both the recoil collection technique and silicon solid-state detectors have been used to obtain the data obtained since the 1960 edition of this report (see Table I). The apparatus and experimental technique also have been previously described. In analysis of the data, transformation of the angular distributions from laboratory system into the center-of-mass system were performed with the measured x^2 values described elsewhere in this report.[1]

The anisotropy in fission reactions has been successfully explained on the basis of a model first proposed by Bohr[2] and subsequently extended by Griffin[3] and by Halpern and Strutinski.[4] According to the latter treatment,

[*] This paper embodies work presented in the Ph. D. thesis of Victor E. Viola, Jr., UCRL-9619, March 1961.

[†] Princeton University.

[1] T. Sikkeland, E. H. Haines, and V. Viola, Jr., this report, B.6.

[2] A. Bohr, in Proceedings of the International Conference on the Peaceful Uses of Atomic Energy, Geneva, 1955, Vol. 2 (United Nations, New York, 1956), p. 151.

[3] J. J. Griffin, Phys. Rev. 116, 107 (1959).

[4] I. Halpern and V. M. Strutinski, in Proceedings of the Second International Conference on the Peaceful Uses of Atomic Energy, Geneva, 1958 Vol. 15, United Nations, Geneva, 1958), p.400.

Table I. Measured fission fragment anisotropies; a refers to recoil collection measurements, b refers to solid-state counter results.

Target	Projectile	Z^2/A	E_{lab} (Mev)	Anisotropy	p	K_0^2	Measurement method
Au^{197}	B^{11}	33.9	100	4.00 ± 0.14	7.3 ± 0.4	115	(a)
			85.6	4.09 ± 0.18	7.6 ± 0.6	80	(a)
			80.1	4.03 ± 0.20	7.1 ± 0.5	73	(a)
			69.5	3.24 ± 0.19	5.2 ± 0.6	68	(a)
Au^{197}	C^{12}	34.6	118	4.18 ± 0.16	7.3 ± 0.3	146	(a)
			108	3.99 ± 0.24	7.2 ± 0.5	123	(a)
Au^{197}	N^{14}	35.1	123	3.66 ± 0.15	6.2 ± 0.3	185	(b)
			96.7	3.41 ± 0.10	5.4 ± 0.4	113	(b)
Au^{197}	O^{16}	35.5	137	3.79 ± 0.15	6.6 ± 0.4	215	(b)
Bi^{209}	B^{11}	35.2	95.9	3.22 ± 0.13	5.1 ± 0.3	150	(a)
			91.0	3.20 ± 0.16	5.0 ± 0.3	139	(a)
			80.4	3.17 ± 0.14	4.8 ± 0.3	108	(a)
			69.5	2.60 ± 0.14	3.5 ± 0.3	100	(a)
			62.7	2.62 ± 0.21	3.3 ± 0.3	74	(a)
Bi^{209}	C^{12}	35.8	105	3.14 ± 0.11	4.6 ± 0.3	176	(a)
			89.7	2.90 ± 0.12	3.9 ± 0.3	141	(a)
	N^{14}	36.3	123	3.04 ± 0.15	4.5 ± 0.3	253	(b)
			116	3.03 ± 0.10	4.5 ± 0.10	228	(a)
			110	2.90 ± 0.15	4.1 ± 0.3	220	(b)
			99.5	2.50 ± 0.14	3.6 ± 0.3	173	(a)
	O^{16}	36.8	137	3.11 ± 0.15	4.7 ± 0.3	292	(b)
			119	2.85 ± 0.15	4.0 ± 0.3	232	(b)
			102	2.48 ± 0.15	3.1 ± 0.4	167	(a)

the anisotropy is characterized by the parameter $p = I_{max}^2 / K_0^2$. Here I_{max} is the maximum total angular momentum of the compound nucleus, and K_0 is the mean value of the projection of I on the nuclear symmetry axis. For spheroidal nuclei K_0^2 can be rewritten as

$$K_0^2 = T j_0 \, \eta^{-2/3} \, (\eta^2 + 1)/(\eta^2 - 1) \; , \tag{1}$$

where T is the nuclear temperature, j_0 is the rigid-body moment of inertia of a sphere with the same volume as a spheroid with a major-to-minor axis ratio η.

Qualitatively, the data agree well with the thoery, and can be summarized as follows:

a. The anisotropy increases with bombarding energy, analogously to the dependence of the orbital angular momentum transfer of the reaction

$$(\ell \approx I).$$

b. Compound nuclei formed from Au yield larger anisotropies than those from Bi. As observed from Eq. (1), this result is expected because of the larger fission barriers (lowest) and greater deformation (larger η) of the lighter compound nuclei.

c. At the same excitation energy, the anisotropy decreases as the mass of the projectile increases. Again, this is explained by the more fissionable compound nuclei formed with ions of higher Z. In this respect N^{14} and O^{16} behave somewhat anomalously at high energies. This has been tentatively explained as being due to nuclear surface reactions which may be more probable for the loosely bound N^{14} structure than the doubly magic O^{16} nucleus.

The principal difficulty in attempting a more quantitative treatment is the uncertainty in our knowledge of the nuclear temperature. From the experimental p values and the calculated values of I_{max},[5] one can determine K_0^2. Our approach has been to examine the variation of T and η for K_0^2 values measured for the various systems. Such an analysis is shown in Fig. B.7-1, where T is plotted versus η for interpolated values of K_0^2 corresponding to a calculated excitation energy above the fission barrier, $E^* - E_f$, of 75 Mev for each initial compound nucleus. If we assume $T = [10(E^* - E_f)/A]^{1/2}$, then Fig. B.7-1 indicates that the corresponding spheroidal deformation of the fissioning nucleus increases with decreasing Z. For the most fissionable compound nuclei, e.g. Pa^{225} and Th^{223}, one finds $\eta \approx 2.5$, which is in the range of values expected for these nuclei. Hence, nearly all the fission is most probably occurring from the initial compound nucleus. For lower-Z systems, η values of 4:1 to 5:1 are required if one assumes only first-chance fission. In this case, the probability for neutron emission, Γ_n/Γ_f, must be large enough to lower T or the saddle-point shapes or both for systems of high angular momentum, and large fission barriers must be substantially deformed.

At values of $E^* - E_f$ near the Coulomb barrier, very large deformations (i.e. from 4:1 to 8:1) are required to be consistent with first-chance fission.

[5] T. D. Thomas, Phys. Rev. 116, 703 (1959).
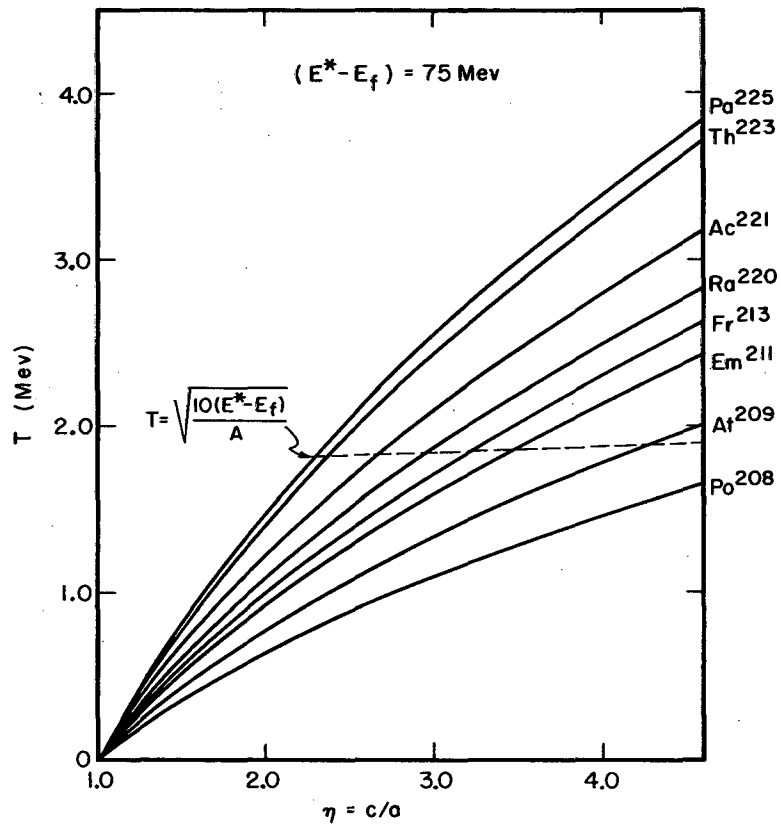
Fig. B.7-1. Plot of variation in nuclear temperature versus spheroidal deformation for measured values of K_0^2 corresponding to $(E^*-E_f) = 75$ Mev. Dotted line represents the nuclear temperature of the initial compound nucleus.

Qualitatively, one would expect these saddle-point shapes to be more deformed than at higher energies. However, such extreme values may be in part due to additional effects, for example:

    a. The moment of inertia of the compound nuclei at low excitation energy may be less than the rigid body moment.

    b. Γ_n/Γ_f .may be large for these excitations..

    c. The spheroidal shape approximation may not be a good one.

    d. The model for calculating I_{max} may not be applicable near the barrier.

8. FISSION FRAGMENT ANISOTROPY IN REACTIONS OF H_2 AND He^4 WITH U^{238}

V. E. Viola, Jr., John M. Alexander, and A. R. Trips

We have measured the angular distributions of the gross fission products and of selected fragments from bombardments of U^{238} with 24-Mev H^2 and 48-Mev He^4 ions. This work was undertaken to study the effect of mass ratio (M_H/M_L) on the anisotropy of the fission fragments. According to Halpern and Strutinski[1] and Griffin,[2] the anisotropy should vary inversely with excitation energy for a system of constant angular momentum. Hence, the anisotropies should give information about the excitation energies or angular momenta, or both, of nuclei that give rise to fission products of differing mass ratio.[3]

In previous recoil-collection experiments on such systems, thin sources of the target material have been deposited on a thick supporting foil, restricting the measurement of the angular distribution to one hemispher.[4,5] The targets for the experiments reported here were prepared by vaporizing 150 to 200 $\mu g/cm^2$ of U^{238} F_4 onto a 220-$\mu g/cm^2$ Ni backing foil. At angles of less than 60° to the target normal, these thicknesses are substantially less than the ranges of even the heaviest fission fragments. This permits measurement of the entire angular distribution in a single experiment. The apparatus and recoil collection technique have been described elsewhere.[6] The angular resolution was increased to about 8° for these experiments.

[1] I. Halpern and V. Strutinski, in Proceedings of the Second United Nations International Conference on the Peaceful Uses of Atomic Energy, Geneva, 1958, Vol. 15 (United Nations, Geneva, 1958) p. 400.

[2] J. J. Griffin, Phys. Rev. 116, 107 (1959).

[3] A. W. Fairhall, E. F. Neuzil, and R. C. Jensen, in Proceedings of the Second United Nations International Conference on the Peaceful Uses of Atomic Energy, Geneva, 1958 Vol. 15 (United Nations, Geneva, 1958), p. 452.

[4] C. T. Coffin and I. Halpern, Phys. Rev. 112, 536 (1958).

[5] University of Washington Annual Progress Report, 1960 and 1961.

[6] V. E. Viola Jr., Angular Distributions from Heavy-Ion–induced Fission (thesis) UCRL-9619, March 1961.

The gross product angular distribution in the center-of-mass system was obtained by the differential range measurement technique[6] and is shown in Fig. B.8-1. Good agreement with the results of Coffin and Halpern is found.[4] These differential range experiments demonstrated that the range distributions were characteristic of the fission process. In Figs. B.8-2 and B.8-3 we show the c.m. angular distributions for the various products. The anisotropy does change with mass ratio of the fragments for deuteron fission. However, for α-particle-induced fission there is little or no difference in the angular distributions of Ag^{111}, I^{131}, and Ba^{140}. The discrepancy between forward and backward measurements for Ba^{140} and Ag^{111} in Fig. B.8-2 is attributed to an error in target positioning. This error was corrected in the other experiments. The c.m. transformations have been made by assuming full momentum transfer.[7]

[7]W. J. Nicholson and I. Halpern, Phys. Rev. 116, 175 (1959).

9. NUMBER OF NEUTRONS EMITTED BY FISSION FRAGMENTS

J. C. D. Milton

At the suggestion of W. J. Swiatecki, some calculations based on the tangent spheroid model of the fissioning nucleus have been performed in the hope of gaining some understanding of the variation of ν with fragment mass.[1,2,3,4] The potential energy of the system of two uniformly charged prolate spheroids in contact is calculated as a function of the ratio of their major to minor axes, c/a, for a number of different relative volumes. In general the potential energy of such a system has a minimum when the c/a for both drops is in the range 1 to 2 for the x values of interest. We refer to this as the liquid drop minimum. If one of the drops is spherical ($c/a = 1$) there is in addition a well-defined value of the deformation of the other drop which gives a minimum along the $c/a = 1$ axis. Normally we consider that shell corrections to the energy of the nucleus are effective only when the nuclear potential is nearly spherical. If this is so then our liquid drop potential surface will be depressed in a narrow region about both axes. The depth of the depression will depend on the size of the shell corrections. If they are large enough the axial minimum may be depressed below the liquid drop minimum. Our simple picture would then be that fission always takes place from the minimum of the potential energy surface and that the deformation energy of each drop at the time of scission is transferred into excitation energy of the fragment, whereas the interaction energy becomes the kinetic energy of the two fragments at infinity. If one of the drops were spherical at the time of scission then it would have no excitation energy and emit no neutrons.

[1]James Terrell, Bull. Am. Phys. Soc. 6, 16 (1961).

[2]J. S. Fraser and J. C. D. Milton, Phys. Rev. 93, 818 (1954).

[3]S. L. Whetstone, Phys. Rev. 114, 581 (1959).

[4]Apalin, Dobrinin, Zaharova, Kutikov, and Mikhaylan, Atomnaya Energ. 8, 15 (1960).
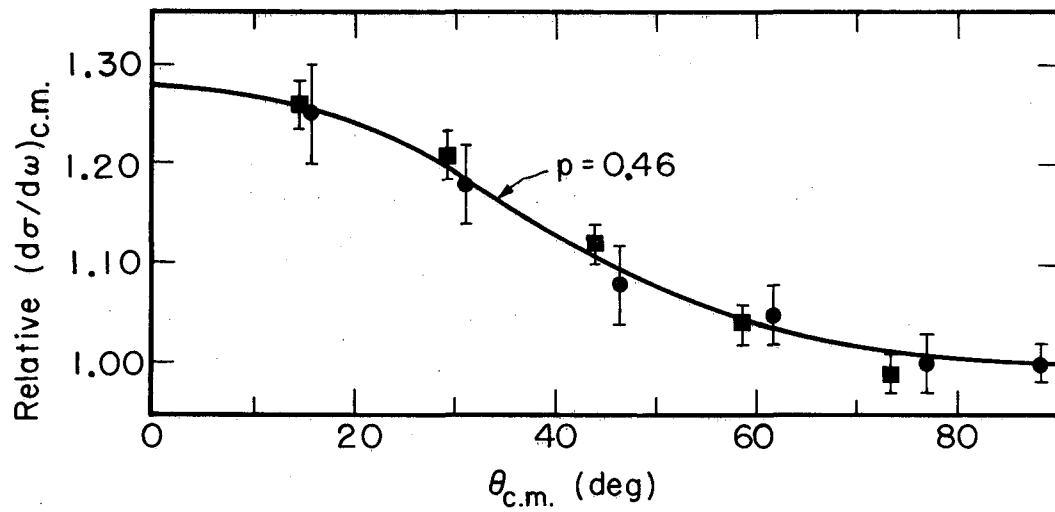
Fig.B.8-1. Center-of-mass angular distribution for gross fission products
from 24-Mev H^2 bombardment of U^{238}. Solid curve is theoretical fit
to the data according to p values of Ref. 1. ⊙ denotes data from angle
θ and ⊡ from π-θ.
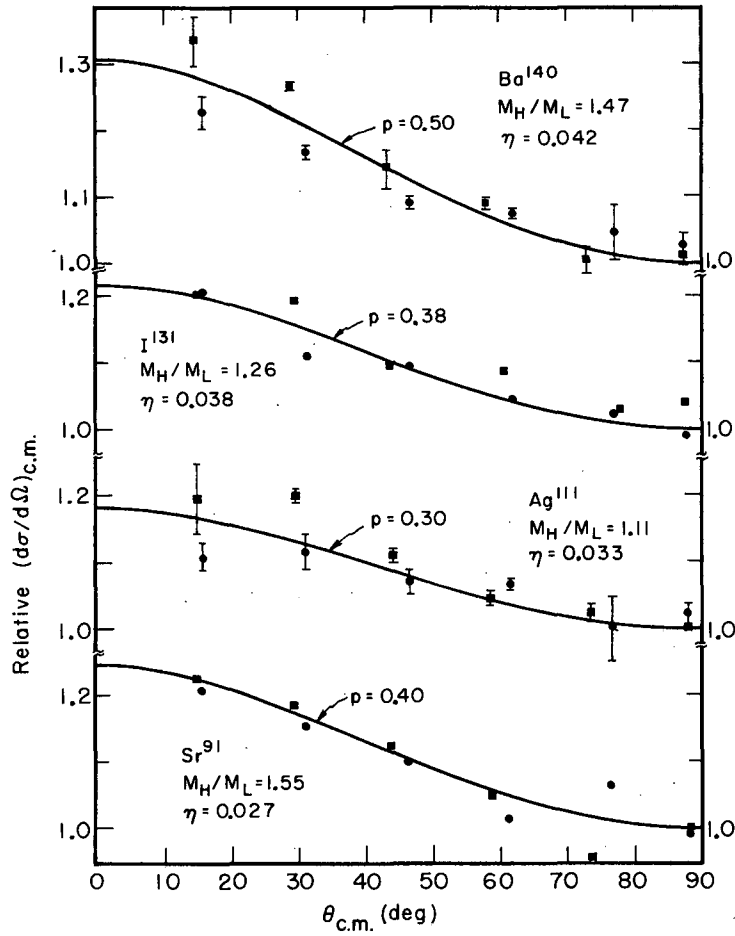
MU-25760

Fig. B.8-2. Center-of-mass angular distribution for fission products from 24-Mev H^2 bombardment of U^{238}. Solid curve is theoretical fit to the data according to p values of Ref. 1. ⊙ denotes data from angles θ and ⊡ from π-θ.
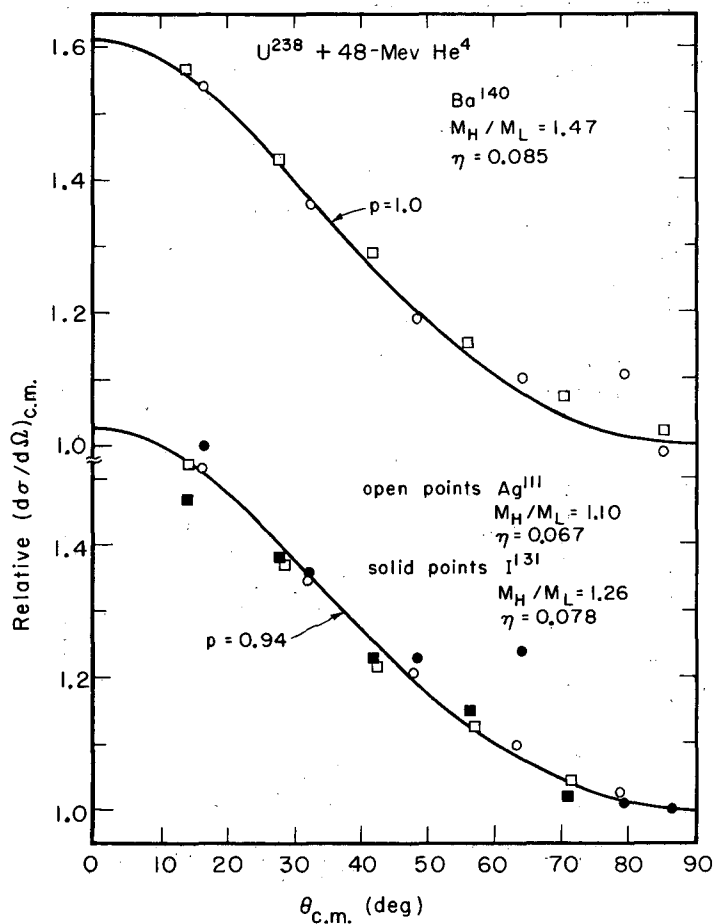
Fig. B.8-3. Center-of-mass angular distribution for fission products from 48-Mev He^4 bombardment of U^{238}. Solid curve is theoretical fit to the data according to p values of Ref. 1. ⊙ denotes data from angles θ and ⊡ from $\pi-\theta$.

In Fig. B.9-1a we have plotted the amount of energy the system has to pay in going from the liquid drop minimum to the axial minimum, and labeled it "liquid drop." The double-peaked line labeled "shell" is the energy gained by the nucleus in forming shells. It has been calculated by comparing the masses obtained by Cameron,[5] which include shell corrections, with those obtained from Green's liquid drop masses[6] as calculated by Fink.[7] Although the shape of this curve is well determined, its position on the vertical axis is somewhat arbitrary, since it depends upon where the smooth reference mass surface is placed. However, if one takes the shell corrections to be zero in the mass region 105, then the curve is as shown. Thus wherever the shell curve lies above the liquid drop line we should expect no deformation energy and hence no neutrons from those fragments. The sum of the deformation energies of both fragments at the liquid drop minimum turns out to be nearly equal to the deformation energy of one of the fragments at the position of the axial minimum. We thus expect the fragment paired with the spherical one to emit twice as many neutrons. The deformation energy at the liquid drop minimum is rather a flat function of relative drop size and is about twice as high as the observed excitation energy. This is no doubt due to the crudeness of the shapes assumed by the model. If we arbitrarily reduce the deformation energy by one-half, the appearance of ν is given approximately by the solid line in Fig. B.9-1b. The experimental observations are shown as a dotted line.

[5] A. G. W. Cameron, Can. J. Phys. 35, 1021 (1957).

[6] A. E. W. Green, Revs. Modern Phys. 30, 569 (1958).

[7] R. D. Fink, Department of Chemistry, MIT (unpublished work).

10. FISSION ENERGY TABLES

J. C. D. Milton

A large table of the energies released during fission as a function of the masses and charges of the fragments has been calculated by use of Cameron's[1] mass formula. The energy released and the neutron binding energies are given both before and after averaging over a Gaussian charge distribution of rms width 0.7 charge unit. The maximum energy release and the charge corresponding to this maximum are also given, and the latter is compared with a prescription given by Apalin[2] for the most probable charge. In general the Apalin prescription gives values of the light fragment charge which are lower than those given by the maximum energy.

In all, 34 cases were computed between Bi^{209} and Fm^{254}, making the full table somewhat bulky--more than 800 pages. Accordingly a summary table was prepared in which only seven of the more commonly investigated isotopes are given in full. The others are represented only by the shorter

[1] A. G. W. Cameron, Can. J. Phys. 35, 1021 (1957).

[2] Apalin, Dobrinin, Zaharova, Kutikov, and Mikhaylan, Atomnaya Energ. 8, 15 (1960).
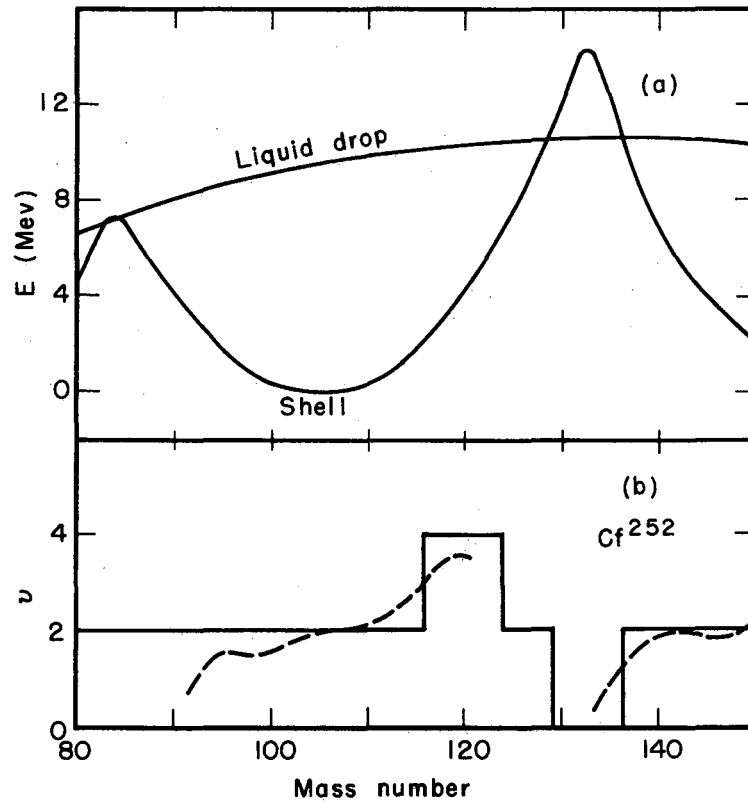
MU-25987

Fig. B.9-1. (a) Comparison of the shell corrections to the mass and the energy it costs to make one of the tangent spheroids into a sphere.

(b) Comparison of the observed neutron emission probability (dotted line) and that predicted by this model (solid line).

table of maximum energy release. This is to be issued as UCRL-9883.

The values in the table given by Cameron's mass formula have been compared with those given by Seeger's.[3] Although the differences are somewhat complex they may be summarized as follows. The value of the maximum total energy release for any fragment pair is insignificantly different, usually less than 2 Mev. The energy release isobaric parabolas given by Seeger are, however, always flatter and slightly skewed relative to Cameron's and in such a way that the maximum energy always occurs at a slightly lower light fragment charge, sometimes as much as 0.6 charge unit lower. Seeger's formula always gives a larger energy release when the light fragment is very neutron-rich, the difference being greatest (approx 15 Mev) when the heavy fragment has a mass near 150.

It will be realized from what has been said that the two formulae differ very much in their predictions for the most probable charge. Unfortunately neither of the predictions agrees very well with the values of most probable charge derived from independent yield data. The extent of the disagreement is illustrated in Fig. B.10-1, where the data compiled by Wahl[4] are compared with the estimates made on the basis of maximum energy release and minimum potential energy postulates.[5] Although the uncertainty of much of the data is great, it appears that the uncertainty in current mass formulae preclude the proper understanding of the charge division.

[3]P. A. Seeger, Nuclear Phys. 25, 1 (1961).

[4]Wahl, Ferguson, Nethaway, Troutner, and Wolfsberg, Washington University, St. Louis, unpublished report, June 1961.

[5]See, for example, H. Marshall Blann, Fission of Gold with 112-Mev C^{12} Ions: A Yield-Mass and Charge-Distribution Study (thesis), UCRL-9190, May 1960.

11. VELOCITY AND ANGULAR DISTRIBUTIONS OF PROMPT NEUTRONS FROM SPONTANEOUS FISSION OF Cf^{252} (*)

Harry R. Bowman, Stanley G. Thompson, J. C. D. Milton, and Wladyslaw J. Swiatecki

The velocity and angular distributions of neutrons associated with light and heavy groups of fission fragments from spontaneous fission of Cf^{252} have been measured. The results can be accounted for within about 10 to 20% by the assumption of isotropic evaporation from moving fragments. Closer examination of the results shows systematic differences from simple evaporation which are outside the statistical errors of the measurements.

The approach used involved coincident measurements of neutron and fission-fragment flight times over a known distance. Measurement of the velocities of both fragments determined their masses and energies. Simultaneous measurement of the velocities of coincident neutrons making known angles with the fragment direction gave the basic information bearing on neutron emission in the fission process.
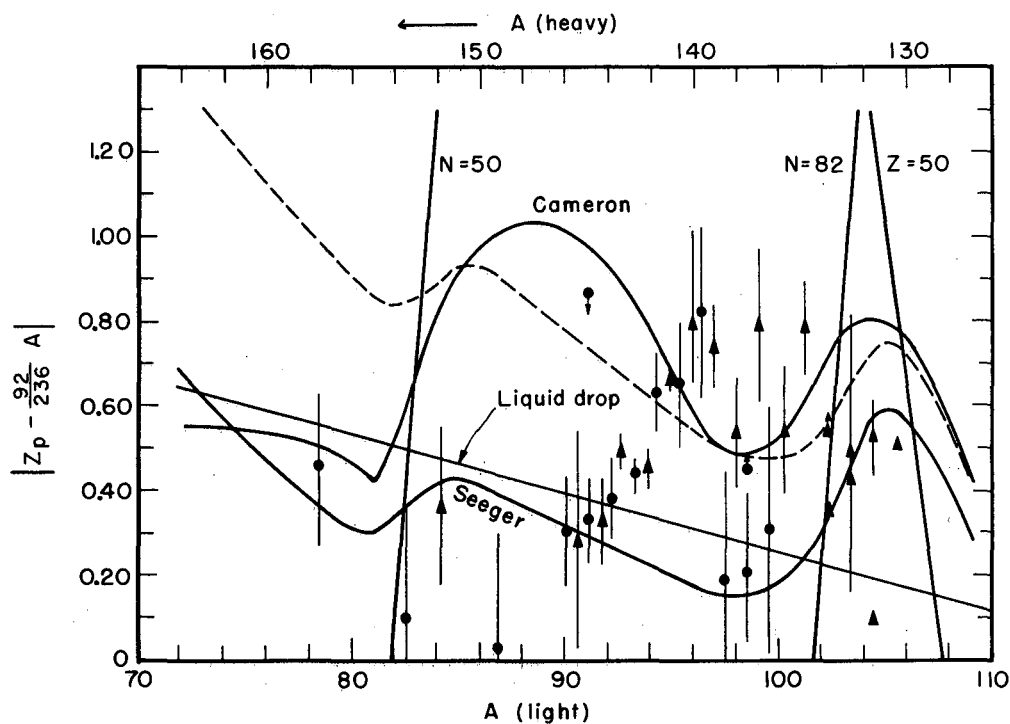
MU-25988

Fig. B.10-1. Comparison of most probable charge Z_p as obtained from
independent yield data. The solid lines are the values calculated
from the mass formulae of Cameron and Seeger based on the mini-
mum-potential-energy postulate. The dotted line corresponds to the
maximum energy release for Seeger. The straight line labeled
"liquid drop" is the minimum potential energy prediction using smooth
liquid drop masses.

The velocities of fragments and neutrons were determined by measuring their flight times over a known distance. These flight times, ranging from about 20 to 200 nanoseconds, were determined through the use of time-to-pulse-height converters of conventional design, in which time is measured by the amount of charge collected on a condenser in the interval between two timing pulses. Time-of-flight measurements were made for those events in which one neutron and two fragments occurred in coincidence. Rare events in which two neutrons were detected in coincidence with both fragments were also measured. The angle of one of the neutron detectors, N_1, relative to the fragments was varied through a range from 22.5 to 90 deg in steps of 11.25 deg. The position of the neutron detector N_2 was held constant at 11.25 deg throughout the series of measurements.

More than 250,000 events were recorded and the final results expressed in terms of the neutron denisty distribution, $\rho(V, \theta)$, in neutrons per unit volume of velocity space at the velocity V and angle θ.

A complete account of the results of the experiments is given in UCRL-9713. The following is a brief summary of the final conclusions.

A. The overall properties of the neutrons are as follows:

    1. The number of neutrons per fission is $\overline{\nu} = 3.8$.
    2. The energy spectrum is a rapidly decreasing one, with an average energy of $2.20 \pm .05$ Mev (lab).
    3. The angular distribution is strongly peaked in the direction of the fission fragments: the relative intensities in the direction of the light fragment, in the direction of the heavy fragment, and at right angles are about 9, 5, and 1, respectively.
    4. The broad features of the energy and angular distributions are reproduced by the assumption of isotropic evaporation of the neutrons from fully accelerated fragments.

B. If the data are analyzed on the basis of isotropic evaporation from fully accelerated fragments, then

    1. The light and heavy fragments emit comparable numbers of neutrons, with virtually identical energy spectra. The average temperature of the spectra is $0.72 \pm .04$ Mev, with an rms deviation $\sigma_T = 0.32$ Mev for both fragments.
    2. The light fragment emits 1.97 neutrons, the heavy 1.70 neutrons ($\nu_L/\nu_H = 1.16$), which represents contributions to the internal excitation energies of 14.7 Mev and 10.7 Mev, respectively.
    3. The observed deviations from the hypothesis of isotropic emission by fully accelerated fragments are such that not more than about 90% of the neutrons can arise from simple isotropic evaporation.

C. The nature of the deviations is less well determined than the overall features of the neutron distributions. The following features are suggested:

    1. There is no indication of a marked anisotropy of the $P_2(\cos \psi)$ type in the emission of the neutrons from the fragments.
    2. Most of the systematic deviations from the hypothesis of isotropic emission from moving fragments could be accounted for by assuming a small fraction of rather energetic neutrons (for example 10%) to be emitted isotropically from a source not sharing the motion of the fragments.

3. The remaining observed deviations appear at the single small-angle settings (11.25 and 168.75 deg) and would require for their explanation either a small number of neutrons collimated along the fission direction or an unknown instrumental difference in the efficiencies of the two neutron-counter systems used in the experiment.

12. KINETIC ENERGY RELEASE IN DEUTERON FISSION OF U^{238}

John M. Alexander and M. F. Gazdik

One of the interesting features of the fission process is the dependence of kinetic energy on mass asymmetry. Various studies of thermal-neutron fission of U^{235} show that the total kinetic energy of near-symmetric fragments is about 35 Mev less than the maximum total kinetic energy.[1,2,3] Similar "kinetic energy deficits" for near symmetric fission have been indicated for fissioning nuclei of Pu^{240} and U^{234} excited to about 6 Mev.[2,3,4] At present it is not possible to make a satisfactory energy balance for these cases of near-symmetric fission. No theoretical explanation of this effect has been proposed.

The purpose of this work is to make an investigation of the kinetic energy released in fission for a more highly excited fissile nucleus. We have performed integral recoil range experiments for the products Sr^{89}, Ag^{111}, Cd^{115}, I^{131}, and Ba^{140} from 23-Mev deuteron fission of natural uranium. Uranium foils 0.001 in. thick were used with Au catcher foils for all products except I^{131}; for this case Al catchers were used. Experiments by J. B. Niday have shown that the range values from experiments using Al catchers are 3% greater than those using Pb catchers.[1] Using this result, we have corrected the range values for I^{131}. The range values are shown in the Table along with the ratio to the corresponding range for thermal-neutron fission of U^{235}. In calculating these range values we have used preliminary angular distribution data obtained from other measurements.[5]

From the table we see that the ranges of the near-symmetric products are somewhat greater for deuteron fission; however, the ranges of asymmetric fission products are somewhat smaller. A more quantitative comparison can be made by converting the ranges to kinetic energies, and the kinetic energies to total kinetic energy release. The results of such a conversion are shown in Fig. B. 12-1. (We have used range-energy relationships proposed by Niday.[1]) The "kinetic energy deficit" is only about 8 Mev for deuteron fission of U^{238}. It appears that the additional excitation energy has significantly changed the nature of the fission process.

[1] J. B. Niday, Phys. Rev. 121, 1471 (1961).

[2] J. C. D. Milton, Phys. Rev. Letters 7, 67 (1961).

[3] J. M. Alexander and M. F. Gazdik, Phys. Rev. 120, 874 (1960).

[4] S. Katcoff, J. A. Miskel, C. W. Stanley, Phys. Rev. 74, 631 (1948).

[5] V. Viola, J. M. Alexander, and A. Trips, this report, B. 8.

Table I. Corrected range values for recoil range experiments.

Product	Range in U (mg/cm^2)		$\dfrac{\text{Range for } d + U^{238}}{\text{Range for } n + U^{235}}$
	23-Mev $d + U^{238}$ [a]	$n + U^{235}$	
Sr^{89}	$11.1 \pm .16$	11.20 [b]	0.991
Ag^{111}	$9.74 \pm .03$	9.45 [b]	1.031
Cd^{115}	$9.52 \pm .10$	9.23 [b]	1.031
I^{131}	$8.94 \pm .13$ [b]	9.15 [b]	0.977
Ba^{140}	$8.47 \pm .05$	8.50	0.996

a. The quoted errors are the standard deviation of the mean. These do not reflect the error due to use of preliminary angular distribution parameters.

b. These ranges were measured with Al catchers and have been multiplied by 0.97 to correct to Pb or Au catchers. See Ref. 1.
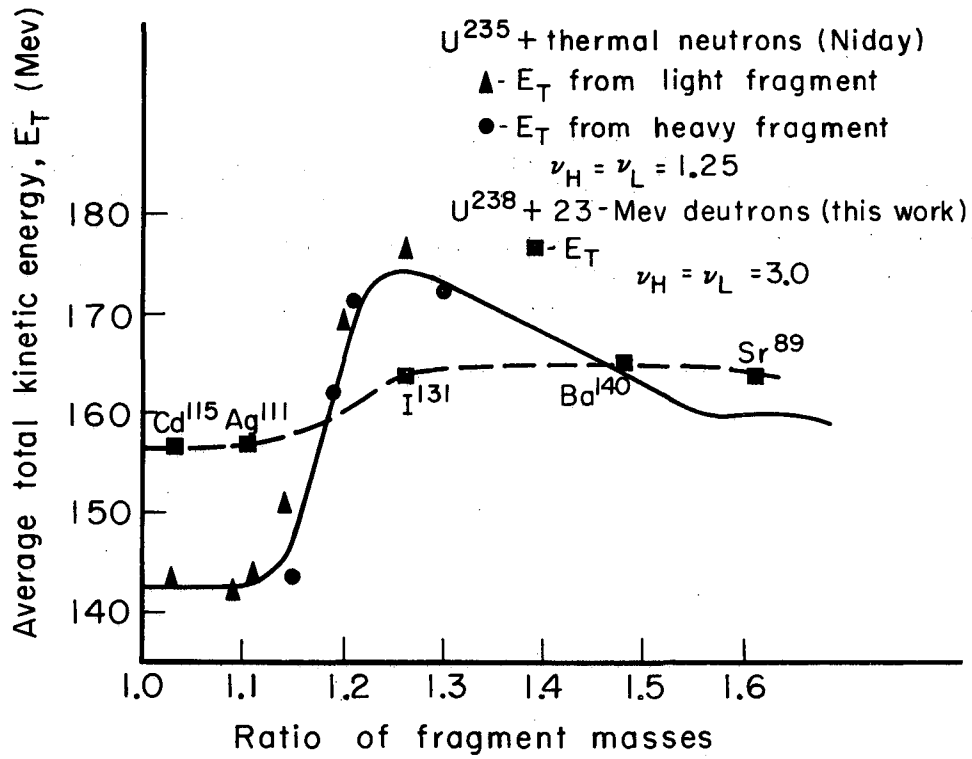
Fig. B.12-1. Kinetic energy release in deuteron fission of U^{238}.

C. NUCLEAR REACTIONS

1. RECOIL PROPERTIES OF Tb^{149} PRODUCED IN HEAVY-ION-INDUCED REACTIONS

John M. Alexander and David Sisson

In earlier work we have reported some recoil range measurements for the product Tb^{149} formed in (HI, xn) and (HI, pxn) reactions.[1] These measurements have been extended to include a large variety of heavy ions (HI), many possible reactions, and a wide range of energies. The experimental techniques were very similar to those previously described.[1] Values of the average range, R_0, and the range straggling parameter, ρ are given in Table I.

The values of the average range are used as a test of the compound-nucleus model. If a compound nucleus is formed the products recoil almost directly along the beam direction with an average kinetic energy E_{CN} where

$$E_{CN} = E_b \left[\frac{A_b \, A_R}{(A_T + A_b)^2} \right] .$$
(1)

The symbol E_b denotes incident bombarding energy; A denotes mass number, with subscripts b for bombarding particle, T for target, and R for final recoil atom.

If range-energy data for Tb^{149} were available, the measured average ranges could be converted to average kinetic energies for comparison with Eq. (1). However, since no such data are available, we resort to an internal-consistency agreement. First, we calculate E_{CN} from Eq. (1), assuming the validity of the compound-nucleus model. Then we plot the measured average ranges against E_{CN} as shown in Fig. C.1-1. If the compound nucleus model is adequate one smooth curve (namely the range-energy curve) should result. It is very unlikely that partial momentum transfer reactions could take place in such a way as to give one single curve through all the measurements. From Fig. 1 we note that indeed one smooth wave can be drawn through the data points. We conclude that Tb^{149} is produced by compound-nucleus reactions for all reactions and energies studied.

The measured range straggling ρ is due to the following effects: (a) foil inhomogeneities, ρ_f, (b) the statistics of the stopping process, ρ_s, (c) the nuclear reaction, ρ_n, (d) finite target thickness, ρ_W. For the $(HI, xn)Tb^{149}$ reactions we can calculate the range straggling due to the nuclear reaction. The calculation of straggling has been performed by the Monte Carlo method using evaporation theory. Then we can deduce the straggling due to foil inhomogenieties and stopping effects by subtraction of ρ_n and ρ_W. Both these latter effects (ρ_n and ρ_W) comprise only a relatively small part of the measured range straggling. Therefore we are able to make

---

[1] L. Winsberg and J. M. Alexander, Phys. Rev. 121, 518 (1961); J. M. Alexander and L. Winsberg, Phys. Rev. 121, 529 (1961).
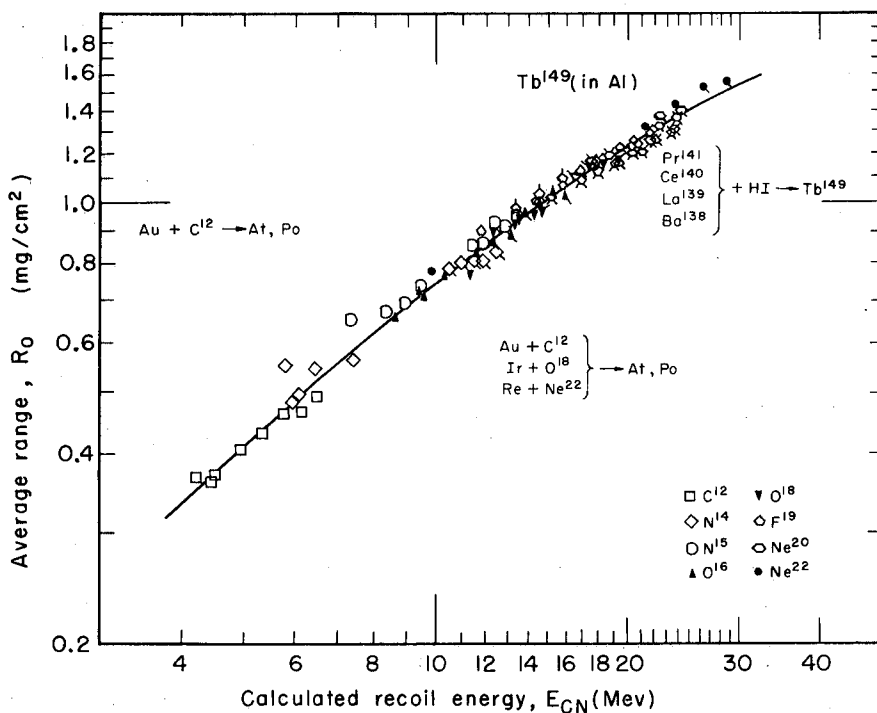
Fig. C. 1-1. Average range as a function of calculated recoil energy. The symbols are as follows: C^{12} □ ; N^{14} ◇ ; N^{15} D O^{16} ▲ ; O^{18} ▼; F^{19} ⬡; Ne^{20} ⬦ ; Ne^{22} ●; Four bars are for reactions forming compound nuclei of Z = 69; three bars for Z = 68; two bars for Z = 67; one bar for Z = 66; no bars for Z = 65.
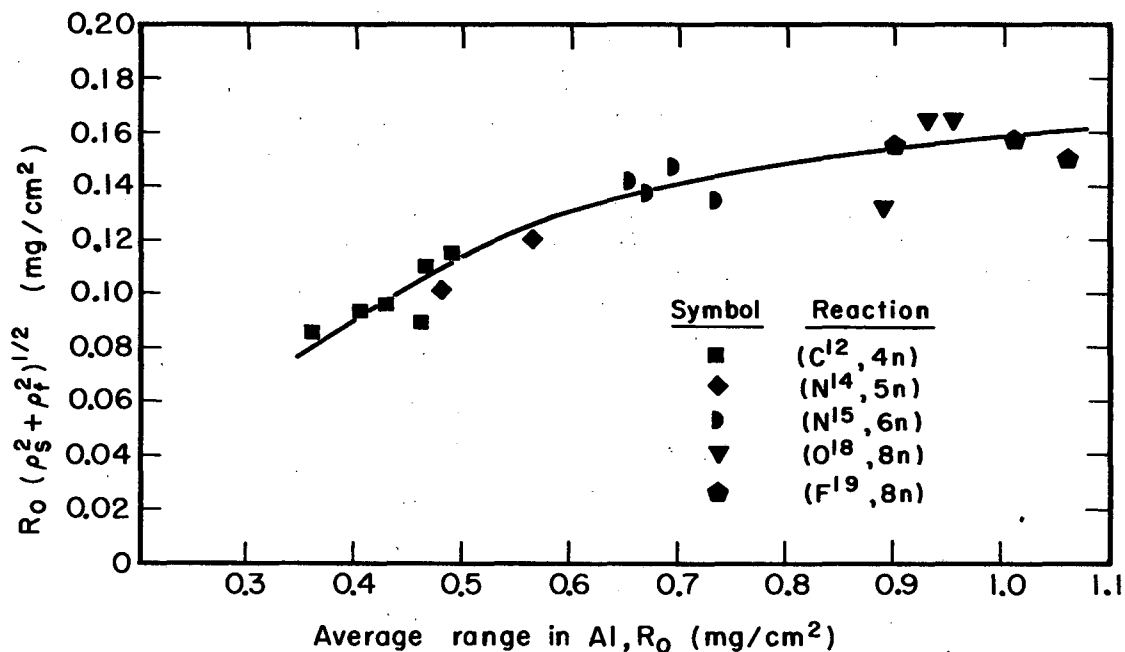
Fig. C. 1-2. Range straggling of Tb^{149} due to foil inhomogeneities and stopping phenomena as a function of average range.

the subtractions with confidence. The resulting values of the range straggling from foil inhomogeneities and the stopping effect are shown in Fig. C-1-2. Some experiments to be described later indicate that these range straggling values are probably due in large measure to the stopping process itself.

Using the results shown in Fig. 2, we can subtract ρ_f and ρ_s from the measured range straggling for the more complex reactions. Thus we can determine values of ρ_n that may give insight into the mechanism of the more complex reactions.

Table I. Summary of the Tb^{149} recoil data

Reactions	Bombarding energy, E_b (lab)(Mev)	Average range R_0 (mg/cm^2)	Straggling parameter, ρ
(leading to $_{65}Tb$ compound nuclei)			
$Pr^{141} + C^{12}$	85.1	0.491	0.298
	80.3	0.465	0.295
	75.2	0.461	0.255
	69.8	0.430	0.273
	64.6	0.405	0.270
	58.3	0.360	0.273
$Ce^{140} + N^{14}$	84.4	0.566	0.240
	67.6	0.482	0.230
$Ce^{140} + N^{15}$	108.3	0.735	0.220
	102.2	0.696	0.242
	95.8	0.671	0.233
	88.5	0.654	0.237
$La^{139} + O^{18}$	131.0	0.955	0.208
	122.4	0.932	0.203
	113.9	0.892	0.175
$Ba^{138} + F^{19}$	137.6	1.059	0.177
	125.8	1.010	0.181
	111.9	0.90	0.19

Table I. (cont)

	E_b	R_0	ρ
(leading to $_{66}$Dy compound nuclei)			
$Pr^{141} + N^{14}$	142.8	0.833	0.25
	137.2	0.810	0.233
	132.0	0.810	0.222
	126.4	0.808	0.197
	120.8	0.789	0.216
$Pr^{141} + N^{15}$	153.0	0.942	0.190
	147.9	0.917	0.193
	142.8	0.926	0.199
	137.4	0.856	0.203
	132.0	0.856	0.209
	113.1	0.779	0.207
$Ce^{140} + O^{16}$	163.0	1.028	0.213
	155.5	1.042	0.204
	148.6	0.992	0.219
	141.3	0.964	0.189
	133.6	0.889	0.187
	126.2	0.863	0.199
	118.4	0.830	0.177
$La^{139} + F^{19}$	192.9	1.312	0.166
	182.4	1.248	0.174
	170.8	1.236	0.163
	160.7	1.169	0.161
$Ba^{138} + Ne^{20}$	202.6	1.402	0.155
	188.8	1.381	0.153
	175.6	1.199	0.169
	162.0	1.251	0.144
	148.0	1.158	0.160
(leading to $_{67}$Ho compound nuclei)			
$Pr^{141} + O^{16}$	162.9	1.035	0.180

Table I. (cont)

Reactions	E_b	R_0	ρ
$Pr^{141} + O^{18}$	179.8	1.169	0.202
	172.4	1.162	0.181
	164.3	1.145	0.183
	156.2	1.100	0.188
	139.0	0.976	0.205
$Ce^{140} + F^{19}$	192.9	1.293	0.179
	182.6	1.258	0.177
	172.1	1.228	0.170
	160.2	1.173	0.171
	148.4	1.106	0.196
$La^{139} + Ne^{20}$	202.6	1.371	0.162
	188.8	1.325	0.163
	174.6	1.222	0.162
	162.0	1.179	0.164

(leading to $_{68}$Er compound nuclei)

Reactions	E_b	R_0	ρ
$Pr^{141} + F^{19}$	191.7	1.227	0.220
	182.0	1.152	0.230
	171.8	1.126	0.240
	161.5	1.094	0.229
	151.2	1.096	0.205
	138.9	1.033	0.191
	126.7	0.975	0.178
$Ce^{140} + Ne^{20}$	203.2	1.308	0.201
	188.8	1.251	0.236
	174.0	1.209	0.202

Table I. (cont)

Reactions	E_b	R_0	ρ
	160.0	1.175	0.213
	145.2	1.148	0.191
	129.6	1.017	0.188
(leading to $_{69}$Tm compound nuclei)			
$Pr^{141} + Ne^{20}$	202.8	1.295	0.213
	188.6	1.270	0.206
	175.6	1.200	0.207
	161.8	1.189	0.166
	147.2	1.078	0.173

2. EXCITATION FUNCTIONS FOR Tb^{149}, Dy^{150}, AND Dy^{151} PRODUCED IN HEAVY-ION REACTIONS

John M. Alexander

The properties of nuclei excited to energies greater than about 40 Mev are almost completely unknown. The reason for our ignorance of these properties lies in our past inability to produce these nuclei in a relatively pure way. In the preceding report we have shown that recoil range data indicate that the compound-nucleus mechanism is operative for Tb^{149} produced by heavy-ion reactions. This result means that we can produce excited compound nuclei and study their properties with little or no interference from "direct reactions." Interference from direct reactions is always present in measurements of the energy spectra of nucleons, a particles, etc., emitted in medium- and high- energy reactions (> 30 Mev).

Several kinds of measurements can give information about the highly excited compound-nuclei excitation functions, angular distributions, and range distributions. In this work we present some of the systematics of the excitation functions for Tb^{149}, Dy^{150}, and Dy^{151}.

First, let us consider the reactions (Hi, xn)Tb^{149}, where HI devotes the heavy-ion projectile. Recently, Macfarlane has found a 4.0-min isomeric state of Tb^{149}.[1] This isomeric state has higher spin than the 4.1-hr ground state and has a very small probability for decay to the ground state.[1] Therefore we can expect the higher-angular-momentum states of the excited Tb compound nuclei to decay predominantly to 4.0-min Tb^{149m} while the lower-angular-momentum states should populate 4.1-hr Tb^{149}. Thus, studies of 4.1-hr Tb^{149} will reflect the properties of the Tb compound nuclei having small angular momenta.

An informative way to compare cross-section data is to plot the fraction of the reaction cross section against the available kinetic energy per nucleon. Such a plot for (HI, xn)Tb^{149} reactions is shown in Fig. C.2-1. We note that these reactions are not very probable (peak cross sections of approx 5 to 0.5% of the total reaction cross section), and that 3 to 4 Mev is the most probable energy released per emitted nucleon. This result is very different from (HI, xn)Dy^{150} and (HI, xn)Dy^{151} reactions. In Fig. C.2-2 we see a similar plot for a typical pair of these latter reactions. These excitation functions peak at about 40% of the total reaction cross section and at 5 to 6 Mev per nucleon. We attribute this very different behavior to effects of angular momentum on the decay of the compound nucleus. The compound nuclei of high angular momentum are probably de-exciting, with much larger energies going into photon emission.[2,3] We are initiating measurements of the angular

---

[1] R. D. Macfarlane, An Alpha-Emitting Isomeric State of Tb^{149} (UCRL-9870, Sept. 1961), submitted to Phys Rev. Letters.

[2] James F. Mollenauer, Effects of Angular Momentum on Gamma-Ray Production in Compound-Nucleus Reactions (thesis), UCRL-9724, July 1961.

[3] John R. MortonIII, Investigation of Nuclear Reactions by Recoil Studies of Radioactive Products (thesis), UCRL-9595, April 1961.
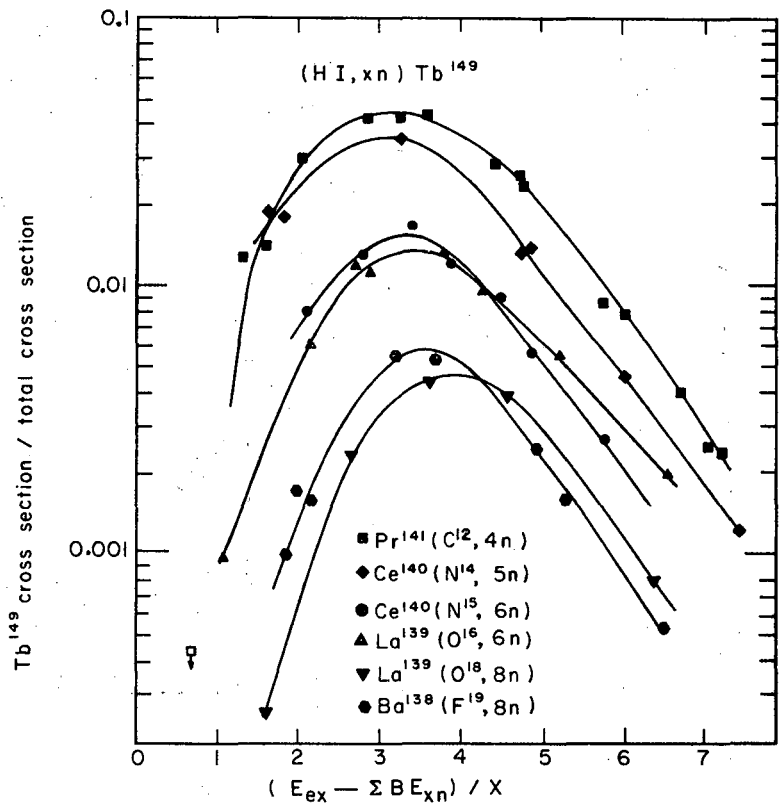
Fig.C.2-1. Fractional cross section for 4.1-hr Tb^{149} from (HI, xn)Tb^{149} reactions as a function of available energy per emitted nucleon.
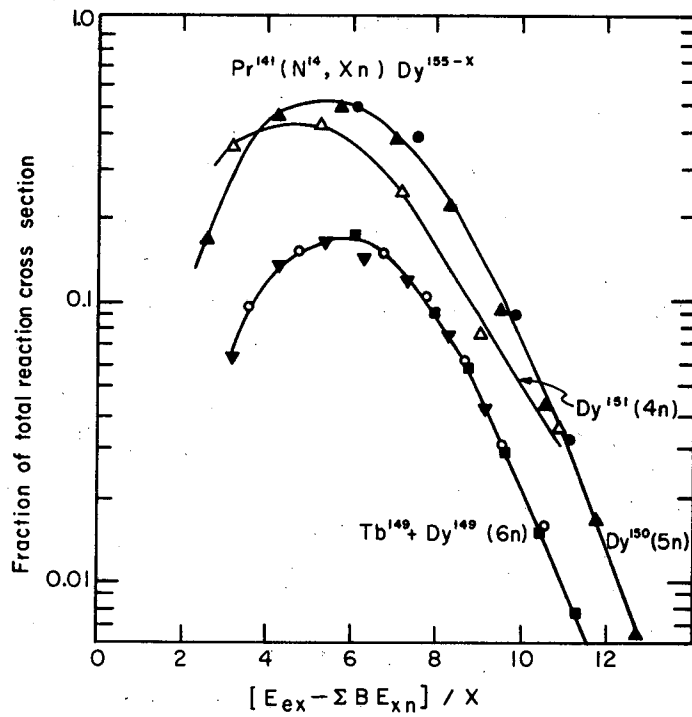
Fig. C.2-2. Fractional cross sections for several products from reactions
    of N^{14} with Pr^{141} as a function of available energy per emitted nucleon.

and range distributions of these products in order to make a more definite energy balance between photons and kinetic energy of emitted nucleons.

It is interesting to compare cross-section data for the same compound nucleus produced by different reactions. Several such comparisons are shown in Figs. C.2-3 through C.2-6. Evidently the angular momentum differences for these different reactions do not drastically alter the decay properties of these excited compound nuclei. Significant differences are observed for the magnitudes but not the energy dependence of these cross sections.

A large body of additional cross section measurements has been obtained. We are in the process of correlating these data and comparing with nuclear evaporation theory.

3. A DETAILED STUDY OF THE COMPOUND NUCLEUS Dy^{156} AT EXCITATION ENERGIES OF 65 to 125 Mev

Gabriel Simonoff and John M. Alexander

In preceding reports we have mentioned several interesting features of heavy-ion nuclear reactions:
  (a) Recoil range data indicate the validity of the compound-nucleus mechanism for a large variety of heavy-ion reactions leading to 4.1-hr Tb^{149}.
  (b) The energetics of the reactions $(HI, xn)Tb^{149}$ and $(HI, xn)Dy^{150}$ and Dy^{151} are very different.
  (c) Different reactions leading to Tb^{149}, Dy^{150}, and Dy^{151} give excitation functions that have almost the same dependence on excitation energy of the compound system.
In this work we produce and study the compound nucleus Dy^{156} by two reactions: $Ce^{140} + O^{16}$ and $Nd^{144} + C^{12}$. The linear and angular momentum given to the compound nucleus by these two projectiles differ significantly. We measure for the products Tb^{149}, Dy^{150}, and Dy^{151} the excitation functions, the average range, R_0; the range straggling, ρ; and the laboratory-system angular distribution, $W(\theta_L)$.

  Each of these measurements has a different dependence on the properties of the compound nucleus. If a compound nucleus is formed, the recoil velocity of the final product can be resolved into two components,
  (a) a velocity component (denoted $\vec{v}$) along the beam direction due to the impact of the heavy ion with the target,
  (b) a velocity component (denoted $\vec{V}$) due to the sum of all recoils from the evaporated particles.
The velocity $\vec{V}$ has an angular distribution $W(\theta)$ that is symmetric about the 9--deg plane in the c.m. system and is expected to show some preference for forward and backward angles, θ(in the c.m. system). If this compound-nucleus mechanism is correct one can show that the following relationships hold to a first approximation in the ratio of the average quantity $\langle V \rangle$ to v.
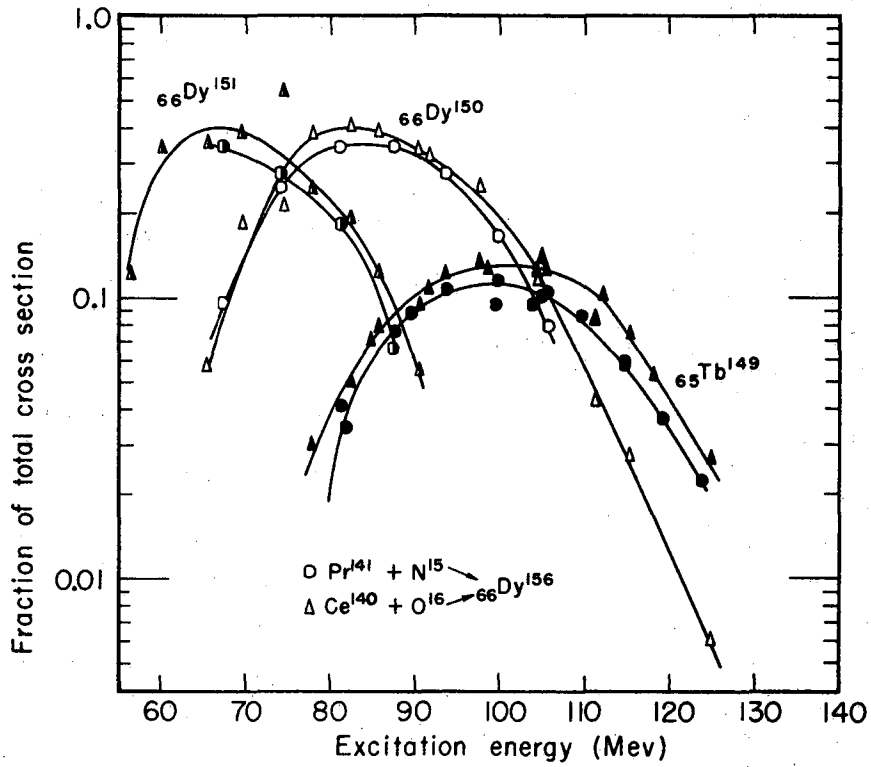
Fig. C.2-3.   Fractional cross sections for several products from Dy^{156} compound nuclei.
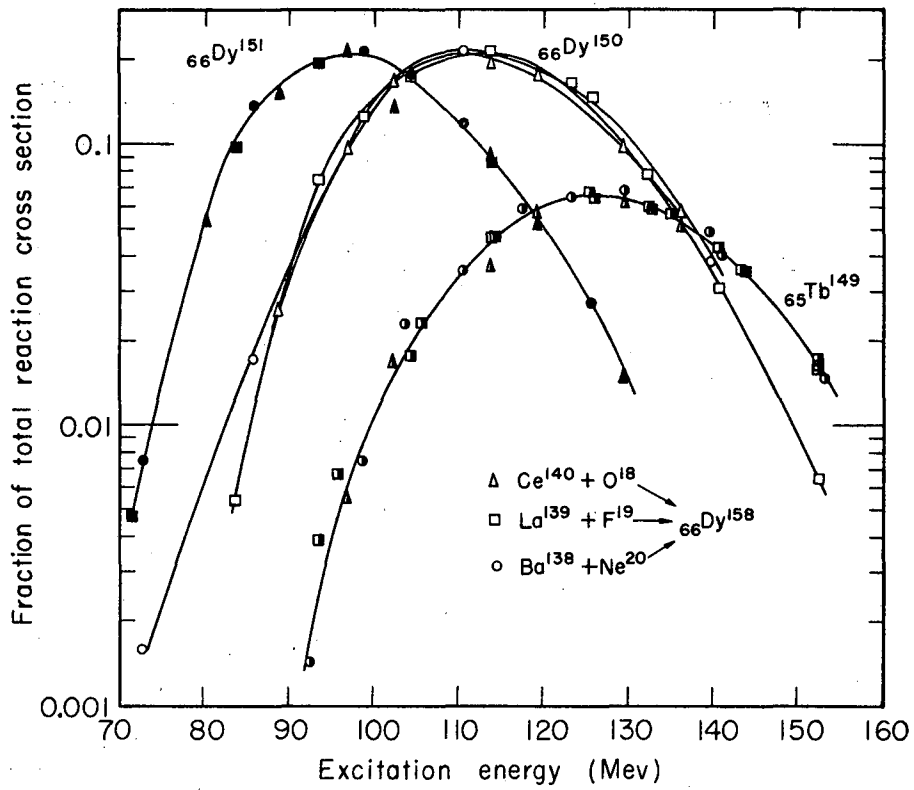
Fig. C.2-4. Fractional cross sections for several products from Dy^{158} compound nuclei.
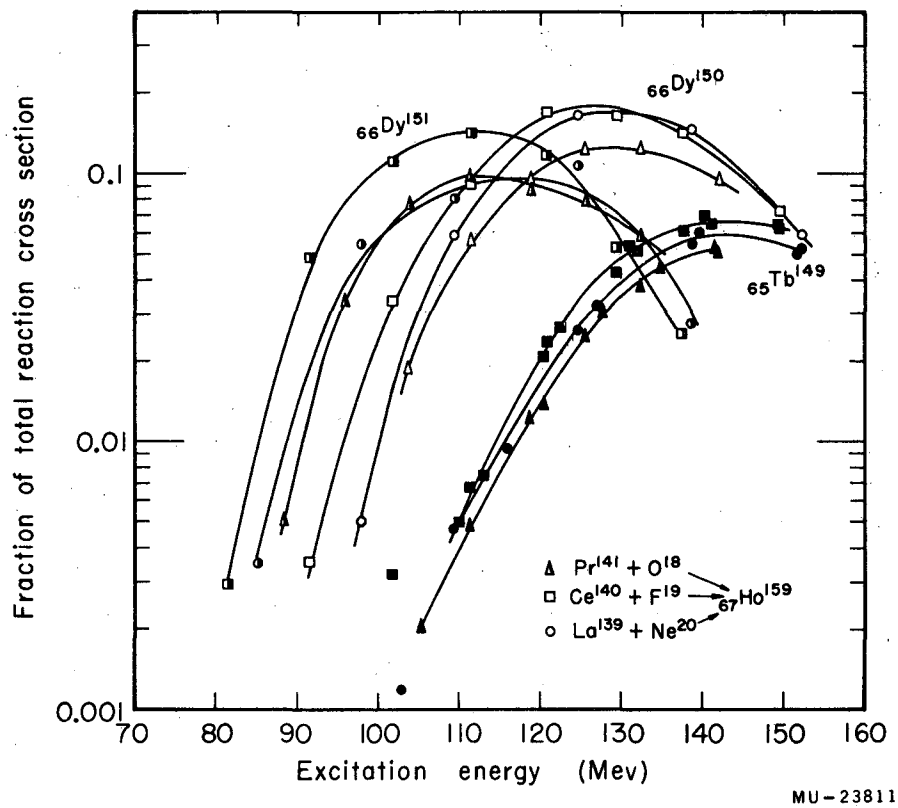
Fig. C.2-5. Fractional cross sections for several products from Ho^{159} compound nuclei.
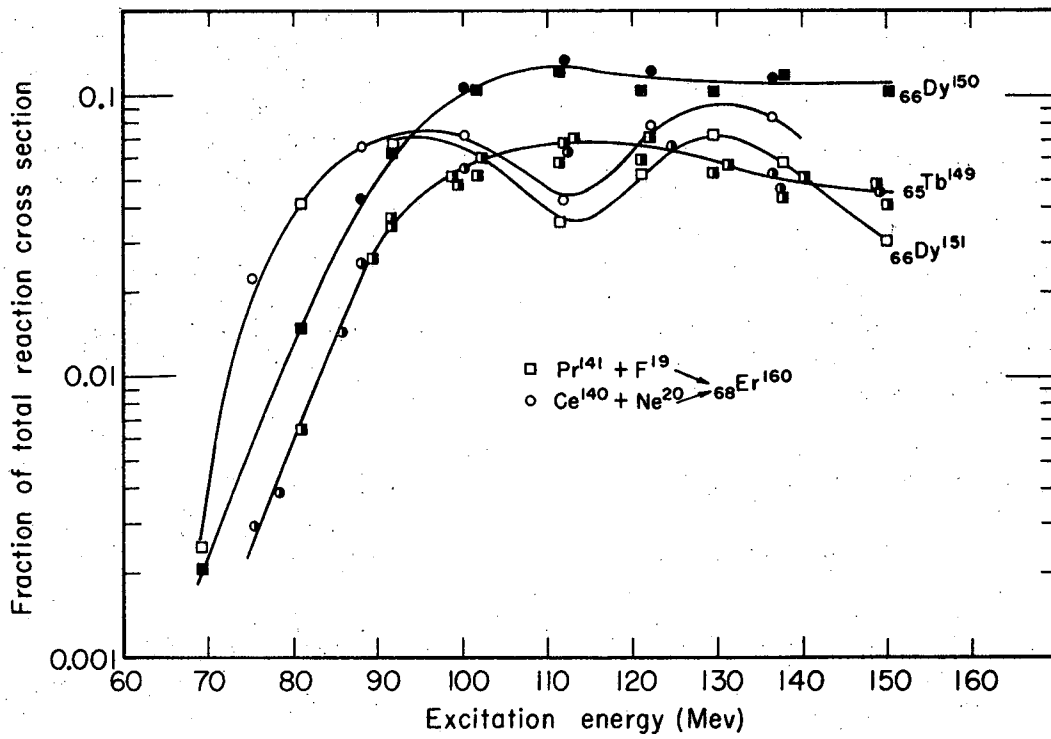
MU-23812

Fig. C.2-6. Fractional cross sections for several products from Er^{160} compound nuclei.

$$\langle R_0 \rangle \approx k v^N \qquad \text{for } W(\theta) = 1 \text{ or } 1/\sin\theta,$$

$$\langle (R-R_0)^2 / R_0^2 \rangle = \rho^2 \approx N^2 \langle v^2 \rangle /3v^2 \quad \text{for } W(\theta) = 1,$$

$$\langle (R-R_0)^2 / R_0^2 \rangle = \rho^2 \approx N^2 \langle v^2 \rangle /2v^2 \quad \text{for } W(\theta) = 1/\sin\theta,$$

$$\langle \theta_L \rangle \approx \pi \langle v \rangle /4v \qquad \text{for } W(\theta) = 1,$$

$$\langle \theta_L \rangle \approx 2 \langle v \rangle /\pi v \qquad \text{for } W(\theta) = 1/\sin\theta.$$

The approximation has been made that $R = k \left| (\vec{v} + \vec{V}) \right|^N$.

From these equations we see that the average range $\langle R_0 \rangle$ is sensitive only to the impact velocity, v (if $W(\theta)$ is symmetric about the 90-deg plane), and therefore provides a measure of the momentum transfer and a severe test of the compound-nucleus mechansim. The range straggling, as characterized by ρ, and the angular distribution, as characterized by $\langle \theta_L \rangle$, are sensitive both to $\langle V \rangle$ and to $W(\theta)$. However, $\langle \theta_L \rangle$ is decreased while ρ is increased by increasing forward-backward preference in $W(\theta)$. Thus the measurement of both ρ and $\langle \theta_L \rangle$ offers a possibility of separating the effects of the magnitude of $\vec{V}$ and of its angular distribution. The magnitude of $\vec{V}$ depends on the division of energy released to photon emission and to kinetic energy of the evaporated nucleons. The excitation functions provide a measure of the energy dependence of the probabilities for various modes of decay (neutron emission, photon emission, etc.) of the compound nucleus. We present these first approximations as a qualitative description only. Actually more detailed evaporation calculations are in progress, using the Monte Carlo method and the IBM 704 computer.

The excitation functions have been measured and are shown in Fig. C.3-1. The recoil range distributions in Al have been measured and are given in the table. In every case the average ranges indicate total momentum transfer and therefore compound-nucleus formation. (Compare with data for Tb^{149}.[1] A preliminary subtraction of straggling due to foil inhomogeneities, target thickness, and stopping phenomena has been made, and the resulting straggling due to the nuclear reaction, ρ_n, is shown. These straggling parameters ρ_n are not very accurate, and it may be necessary to use another experimental technique.

An apparatus has been constructed for measuring angular distributions with approx 1-deg resolution. This apparatus is similar to that used by Harvey et al.,[2] but has considerably improved angular resolution. The values of $\langle \theta_L \rangle$ are expected to be only 3 to 10 deg, and thus this improved angular resolution is necessary. The results of two angular distribution experiments are shown in Fig. C.3-2.

---

[1] This report, C.1.

[2] Paul F. Donovan, B. G. Harvey, and W. H. Wade, Phys. Rev. 119, 218 (1960); B. G. Harvey, W. H. Wade, and Paul F. Donovan Phys. Rev. 119, 225, (1960).
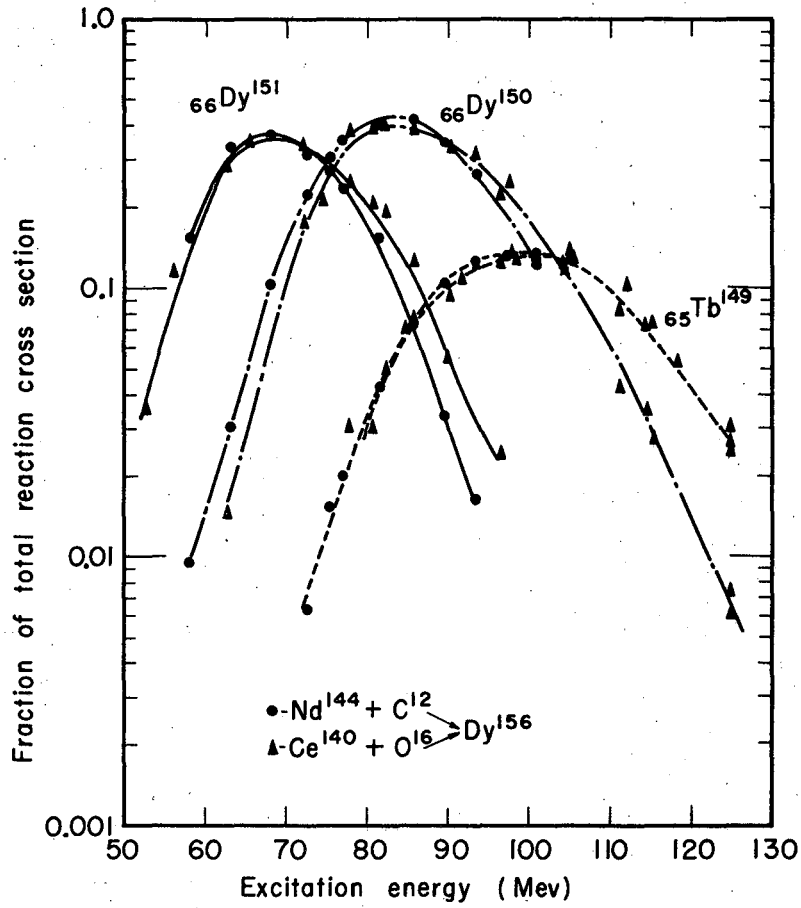
Fig. C.3-1. Fractional cross sections for several products from the
   compound system Dy^{156}.
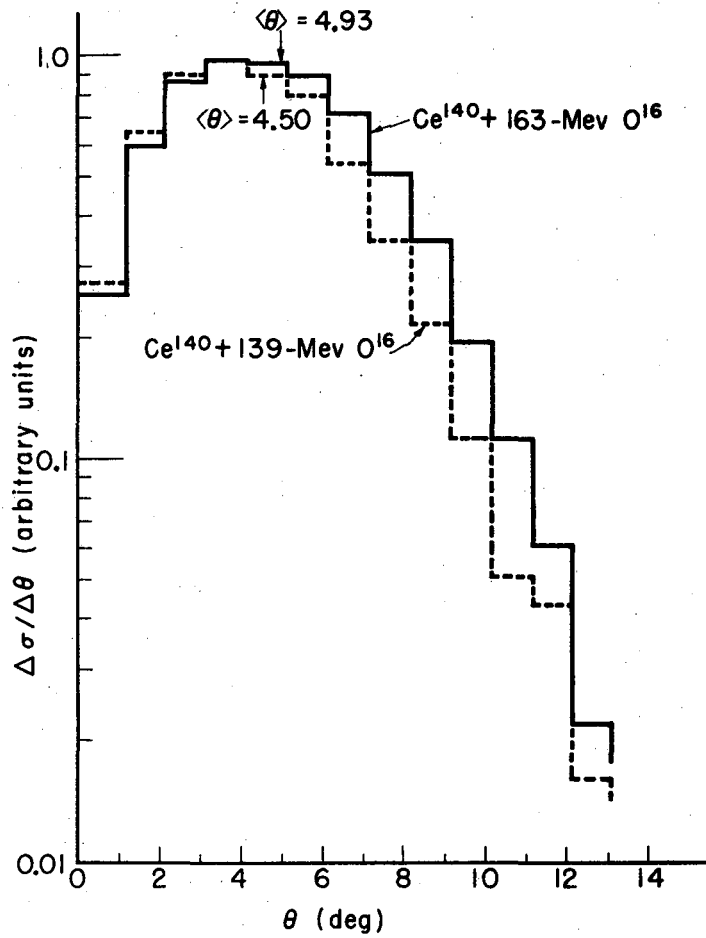
Fig. C.3-2. Angular distributions for $Dy^{149} + Tb^{149}$ from reactions of O^{16} with Ce^{140}.

Recoil range distributions

Reaction	Bombarding energy, E_b (Mev)(lab)	Observed product	Average range, R_0 (mg/cm^2)	Measured straggling parameter, ρ	Nuclear reaction straggling parameter, ρ_n[a]
$Ce^{140} + O^{16}$	146.0	Tb^{149}	.996	.183	$.09 \pm .035$
		Dy^{150}	.991	.190	$.102 \pm .03$
	140.0	Tb^{149}	.953	.186	$.083 \pm .04$
		Dy^{150}	.958	.197	$.105 \pm .03$
	128.1	Tb^{149}	.910	.196	$.089 \pm .033$
		Dy^{150}	.912	.202	$.10 \pm .03$
	112.4	Tb^{149}	.803	.193	≈ 0
	100.4	Dy^{151}	.758	.200	≈ 0
	100.0	Dy^{151}	.730	.196	≈ 0
	88.2	Dy^{151}	.677	.199	≈ 0
$Nd^{144} + C^{12}$	120.5	Tb^{149}	.661	.245	$.082 \pm .03$
		Dy^{150}	.656	.248	$.085 \pm .03$
	95.0	Tb^{149}	.549	.224	≈ 0
		Dy^{150}	.551	.223	≈ 0
		Dy^{151}	.554	.237	≈ 0

a. The value of ρ_n is given only if it is significantly different from zero.

4. A RECOIL STUDY OF THE REACTION $C^{12}(p, pn)C^{11}$

Sarjant Singh and John Alexander

The usual theoretical approach to high-energy nuclear reactions rests on considerations of nucleon-nucleon collisions inside nuclei. Calculations of most experimental observables involve the consideration of a complex spectrum of various kinds of collisions. One of the most direct studies of these collisions is the observation of products of the so-called simple reactions (p, pn), (p, 2p), (p, pπ$^+$), etc. These reactions involve only a small number of collisions and result in residual nuclei with small energies of excitation. Therefore the complexities of the inter-actions are minimized. These simple reactions are, however, sensitive to the individual properties of the target nuclei. Nuclear shell structure, for example, appears to have a significant effect on cross sections for (p, pn) reactions.[1]

At present, the experimental information concerning simple reactions consists mainly of excitation-function measurements for (p, pn) reactions. A few studies of (p, 2p) and (p, pπ$^-$) reactions have been made. In order to gain a more detailed picture of the kinematics of these reactions, measurements of angular and energy distributions are needed. It is very difficult to obtain velocity measurements for protons and neutrons ejected in these simple reactions, because of the occurrence of many reactions that are more complex. However, radiochemical techniques are suitable for observations of the recoil properties of the heavy residual nuclei.

Many different kinds of recoil measurements can be made--each having its own particular experimental difficulties. Most of the experimental difficulties arise from the fact that the recoil energies and ranges of (p, pn) products are expected to be very small (kev region). We have chosen the very simple thick-target integral range technique in order to get an initial survey of some features of the recoil properties of (p, pn) reactions. The reaction $C^{12}(p, pn)C^{11}$ has been selected because a very simple experimental method is possible for this case.

The experimental method consists of exposing a foil stack of thick plastic targets and thick Be catcher foils. The fraction of the C^{11} atoms that recoils from the target into the Be catchers was measured by direct observation of the beta radiation from target and catcher foils. From these measurements we obtain the average components of the recoil range (a) along the beam direction $F_F W$, (b) opposite to the beam direction $F_B W$, and (c) perpendicular to the beam direction $\pi^{-1}4F_p W$. In Fig. C.4-1 we show the energy dependence of these "effective ranges."

We have compared these data with the predictions of several simple reaction mechanisms: (a) neutron evaporation after deposition of a small amount of energy by a single elastic nucleon-nucleon collision, (b) fast reaction consisting of a single inelastic nucleon-nucleon collision. From these comparisons we conclude that neutron evaporation cannot be the major mechanism for any incident energy between 0.25 and 6.2 Gev. The results

---

[1] P. A. Benioff, Phys. Rev. 119, 324 (1960).
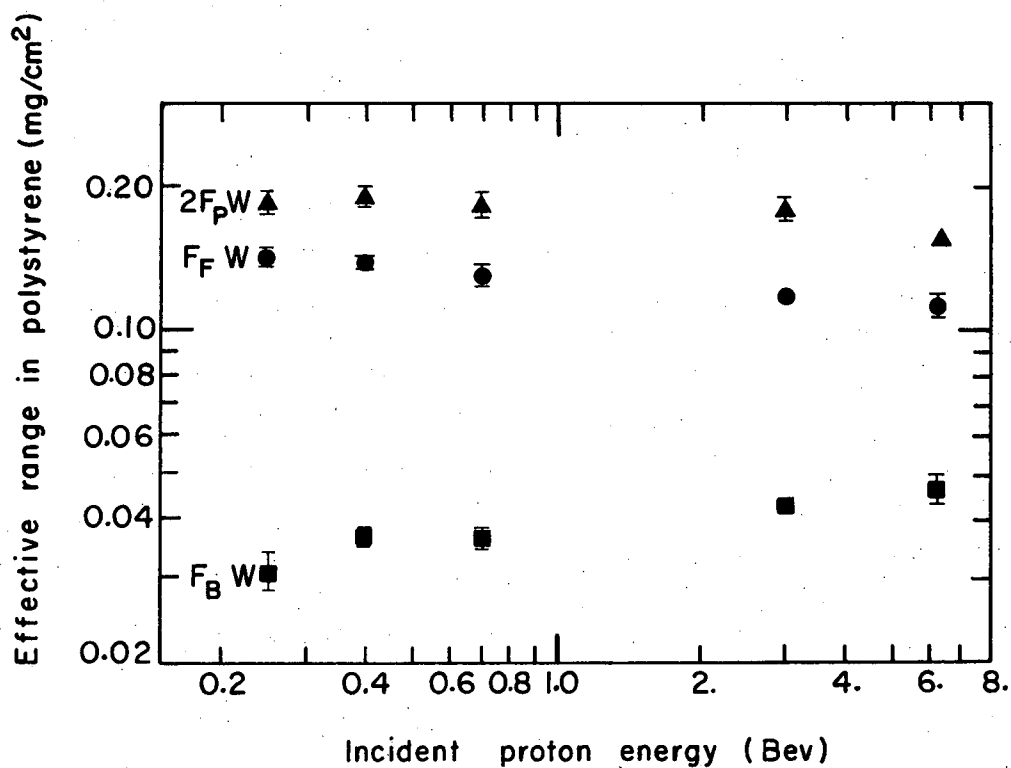
Fig. C.4-1. Effective ranges for C^{11} from $C^{12}(p,pn)C^{11}$.

MU-25283

for 3 and 6.2 Gev are consistent with a fast or "knock-on" reaction consisting of a single inelastic nucleon-nucleon collision. If this mechansim is assumed, an average kinetic energy of 19 Mev can be deduced for the struck neutron (before the collision) in the C^{12} nucleus.

5. THE REACTION N^{15} $(a, d)O^{17}$

Joseph Cerny and Bernard G Harvey

The reaction $N^{15}(a, d)O^{17}$ has been investigated by bombarding gaseous, 94.6% enriched N^{15} obtained from the Isomet Corporation with 48-Mev helium ions from the Crocker Laboratory 60-inch cyclotron. The deuterons were detected and identified by means of an E -dE/dx counter telescope system operated in conjunction with a pulse multiplier. The dE/dx component was a diffused-junction silicon detector and the E component was first a NaI(Tl) crystal and later a lithium-drifted semiconductor. A typical multiplier spectrum showing the separated p, d, and t peaks is given in Fig C.5-1. Figure C.5-2 shows an energy spectrum of the emitted deuterons; a comparison of the states observed in this reaction with those previously reported[1] again illustrates that the (a, d) reaction is fairly selective in populating final states.

Deuteron groups from transitions to the ground, 0.87-Mev, and 3.85-Mev levels of O^{17} were separately resolved. These three levels are expected to arise primarily from the coupling of a 1 $d_{5/2}$, a 1 $s_{1/2}$, and a 1 $f_{7/2}$ neutron, respectively, to an O^{16} core.[2] Since the formation of these states in an (a, d) reaction involves the capture of a $p_{1/2}$ proton and a $d_{5/2}$, $s_{1/2}$, or $f_{7/2}$ neutron, respectively, it is interesting to compare their statistically weighted cross sections. The absolute cross section of the ground-state transition integrated from 11 to 102 deg (c.m.) is 1.1_8 mb, which is expected to be accurate to ±10%. After background subtraction, the statistically weighted cross sections to the 0.87- and 3.85-Mev levels are as follows relative to the statistically weighted ground-state cross section:

$$\frac{\sigma_J (0.87)}{\sigma_J (g \cdot s.)} = 0.58, \qquad \frac{\sigma_J (3.85)}{\sigma_J (g \cdot s.)} = 0.12.$$

These results indicate that the cross sections for stripping particles across shells onto a N^{15} core vary in the following manner:

$$\sigma_J (d_{5/2} \ p_{1/2} \ \text{capture}) > \sigma_J (p_{1/2} \ s_{1/2} \ \text{capture}) > \sigma_J (p_{1/2} \ f_{7/2} \ \text{capture}).$$

Apparently stripping across shells becomes less likely with increasing energy separation of the shells into which the particles are captured.

[1] J. Cerny, B. G. Harvey, and R. H. Pehl, Nuclear Phys. 29, 120 (1962)

[2] E. L. Keller, Phys. Rev. 121, 820 (1961).
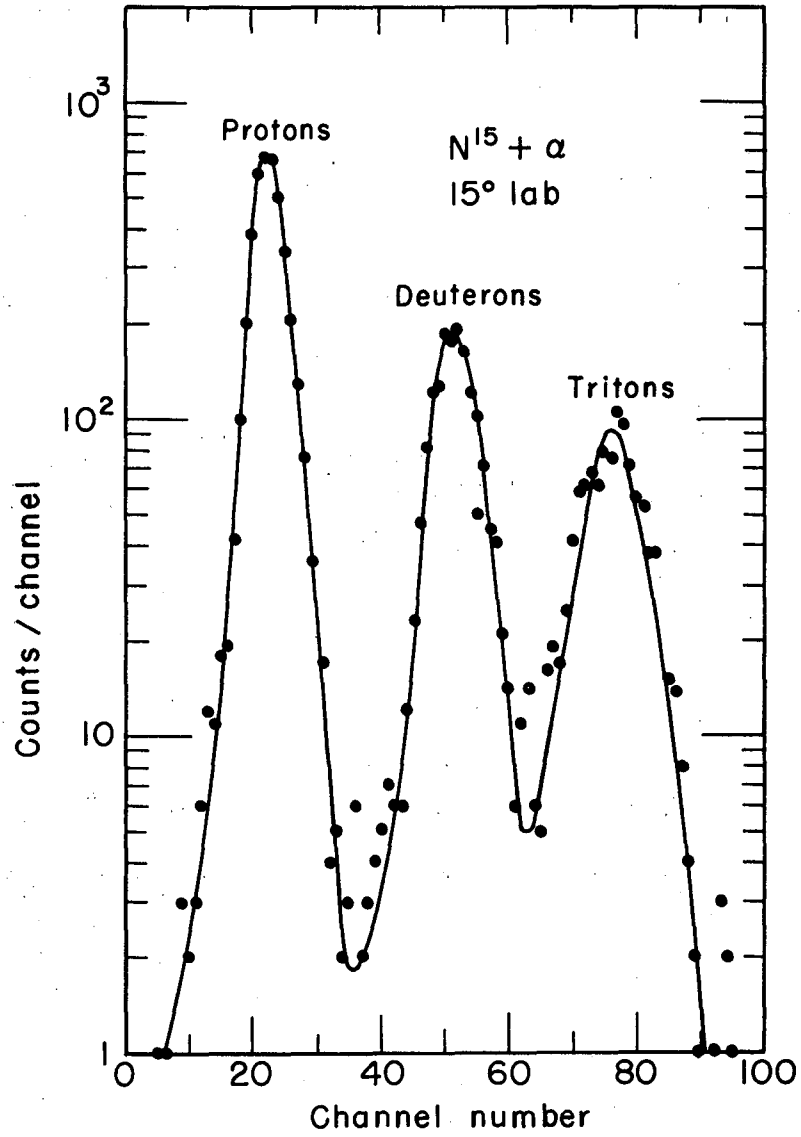
Fig. C.5-1. Multiplier spectrum from bombardment of N^{15} with 46.5-Mev helium ions.
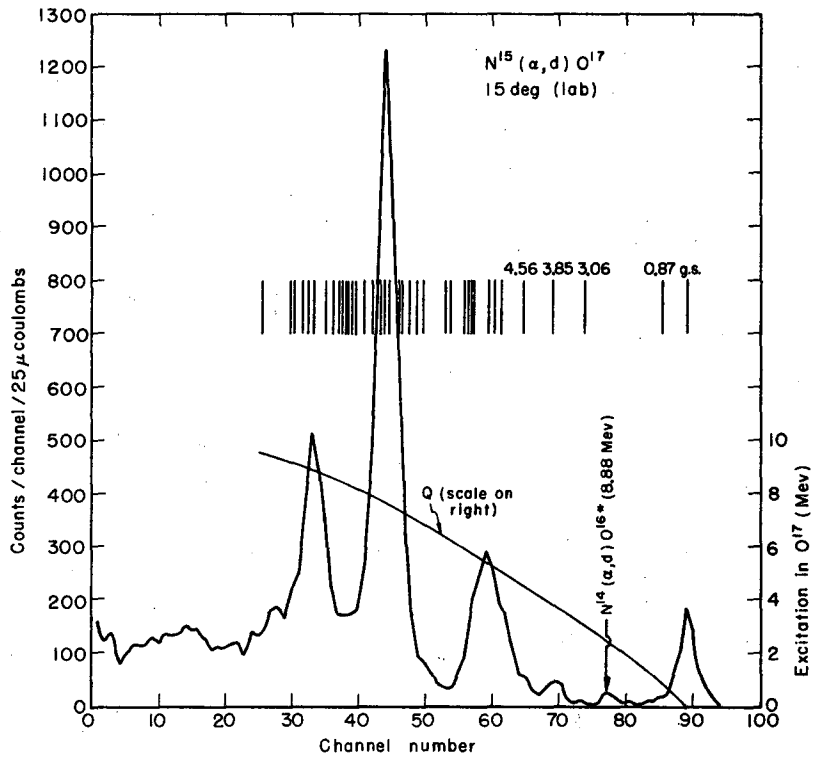
MU-23782

Fig. C.5-2. Deuteron energy spectrum from the reaction $N^{15}(\alpha, d)O^{17}$. Q values for the various peaks are shown.

Figure C.5-3 shows the angular distribution of the deuterons from the $N^{15}(\alpha, d)O^{17}$ (g. s.) transition. In analyzing these results by using the Glendenning two-nucleon stripping theory,[3] two different final states were assumed in order to determine whether a unique fit was possible. The expected shell-model transition

$$\left[(core)_0 + p_{1/2} \right]_{1/2-} \longrightarrow \left[(core)_0 + (p_{1/2})^2_{J=0} (d_{5/2}) \right]_{5/2+} ,$$

which allows the neutron and proton to be captured with total orbital angular momentum (L) values of 1 and 3, was one of these; the other transition was

$$\left[(core)_0 + p_{1/2} \right]_{1/2-} \longrightarrow \left[(core)_0 + (p_{1/2})^2_{J=0} (s_{1/2}) \right]_{1/2+} , \quad L = 1 \text{ only},$$

which assumes, solely for the comparison, that the $s_{1/2}$ level lies lower than the $d_{5/2}$ level in O^{17}. However, reasonably good fits were obtained for both configurations; the fit from the expected shell-model transition is shown in Fig. C.5-3. This again[1] indicates that no spectroscopic identification of unknown final states would be possible at these high momentum transfers.

---

[3]N. K. Glendenning, Nuclear Phys. **29**, 109 (1962).

6. A TWO-NUCLEON STRIPPING ANALYSIS
OF THE $C^{12}(He^3, p)N^{14}$ REACTION

Ernest Rivet, Joseph Cerny, Bernard G. Harvey, and Richard H. Pehl

The 31.2-Mev He^3 beam of the Berkeley Hilac has been used to investigate the two-nucleon transfer reaction $C^{12}(He^3, p)N^{14}$. Proton energy spectra were recorded in NaI(Tl) crystals and lithium-diffused semiconductors: both counters were preceded by sufficient absorber to stop all shorter-range reaction products. A typical energy spectrum from the semiconductor counter is shown in Fig. C.6-1. These $C^{12}(He^3, p)N^{14}$ spectra are remarkably similar to the $C^{12}(\alpha, d)N^{14}$ spectra obtained earlier,[1] except that for the (He^3, p) reaction $\Delta T = 1$ transitions are not forbidden. The absence of transitions to the 7.40- and 7.60-Mev levels in both reactions is in agreement with the prediction of True[2] that these levels arise from core excitation of the target nucleus, since no known core-excited states have been observed in any of our (α, d) investigations.

Angular distributions of protons from transitions to the ground, 2.31-Mev, and 3.95-Mev states have been obtained. These data and those of Priest et al.[3] at 13.9 Mev have been compared with the Glendenning two-nucleon

---

[1]B. G. Harvey and J. Cerny, Phys. Rev. **120**, 2162 (1960).

[2]W. W. True (University of California, Davis), private communication.

[3]J. R. Priest, D. J. Tendam, and E. B. Bleuler, Phys. Rev. **119**, 1295 (1960).
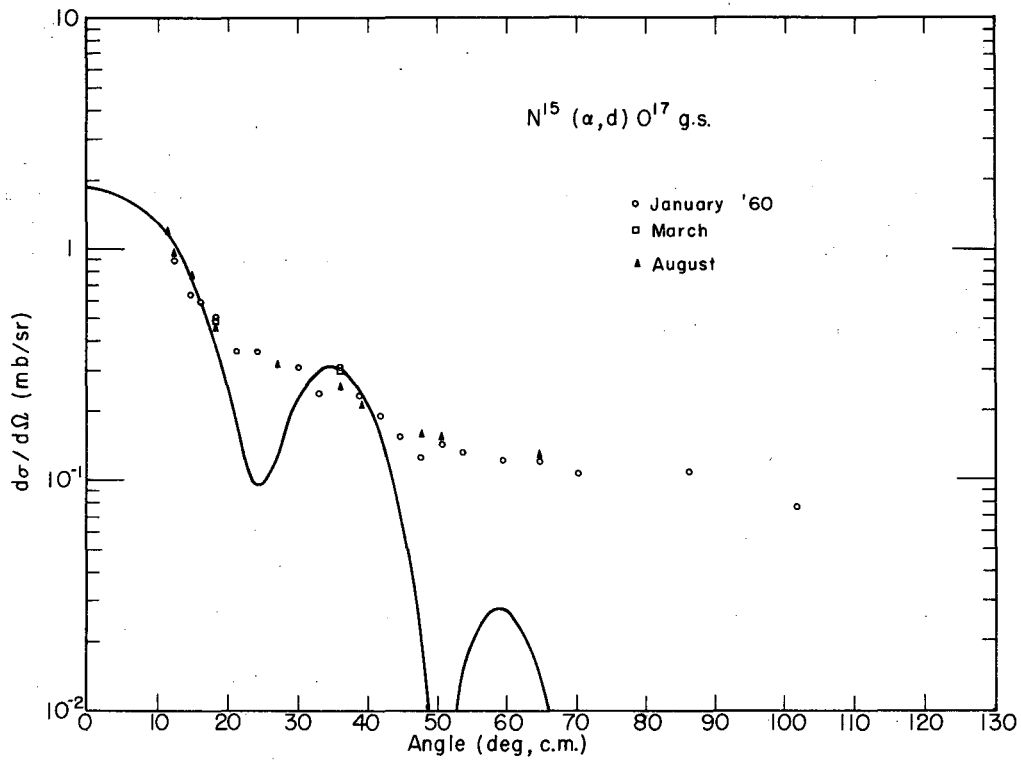
Fig. C.5-3. Angular distribution of deuterons from formation of the ground
state of O^{17}. The solid line was calculated from the Glendenning equation
by using $j_n = 5/2$, $j_p = 1/2$, $R_0 = 6.0$ fermis.
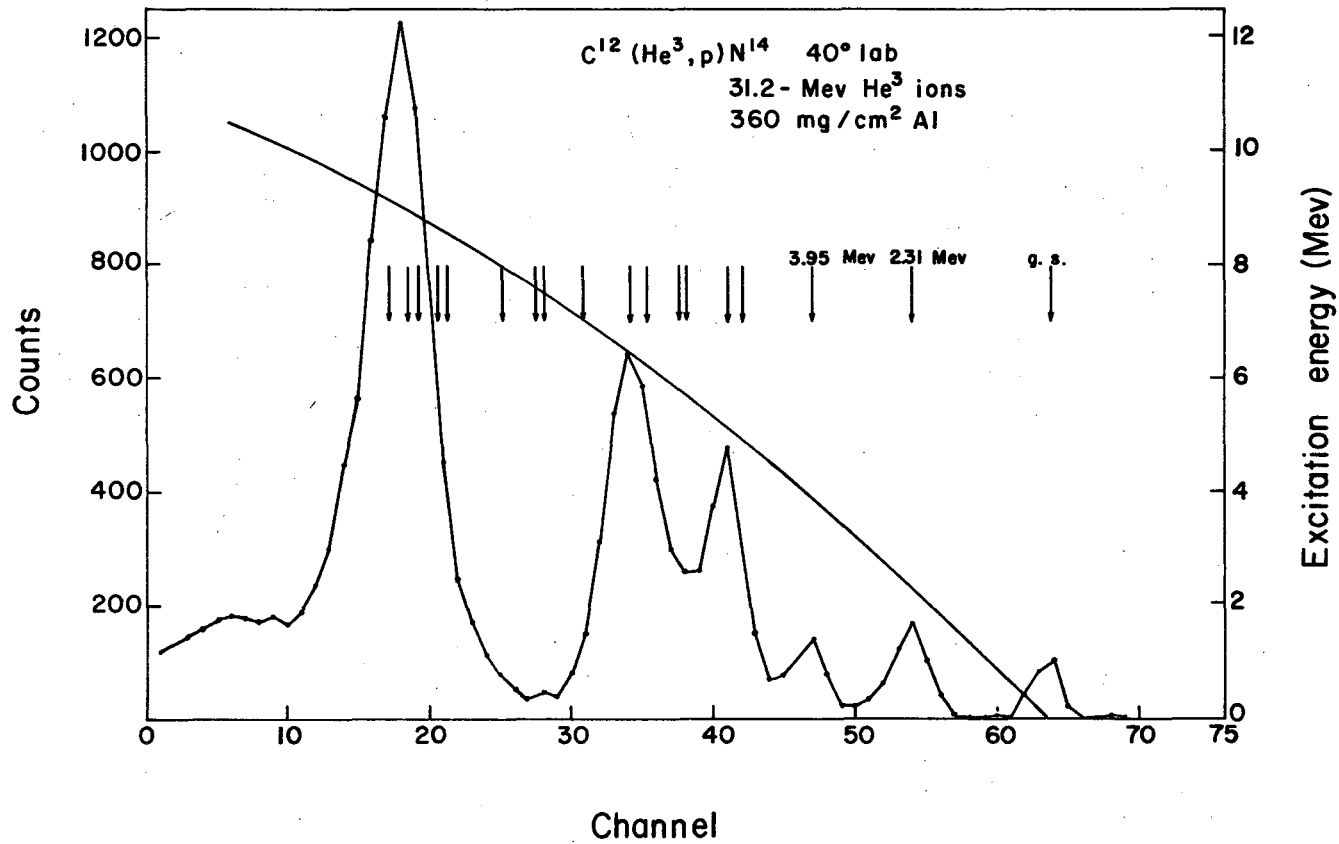
Fig. C.6-1. Proton energy spectrum from the reaction $C^{12}(He^3, p)N^{14}$.
Q values for the various peaks are shown.

MUB-880

stripping theory.[4] Since this theory was initially formulated for (α, d) reactions, some modification has been required[5] to make it applicable to (He^3, p) reactions; the major change is that the nuclear structure factors now account for the fact that the captured particles can go into signlet as well as triplet states. The differential cross section for reactions on an even-even target is given by

$$\frac{d\sigma}{d\Omega} \propto e^{-\kappa^2/4\gamma^2} \sum_L \frac{C_L}{2L+1} \left| B(\ell_n \ell_p L; Q) \right|^2 ,$$

where

$$C_L = \sum_{S=0}^{1} (a_{LSJ_f})^2 ,$$

$$B(\ell_n \ell_p L; Q) = \sum_{n=0}^{\infty} (-1)^n (2n+1) I_{n+1/2} (3\gamma^2 R_0^2) \sum_{\lambda_n = |\ell_n - n|}^{\ell_n + n, 2}$$

$$\times \sum_{\lambda_p = \max(|\ell_p - n|, |L - \lambda_n|)}^{\min(\ell_p + n, L + \lambda_n), 2} J_{\lambda_n}(QR_0/2) J_{\lambda_p}(QR_0/2) \sqrt{(2\lambda_n + 1)(2\lambda_p + 1)}$$

$$\times i^{\lambda_n + \lambda_p} W(\ell_n \ell_p \lambda_n \lambda_p; Ln) C_{0\ 0\ 0}^{\lambda_n \lambda_p L} C_{0\ 0\ 0}^{l_n n \lambda_n} C_{0\ 0\ 0}^{l_p n \lambda_p} .$$

All the symbols are defined elsewhere.[6]

    In order to fit adequately the experimental angular distributions, it was necessary to introduce a radius parameter for the He^3, R_{He3}, which was greater than that used for the He^4 in the (α, d) analysis. A value of R_{He3} of 1.61 f has been used, although any value between 1.45 and 1.90 f would give approximately the same overall agreement. This trend is in accord with our expectations, since the more loosely bound He^3 would be expected to possess fewer high-momentum components in its wave function. The transitions to the ground and 3.95-Mev states of N^{14} are both $0+ \longrightarrow 1+$, so that conservation of angular momentum and parity permits $L = 0, 2$ capture for both. However, the ground-state transition is expected to possess a dominant $L = 2$ component

[4] N. K Glendenning, The Two-Nucleon Stripping Reaction, Nuclear Phys. (in press).

[5] Norman K. Glendenning (lawrence Radiation Laboratory, Berkeley), private communication.

[6] J. Cerny, Two-Nucleon Transfer Reactions in the Light Elements (thesis), UCRL-9714, May 1961.

(well represented by $(p_{1/2})^2$ capture), whereas the transition to the 3.95-Mev state should possess a dominant L = 0 component [the nuclear structure factors for this can be represented by $(d_{5/2})^2$ or $(s_{1/2})^2$ capture].[6]

The $(p_{1/2})^2$, $(d_{5/2})^2$, and $(s_{1/2})^2$ capturing configuartions were tried in attempting to fit the experimental angular distributions of these two states at both bombarding energies. The 13.9-Mev data were acceptably fitted only as predicted. At 31.2 Mev, though, the fits to the angular distributions did not follow these predictions: the ground-state transition required a dominant L = 0 configuration rather than the expected L = 2, and the 3.95-Mev transition could be fitted by all three configurations. Although the latter result is to be expected as the momentum transfer increases, the former is anomalous and is not understood at present. Figures C.6-2 and C.6-3 show the angular distributions and fits to the ground-state transition at both energies.

The transition to the 2.31-Mev state, $0+ \longrightarrow 0+$, permits L = 0 capture only. Quite acceptable fits were obtained at both energies for $(p_{1/2})^2$ capture. Figure C.6-4 shows the experimental angular distribution and fit at 31.2 Mev bombarding energy.

7. INVESTIGATION OF ISOBARIC-SPIN CONSERVATION IN THE $O^{16}(d, a)N^{14}$ REACTION USING A HIGH-RESOLUTION SEMICONDUCTOR E - dE/dx SYSTEM

Richard H. Pehl, Joseph Cerny, and Bernard G. Harvey

An advance in thin semiconductor detector design[1] has enabled us to obtain very low backgrounds in an investigation of the effects of angular momentum and parity conservation and isobaric-spin conservation in restricting $0+$, $T = 0 \longrightarrow 0+$, $T = 1$ (d, a) transitions. An upper limit for the ratio of the cross section for the $O^{16}(d, a)N^{14}$ * (2.31-Mev) $0+$, $T = 1$ transition to the cross section for the $O^{16}(d, a)N^{14}$ ground-state transition with 24-Mev incident deuterons of $0.7 \pm .6\%$ has been obtained.

This 0.0025-inch detector was incorporated as the dE/dx component in a counter telescope; the E component was a 0.0165-inch diffused-junction silicon detector which has been described previously.[2] Pulses from these detectors were used to operate a pulse multiplier, in order to separate the a particles from other reaction products. A typical multiplier spectrum is shown in Fig. C.7-1a. Multiplied pulses corresponding to a particles were then used to trigger a RIDL 400-channel pulse-height analyzer which recorded the energy spectrum of the a particles. A block diagram of the electronics is shown in Fig. C.7-1b. The experimental apparatus and general techniques have been described previously.[2]

---

[1] J. H. Elliott and R. H. Pehl, A Thin Semiconductor Transmission-Counter System for Nuclear Particle Detection, to be submitted to Rev. Sci. Instr.

[2] J. Cerny, B. G. Harvey, and R. H. Pehl, (a, d) Reactions on Odd-Odd Targets Nuclear Phys. (in press).
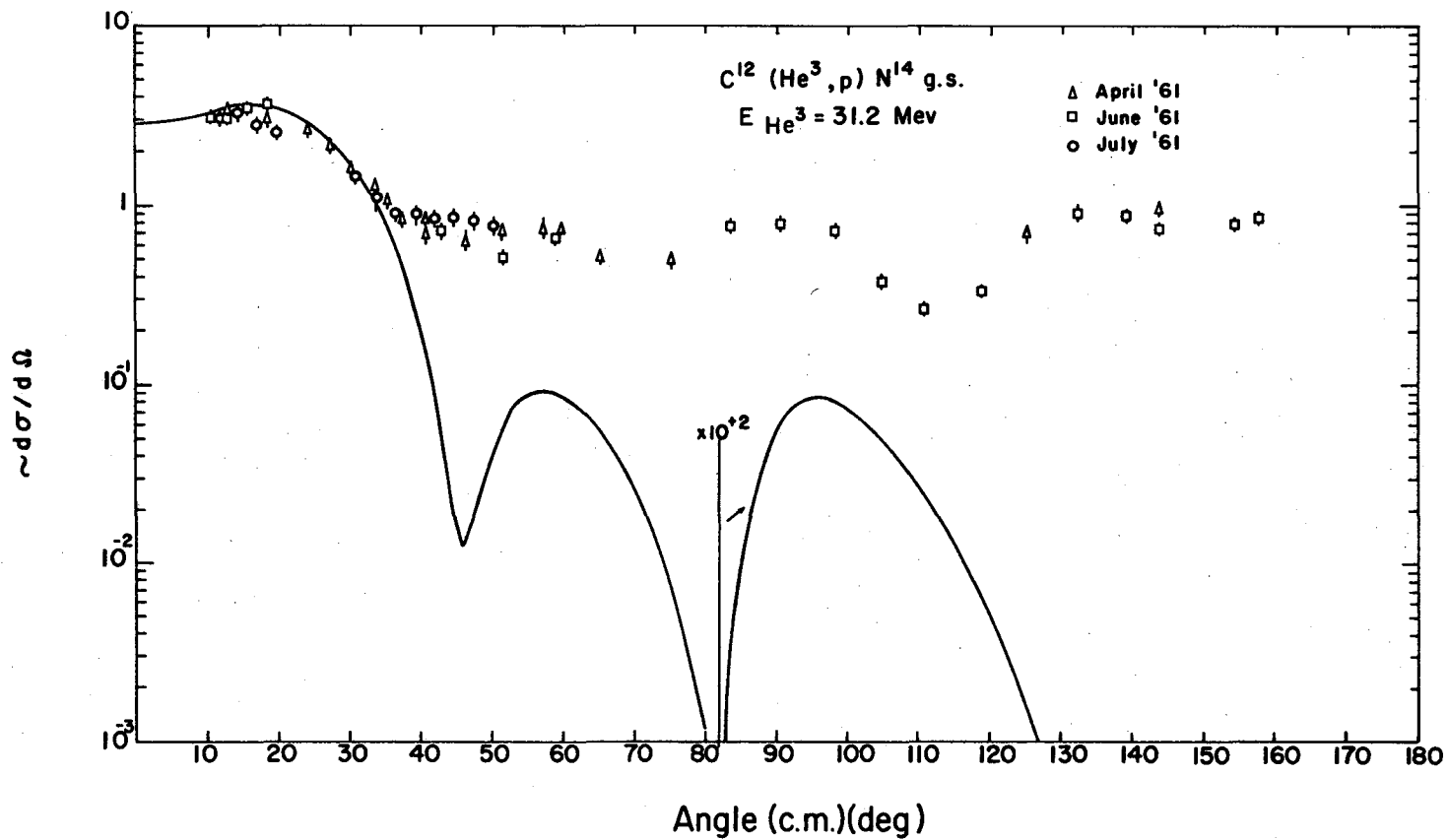
Fig. C.6-2. Angular distribution of protons from the $C^{12}(He^3, p)N^{14}$ (g.s.) reaction with 31.2-Mev He^3. The solid line was calculated from the Glendenning equation by using $(d_{5/2})^2$ capture, $R_0 = 5.1$ fermis.
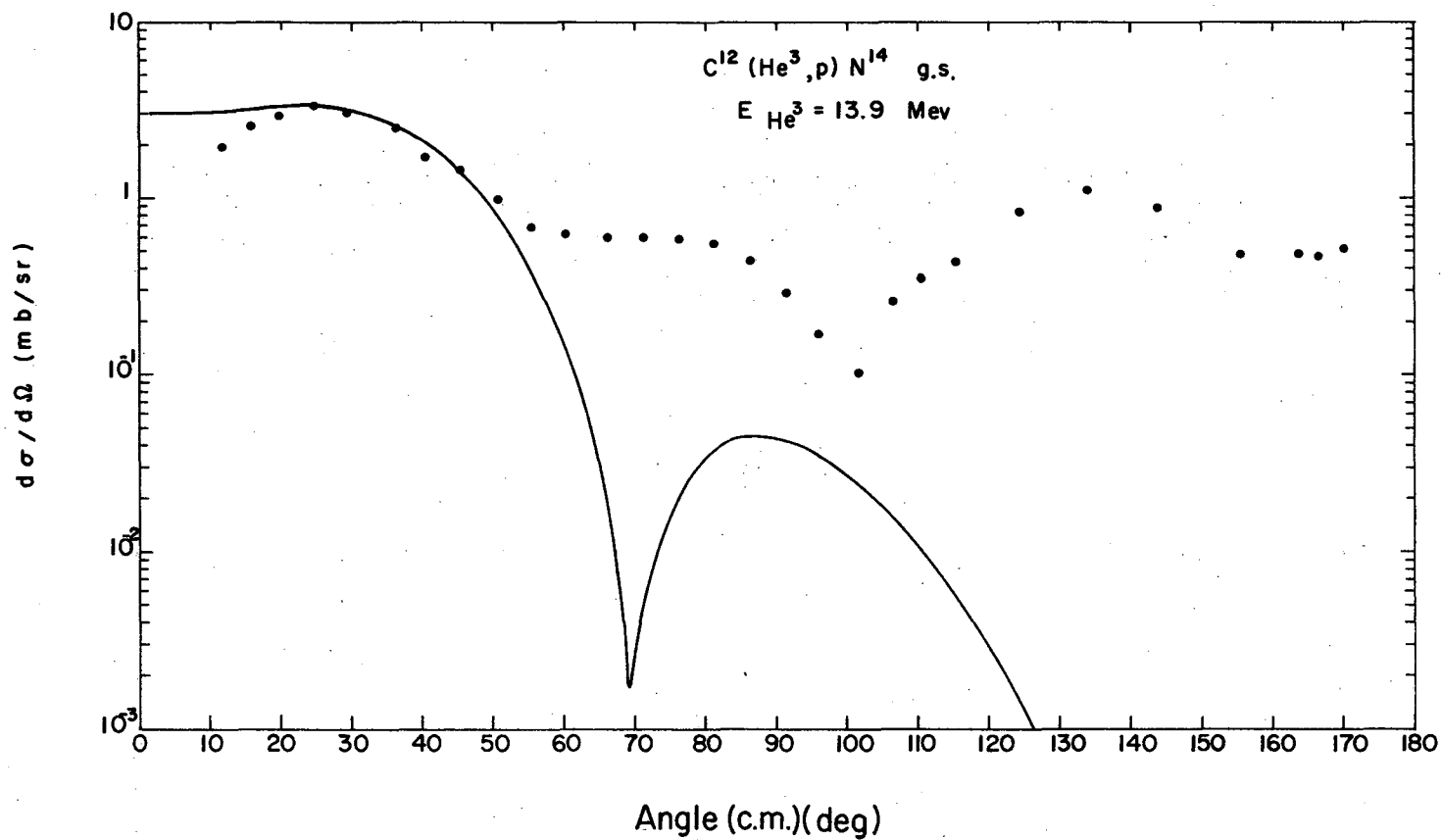
Fig. C.6-3. Angular distribution of protons from the $C^{12}(He^3, p)N^{14}$ (g. s.) reaction with 13.9-Mev He^3. The solid line was calculated from the Glendenning equation by using $(p_{1/2})^2$ capture, $R_0 = 5.5$ fermis.
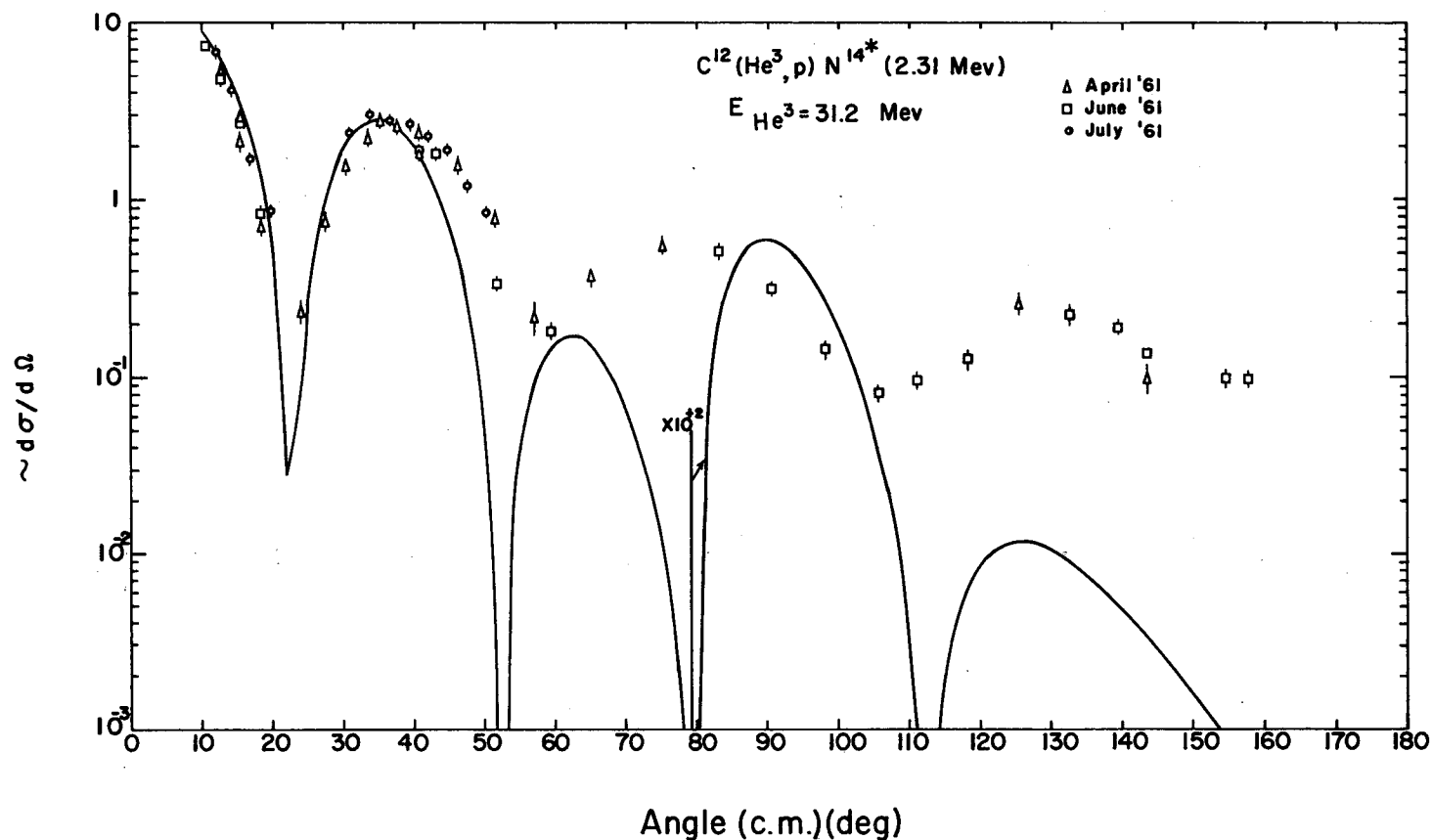
Fig. C.6-4. Angular distribution of protons from the $C^{12}(He^3, p)N^{14}$ (2.31-Mev) reaction with 31.2-Mev He^3. The solid line was calculated from the Glendenning equation by using $(p_{1/2})^2$ capture, $R_0 = 7.2$ fermis.

Fig. C.7-1. (a) Typical multiplier spectrum with 24-Mev deuterons.
(b) Block diagram of the electronics.

(a)

1000
900
800   ↑5000
700   ←Charge I particles   Charge 2 particles
600   (predominantly He⁴)
500
400
300
200
100
0   10 20 30 40 50 60 70 80 90 100

Counts per channel

Channel number

(b)

Scattering- chamber area   Counting area

RIDL
pulse-height analyzer

Incident particles

Diffused-junction silicon detector

E counter

Silicon detector

d E/dx counter

PA
Preamplifier

PA

70 ft
RG 58
cable

DD2

DD2

Double-differentiating linear amplifiers

DD2

DD2

Los Alamos
pulse
multiplier

Cathode
follower

Mod. VI
Linear
amplifier

Pulse adder

1000 Ω

1000 Ω

E + d E/dx pulse

Mod. VI

Upper
and
lower
discr.

Trigger pulse
only for alphas

Signal
for analysis

400-
channel
pulse-
height
analyzer

MUB-893

UCRL-10023

The resolution (FWHM) in the (d, α) experiments was 1.1% when a carbon target, approx 0.3 mg/cm^2, was used (a $C^{12}(d, \alpha)B^{10}$ spectrum is shown in Fig. C.7-2a. The resolution was limited by the approximately 0.8% energy spread in the cyclotron beam.

The $O^{16}(d, \alpha)N^{14}$ reaction was investigated, using a gas target, in the angular range from 13° to 61°. A typical energy spectrum is shown in Fig. 2b. The 1.8% energy resolution is well accounted for by the beam spread plus the target thickness. At no angle does an α-particle group corresponding to the $O^{16}(d, \alpha)N^{14}$ * (2.31-Mev) transition appear. After background subtraction, we are able to set an upper limit of 0.7 ± .6% for the cross section to this state relative to that to the ground state.

Since (d, α) 0+, T = 0 $\longrightarrow$ 0+, T = 1 direct-reaction transitions are forbidden by both angular momentum and parity conservation and by isobaric spin conservation,[3] it is likely that any observed transitions to the 2.31-Mev state would occur through a compound-nucleus reaction. At high excitation, as arises under our experimental conditions, the states of the compound nucleus are expected to possess a low "effective" i-spin impurity;[4] in addition, the initial and final states of this reaction have been calculated to possess small impurities.[5] Thus a very low cross section for the $O^{16}(d, \alpha)N^{14}$ * (2.31-Mev) transition could possibly be observed.

Although our result is in agreement with this prediction, two additional effects should be included in this analysis, both of which tend to increase the upper limit for the relative cross section observed. First, only the compound-nucleus contribution to the ground state should be included in this comparison, and second, correction should be made for the fact that compound-nucleus 0+, T = 1 $\longrightarrow$ 0+, T = 1 (d, α) transitions are also significantly reduced by restrictions arising from angular momentum and parity conservation.[6]

---

[3] B. G. Harvey and J. Cerny, Phys. Rev. 120, 2162 (1960).

[4] D. H. Wilkinson, Phil. Mag. [8] 1, 379 (1956).

[5] W. M. Macdonald, Nuclear Spectroscopy, Part B F. Ajzenberg-Selove, Ed. (Academic Press, New York and London, 1960), p. 932.

[6] Y. Hashimoto and W. Parker Alford, Phys. Rev. 116, 981 (1959).

8. ELASTIC SCATTERING OF C^{12} (*)

Jonas Alster[†] and H. E. Conzett

Differential cross sections for the elastic scattering of 124.5-Mev C^{12} ions on Fe, Ni, Ag^{107}, Ir, and Ta have been measured. Because of its short de Broglie wave length and its large absorption (i.e., any transition out of the entrance channel), the heavy ion is an ideal probe for investigating nuclear surfaces. That is, it satisfies the requirements for a straightforward diffraction-theory treatment of elastic scattering. There, one works directly with partial-wave scattering amplitudes, and from them derives information concerning the nuclear surface, with no reference to the concept of an

---
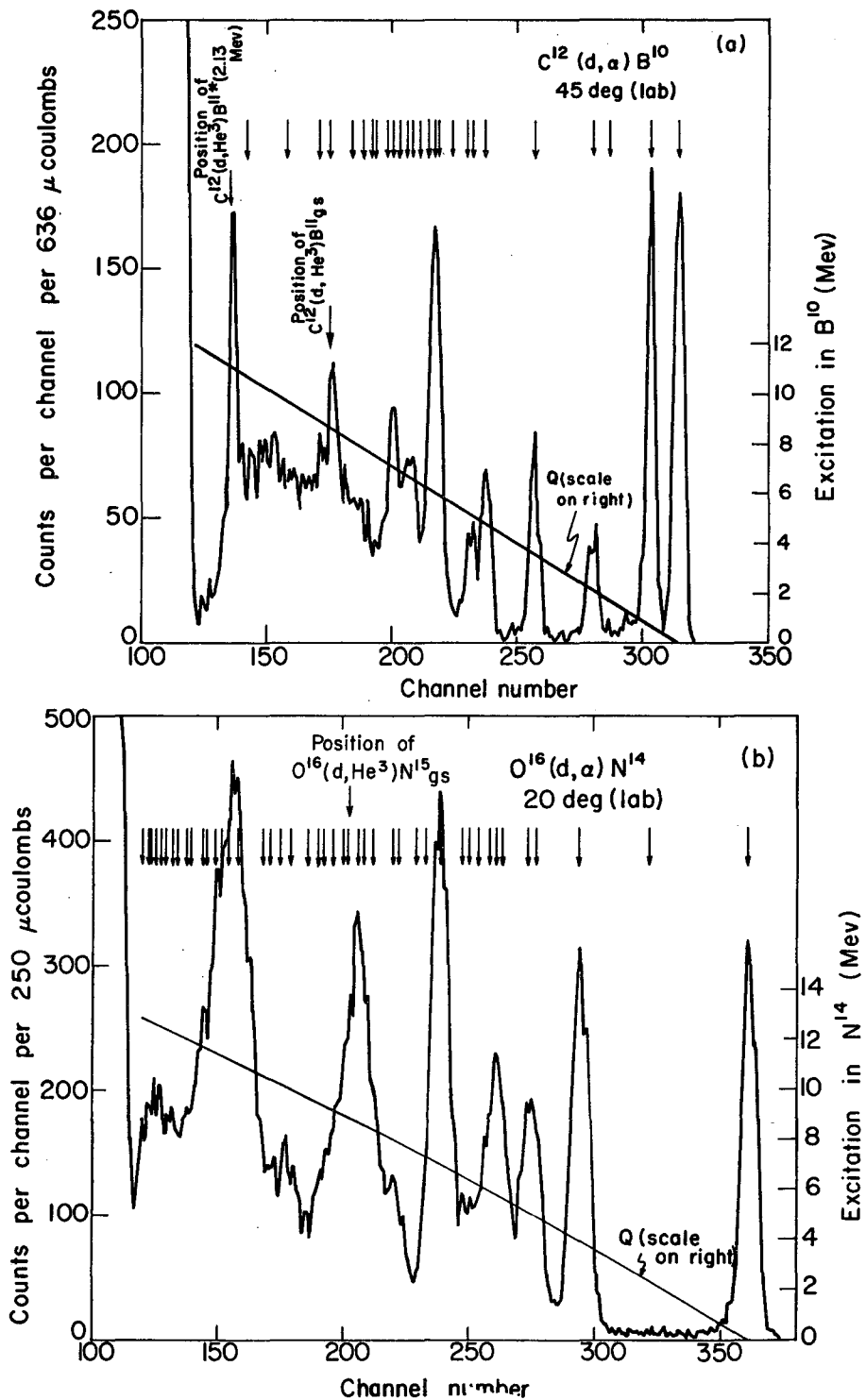
Fig. C.7-2. (a) Alpha energy spectrum from the reaction $C^{12}(d,\alpha)B^{10}$.
Q values for the various peaks are shown. Arrows indicate the
positions of known levels.
(b) Alpha energy spectrum from the reaction $O^{16}(d,\alpha)N^{14}$.

interaction potential. The sharp-cutoff model[1] assumes that the amplitude, A_ℓ, of the ℓth outgoing partial wave is zero for $\ell \leq \ell_A$, where $\hbar[\ell_A(\ell_A+1)]^{1/2}$ is taken to be the orbital angular momentum of the projectile which classically can just reach the nuclear interior. Thus, there is complete absorption of these partial waves. For $\ell > \ell_A$, the A_ℓ are taken to be those for Coulomb scattering, for which there is no nuclear absorption. The "fuzzy"-cutoff treatment[2,3] more realistically describes the change from complete absorption to no absorption as occurring over a number of partial waves. Also, a real phase shift, δ_ℓ, resulting from the nuclear interaction, is taken into account. Thus, A_ℓ and δ_ℓ are given by

$$A_\ell = \{1 + \exp[(\ell_A - \ell)/\Delta\ell_A]\}^{-1} \, ,$$

$$\delta_\ell = \delta_0 \{1 + \exp[(\ell - \ell_\delta)/\Delta\ell_\delta]\}^{-1} \, ,$$

and are shown in Fig. C.8-1.

The excellent agreement between the experimental and calculated differential cross sections is demonstrated in Fig. C.8-2. The values of the parameters ℓ_A and $\Delta\ell_A$, determined by best agreement with the experimental results, are then used to calculate an interaction radius, the surface thickness in which the absorption occurs, and the reaction cross section.

[1] J. S. Blair, Phys. Rev. 95, 1218 (1954); Phys. Rev. 108, 827 (1957).

[2] J. A. McIntyre, K. H. Wang, and L. C. Becker, Phys. Rev. 117, 1337 (1960).

[3] K. R. Greider and A. E. Glassgold, Ann. Phys. 10, 100 (1960).

9. (α, t) REACTIONS

José G. Vidal

Part of the experimental work on the differential cross section of the (α, t) reaction has been previously reported.[1] It is the object of this report to present a theoretical expression for the angular distribution of this process on the basis of a plane-wave Born-approximation model.[2]

Previous work on this subject has been done by El Nadi;[3] however, the present calculation differs from that one in several respects: initial, rather then final, interactions are considered, finite range interactions are used whenever possible, exchange effects are included, and a different radial cut-off procedure is used.

The differential cross section for an (α, t) reaction is given, in a familiar notation, by

[1] J. Gonzaléz-Vidal, H. C. Conzett, and W. H. Wade, Bull. Am. Phys. Soc. Series II 5, 230 (1960).

[2] S. T. Butler, Phys. Rev. 106, 272 (1957).

[3] M. El Nadi, Phys. Rev. 120, 1360 (1960).
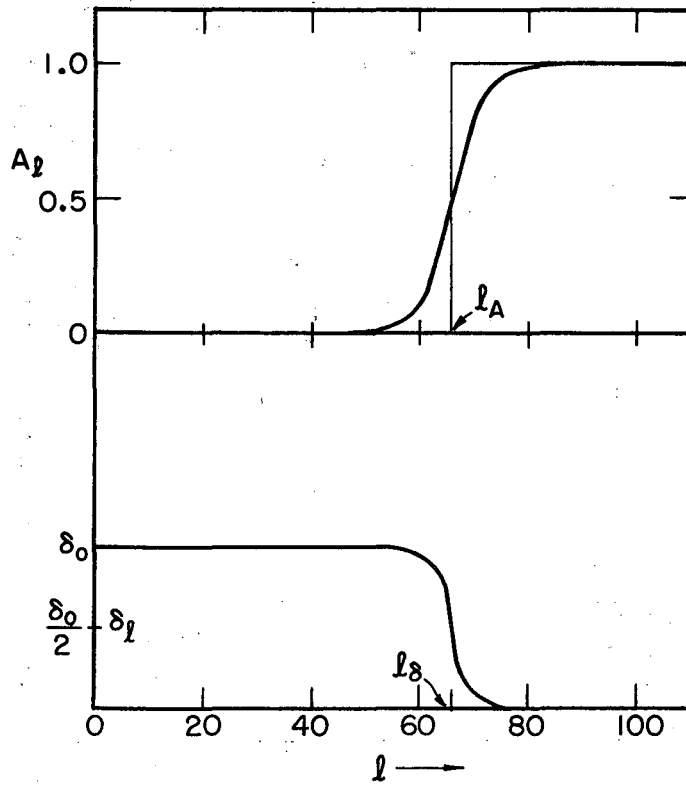
Fig. C. 8-1. The amplitude of the outgoing partial wave and the
real nuclear phase shift as a function of ℓ.

MU-23523

Ta + C^{12}
• Experimental points
— Calculated points
$\ell_A=65$

$\dfrac{\sigma}{\sigma_R}$

1.2
1.0
①

1.2
1.0
②

1.2
1.0
③
0.5
0.2
0.1
0.05

0   10   20   30   40   50

$\Theta_{c.m.}$
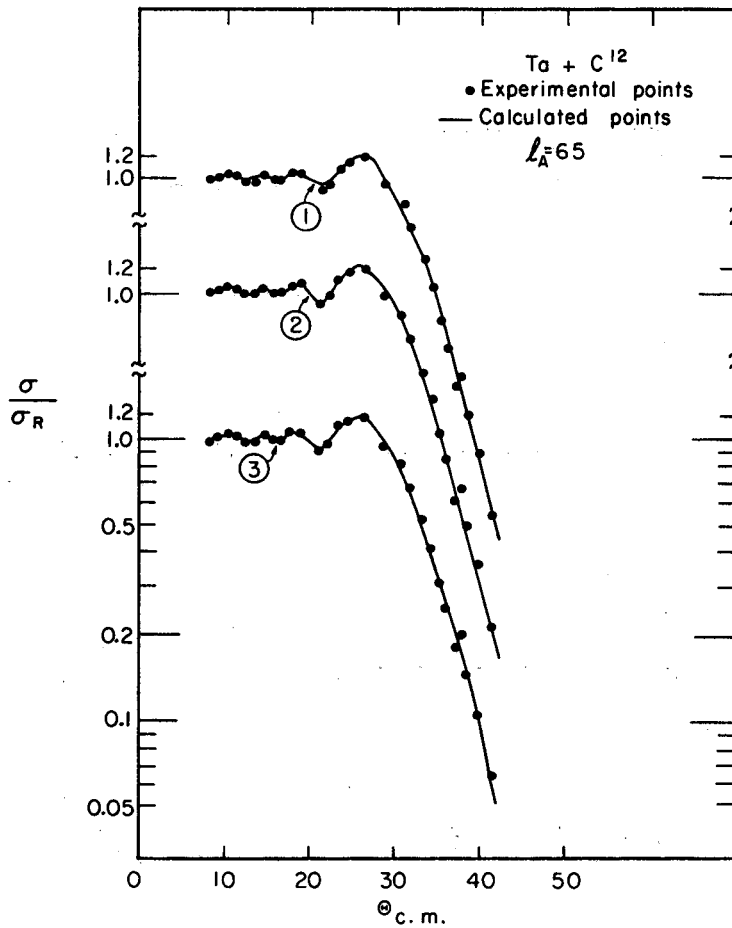
MU-23622

Fig. C.8-2.   Angular distribution of C^{12} ions elastically scattered from Ta at $E_{lab} = 124.5$ Mev.   The dots are the measured cross sections and the solid line is the calculated cross section with the following parameters.

	ℓ_A	$\Delta\ell_A$	δ	ℓ_δ	$\Delta\ell_\delta$
1	65	3.6	0.3	65	3.0
2	65	3.0	0.4	65	3.0
3	65	3.3	0.3	66	2.6

$$\sigma(\theta) = \frac{M_t^* M_\alpha^*}{(2\pi\hbar^2)^2} \cdot \frac{k_t}{k_\alpha} \cdot \frac{1}{2J_i + 1} \sum_{\mu_f \mu_i \mu_t} |I|^2 \ ,$$

with $I = \int d\tau \ \overline{\Phi}_t^{1/2} \ \overline{\Phi}_{J_f}^{\mu_f} \exp(-i\vec{k}_t \cdot \vec{r}_t) \ V \ \Psi$

where $\Phi_t^{1/2}$ is the internal wave function of the triton (radial part is taken

as a Gaussian: $\exp(-\gamma \sum\limits_{i>j}^{3} r_{ij}^{2})$). The $\Phi_{J_f}^{\mu_f}$ is the wave function of the residual

nucleus, and the exponential is a plane wave representing the relative motion of the final system.

Ψ, the exact wave function of the process, will be approximated by $P \exp(i\vec{k}_\alpha \cdot \vec{r}_\alpha) \Phi_0^0 \ \Phi_{J_i}^{\mu_i}$, where Φ_0^0 is the internal wave function of the incoming

α particle (with radial part $\exp(-\mu \sum\limits_{i>j} r_{ij}^{2})$), and $\Phi_{J_i}^{\mu_i}$ is that of the target nucleus.

P is an operator that interchanges the nucleons in the α-particle with those of the target. It is through this antisymmetrization operator that the exchange effects are introduced when we consider the wave function of the residual nucleus to have contributions from a core plus one proton state and a different core plus an α-cluster state; correspondingly the initial nucleus wave function will be made up of contributions from a core state and a different core plus triton cluster state. We shall assume the cluster state cores to be even-even systems with spin 0. We will consider only those terms of the anti-symmetrized initial wave function in which the protons in the α particle exchange with the least bound proton in the target and those in which all the nucleons in the triton cluster in the target exchange with the nucleons in the α particle.

Then I = 2D-E, where D represents the direct term (a term in which the outgoing triton contains only nucleons initially found in the incoming α particle), and E represents the exchange term (a term in which the outgoing triton contains nucleons found initially in the target nucleus).[4] The factor of two in the direct term appears because there are two equivalent protons in the α particle.

In this report we limit ourselves to j-j coupling. To insure consistency in the interference terms all expansions are done with

$\vec{Q} (= -\vec{k}_\alpha + \frac{MT}{M_R} \vec{k}_t)$ taken as the polar axis.

[4] M. A. Nagarajan and M. K. Banerjee, Nuclear Phys. <u>17</u>, 341 (1960).

For the direct matrix element the potential is made up of two terms: the interaction between a proton in the α particle and the "rest" of the α particle, and the interaction of the "rest" of the α particle with the target nucleus. The first term is identified with a stripping mechanism and the second term, representing a distortion of the plane waves, is neglected.[5]

Two forms are chosen for the stripping potential; the first one is $-\dfrac{V_0}{y^3 \pi^{3/2}} \exp(-\rho^2/y^2)$, where y is a range parameter. This potential goes to $-V_0 \delta(\vec{\rho})$ as y approaches zero. This form represents the interaction potential as an average potential between the captured proton and the "rest" of the α particle. This potential yields

$$D = -\frac{(4\pi)^{7/2}}{2^{1/2}} \frac{V_0 \Lambda_F \Lambda_i N}{y^3 \pi^{3/2}} (i^{-\ell_p})(2\ell_p + 1)^{1/2}[(-)^{(1/2)-\mu_t}] \, C(J_i, j_p \, J_f; \mu_i, -\mu_t, \mu_f)$$

$$\times C(\ell_p, 1/2, j_p; 0, -\mu_t, -\mu_t) F_{\ell_p 0} \, ,$$

where Λ_F^2 is the probability of finding the final nucleus in a core-plus-proton state, Λ_i^2 is the probability of finding the initial nucleus in the core state, ℓ_p is the orbital angular momentum of the captured proton, N includes the normalization constants.

The form of $F_{\ell_p 0}$ depends on the radial wave functions used for the proton bound state; for square-well wave functions it is

$$F_{\ell_p 0} = \frac{\pi^{3/2} R_0^2 \exp[-K^2 y^2/4(3\mu y^2+1)] B_{\ell_p}}{4^3 \left\{\dfrac{1}{y^2}(3\mu y^2+1)(2\mu+3\gamma/2)(8\mu/3 + 2\gamma)\right\}^{3/2}} \quad \frac{W\left\{j_{\ell_p}(Q_{r_p}), h_{\ell_p}^{(1)}(i\beta r_p)\right\}_{r_p = R_0}}{Q^2 + \beta^2}$$

where $\vec{K} = (3/4)\vec{k}_\alpha - \vec{k}_t$. The region 0 to R_0 is excluded from the r_p integration in order to avoid the inner region of configuration space where compound-nucleus formation is important. B_{ℓ_p} is a normalization constant.

The second form of the stripping potential is a more realistic one and is given by a sum of two-body potentials, $\sum_{i=1}^{3} V_i(r_{p_i})$, where $V_i(r_{p_i}) = -V_0' e^{-\beta_0 r_{p_i}^2}$. For this case

$$D = -(4\pi)^{7/2} 27 \Lambda_F \Lambda_i V_0' (i^{-\ell_p})(2\ell_p+1)(-)^{1/2-\mu_t} C(J_i, j_p, J_f; \mu_i, -\mu_t, \mu_f)$$

$$\times C(\ell_p', 1/2, j_p; 0, -\mu_t, -\mu_t) \left\{ A \exp(-A_1 K^2) + B \exp(-B_1 K^2) \right\}$$

---
[5] T. B. Day, L. S. Rodberg, G. A. Snow, and J. Sucher, Phys. Rev. 123, 1051 (1961).

where $F_{\ell_p} = \dfrac{R_0^2 B_{\ell_p}}{Q^2+\beta^2} \, W\left\{ j_{\ell_p}(Q_{r_p}), \, h_{\ell_p}^{(1)}(i\beta r_p)\right\}_{r_p = R_0}$

$$A = 1/16\left[bu\left(a + \frac{v^2}{4\mu}\right)\right]^{3/2} ; \quad A_1 = \left\{ 4\left(a - \frac{v^2}{4\mu}\right)\right\}^{-1}$$

$$B = \beta_1 \left[a_0\left(\gamma_0 - \frac{\beta_0^2}{4\beta_1}\right) - \frac{v_0^2}{4}\right]^{-3/2} ; \quad B_1 = \left\{ 4\left[a_0 - \frac{v_0^2}{4\left(\gamma_0 - \frac{\beta_0^2}{4\beta_1}\right)}\right]\right\}^{-1} ,$$

and $u = 6\mu + 9/2\gamma + \beta$; $a = 9(\mu + 1/2\,\gamma)$; $\beta_1 = 2\mu + 3/2\,\gamma + \beta/4$;

$\gamma_0 = 24\mu + 18\gamma + \beta$; $a_0 = 9(3\mu + 2\gamma)$; $b = 2\mu + 3/2\,\gamma$.

    The exchange matrix element potential is made up of two terms: the interaction between the incoming α particle and the triton cluster (giving rise to a knockout process), and the interaction between the triton cluster and the core, giving rise to a heavy-particle stripping process.[6] Let us write, then,

$$E = E_{KO} + E_{HPS}.$$

    A zeroth-order approximation for the knockout potential is to represent it by a delta potential: $-V_{KO}\,\delta(r_{at_c})$. This probably is not a very good approximation at low energies, because of the finite sizes of the α particle and the triton cluster.

    This approximation yields

$$E_{KO} = -(4\pi)^{11/2}\, V_{KO}\Gamma_T\Gamma_F N' \sum_{m'_t\, m_t\ell_t} i^{-\ell_t}\left\{ \frac{(2\ell_t + 1)(2\ell'_t + 1)}{(2J_f + 1)}\right\}^{1/2}$$

$$C\left(\ell'_t, \tfrac{1}{2}, J_i; m'_t, \mu_t, \mu_i\right)\, C\left(\ell'_t, \ell_t, J_f; m'_t, -m_t, \mu_f\right) C\left(\ell'_t, \ell_t, J_f; 0, 0, 0\right)\overline{Y}_{\ell_t m_t}$$

$$(\theta_M, \phi_M)F_{J_f\ell'_t\ell_t} ,$$

where we have assumed the triton cluster to be in a definite state, ℓ'_t, of orbital angular momentum. Γ_T^2 and Γ_F^2 represent the probabilities of

---

[6]L. Madanski and G. E. Owen, Phys. Rev. 99, 1608 (1955); 105, 1766 (1957).

finding the target and the residual nuclei in cluster states. N' involves normalization factors. We also have

$$F_{J_f \ell_t' \ell_t}' = - \frac{\pi^{5/2} B_{J_f} B_{\rho t'}}{4^5 (abcd\epsilon)^{3/2}} \int_{R_0}^{\infty} dr_t \, r_t^2 \, h_{J_f}^{(1)}(i\beta_a r_t) h_{\ell_t'}^{(1)}(i\beta_{tc} r_t) j_{\ell_t}(Mr_t) \, ,$$

with $\vec{M} = \frac{M_{core}}{M_T} \vec{k}_a - \frac{M_{core}}{M_R} \vec{k}_t$ and $a = 3(\mu'+\mu)$, $b = 2(\mu'+\mu)$, $c = \frac{8}{3}(\mu'+\mu)$,

$d = 2(\gamma'+\gamma)$, $\epsilon = \frac{3}{2}(\gamma'+\gamma)$ where the primes are introduced to take into account binding energy differences between the clusters and the free-particle states of the α particle and the triton.

If $J_f = 0$, $F_{J_f \ell_t' \ell_t}$ can be approximated by

$$\frac{\pi^{5/2}}{4^5(abcd\epsilon)^{3/2}} \frac{(\beta_{tc}+\beta_a)}{\beta_{tc}\beta_a} \frac{R_0 B_0 B_{\ell_t'}}{(M^2+[\beta_{tc}+\beta_a]^2)} W\left\{ j_{\ell_t}(Mr_t), h_{\ell_t}^{(1)}[i(\beta_a+\beta_{tc})r_t] \right\}_{r_t=R_0},$$

if $\beta_{tc}R_0 > \ell_t'$.

The heavy-particle stripping term yields

$$E_{HPS} = - T\Gamma_T\Gamma_F (4\pi)^7 N' \sum_{m_t} (-)^{m_t} i^{J_f+\ell_t} C(\ell_t', \tfrac{1}{2}, J_i; m_t, \mu_t, \mu_i)$$

$$\times \bar{Y}_{J_f, \mu_f}(\vec{Q}_0) \, \bar{Y}_{\ell_t, -m_t}(K_0) \, G_{J_f \ell_t},$$

where $\vec{Q}_0 = \vec{k}_a - \frac{M\alpha}{MR}\vec{k}_t$; $\vec{K}_0 = -\frac{M_t}{M_T}\vec{k}_a - \vec{k}_t$; $T = \left(\frac{Q_0^2}{2m_{tc}} + \epsilon\right)$, with m_{tc} as the

reduced mass of the triton-cluster-plus-core system and ϵ as the absolute value of the binding energy of the triton-cluster to the core; and

$$G_{J_f \ell_t} = \frac{R_1^2 R_2^2 B_{J_f} B_{\ell_t}}{(Q_0^2 + \beta_a^2)(K_0^2 + \beta_{tc}^2)} W\left\{ j_{J_f}(Q_0 r_a), h_{J_f}^{(1)}(i\beta_a r_a) \right\}_{r_a=R_1}$$

$$\times W\left\{ j_{\ell_t}(K_0 r_t), h_{\ell_t}^{(1)}(i\beta_{tc} r_t) \right\}_{r_t=R_2}$$

In all the processes considered the selection rules are $|\vec{J}_i + \vec{J}_f + \frac{1}{2}|_{\min}$ $\leq \ell \leq J_i + J_f + \frac{1}{2}$. The expression for $\sum\limits_{\substack{\mu_i \mu_f \\ \mu_t}} |I|^2$ for the special case $J_f = 0$

(assuming pure states and average interaction for the stripping contribution) is

$$
\sum_{\substack{\mu_i \\ \mu_t}} |I|^2 = \frac{4^8 \pi^4 V_0^2 \Lambda_F^2 N^2 \Lambda_i^2}{2y^6} F^2_{\ell_p 0} + (4\pi)^{10}(2J_i+1)N'^2 V_{K0}^2 \Gamma_T^2 \Gamma_F^2 |F_{0\ell_t \ell_t}|^2
$$

$$
+ (4\pi)^{12}(2J_i+1)N'^2 T^2 \Gamma_T^2 \Gamma_F^2 |G_{0\ell_t}|^2 + 4 \frac{(4\pi)^{17/2}}{\sqrt{2}} \Lambda_i \Lambda_F \Gamma_T \Gamma_F NN' V_0 (2J_i+1)^{1/2} \overline{F}_{\ell_p 0}
$$

$$
\times \left\{ V_{K0} P_{\ell_t}(\cos\phi_{MQ}) F_{0\ell_t \ell_t} + 4\pi T P_{\ell_t}(\cos\phi_{K_0 Q}) G_{\ell_t 0} \right\} \delta_{\ell_t \ell_p}
$$

$$
+ (4\pi)^{11}(N'\Gamma_T \Gamma_F)^2 V_{K0} T(2J_i+1) P_{\ell_t}(\cos\phi_{K_0 M}) \overline{G}_{0\ell_t} F_{0\ell_t \ell_t} \quad,
$$

where the first three terms represent pure stripping, pure knockout, and pure heavy-particle stripping, respectively. The fourth term represents the interference between the direct and exchange processes. The last term represents the interference between knockout and heavy-particle stripping. We have taken advantage of the properties of $F_{\ell_p 0}$, $G_{0\ell_t}$, and $F_{0\ell_t \ell_t}$ to simplify the expression.

In general we should expect the stripping term to be the dominant one, and the exchange terms to be important only when there is an appreciable probability of cluster states.

Then if the exchange effects are not important we have

$$
\sigma(\theta) = \frac{M_a^* M_t^*}{(2\pi \hbar^2)^2} \frac{k_t}{k_a} \frac{(2J_f+1)}{2(J_i+1)} \Lambda_i^2 \Lambda_F^2 \left[\frac{(4\pi)^{7/2} V_0 N}{y^3 \pi^{3/2}} \right]^2 |F_{\ell_p 0}|^2 .
$$

If only knockout is important,

$$
\sigma(\theta) = \frac{M_a^* M_t^*}{(2\pi \hbar^2)^2} \frac{k_t}{k_a} (N'\Gamma_T \Gamma_F V_{K0})^2 (4\pi)^{10} \sum_{\ell_t} (2\ell_t+1) C(\ell_t', \ell_t, J_f; 000) |F_{J_f \ell_t' \ell_t}|^2 .
$$

If only heavy-particle stripping is important,

$$\sigma(\theta) = \frac{M_a^* \, M_t^*}{(2\pi \, \hbar^2)^2} \; \frac{k_t}{k_a} \; (N' \Gamma_T \Gamma_F T)^2 \, (4\pi)^{12} \, (2J_f + 1) \, |G_{J_f \ell_{t'}}|^2 .$$

10. MESON-INDUCED NUCLEAR REACTIONS

Paul L. Reeder and Samuel S. Markowitz

The reactions of π mesons with complex nuclei are being studied with the aid of pion beams from the 184-inch cyclotron. The purpose of these experiments is to give information on the mechanism of high-energy reactions occurring in various nuclei, especially at the nuclear surface. Mesons with energy greater than 140 Mev have a mean free path in nuclear matter of about 1 pion Compton wave length (1.41×10^{-13} cm). This distance is roughly equal to surface-thickness parameter of Hofstadter[1] for complex nuclei. Therefore we can assume that simple nuclear reactions of the type

$$Z^A + \pi^- \longrightarrow Z^{A-1} + \pi^- + n,$$

$$Z^A + \pi^- \longrightarrow (Z-1)^{A-1} + \pi^- + p$$
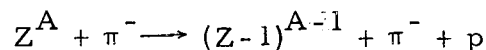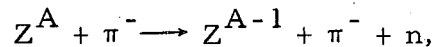
can occur only at the surface of the nucleus. By comparison of the excitation functions for these reactions with the excitation functions for the analogous reactions induced by protons, we hope to test whether or not the proton reactions

$$Z^A + p \longrightarrow Z^{A-1} + p + n,$$

$$Z^A + p \longrightarrow (Z-1)^{A-1} + p + p$$
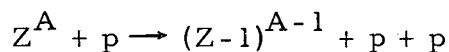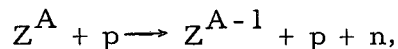
likewise proceed by an individual-particle surface collision mechanism.

The reaction $C^{12}(\pi^-, \pi^- n)C^{11}$ was chosen as a starting point despite its relatively small "size," because a simple electronic technique for observing the 20.4-min C^{11} activity with high efficiency is available without the need for chemical separation. Since presently available magnetically analyzed pion beams have low intensities (approx $10^6 \pi/\text{min}$) the short half-life of C^{11} enables one to obtain observable amounts of activity with reasonable bombardment times (30 min). The pion beam is measured by a two-counter telescope and fast (40-Mc) scaling circuit. The targets are 2.5-in.-diameter by 1-in.-thick disks of plastic scintillator (91.5% C^{12}). After bombardment in the pion beam the targets are mounted on a photomultiplier tube and the pulses are led to a linear amplifier and scaler. The detection efficiency of this system was measured by a β-γ coincidence technique and is about 82%.

---

[1] R. Hofstadter, in Proceedings of an International Conference on Nuclear Physics, Paris, July, 1958.

The cross sections obtained so far are given in Table I.

Table I. $C^{12}(\pi^-, \pi^- n)C^{11}$ cross sections.

Pion energy (Mev)	σ (mb)
60 ± 6	11 ± 2
127 ± 9	23 ± 3
310 ± 4	11 ± 2
370 ± 5	36 ± 5
430 ± 5	34 ± 15
1610 ± 20	22 ± 10

With the data obtained to date, the collision of a $\pi^- + n$ within the C^{12} nucleus with both collision partners escaping does not reflect the large res- onance peak in $\pi^- + n$ free-particle total cross sections.

In addition, targets of natural zinc have been bombarded with 310- and 370-Mev π^- and the yield of copper isotopes measured after radiochemical purification. Table II gives the isotopes observed and the yield.

Table II. $Zn^{68}(\pi^-, \pi^- p)Cu^{67}$ cross sections and the "yields" of Cu^{64} and Cu^{61} from $\pi^- +$ zinc

Energy (Mev)	Cu^{67} (mb)	Cu^{64} (mb)	Cu^{61} (mb)
310 ± 4	25 ± 3	14 ± 2	24 ± 5
370 ± 5	23.4 ± 2	14.1 ± 1.5	19.5 ± 2

The cross section for Cu^{67} is calculated with the assumption that the only target nuclide is Zn^{68}, whereas it is assumed that Cu^{64} and Cu^{61} could be produced from any of the natural Zn isotopes. These yields are identical within experimental error with the similar yields for 400- and 560-Mev protons on Zn as measured previously.[2]

The production of Cu^{64} and Cu^{61} probably takes place by complicated reactions in which it is possible for the pion to become scattered in the nucleus and absorbed. Since the proton bombardments give similar results, however, we can speculate that the energy-transfer mechanisms may also be similar.

---

[2] P. Reeder and S. S. Markowitz, in Chemistry Division Semiannual Report, UCRL-9093, Nov. 1959, p. 6.

It has been previously assumed that pion production and reabsorption were responsible for large energy transfers in high-energy proton-induced nuclear reactions.[3] The present direct pion studies therefore give strong experimental indication that pion scattering and absorption in nuclear matter is an essential feature of high-energy reactions. This work is being continued.

[3] R. Wolfgang, E. Baker, A. A. Caretto, J. Cumming, G. Friedlander, and J. Hudis, Phys. Rev. 103, 394 (1956).

11. SCATTERING OF 915-Mev α PARTICLES FROM CARBON AND HELIUM: DIRECT EVIDENCE FOR α-PARTICLE CLUSTERING IN NUCLEI[*]

Terence J. Gooding and George Igo

We have obtained direct evidence for α-particle clustering in C^{12} from the (α, 2α) reaction at 915 Mev. Measurements of the energies of the two outgoing α particles and the angular correlation getween them show that the reaction proceeds via a direct collision between the incident α particle and an α-particle cluster in the nucleus. An estimate of the preformation probability has been obtained by comparing the carbon and helium differential cross sections.

Figure C.11-1a is a diagram of the experimental arrangement. The 915-Mev α-particle beam from the Berkeley synchrocyclotron was focused at the center of an 18-in.-diam scattering chamber to a spot 1 in. wide by 3/4 in. high. The beam intensity was about 3×10^8 α particles per sec and was monitored by an 8-in.-diam ionization chamber. The duty cycle was increased from about 60 μsec per burst to 12 msec per burst by means of an extraperipheral dee. Measurements were made first with the chamber filled to 65 psi of helium and then with a thin graphite target (approx 260 mg/cm^2 for θ_L= 17 deg and approx 600 mg/cm^2 for θ_L= 26 deg) placed at the center of the scattering chamber.

Particles scattered from the target were detected by counters placed at angles θ_L and θ_R with respect to the α-particle beam. The particles were identified by measuring their total energy, E, and their rate of energy loss, dE/dX. The dE/dX counters were disks of plastic scintillator, 1.0 in. in diam by 0.1 in. thick, and the E counters were cylinders of plastic scintillator, 3.5 in. in diam by 11 in. long. The response of the counters to α particles and protons of various energies was determined by placing the counters, preceded by an appropriate absorber, in the direct α-particle and proton beams. The response was in reasonable agreement with calculations based on the response of plastic scintillator to lower-energy protons, deuterons, and electrons.[1] The nuclear absorption in the E counters was about 35% and was determined in the direct beam by measuring the low-energy tail of the pulse-height spectrum.

[1] T. J. Gooding and H. G. Pugh, Nuclear Instr. and Methods 7, 189 (1960).

(a)

(b)
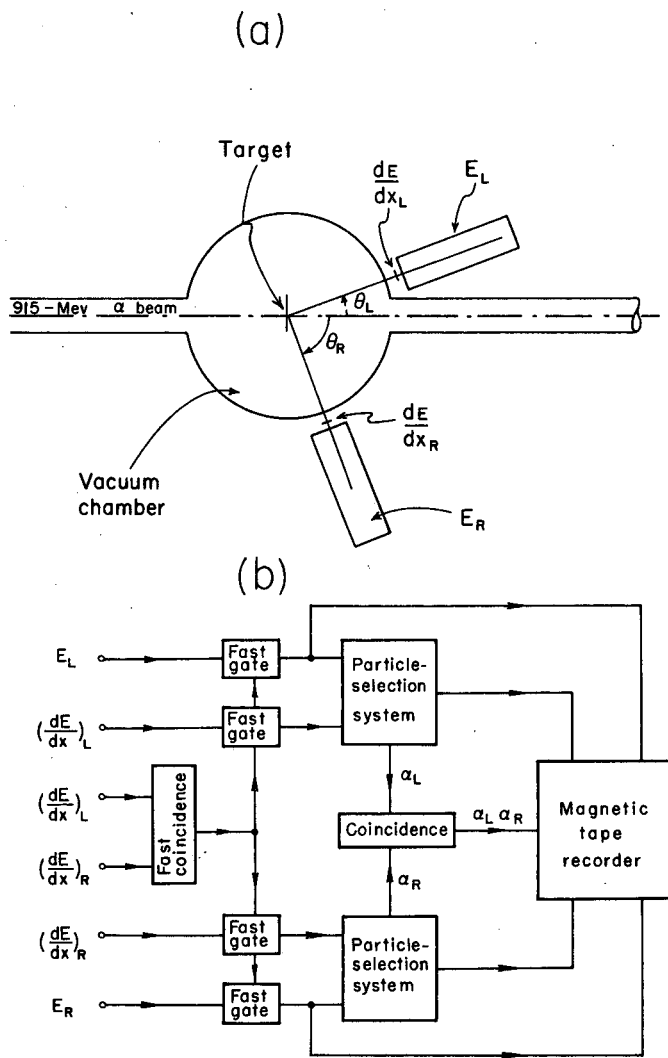
MU-23414-A

Fig. C.11-1. (a) Diagram of the experimental arrangement
(b) Block diagram of the electronics.

A block diagram of the electronics is shown in Fig. C.11-1b. The fast-coincidence resolving time was 5 nsec and was limited by the flight-time difference between high- and low-energy α particles leaving the target. The particle-selection systems consisted of complex arrangements of discriminators and coincidence circuits acting on linear outputs from the dE/dX and E counters. In this way, we were able to sort doubly charged particles (He^3 and He^4) from singly charged particles with a high degree of reliability. Outputs from the particle-selection systems were fed into a slow-coincidence unit which was used to start a magnetic recorder. With the helium target, the fast-coincidence counting rate was typically p per sec, whereas the $(\alpha, 2\alpha)$ coincidence rate was only 1 per min. Outputs from the E counters were pulse-height analyzed in the magnetic recorder. In addition, information concerning the energy range in which each α particle fell was recorded. The magnetic tape was subsequently analyzed by using an IBM-7090 computer.

The differential cross section $d^2/d\Omega_1 d\Omega_2$ for scattering of the α-particle beam by helium and carbon was measured at $\theta_L = 17$, 26, and 45 deg, with $\theta_L + \theta_R = 87$ deg (the separation angle for elastic scattering at 915 Mev). At each angle, we measured the energy spectrum E_L and the spectrum of the sum of the energies $E_L + E_R$.

The spectra from helium at 17 deg are shown in Fig.C.11-2. The peak at 815 Mev in E_L and 915 Mev in $(E_L + E_R)$ corresponds to the elastically scattered group. The second peak at $E_L = 650$ Mev and $(E_L + E_R) = 750$ Mev is thought to be due to stripping of the forward-going α particle into a He^3 plus a neutron. The relative intensities of these two peaks are misleading, since the elastic peak is sharply correlated at these angles, whereas the inelastic group would be expected to have a broader distribution. The third peak may be due to an energy cutoff in the experiment at around 350 Mev. The energy calibration throughout these measurements is uncertain to ±50 Mev. At 26 deg the spectrum looked essentially the same but the cross section was reduced. The cross section at 45 deg was too low to be measured.

The carbon data at 26 deg are shown in Fig. C.11-3. The summed spectrum again shows two peaks, but the relative intensity of the elastically scattered group appears reduced. This is because the angular correlation is broadened by the momentum distribution of the α particles in the carbon nucleus. The peak at 750 Mev in the energy spectrum E_L for events with $E_L + E_R > 850$ (i.e., the elastically scattered group) shows clearly that the reaction is proceeding via a direct collision of the α particle with an α cluster in the nucleus. If, for instance, the initial collision was between the incident α particle and a deuteron, then the energy of the α particle scattered at 26 deg would be about 500 Mev. An α-particle—nucleon collision producing an α particle at 26 deg is kinematically forbidden.

Further evidence in support of this conclusion is given in Fig. C.11-4, which shows the summed spectra for $\theta_L = 17$ deg and $\theta_L + \theta_R$ equal to (a) 87 deg and (b) 57 deg. The intensity of the quasi-elastically scattered group drops by a factor of about four when the separation angle is moved 30 deg from the kinematic angle of 87 deg. Consequently, the recoil α particle is correlated to within $(6 \pm 3)\%$ of the total available solid angle.

In order to obtain the probability of α-particle clustering in carbon, the differential cross sections for elastic scattering from helium and quasielastic
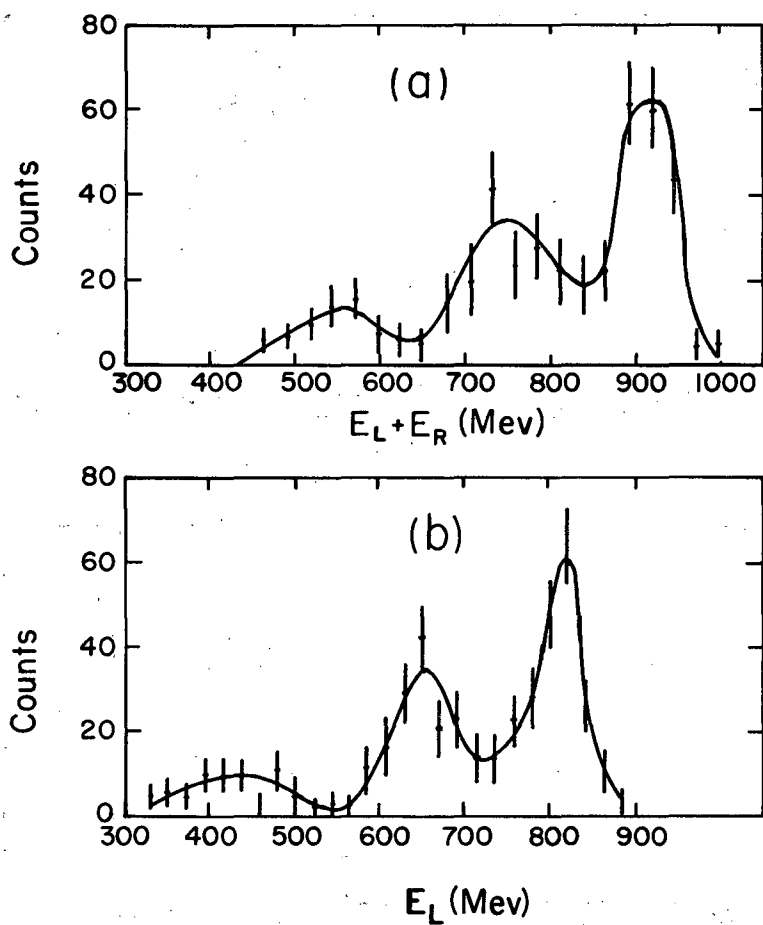
Fig. C.11-2. Scattering from helium at $\theta_L = 17$ deg, $\theta_L + \theta_R = 87$ deg.
(a) Summed energy spectrum $E_L + E_R$; (b) energy spectrum E_L.
The energy calibration is uncertain to ±50 Mev.
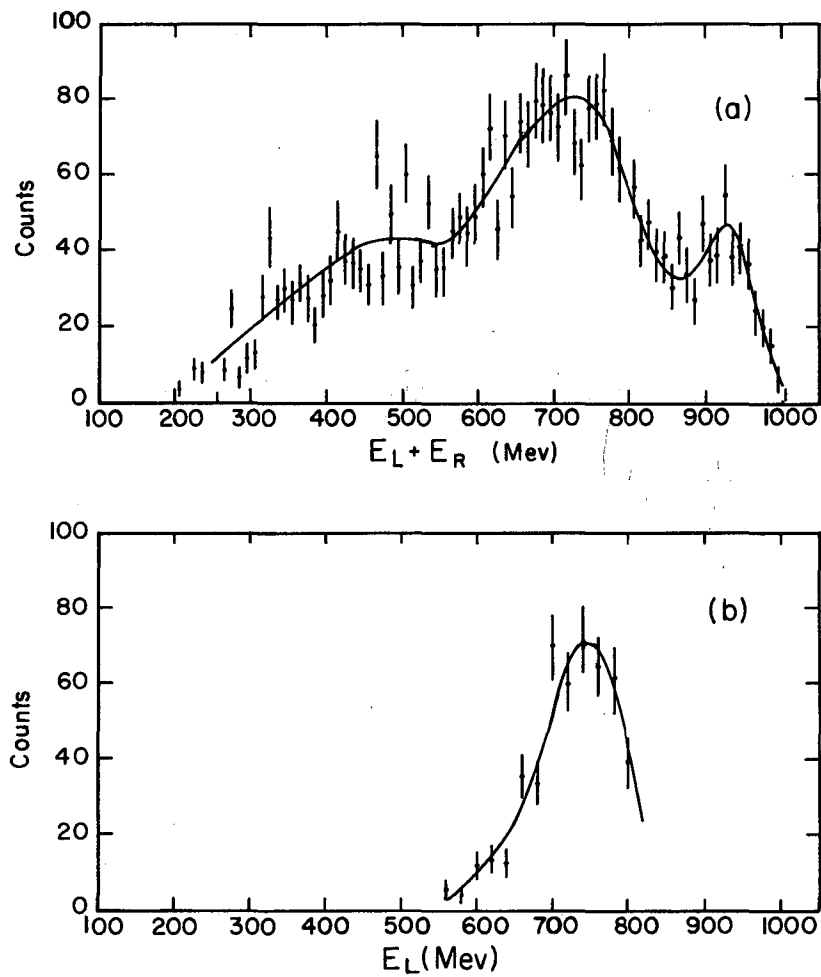
MU-23566

Fig. C.11-3. Scattering from carbon at $\theta_L = 26$ deg, $\theta_L + \theta_R = 87$ deg. (a) Summed energy spectrum $E_L + E_R$; (b) energy spectrum E_L, where $E_L + E_R > 850$ Mev. The energy calibration is uncertain to ± 50 Mev.
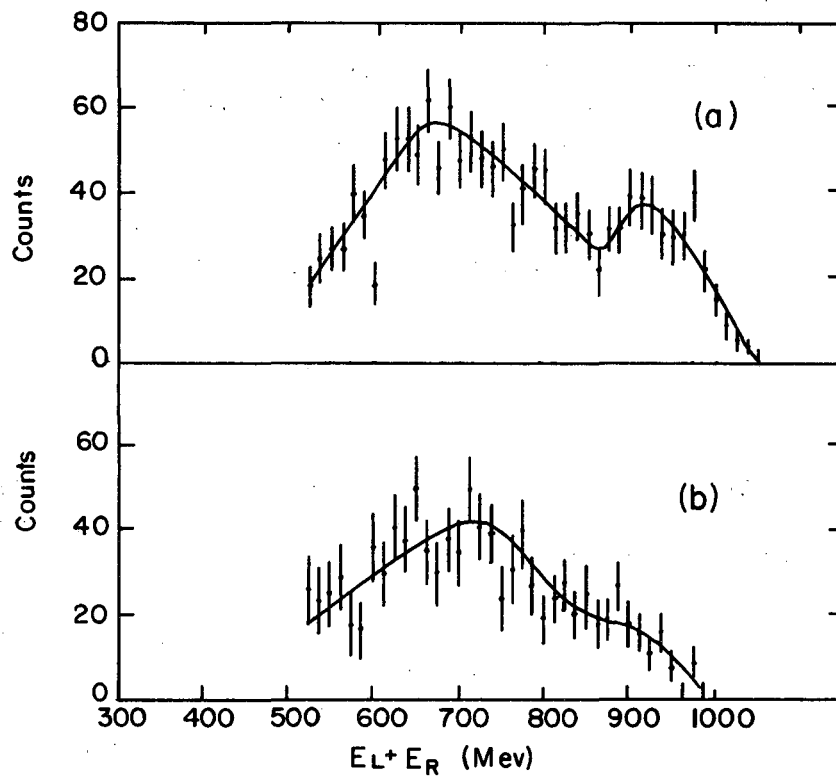
Fig. C.11-4. The carbon summed energy spectrum at $\theta_L = 17$ deg and (a) $\theta_L + \theta_R = 87$ deg; (b) $\theta_L + \theta_R = 57$ deg. The energy calibration is uncertain to ± 50 Mev.

scattering from carbon have been calculated at 17, 26, and 45 deg and are shown in Table I. The differential cross section for helium has been corrected for the finite size of the beam, the finite extent of the helium gas target, and nuclear absorption in the counters. To obtain the cross section for carbon, one must integrate over the solid angle into which the correlated α particle can be scattered.

To perform this integration, we have assumed that the angular correlation follows a triangular distribution through the two experimental points, that the angular correlation at $\theta_L = 26$ deg is the same as at $\theta_L = 17$ deg, and that the width of the distribution out of the plane of scattering is the same as that in the plane of scattering. The large errors on the cross sections quoted in Table I are primarily due to the inadequacy of the data on the angular-correlation function.

The ratio of the (α, 2α) differential cross section for carbon and helium is 1.74 ± 0.9 at 17 deg and 3.9 ± 2.9 at 26 deg. According to the extreme α-particle model for carbon, we would expect this ratio to be about 3.

Further measurements are in progress on the angular-correlation function and the differential cross section for the (α, 2α) reaction for other nuclei.

Table I. The differential cross sections for elastic scattering from helium and quasi-elastic scattering from carbon.

θ_L (deg)	$d\sigma/d\Omega$ (μb/sr)		$\dfrac{d\sigma/d\Omega \ (\text{carbon})}{d\sigma/d\Omega \ (\text{helium})}$
	Helium	Carbon	
17	165 ± 35	287 ± 150	1.7 ± 0.9
26	22 ± 11	86 ± 50	3.9 ± 2.9
45	~ 0	~ 0	...

12.   THE GIANT E1 RESONANCE FOR DEFORMED NUCLEI TREATED BY THE RANDOM-PHASE APPROXIMATION (*)

S. G. Nilsson,[†] J. Sawicki,[‡] and N. K. Glendenning

The giant E1 photonuclear resonance has now been studied for a large number of nuclides, and there appear to be experimental indications that the resonance exhibits a split peak in strongly deformed nuclei.[1] Danos[2] and Okamoto[3] explained this effect qualitatively in terms of a hydrodynamic model with different characteristic frequencies along the major and minor axes of the spheroid. This effect was then also calculated on the basis of the independent-particle picture by Wilkinson[4] and by Mottelson and Nilsson,[5] using the wave functions of an anisotropic harmonic oscillator.

Such a simple description of the E1 giant resonance in terms of non-interacting particles now appears to be contradicted by the empirical fact that the characteristic resonance energy is larger by a factor on the order of 1.5 to 2 than the spacing between two oscillator shells, $\hbar\omega$.[6] Already several years ago Elliott and Flowers[7] were able to explain the photo-excitation spectrum of O^{16} by the perturbation of the simple shell-model states of this nucleus by a residual two-body force of finite range, containing exchange operators. As a result, states of mixed configuration are formed with such proportions of the pure states that the 1- states with T = 1 generally appear above $\hbar\omega$, while those with T = 0 generally appear below. In particular, the two highest-lying E1 states were found to absorb almost all the E1 oscillator strength and thus together constitute a true giant.

Recently the approach based on the random-phase approximation has been applied with success to the study of certain types of collective states

1 Fuller, Petree, and Weiss, Phys. Rev. 112, 554 (1958); E. G. Fuller and M. S. Weiss, Phys. Rev. 112, 560 (1958); and E. G. Fuller, in Proceedings of the International Conference of Nuclear Physics, Paris, 1958 (Dunod, Paris, 1959), p. 642.

2 M. Danos, Bull. Am. Phys. Soc. 1, 135, 246 (1956); Nuclear Phys. 5, 23 (1958).

3 K. Okamoto, Progr. Theoret.Phys. (Kyoto) 15, 75 (1956); Phys. Rev. 110, 143 (1958).

4 D. H. Wilkinson, Phil. Mag. 3, 567 (1958).

5 B. R. Mottelson and S. G. Nilsson, Nuclear Phys. 13, 280 (1959).

6 Schiffer, Lee, and Zeidman, Phys. Rev. 115, 427 (1959).

7 J. P. Elliott and B. H. Flowers, Proc. Roy. Soc. (London) A242, 57 (1957).

in Nuclei.[8-12] This approach has the advantage over a shell-model calcula-
tion in that it accounts approximately for the effects of correlations in the
ground state. Let $|0\rangle$ denote the ground state, which may, as a result of
the residual interaction, be a complicated superposition of 1, 2, $\cdots$ particle
excitations from the degenerate independent-particle system. The type of
collective state in which we are interested differs from the ground state only
in that it consists of a linear combination of single-particle excitations rel-
ative to the ground state, since the electromagnetic interaction can excite
only one particle at a time to lowest order in $e^2/\hbar c$. Introducing creation and
destruction operators, we can thus write the excited state in the form

$$|E\rangle = \sum_{\nu \nu'} C_{\nu \nu'} \hat{\rho}_{\nu \nu'} |0\rangle,$$

where $C_{\nu \nu'}$ are coefficients to be determined and

$$\hat{\rho}_{\nu \nu'} = a^+_{\nu'} a_\nu$$

is the density matrix operator corresponding to the promotion of a praticle
from the state ν to ν'. Employing the random-phase approximation, we find
that the amplitudes

$$\rho_{\nu \nu'} = \langle E| \hat{\rho}_{\nu \nu'} |0\rangle$$

connecting the ground to excited state satisfy the equation

$$(\epsilon_{\nu'} - \epsilon_\nu - E) \rho_{\nu \nu'} = (n_{\nu'} - n_\nu) \sum_{\kappa \kappa'} \langle \nu \kappa' | V(-P^{12}) | \nu' \kappa \rangle \rho_{\kappa \kappa'}.$$

Here ϵ_ν are the shell-model energy levels and n_ν are the occupation numbers
relative to the degenerate system. A more detailed discussion of the calcu-
lations can be found elsewhere[13] and in the longer version of this paper.

    We have applied this method to Mg^{24}, using oscillator and deformation
parameters[14] $\hbar \omega_Z$ = 11.4 Mev, $\hbar \omega_\perp$ = 15.9 Mev, $\eta = 4$, $\kappa = 0.08$. A list of the

[8] G. E. Brown and M. Bolsterli, Phys. Rev. Letters 3, 472 (1960); see also
Brown, Castillejo, and Evans, Nuclear Phys. 22, 1 (1961).

[9] K. Sawada, Phys. Rev. 106, 372 (1957); Sawada, Brueckner, Fukuda, and
Brout, Phys. Rev. 108, 507 (1957).

[10] S. Takagi, Progr. Theoret. Phys. (Kyoto) 21, 174 (1959).

[11] S. Fallieros, Thesis, University of Maryland, 1959.

[12] B. R. Mottelson, in Proceedings of the International Conference on Nuclear
Structure, Kingston (University of Toronto Press, 1960).

[13] J. Sawicki, Nuclear Phys. 23, 285 (1961).

[14] S. G. Nilsson, Kgl. Danske Videnskab. Selskab Mat.-fys. Medd. 29, No.
16 (1955).

single-particle states contributing to the formation of the excited state can be found in Ref. 14. Our results are illustrated in Fig. C.12-1, where the independent-particle radiative widths can be compared with those of this calculation. The several states collecting the giant strength now appear at higher energies for the interacting system, about 5 Mev for K = 0 and about 7 Mev for K = 1.

The table shows the average peak positions found by weighting the energy levels according to their absorption cross sections. Notice that the splitting of the giant peak into K = 0 and K = 1 components is increased by about 2.1 Mev over what the independent-particle calculation predicts.

Table I. Position of the average giant peaks for the interacting and non-interacting system (Mev)

	K = 1	K = 0	Difference
Interacting-particle system	23.5	17.8	5.7
Independent-particle system	16.4	12.8	3.6
Difference	7.1	5.0	2.1

An important result which emerges from this work is the fact that, while the shell-model calculation (even for a pure Wigner force) leads to a large excess value of the Thomas-Kuhne-Reiche sum over the value NZ/A derived for velocity independent nonexchange forces, the inclusion of the ground-state correlation leads to a large reduction of this excess. Empirically, below an energy of 2 or 3 $\hbar\omega$ this sum rule value is exceeded by only 10 to 20%.

13. NUCLEON-NUCLEON TRIPLET-EVEN POTENTIALS (*)

Norman K. Glendenning and Gustav Kramer[†]

There are still not sufficient scattering data to define the force acting in the n-p system as well as the force in the p-p system. However, the proerties of the deuteron serve as constraints on the definition of the triplet-even force. In addition there is one other important constraint: all meson-theoretic derivations of nuclear forces agree that at large distance the potential must behave like the one-pion exchange potential (OPEP) which for the triplet-even states is[1]

[1]See, for example, L. Hulthén and M. Sugawara, The Two-Nucleon Problem, in Handbuch der Physik Vol. XXXIX, (Springer-Verlag, Berlin, 1957) p. 17.
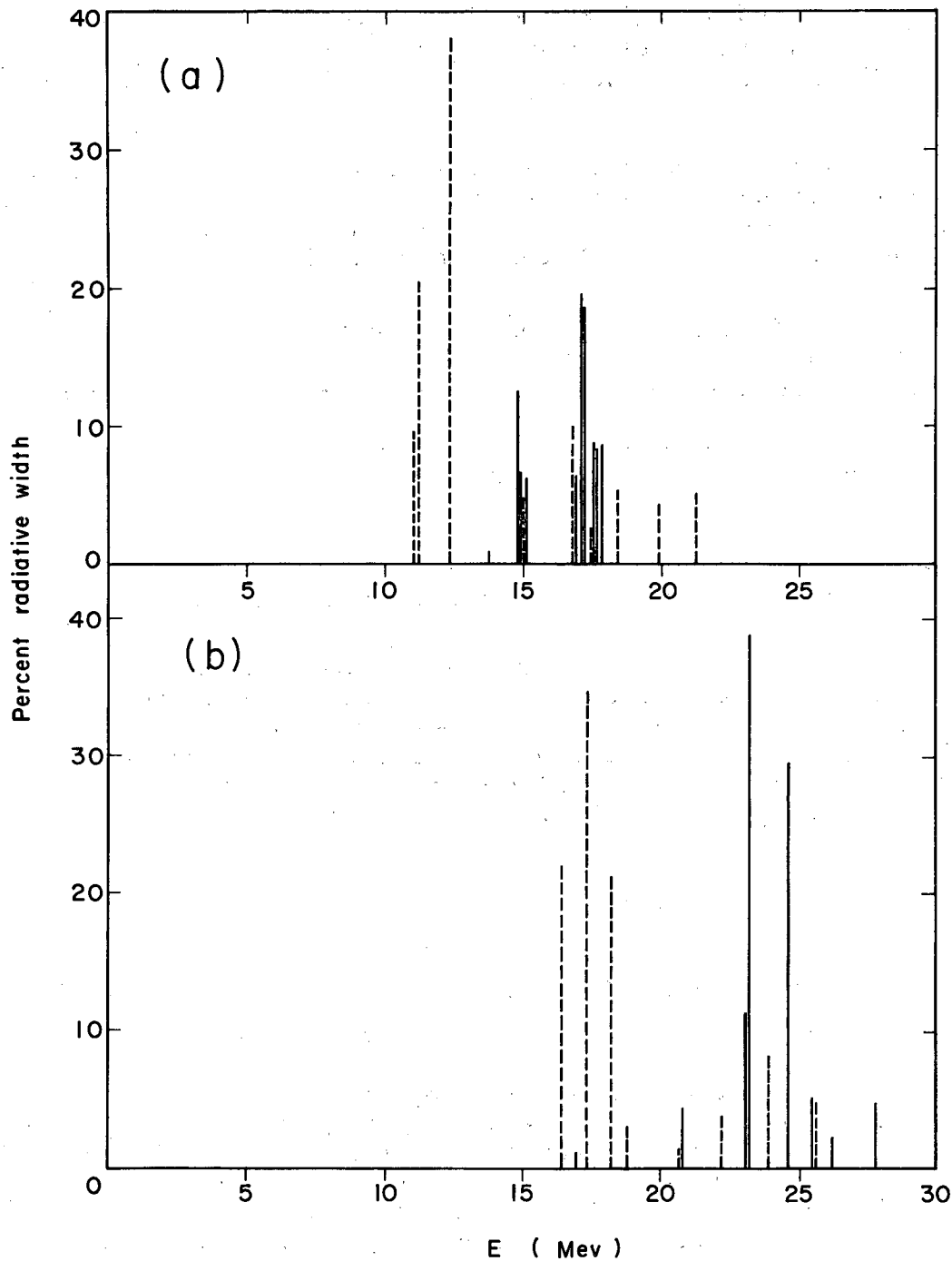
MUB-869

Fig. C.12-1. The calculated positions and relative radiative widths of the K = 0 (dashed lines) and K = 1 (solid lines) dipole states of Mg^{24} are shown (a) for the independent-particle model and (b) for the interacting system treated by the random-phase approximation described in the text. Levels with widths less than 1% of the total width for a given K have been omitted.

$$V = -\frac{f^2}{4\pi}\frac{e^{-\mu r}}{r}\left[1 + \left(1 + \frac{3}{\mu r} + \frac{3}{(\mu r)^2}\right) S_{12}\right] .$$

Here $1/\mu$ is the pion Compton wave length, $f^2/4\pi$ is the pion-nucleon coupling constant, and S_{12} is the usual tensor operator. This knowledge of the asymptotic behavior of the ptoential has been put to good use in recent phase-shift analyses of nucleon-nucleon scattering in reducing the number of phase shifts that have to be searched for.[2] The procedure rests on the fact that the higher-angular-momentum phases are insensitive to the interior region of the force because of the centrifugal barrier and hence can be set equal to the OPEP phases. In this way the effect of all higher phases can be accounted for. Concerning the inner region of the potential, meson theory cannot make a unique prediction. It must therefore be treated phenomenologically if one seeks to construct a potential model of the two-nucleon force.

Many phenomenological potentials have been constructed to reproduce some of the experimental data, such as these of Signell and Marshak,[3] Gammel and Thaler,[4] and Hamada.[5] However, neither the Signell-Marshak nor the Gammel-Thaler potential fits the deuteron data, while the latter in addition does not satisfy the OPEP constraint. On the other hand, Hamada has been fairly successful in reproducing the deuteron properties and the n-p scattering data with potentials that do have OPEP tails.

The purpose of this work was (a) to construct triplet-even potentials that are asymptotic to the OPEP and are modified in the inner region with ranges corresponding to the exchange of more than one pion in such a way that a bound state with the deuteron properties is obtained together with a phase shift at zero energy consistent with the known triplet scattering length; and (b) from these potentials to compute the D-state probability, the deuteron effective range, the shape-dependent parameter, scattering phase shifts for higher energies, and the deuteron electromagnetic form factor.

In principle the deuteron form factor, which can be measured by electron-deuteron elastic scattering, can yield information about the nucleon force, but this source has not been exploited to any extent as yet.[6, 7]

The analytic forms of the central, spin-orbit, and tensor parts of the potential are defined for $r > r_c$ as

---

[2] M. J. Moravcsik, UCRL-5317-T (1958). See also the review article, M. H. Mac Gregor, M. J. Moravcsik and H. P. Stapp, Nucleon-Nucleon Scattering Experiments and their Phenomenological Analysis, Annual Review of Nuclear Science, Vol 10 (Stanford University Press, Stanford, California, 1960).

[3] P. S. Signell and R. E. Marshak, Phys. Rev. 106, 832 (1957).

[4] J. L. Gammel and R. M. Thaler, Phys. Rev. 107, 1337 (1957).

[5] T. Hamada, Progr. Theoret. Phys. (Kyoto) 24, 126 (1960); ibid. 25, 247 (1961).

[6] V. Z. Jankus, Phys. Rev. 102, 1586 (1956).

[7] J. A. Mc Intyre and S. Dahr, Phys. Rev. 106, 1074 (1957); J. A. Mc Intyre and G. R. Burleson, Phys. Rev. 112, 2077 (1958).

$$V_c = -\mu \frac{f^2}{4\pi} \frac{e^{-x}}{x} \left\{ 1 + \frac{e^{-x}}{x} \sum a_n / x^n \right\} ,$$

$$V_{LS} = -\mu \frac{f^2}{4\pi} \left(\frac{e^{-x}}{x} \right)^2 \sum b_n / x^n ,$$

$$V_T = -\mu \frac{f^2}{4\pi} \frac{e^{-x}}{x} \left\{ \left(1 + \frac{3}{x} + \frac{3}{x^2} \right) \right.$$

$$\left. + \frac{e^{-x}}{x} \sum c_n / x^n + \left(\frac{e^{-x}}{x} \right)^2 \sum d_n / x^n \right\} ,$$

where $x = \mu r$. The core radius r_c is chosen such that the potential yields the deuteron binding energy, by a method given by Hamada.[5] The sums on n extend from 0 to 3.

A number of potentials which satisfy the requirements set down above together with a list of the corresponding properties of the n-p system are given in a full report of this work.[8] The scattering phase shifts δ_{LJ} calculated from these potentials are represented in Figs. C.13-1 to C.13-3 in the energy range 95 to 310 Mev and compared with two of the phase-shift solutions to the experimental data found by Breit and co-workers,[9] and with the solution at 95 Mev by MacGregor.[10] The experimental data, however, are not sufficiently abundant to assure that even other phase-shift solutions do not exist.

The deuteron electromagnetic form factor corresponding to our potentials was also computed. Of course this quantity depends not only on the deuteron wave function but also on the distribution of charge and magnetic moment in the nucleons themselves. In Fig. C.13-4 we illustrate our results by showing the boundaries between which all form factors corresponding to our potentials fall. For the nucleon form factors we have used the measurements by Hofstadter et al.[11] Note that the deuteron form factor depends most sensitively on the nuclear force for large momentum transfer q. Thus if the nucleon form factors are well known, the region $q \gtrsim 6f^{-1}$ if appropriate for studying the details of the inner region of the triplet-even force. Conversely if the force were well known one could deduce the nucleon form factors (in the combination $F^n + F^p$). We note, however, that for small q the boundaries on the deuteron

---

[8] N. K. Glendenning and G. Kramer, Nucleon-Nucleon Triplet-Even Potentials (Phys. Rev., to be published) (UCRL-9904, Dec. 1961).

[9] M. H. Hull, K. E. Lassila, H. M. Ruppel, F. A. McDonald, and G. Breit, Phys. Rev. 122, 1606 (1961).

[10] M. H. MacGregor, Phys. Rev. 123, 2154 (1961).

[11] R. Hofstadter and R. Herman, Phys. Rev. Letters 6, No. 6, 293 (1961).
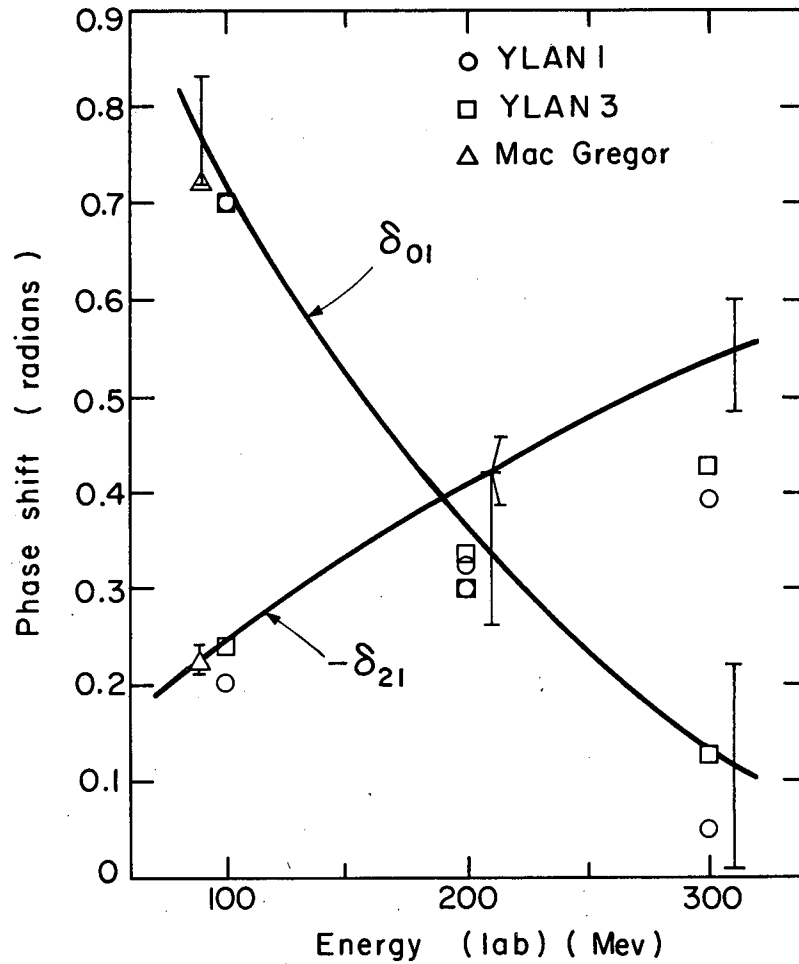
Fig. C.13-1. The coupled phase shifts δ_{01} and δ_{21}, computed from the
    potentials described in the text, are illustrated by indicating with
    a vertical bar the range in which they fall at each of three energies.
    The centers of these ranges are joined by a smooth curve. The phase-
    shift solutions of the data by Hull et al. (Ref. 9) are shown (referred
    to in their notation by YLAN1 and YLAN3) together with MacGregor's
    95-Mev results (Ref.10).
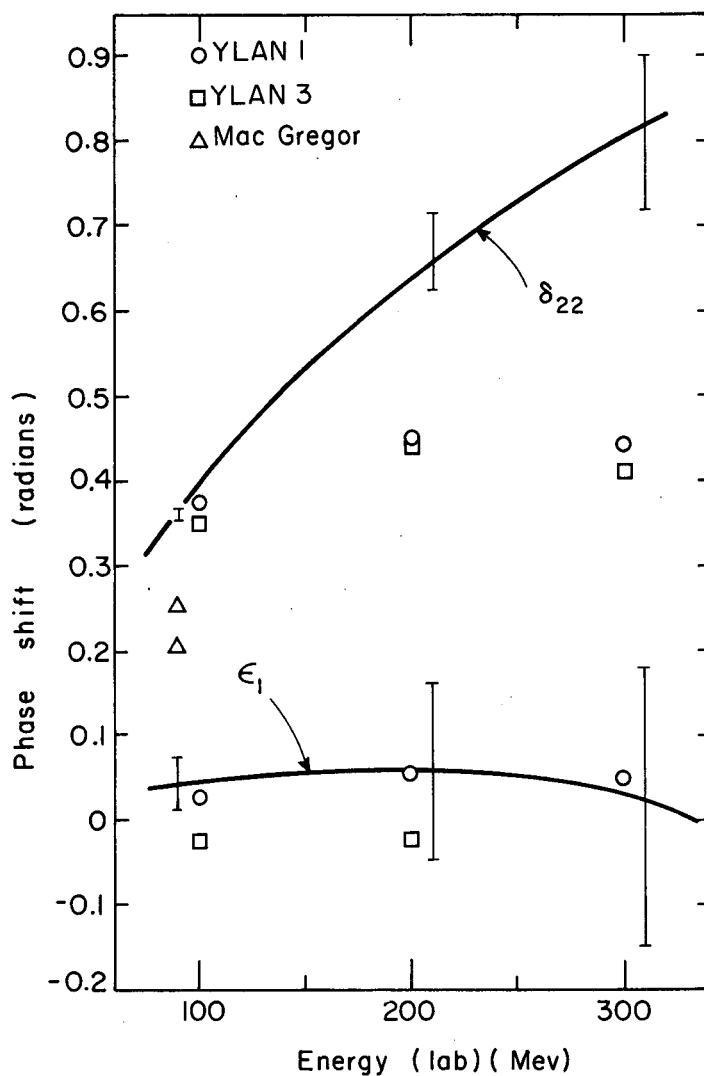
Fig. C.13-2. The coupling parameter ϵ_1 and uncoupled phase δ_{22},
computed from the potentials described in the text, are illustrated
by indicating with a vertical bar the range in which they fall at each
of three energies. The centers of these ranges are joined by a smooth
curve. The phase-shift solutions of the data by Hull et al. (Ref.9) are
shown (referred to in their notation by YLAN1 and YLAN3) together
with Mac Gregor's 95-Mev results (Ref.10).
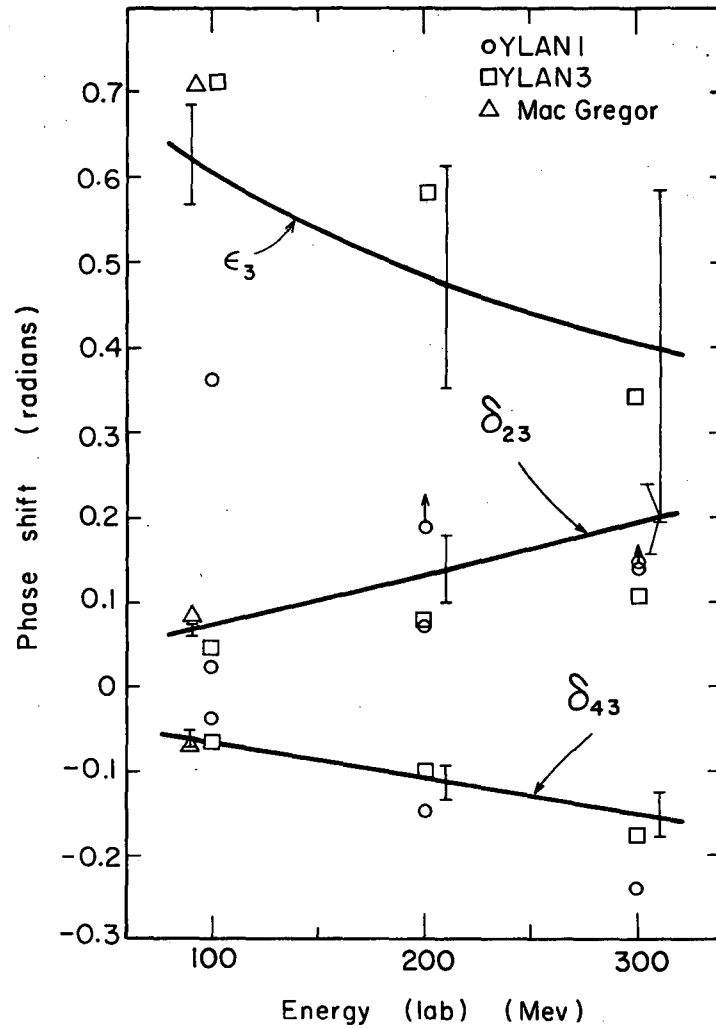
Fig. C.13-3. The coupled phases δ_{23}, δ_{43} and coupling parameter ϵ_3, computed from the potentials described in the text, are illustrated by indicating with a vertical bar the range in which they fall at each of three energies. The centers of these ranges are joined by a smooth curve. The phase-shift solutions of the data by Hull et al. (Ref.9) are shown (referred to in their notation by YLAN1 and YLAN3) together with Mac Gregor's 95-Mev results (Ref.10).
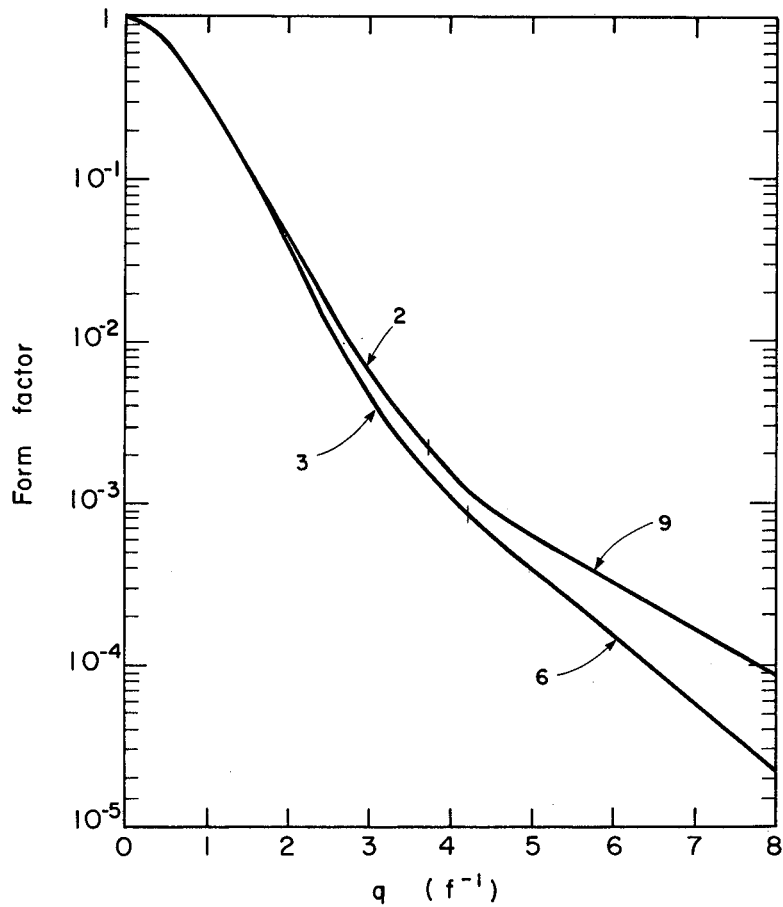
MU-24889

Fig. C.13-4. The two curves represent the upper and lower bounds on the
    deuteron electromagnetic form factor as calculated from the potentials
    described in the text. For purposes of illustration we have used a con-
    stant scattering angle $\theta = 90$ deg. The numbers on the curves correspond
    to the potential numbers in Table I of Ref. 8.

form factor do lie close together, indicating that to a high degree of accuracy it depends only on the well-established tail of the nucleon potential. In such a momentum-transfer region we can therefore use the elastic electron-deuteron scattering experiments to deduce the scalar nucleon form factor $F_1^n + F_1^p$ as we have done elsewhere.[12]

The D-state probability P_D is not susceptible to direct measurement, but it is relevant to the deuteron magnetic moment, hyperfine structure, photodisintigration and the form factor of the deuteron. We found that a triplet-even potential that has the correct asymptotic behavior and yields the deuteron binding energy and quadrupole moment will permit an almost unique prediction for the D-state probability if the triplet scattering length a_t is accurately known.[13]

---

[12] N. K. Glendenning and G. Kramer, Scalar Nucleon Form Factor, Phys. Rev. Letters (to be published).

[13] The scattering length a_t is variously reported as lying between 5.36 and 5.46. These limits do not constitute a very stringent condition on the potential.

14. THE SCALAR NUCLEON FORM FACTOR $F_1^n + F_1^p$ (*)

Norman K. Glendenning and Gustav Kramer[†]

All meson theoretic derivations of nucleon-nucleon potentials agree that the outer region should behave like the one-pion exchange potential (OPEP). The inner region cannot be calculated unambiguously, however, and is therefore usually treated phenomenologically.

The modification of the inner region in such a way as to fit the low-energy n-p data is the subject of a forthcoming work.[1] There we discovered that the integrals that enter the deuteron electromagnetic form factor G^2 are quite insensitive to the inner region of the potential for $q \lesssim 3$ f^{-1}, and are therefore determined by the well-established OPEP tail. This fact can be

---

[1] N. K. Glendenning and G. Kramer, Nucleon-Nucleon Triplet-Even Potentials, Phys. Rev. (to be published) (UCRL-9904, Nov. 1961). The potentials were required to yield the deuteron binding energy and quadrupole moment and give a scattering phase shift at zero energy consistent with the known scattering length. In addition, the phase shifts at higher energies were calculated and they agree roughly with the analysis of the experimental data at 95 Mev by M. H. MacGregor, Phys. Rev. 123, 2154 (1961), and two of the solutions in the energy range up to 300 Mev of M. H. Hull, K. E. Lassila, H. M. Ruppel, F. A. McDonald, and G. Breit, Phys. Rev. 122, 1606 (1961).

used to extract the sum of the neutron and proton charge form factors $F_1^P + F_1^n$ with practically no uncertainty arising from our imperfect knowledge of the n-p force. The sum $F_1^P + F_1^n$ is obtained from the expression[2]

$$G_{exp}^2 = (F_1^P + F_1^n)^2 (G_0^2 + G_2^2) + (2 \tan^2 (\theta/2) + 1) G_{mag}^2, \qquad (1)$$

where G_0, G_2, G_{mag} are respectively the contributions from the spherical and quadrupole charge distributions and the magnetic moment.[3] In addition to F_1^P and F_1^n, G_{mag} contains also the magnetic parts of the nucleon form factors F_2^P and F_2^n. Since G_{mag} is almost everywhere at least two orders of magnitude less than $G_0^2 + G_2^2$, its value will affect at most the third figure of $F_1^P + F_1^n$ (except at large angles, which we avoid). Since the already published neutron form factors of Hofstadter et al.[4] should allow us to compute G_{mag} to at least one significant figure, we shall use the published values of the nucleon form factors in G_{mag}.

We have used the experimental cross section for elastic electron-deuteron scattering of Friedman, Kendall, and Gram[5] to find $G_{exp}^2 = (d\sigma/d\Omega)_{exp}/(d\sigma/d\Omega)_0$, where $(d\sigma/d\Omega)_0$ is the cross section for electron scattering from a spinless point charge.

Drawing a smooth curve through a recent experimental measurement[6] of the proton charge form factor F_1^P, we obtained values for this quantity which we subtracted from our value of $F_1^P + F_1^n$ to get the neutron charge form factor. Our results are shwon in the Fig. C.14-1. The upper and lower limit on $F_1^n + F_1^P$ come both from the experimental uncertainty in G_{exp}^2 and the slight uncertainty in the integrals appearing on the right side of Eq. (1) arising from our imperfect knowledge of the nucleon force at small distances.

As can be seen from the figure, it is consistent with the existent data to say that the neutron charge form factor F_1^n is zero, at least up to a momentum transfer $q = 3f^{-1}$. However, most of the data suggest a very small negative value of the form factor.

Our results do not agree with those of the Stanford[4] and Cornell[7] groups who analyzed the inelastic (deuteron breakup) process. However, no analysis

[2] V. Z. Jankus, Phys. Rev. 102, 1586 (1956).

[3] R. Hofstadter, Nuclear and Nucleon Scattering of High-Energy Electrons, in Annual Review of Nuclear Science (Stanford University Press, Stanford, California, 1957), Vol. VII.

[4] R. Hofstadter, C. deVries, and R. Herman, Phys. Rev. Letters 6, No. 6, 290 (1961); R. Hofstadter and R. Herman, Phys. Rev. Letters 6, No. 6, 293 (1961). We used Eqs. (9) through (12) in the second of these references.

[5] J. I. Friedman, H. W. Kendall, and P. A. M. Gram, Phys. Rev. 120, 992 (1960).

[6] F. Bumiller, H. Croissiaux, E. Dally, and R. Hofstadter, Phys. Rev. (to be published).

[7] D. N. Olson, H. F. Schopper and R. R. Wilson, Phys. Rev. Letters 6, No. 6, 286 (1961); R. M. Littauer, H. F. Schopper, and R. R. Wilson, ibid. 6, No. 7, 141 (1961); ibid 6, No. 7, 144 (1961).
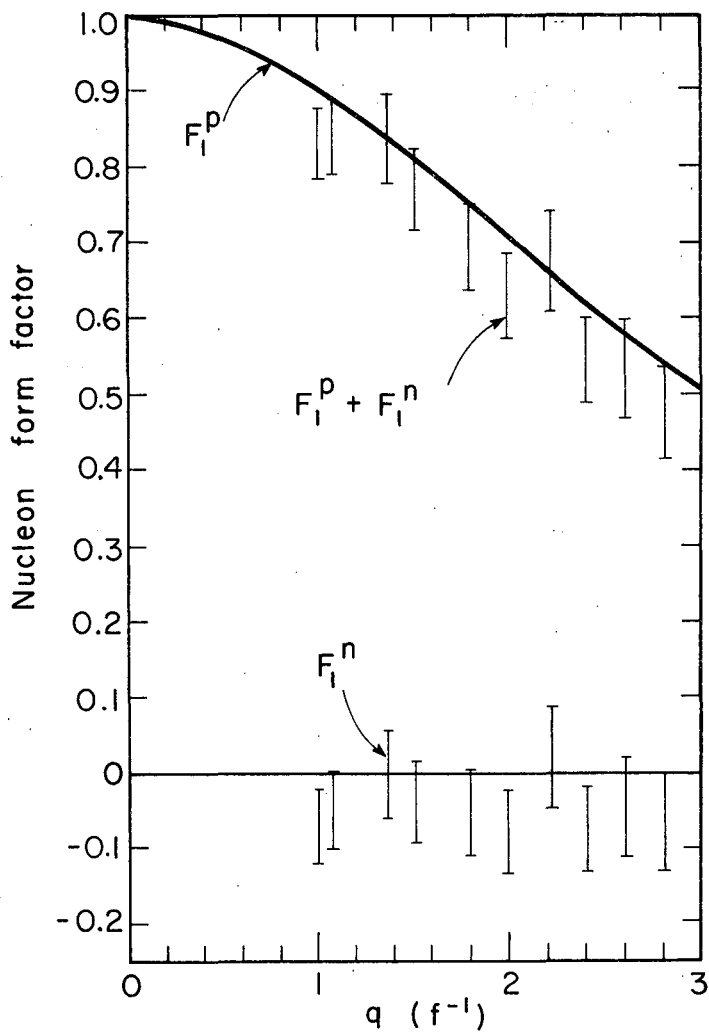
Fig. C.14-1. The sum of the charge parts of the nucleon form factors
$F_1{}^n + F_1{}^p$ which is deduced from Eq. (15) is shown. At $q \approx 1$ f^{-1}
about 20%, and at $q \approx 3$ f^{-1} about 50%, of the spread is due to our
incomplete knowledge of the triplet-even force. The rest is ex-
perimental error in the elastic scattering experiment. The proton
charge form factor $F_1{}^p$ is obtained from Ref. 6 by drawing a smooth
curve through the experimental results. There is an error on this
curve of about ±0.03. The neutron charge form factor is obtained by
subtracting the smoothed proton data from the points for $F_1{}^p + F_1{}^n$.
The error on the proton form factor should be added to those already
shown on $F_1{}^n$ to get the total uncertainty.

of the inelastic process to date has accounted for the presence of the D states in the deuteron, nor all of the final-state interactions, except in a rough manner.[2-8]

  There is some uncertainty introduced into our results by unknown relativistic and meson-current effects. Nevertheless we feel that these effects will be small in the region of low momentum transfer considered here.[9]

---

[8] L. Durand III, Phys. Rev. Letters $\underline{6}$, No. 11, 631 (1961); Phys. Rev. $\underline{123}$, 1393 (1961).

[9] R. Blankenbecler (Thesis, Stanford University, 1958) has studied relativistic corrections, using a simplified model of the deuteron (two bosons, one of which is charged, bound by a separable potential). In this model the corrections can give rise to a 25 to 30% reduction in the cross section at $q = 3$ f^{-1}, which would mean that the scalar charge form factor would be larger by as much as 15%. Whether the corrections would be as large in a realistic model is not clear. However, suppose that this is the correction that obtains at $q = 3$ f^{-1}. Then if we applied a correction that is 15% at $q = 3$ f^{-1} and goes linearly to zero as $q \rightarrow 0$, the limits we place on F_1^n would lie one above and one below the zero value for all values of q listed in our table except at $q = 2.2$ f^{-1}, where both limits are positive.

15. COMPARISON OF DIFFRACTION THEORY AND THE OPTICAL MODEL (*)

Jonas Alster[†] and H. E. Conzett

  The optical model describes the nuclear interaction between an incident particle and a nucleus in terms of a complex potential well, generally of the form

$$-[V + i W] \{1 + \exp[(r - R)/d]\}^{-1}.$$

The real (V) and imaginary (W) parts, the radius (R), and the surface thickness (d) parameters are determined from fitting the elastic scattering differential cross sections and the reaction cross section. The calculation involves solving (numerically) the Schrödinger equation for the system and determining the amplitudes, A_ℓ, and (nuclear) phase shifts, δ_ℓ, of the outgoing partial waves. From A_ℓ and δ_ℓ the cross sections are calculated.

  In the diffraction-theory treatment (Paper C.8), one starts directly with the A_ℓ and δ_ℓ, determines their ℓ dependence from fitting the elastic scattering data, and then calculates the interaction radius, surface thickness, and reaction cross section. Computationally, this is a much simpler task, especially for heavy-ion scattering in which a large number of partial waves contribute to the process.

  Because of the excellent agreement between theory and experiment achieved in the C^{12} scattering, it was of interest to make detailed comparisons between the two models. Therefore, we made a "fuzzy"-cutoff (diffraction) analysis of existing α-particle elastic scattering data which previously had been compared to an optical-model analysis.[1] One example of the comparison is given in Fig. C.15-1, where it is seen that an equally good fit to the experimental data is achieved by the diffraction treatment.

---

[1] G. Igo, Phys. Rev. $\underline{115}$, 1165 (1959).
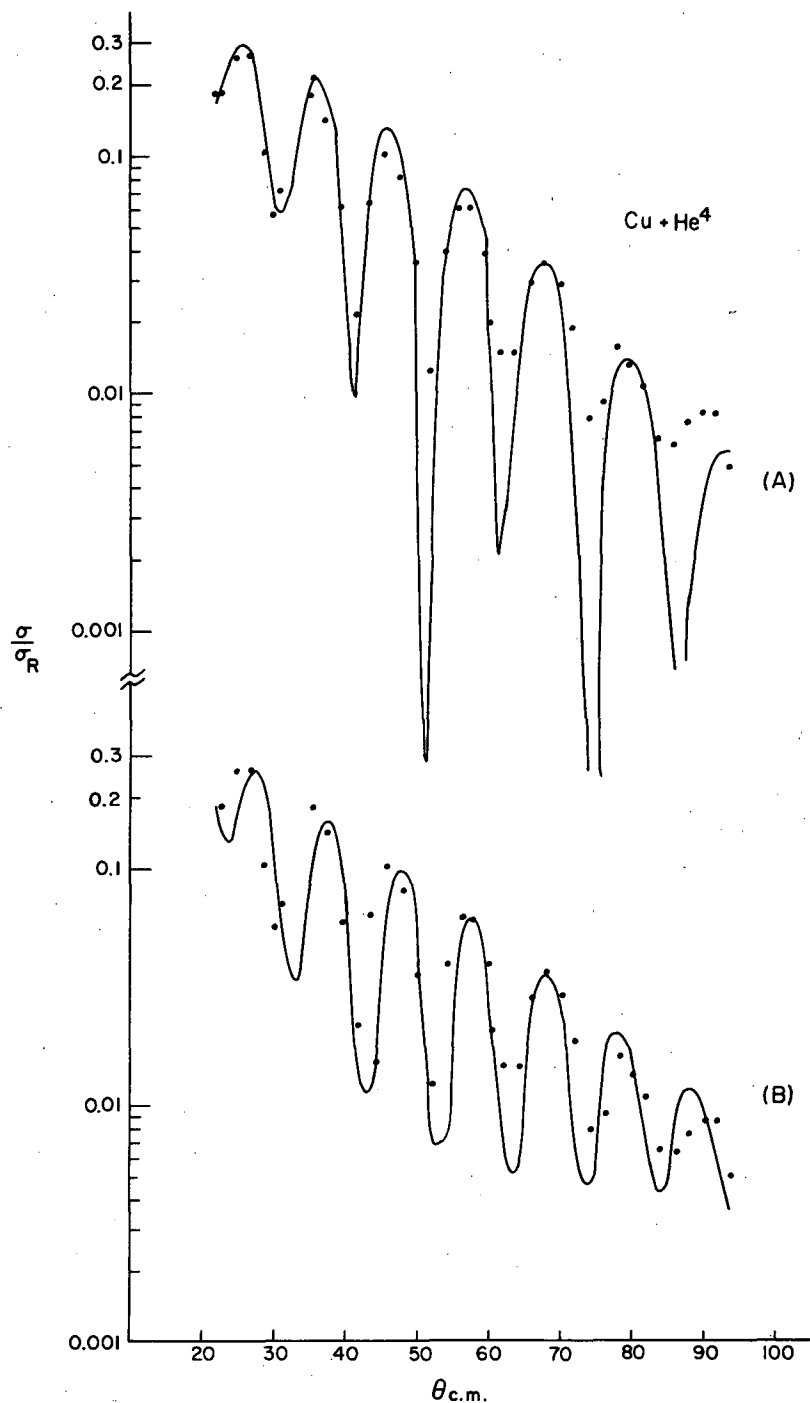
MUB-660

Fig. C.15-1. (a) The solid line is the optical-model fit to the elastic
scattering of 40-Mev α's from Cu (Ref. 1). Parameters are
$V = 49.3$ Mev, $W = 11$ Mev, $R = (1.14A^{1/3} + 2.24)f$, $d = 0.5$ f.
The points give the experimental values.
(b) The solid line gives the "fuzzy" - cutoff model fit to the same
data with the parameters $\ell_A = 17$, $\Delta \ell_A = 0.8$, $\delta = 0.7$, $\ell_\delta = 17$,
$\Delta \ell_\delta = 1.0$.

D. PHYSICAL CHEMISTRY

1. THE SOLVENT EXTRACTION OF HClO$_4$ BY DILUTE SOLUTIONS OF TRIBUTYL PHOSPHATE IN CCl$_4$

David C. Whitney and Richard M. Diamond

As part of a larger program of studying the extraction of inorganic compounds into organic solvents, the species and the mechanism for the solvent extraction of HClO$_4$ into tributyl phosphate (TBP) solutions in CCl$_4$ have been determined for the cases in which the organic phase in the extraction conforms reasonably well to the laws governing ideal solutions. The upper limit for such behavior has been found to be at TBP concentration on the order of a few tenths molar. Direct titrations of the acid and water (Karl Fischer determination) extracted into the organic phase, as well as infrared studies of the organic extracts, were used in the analysis. It was found that the extracting species present when the aqueous phase concentration is less than 6 M has the formula [3TBP·H$^+$·XH$_2$O] [ClO$_4^-$], having a minimum value of $\overline{1}$ at very low TBP concentrations and rising to 4 as the TBP concentration leaves the region of ideality; above 6 M this species starts to become replaced by a new species [TBP·H$^+$] [C$\overline{\text{lO}}_4^-$], the latter species apparently being the only one present by the time the aqueous phase HClO$_4$ concentration reaches 11.6 $\underline{M}$.

In the dilute HClO$_4$ case the extracted complex is built around the hydronium ion. Each of the hydrogens of this ion is hydrogen-bonded to either a TBP molecule (in the very dilute TBP solutions, which are mostly hydrophobic CCl$_4$) or to a water molecule which is in turn hydrogen-bonded to a TBP molecule (in the more concentrated TBP solutions, where the presence of the polar TBP reduces the repulsion of the organic phase for the water molecules). As the aqueous HClO$_4$ concentration rises the water activity drops in both phases, so that after the 6 $\underline{M}$ point is reached the TBP is able to displace the water in the hydronium ion to form a nonhydrated salt, similar to the reaction which takes place between acids and amines.

2. ON ANION-EXCHANGE RESIN SELECTIVITIES [*]

Benjamin Chu, [†] David C. Whitney, and Richard M. Diamond

Various explanations have been advanced for experimentally observed anion resin selectivities, but they usually fall into two classes. One of them attributes resin specificity to electrostatic ion pairing between the resin ionic groups and the anion,[1-3] and the other class explains specificity as due

---

[*] Condensation of UCRL-9907, Nov. 1961, submitted to J. Inorg. and Nuclear Chem.

[†] Department of Chemistry, Cornell University, Ithaca, New York.

[1] H. P. Gregor, J. Am. Chem. Soc. 70, 1293 (1948); ibid. 73, 642 (1951).

[2] S. A. Rice and F. E. Harris, Z. physik. Chem. 8, 207 (1956).

[3] J. L. Pauley, J. Am. Chem. Soc. 76, 1422 (1954).

to the polarizability of the anion in the field of the resin cation.[4,5] However, there are so many exceptions to the theoretically predicted orders of preference of the resin, regardless of which model is used, that there must be some other explanation for anion-exchange behavior. We would like to suggest that the difference in the local water structure inside and outside the resin and the extent of hydration of the ion play the major roles in determining resin selectivities.

In water, each H_2O molecule is hydrogen-bonded on the average to about three other H_2O molecules. In the resin, however, the high concentration of ionic groups and the intrusion of the resin matrix causes this normal water structure to be broken up into smaller units with one or two dimensions of the order of 10 angstroms, so that each H_2O molecule is hydrogen-bonded on the average to fewer H_2O molecules than in the aqueous phase. An anion which because of its large size tended to disrupt the water structure might thus be expected to be more readily exchanged into the already more disrupted resin phase from the more highly (hydrogen-) bonded aqueous phase than would a small highly hydrated ion. The effect would be greater, the larger (more disruptive) the ion is. If, however, there are strongly hydrophilic groups on the anion, it will have a very strong attraction for the aqueous phase where it can be better solvated, and it will not readily undergo exchange, this tendency becoming more pronounced as the anions get more basic (more highly hydrated).

These two ideas were tested by using two series of fatty acid anions. First the series acetate, butyrate, trimethylacetate, valerate, and caproate was studied. These anions are derived from acids of the same strength, so that the carboxylate group in each is hydrated to the same degree. But as the size of the hydrocarbon tail is made larger the water structure in the dilute aqueous phase is disturbed to an increasing extent, and the larger the anion the more strongly it is pushed into the resin phase in the exchange with chloride ions. With the second series of anions, trimethylacetate, methyldichloroaceteate, and trichloroacetate, the size of the anion is held relatively constant, but the replacement of methyl groups by chloring atoms causes a decrease in the basic strength of the ion (increase in acidity of the parent acid) and hence a decrease in its degree of hydration. The smaller its tendency to hydrate, the more easily the anion would go into the resin phase in exchange with chloride ion, yielding the observed selectivity order. These results and those obtained by other investigators[1-8] tend to confirm the idea that the principal origin of anion selectivity with quaternary ammonium resins comes from the attempt by the system to maximize the water-water and ion-water interactions, and not in any specific resin group —counter ion interaction.

---

[4] H. P. Gregor, Jack Belle, and R. A. Marcus, J. Am. Chem. Soc. 77, 2713 (1955).

[5] J. Aveston, D. A. Everest, and R. A. Wells, J. Chem. Soc. 231, (1958).

[6] R. M. Wheaton and W. C. Bauman, Ind. Eng. Chem. 43, 1088 (1951).

[7] K. A. Kraus and F. Nelson, J. Am. Chem. Soc. 76, 984 (1954).

[8] G. E. Boyd, S. Lindenbaum, and G. E. Myers, J. Phys. Chem. 65, 577 (1961).

3. THIN CATION-EXCHANGE FOILS. [*]

Sven Bjørnholm and C. Michael Lederer

Treatment of commercial polystyrene sheet with fuming sulfuric acid produces a thin layer of cation exchanger. Sources for α and β spectroscopy can be made by applying a solution containing a radioactive cation to this layer.

Sulfonated foils can be made in a few minutes; a simple press and standardized fuming sulfuric acid are the only required materials. They generally absorb polyvalent cations from solutions which are 0.001 to 0.1 $\underline{M}$ in H^+ or other monovalent ions. Selective absorption of one ion in preference to another is often possible. Details of the sulfonation and absorption procedures are contained in the unabridged paper.

Important properties of the sulfonated layer are its thickness, which determines the energy spread of emerging radiation; the capacity per unit area (millimicro equivalents of exchangeable hydrogen per cm^2) which determines the number of ions that can be absorobed; and the specific capacity (milliequivalents per gram), which determines how quantitative the absorption will be. [Equilibrium for absorption of an n-valent cation depends on a factor (specific capacity).^{n}] These parameters depend on the concentration of SO_3 in sulfonating solution and the length of time of sulfonation. They were measured by a Th^{228} recoil method described in the full paper.

The table gives the results of a series of measurements in which sulfonation time and the concentration of fuming sulfuric acid have been varied. The numbers are averages of several determinations, the errors indicating the reproducibility of the sulfonation process.

The specific capacity reaches a saturation value of 5.6 milliequivalents per gram when the volume ratio, fuming H_2SO_4: conc. H_2SO_4, is 1:1 or more. This capacity corresponds to the introduction of one sulfonic acid group per benzene ring. The capacity at various points on the sulfonated surface was shown to be constant to within 20%.

Foils of high specific capacity are easily produced with thicknesses between 8 and 200 $\mu g/cm^2$. They have been used to prepare sources of curium, californium, einsteinium, and fermium. Selective absorption was manifest in several cases.

---

[*] Abstracted from a paper (UCRL-9957, Dec. 1961) to be submitted to Nuclear Instr. and Methods.

Thickness, capacity, and specific capacity of sulfonated foils.

Sulfonating agent Ratio of fuming H_2SO_4[a] to conc. H_2SO_4[b]	Normality (eq/liter)	Sulfonation time[e]	Thickness ($\mu g/cm^2$)	Capacity[d] $m\mu eq/cm^2$)	Specific capacity[e] (meq/g)
1:3	35.7 ± .1	4 min	2.8 ± 1	0.29 ± .08	0.11 ± .02
		12 min	3.5 ± 1	0.35 ± .08	0.11 ± .02
		25 min	3.7 ± 1	0.42 ± .08	0.12 ± .02
1:1.8	36.9 ± .1	2 min	3.8 ± 1	0.86 ± .2	0.23 ± .04
1:1	38.0 ± .1	5 sec	9 ± 3	39 ± 15	4.3 ± 1.0
		15 sec	14 ± 3	82 ± 20	5.7 ± .4
		1 min	23 ± 5	130 ± 30	5.8 ± .4
		2 min	52 ± 10	280 ± 60	5.4 ± .4
2:1	39.1 ± .1	5 sec	13 ± 4	80 ± 20	5.8 ± .4
		15 sec	16 ± 4	90 ± 30	5.5 ± .4
		1 min	39 ± 8	200 ± 40	5.2 ± .4
		2 min	88 ± 18	490 ± 100	5.6 ± .4

The polystyrene is an ordinary biaxially oriented product, Trycite, made by extruding pure polystyrene with no plasticizer (manufactured by Dow Chemical Co., U.S.A.).

[a]Fuming sulfuric acid: 30 to 33% SO_3 in H_2SO_4 by weight; reagent grade.

[b]Concentrated sulfuric acid: 96% H_2SO_4 by weight; reagent grade.

[c]At room temperature.

[d]$m\mu eq = 10^{-9}$ eq $= 6 \times 10^{14}$ sulfonic acid groups.

[e]It is assumed that thorium is absorbed as a quadrivalent cation.

4. ISOLATION OF TRANSCURIUM ELEMENTS

Sherman Fried and Hugo Schumacher [*]

The irradiation of Cm^{244} in a high flux of neutrons is currently the only practical method of preparing the heavy elements berkelium, californium, einsteinium, and fermium in "substantial" quantities. The reactions may be diagrammatically indicated below.

$$Cm^{244} + X \text{ neutrons} = Cm^{245, 246, 247, 248, 249}$$

$$Cm^{249} \longrightarrow Bk^{249} + \beta^-$$

$$Bk^{249} \longrightarrow Cf^{249} + \beta^-$$

$$Cf^{249} + X \text{ neutrons} \longrightarrow Cf^{250, 251, 252, 253, 254}$$

$$Cf^{253} \longrightarrow Es^{253} + \beta^-$$

$$Es^{353} + n \longrightarrow Es^{254}$$

$$Es^{254} \longrightarrow Fm^{254} + \beta^-.$$
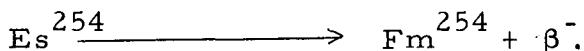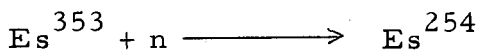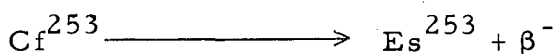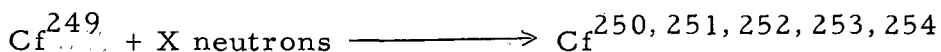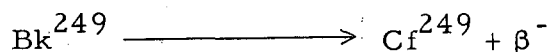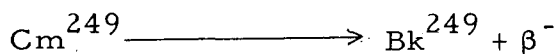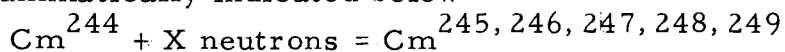
The reactions listed above do not by any means represent the complete set, but will serve as an outline. In general most of the actinides formed in such a bombardment are alpha emitters. The notable exceptions are Bk^{249}, Cf^{252}, and Cf^{253}. Berkelium-249 is a beta emitter, as is Cf^{253}, and the radiation hazards from these nuclides is negligible. Californium-252, on the other hand, decays to some extent by spontaneous fission ($t_{1/2} \approx 60$ yr) and thus is an intense source of fast neutrons. In addition, various fission products accumulate during the irradiation (mainly from the fission of Cm^{245}) and these are sources of high-energy gamma and beta activity.

From what has been stated above it is clear that suitable protective precautions had to be taken, and in fact the separations and purifications were carried out by using a novel type of shielding arrangement devised by the Health Chemistry Department of this Laboratory.

The shielding arrangement consisted of a set of interlocking water-filled tanks 4 ft thick surrounding a totally enclosed master-slave-equipped box in which the actual manipulations were carried out. The shield contained openings for introduction and removal of lines, cables, samples, equipment, etc., and viewing was made possible by means of a water-filled window 2.5X4.5 ft. In addition--and perhaps most important--was the provision made for assaying and removing samples during the course of the run. Remote-control pipetters were developed and the use of a Kollmorgen magnifying periscope as well as binoculars permitted the determination and removal of very small accurately known quantities of solutions for assay. A fast neutron-uranium fission proportional counter, developed by A. E. Larsh,[1] was made

---

[*] On leave from Eidgenössisch Institut für Reaktorforschung, Würenlingen, Aargau, Switzerland.

[1] Almon E. Larsh (Lawrence Radiation Laboratory), Private communication.

integral with the enclosure box, and this made possible the determination of the amount of Cf^{252} present in various samples without their removal from the box. This greatly facilitated the analysis of elution fractions, since they could be assayed in place and the progress of the separation observed concurrent with the elution. With this facility available the operations attendant on purification and separation of the heavy elements were carried out without any undue difficulty. The cave facility is fully discussed in a separate report by the Health Chemistry Division.[2]

Approximately 120 mg of "Cm^{244}", whose actual isotopic composition was

Mass	Atom %
244	89.35
245	1.22
246	8.89
247	0.29
248	0.25

was irradiated in the Materials Testing Reactor at a nominal flux of 5×10^{14} for a total nvt of approximately 2.4×10^{22}. The curium was irradiated as the oxide and was packed in an aluminum capsule approximately 0.5×1 in. After irradiation, the capsule was dissolved and subjected to the various chemical precesses designed to separate the actinide elements from each other.

The curium fraction after separation from the rare earth fission products and from the other actinide elements consisted of approximately 90 mg of material of the following isotopic composition.

Mass	Atom %
243	0.7
244	81.81
246	0.833
246	15.9
247	0.547
248	0.914

The separation process depended largely on the use of ion-exchange resins. In particular, the use of anion-exchange resins in the presence of very concentrated lithium chloride solutions permitted the gross separation of the actinides from each other as well as from the rare earth fission products, ordinarily a rather difficult and tedious problem. The flow sheet for this separation is given below.

---

[2]P. W. Howe, T. C. Parsons, and L. E. Miles, The Water-Shielded Cave Facility for Totally Enclosed Master-Slave Operations at Lawrence Radiation Laboratory, UCRL-9657, Oct. 9, 1961.

D.4   -166-   UCRL-10023

```
                    ┌─────────────────────────┐
                    │ irradiated Al capsule    │
                    │ containing Cm            │
                    └─────────────────────────┘
                               │
                               │  dissolved in
                               │  NaOH + NaNO₃
         ┌──────────────┐      │        ┌──────────────────────┐
         │ sol. of Al   │──────┴────────│ ppt of lanthanide     │
         │ fission prod │               │ & actinide oxides     │
         └──────────────┘               │ + fission prod.       │
                                         └──────────────────────┘
                                                │ centrifuge &
                                                │ wash
    ┌──────────────┐                            │
    │ supernatant  │────────────────┐           │
    │ discarded    │                │           │
    └──────────────┘                │    ┌──────────────────────┐
                                     │    │ actinide & lanthanide │
                                     │    │ hydroxides            │
                                     │    └──────────────────────┘
                                                │
```

Dissolve in 6 $\underline{M}$ HCl, add Fe carrier, ppt
with NH₄OH, centrifuge, dissolve, in
0.1 $\underline{M}$ HCl

┌──────────────────────┐
│ solution of actinides │
│ lanthanides + Fe   │
└──────────────────────┘

absorb on
cation resin
and wash with 2M
HCl, elute with 6M HCl

┌──────────────┐   ┌──────────────────────┐
│ Fission prod.│   │ purified actinides   │
│ + Fe   │   │ and rare earths in   │
└──────────────┘   │ 6 $\underline{M}$ HCl solution │
                                     └──────────────────────┘

evaporate & take
up in 12 $\underline{M}$ LiCl

┌──────────────────────┐
│ Solution of actinides │
│ & lanthanides in 12 $\underline{M}$ LiCl │
└──────────────────────┘

adsorb on anion
resin and then elute
with 10 $\underline{M}$ LiCl

(next page)

| 1st fraction: rare earth fission prod | 2nd fraction: Cm & Am | 3rd fraction: berkelium | 4th fraction: Cf, Es, & Fm |

Add Fe carrier, ppt with NH_4OH, centrifuge & diss. in 6 M HCl, adsorb on anion resin

Cf, Es, & Fm in 6 M HCL

evaporate, dissolve in 0.05 M HCl, adsorb on cation resin (Dowex-50) and elute with α hydroxy-isobutyric acid

| 1st fraction Fm | 2nd fraction Es | 3rd fraction Cf |

After the gross separations had been performed specialized ones were carried out, using the cation-exchange resin Dowex-50 employing α-hydroxy-iso-butyric acid as the eluting agent. Separations of einsteinium and fermium from californium were carried out using this method.

The separation of berkelium was carried out on that fraction of the LiCl eluate between the end of the curium fraction and the beginning of the californium. The method of isolating this element was that due to Peppard,[3] in which advantage is taken of the fact that Bk may be oxidized to the IV state. In this state it may be extracted into di-(2-ethyl hexyl) ortho phos-phoric acid from 10 N HNO_3. Under these conditions it is extracted to the virtual exclusion of the actinides in the III state. The quantity of berkelium was determined by following the rate of growth of its Cf^{249} daughter. In general these separation methods were quite satisfactory. The lone exception has been in the recovery of the element berkelium. According to the rough calculations possible at the present state of the knowledge of cross sections, approximately 7 μg of Bk^{249} should have been recovered. Instead, only

[3] D. F. Peppard, S. W. Moline, and G. W. Mason, J. Inorg. Nuclear Chem. 4, 344-8 (1957).

1.5 μg has been found. It is very difficult to trace this element and thus far it has not been possible to determine where the loss occurred. Californium, on the other hand, was obtained in somewhat greater quantities than expected on the basis of previous experiences. The yield of Cf^{252} as determined both by fission counting and alpha pulse-height analysis was 29.5 μg.

The amount of einsteinium-253 recovered on the first separation was 0.289 μg. Later other milkings of the californium yielded further samples of E^{253}. The isotopic composition of the californium resulting from this irradiation was

Mass	Atom %
249	5.01
250	12.34
251	3.91
252	78.12
253	0.58
254	0.04

5. THE CRYSTAL STRUCTURE AND PHYSICAL PROPERTIES OF AMERICIUM METAL (*)

D. B. McWhan[†] and B. B. Cunningham

X-ray diffraction patterns obtained from a number of polycrystalline samples of americium metal have been indexed as arising from a hexagonal structure with a "c" axis double that to be expected for normal hexagonal close packing. The lattice constants are

$$a = 3.4681 \pm 0.0008 \text{ A},$$

$$c = 11.240 \pm 0.004 \text{ A} \quad \text{at } 20^\circ C.$$

The doubling of the c axis suggests that americium crystallizes in the lanthanum-type structure, which is $P6_3/mmc$ (D_{6h}^4) with metal atoms in 2(a)000;00$\frac{1}{2}$, and 2(C) 1/3, 2/3, $\frac{1}{4}$; 2/3, 1/3, 3/4. In general, calculated and observed intensities of the diffraction lines are in satisfactory agreement except for a few lines in which the discrepancies may be attributed to stacking faults such as have been observed in cobalt.[1]

---

[1]O. S. Edwards and H. Lipson, Proc. Roy. Soc. (London) A180, 268 (1942).

The calculated americium metal density at $20°$ C is $13.67 \pm .005$ g/cm^3. Each americium has six nearest neighbors at 3.468 A and six at 3.450 A, which gives a metallic radius for coordination number 12 of 1.730 A.

Metal prepared by condensing americium vapor obtained by the high-temperature reaction of americium dioxide with liquid lanthanum metal gave a diffraction pattern which was indexed as face-centered cubic with an average a for several productions of $4.895 \pm .005$ A, giving a calculated density of $13.65 \pm .05$ g/cm^3 and a metallic radius for CN12 of 1.73 A.

The dhcp metal studied in the present work has a density some 16% higher than that of dhcp americium prepared previously,[2] for which a and c were found to be

$$a = 3.642 \pm .005 \text{ A},$$

$$c = 11.76 \pm .01 \text{ A},$$ giving a density of $11.87 \pm .05$ g/cm^3 and a metallic radius 1.82 A (CN12).

X-ray diffraction studies on americium metal have been carried out in a temperature range from $-120°$ C to $605°$ C. The data were fitted to a polynomial of second order in temperature by the method of least squares yielding the following calculated coefficients of thermal expansion at $20°$ C:

$$a_a = (7.5 \pm .2) \times 10^{-6} /°C,$$

$$a_c = (6.2 \pm .4) \times 10^{-6} /°C.$$

Up to $605°$ C there is no definite indication of any change in structure.

The melting point of americium metal was found to be $994 \pm 7°$ C on the basis of two separate determinations.

The magnetic susceptibilities of six samples of americium metal have been investigated, with the results listed in the table.

The best value for the magnetic susceptibility of americium metal at $20°$ C is

$$X_{20°C} = (881 \pm 46) \times 10^{-6} \text{ erg/ gauss}^2 / \text{mole}.$$

In the temperature range over which the magnetic susceptibility was measured, $-196°$ C to $550°$ C, there was no evidence for any magnetic transitions, and between -196 and $20°$ C there was less than 2% change in the susceptibility of americium metal; the limit to the temperature dependence between 20 and $550°$ C may be set $\leq 5\%$.

The work on americium metal is continuing in an effort to determine the reason for the existence of two stable dhcp americium metal structures. The freedom of the metal samples from anionic impurities, especially oxygen, is unproven and efforts to determine the oxygen content by activation analysis will be continued.

---

[2] P. Graf, B. B. Cunningham, C. H. Dauben, J. C. Wallmann, D. H. Templeton, and H. Ruben, J. Am. Chem. Soc. **78**, 2340 (1956).

Magnetic susceptibility of americium metal

Sample	$\chi_{20^\circ C} \times 10^6$ (ergs/gauss^2/mol)	Mol % Am	Weight (mg)	$\dfrac{d\chi}{d(1/i)}$
28[a,b]	881 ± 32	99.8	2.529	-
27[b]	876 ± 55	98.5	0.336	-
25[a,b]	885 ± 50	96.9	3.423	175
9[c,d]	900 ± 100	94.4	0.631	1780
17[c,d]	928 ± 100	89.6	1.028	103
13[c,d]	738 ± 100	88.7	1.295	519

[a] Samples 28 and 25 were measured with tantalum and corrected with a blank run.

[b] Samples 25, 27, and 28 were run with a fiber calibrated against $Ni(NH_4)_2(SO_4)_2 \cdot 6H_2O$ and Nd_2O_3 .

[c] Samples 9, 17, and 13 were sealed in quartz capillaries, and the gram susceptibility of quartz was assumed to be -0.493×10^{-6} cgs units.

[d] Samples 9, 17, and 13 were run with a fiber calibrated against $Fe(Nh_4)_2(SO_4)_2 \cdot 6H_2O$, and used the small pole faces, which resulted in an apparent shape factor.

6. CRYSTAL STRUCTURE OF CESIUM MANGANESE FLUORIDE [*]

Allan Zalkin, Kenneth Lee, and David H. Templeton

The magnetic properties of compounds $KMeF_3$, were Me is a 3d transition ion, have attracted considerable attention. These compounds crystallize in the perovskite structure and are ferromagnetic at low temperatures. As a continuation of studies of $KMnF_3$,[1] crystals of $CsMnF_3$ were prepared. X-ray diffraction examination revealed that the structure is not that of perovskite, but rather that of the hexagonal form of barium titanate.[2,3] This result is of importance to the magnetic properties, because the geometry of the surroundings of Mn ions is quite different in the two structures.

[1] A. J. Heeger, O. Beckman, and A. M. Portis, Phys. Rev. 123, 1652 (1961).

CsMnF$_3$ was prepared by heating CsF and MnF$_2$ in HF at 900° and by precipitation from solution. Single crystals were obtained by slow traversal of a thermal gradient, with the melting point of 750±20° near the center of the gradient. Pink single crystals of approximately 2 mm size were obtained.[4]

Weissenberg photographs were taken of a small fragment to establish the symmetry and orientation. From these patterns it was recognized that the structure was essentially the same as that of hexagonal barium titanate.[2] The crystal was mounted on a General Electric XRD-5 diffractometer equipped with a single-crystal orienter, a scintillation counter, and a Mo x-ray tube ($\lambda = 0.70929$ A for Kα_1). With this instrument the cell dimensions were determined to be

$$a = 6.213 \text{ A},$$

$$c = 15.074 \text{ A}.$$

The intensities of 326 independent reflections were measured, including 31 which were recorded as zero. The crystal was large enough that absorption was occurring, but because of the complex shape this correction was not made.

The atomic parameters were refined by least squares, using the full matrix, starting with the values reported for BaTiO$_3$. Five coordinates, six isotropic temperature factors, and one scale factor were refined. Because the absorption effect is largest for the small-angle data, the final refinement was done with only the 274 reflections with $(\sin\theta)/\lambda$ greater than 0.35. For these reflections the conventional unreliability factor R was reduced to 0.096, and the parameters listed in the Table were obtained. The temperature factors are unreliable because of the neglect of absorption, but it is believed that the coordinates are not much affected by this error.

Atomic parameters for CsMnF$_3$.

Atom	x	y	z	$\sigma(x)$	$\sigma(z)$	B, A^2
Cs$_1$	0	0	1/4	...	...	0.8
Cs$_2$	1/3	2/3	0.0986	...	0.0001	0.8
Mn$_1$	0	0	0	...	...	0.7
Mn$_2$	1/3	2/3	0.8498	...	0.0004	0.6
F$_1$	0.522	0.044	1/4	0.002	...	1.4
F$_2$	0.834	0.668	0.078	0.002	0.001	1.2

[2]R. D. Burbank and H. T. Evans, Acta Cryst. 1, 330 (1948).

[3]This isomorphism has also been reported by YU. P. Simanov, L. P. Batsanova, and L. M. Kovba, J. Inorg. Chem. U.S.S.R., 2, 2410 (1957), but atomic coordinates were not determined.

The structure contains two kinds of manganese atoms, each surrounded by six fluorine atoms at the corners of an octahedron. For Mn_1 the surroundings are much like the perovskite structure, with each fluorine neighbor shared as the corner of a neighboring octahedron. The six fluorine atoms are at a distance of 2.14 A. The nearest manganese neighbors are six Mn_2 atoms at 4.24 A. The second kind of manganese, Mn_2, has three fluorines at 2.11 A and three at 2.16 A. Each of these octahedra shares a face with another and three corners with octahedra of the first kind. Thus Mn_2 has one Mn_2 neighbor at 3.01 A and three Mn_1 neighbors at 4.24 A.

7. CRYSTAL STRUCTURE OF COBALT SULFATE HEXAHYDRATE [*]

Allan Zalkin, Helena Ruben, and David H. Templeton

Calorimetric measurements by Rao and Giauque[1] showed some unaccountable residual entropy in crystals of $CoSO_4 \cdot 6H_2O$ at low temperatures. We have investigated the crystal structure in search of an explanation of the disorder. The resulting structure offers no possibility of disordered rings of hydrogen bonds such as were found in $Na_2SO_4 \cdot 10H_2O$,[2] nor do we find any other explanation of the entropy discrepancy.

The structure was solved by use of x-ray diffraction photographic data from single crystals of the three isomorphous substances $CoSO_4 \cdot 6H_2O$, $MgSO_4 \cdot 6H_2O$, and $MgSeO_4 \cdot 6H_2O$. Crystals of the two sulfates were grown from saturated solutions at 50 to 55°, because at room temperature the heptahydrates would have been obtained. The selenate was crystallized at room temperature.

The crystals are monoclinic, space group C2/c, with unit cell dimensions as follows.

	$CoSO_4 \cdot 6H_2O$	$MgSO_4 \cdot 6H_2O$	$MgSeO_4 \cdot 6H_2O$
a (A)	10.032 ± .004	10.110 ± .005	10.36 ± .03
b (A)	7.233 ± .003	7.212 ± .004	7.38 ± .04
c (A)	24.261 ± .010	24.41 ± .01	25.1 ± .1
β (deg)	98.37 ± .03	98.30 ± .04	98.1 ± .2

The atomic positions were determined by Fourier methods and refined by least squares with the full-matrix program of Busing and Levy.[3] With 836 independent reflections, the conventional unreliability factor R was reduced to 0.130 (including zeros) and 0.109 (omitting zeros).

[*] Brief version of paper submitted to Acta Crystallographica.

[1] R. V. G. Rao and W. F. Giauque (University of California), private communication, 1960.

[2] H. W. Ruben, D. H. Templeton, R. D. Rosenstein, and I. Olovsson, J. Am. Chem. Soc. 83, 820 (1961).

[3] W. R. Busing and H. A. Levy, Crystallographic Least-Squares Refinement Program for the IBM 704, CF-59-4-37 (ORNL-59-4-37), April 1959.

The unit cell contains eight formula units. Cobalt atoms occur in two sets of special positions:

Co_1 in 4(a): $(0, 0, 0; \ 0, 0, \frac{1}{2}) + C;$

Co_2 in 4(e): $\pm (0, y, \frac{1}{4}) + C,$ with $y = 0.949.$

Sulfur and ten sets of oxygen atoms occur in general positions. The crystal structure, shown in Fig. D. 7-1, consists of the two kinds of cobalt atoms each surrounded by six water molecules at the corners of an octahedron. Each water molecule is coordinated by only one cobalt atom. Between these groups occur the sulfate ions. The entire structure of sulfate and water oxygen atoms is connected by hydrogen bonds (Fig. D. 7-2). These hydrogen bonds are recognized by principles of bond geometry. Only one configuration of hydrogen atoms in these bonds corresponds to neutral water molecules, and therefore there is no opportunity of disorder of the type observed in sodium solfate decahydrate.

To provide more direct evidence of the hydrogen atoms' positions, we have refined the structure of the magnesium sulfate hexahydrate, using more accurate data obtained by direct counting of the x-ray reflections. After refinement of the heavy atoms with anisotropic temperature factors, the hydrogen atoms are seen as the largest peaks in the difference function. Their locations confirm the configuration assigned by the principles of bond geometry. With 2576 independent reflections, isotropic temperature factors for hydrogen, and anisotropic temperature factors for the other atoms, the unreliability factor R has been reduced to 0.055.

8. THE SPECTRUM OF UCl_4 (*)

Ralph McLaughlin

Thin crystals of UCl_4 were obtained by condensing the vapor between closely spaced pyrex plates. The spectrum of these crystals was observed at liquid He temperature. Under these conditions it was possible to resolve what usually appear as broad bands into groups of lines.

Angular momentum quantum numbers (J) were tentatively assigned on the basis of relative widths of line groups. These tentative assignments were modified until a good least-square fit with a reasonable value of the spin-orbit coupling constant ζ was obtained. In this fitting process the positions of all terms and ζ were treated as variable parameters. This process was repeated treating the Slater integrals F_2, F_4, F_6, and ζ as parameters. Essential agreement between these two approaches led to the conclusion that configuration interaction has little effect upon the positions of energy levels in UCl_4. This calculation also resulted in the assignment of the quantum numbers L and S. The parameters giving the best fit were $F_2 = 206.1 \ cm^{-1}$, $F_4 = 30.09 \ cm^{-1}$, $F_6 = 4.516 \ cm^{-1}$, and $\zeta_{5f} = 1,638 \ cm^{-1}$.
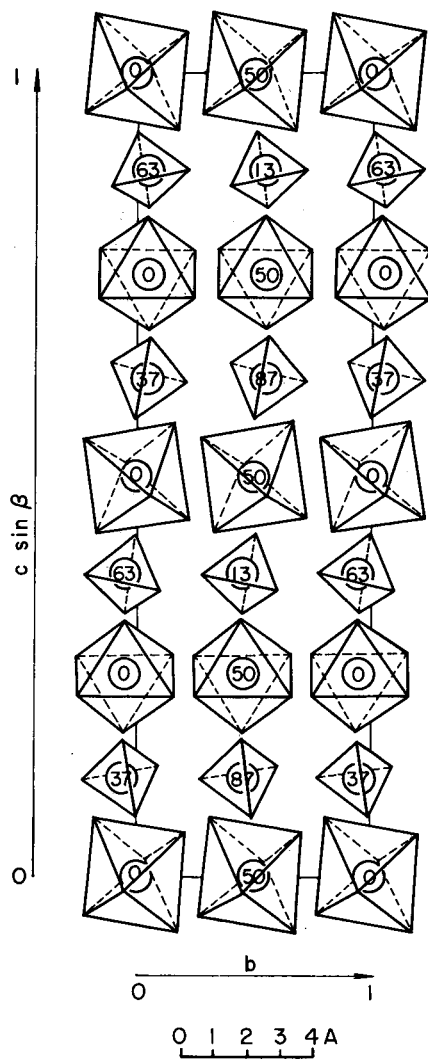
MU-23603

Fig. D.7-1. Packing of $SO_4^=$ tetrahedra and $Co(H_2O)_6^{++}$ octahedra. The encircled numbers are the parameters of the Co and S atoms in the $\underline{a}$ direction.
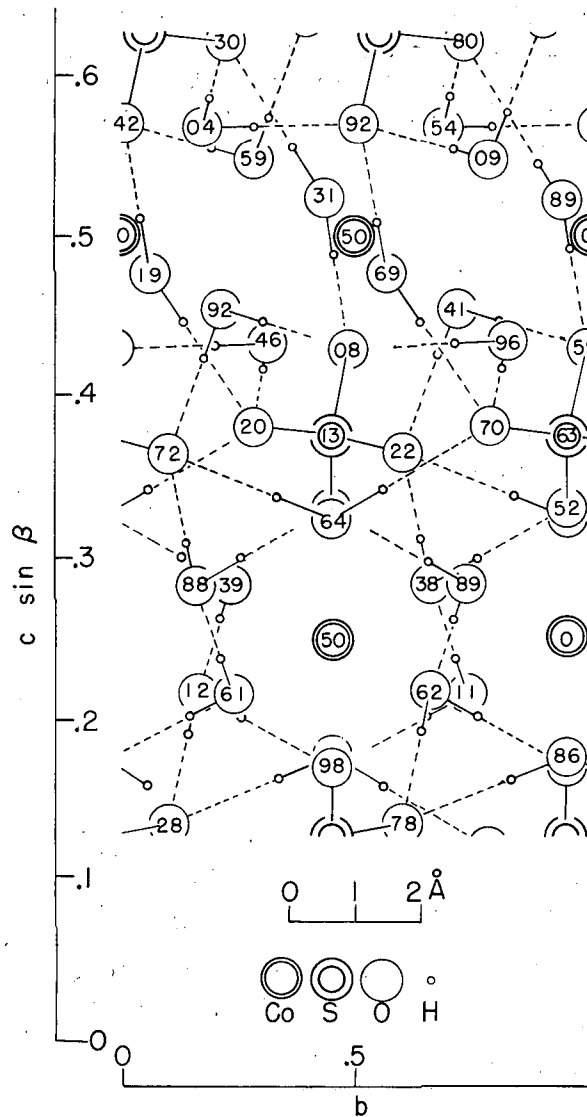
Fig. D.7-2. Hydrogen bond network in $CoSO_4 \cdot 6H_2O$. The numbers are the parameters along the a axis of the Co, S, and O atoms. The complete environment about each of the two different $Co(H_2O)_6^{++}$ and $SO_4^{=}$ is shown.

Eigenvectors obtained from the above treatment were used to calculate the operator equivalent factors needed for the comparison of theoretical and observed positions of crystal field states. Assignment of crystal field states was made on the bases of the polarization properties, relative position within the group, and appearance (sharpness and intensity) of the observed transition. Figures D.8-1 and D.8-2 demonstrate the fit obtained. The crystal field parameters that yielded the best least-squares fit between observed and calculated positions of crystal field states are

$$A_2^0 \left\langle r^2 \right\rangle = -284.2 \text{ cm}^{-1},$$

$$A_4^0 \left\langle r^4 \right\rangle = +154.9 \text{ cm}^{-1} \quad A_4^4 \left\langle r^4 \right\rangle = -1,782 \text{ cm}^{-1},$$

$$A_6^0 \left\langle r^6 \right\rangle = -379.8 \text{ cm}^{-1} \quad A_6^4 \left\langle r^6 \right\rangle = -4,487 \text{ cm}^{-1}.$$

Positions of low-lying states are often useful in the interpretation of magnetic susceptibility data. For this reason the calculated positions of crystal field states relative to the center of gravity of the $^3H_4$ ground level are recorded here.

B_1, -973 B_2, +328

A_1, -422 A_1, +486

E,   -297 E, +596 .

A_2, -18.9

Knowing the values of F_k and ζ for U^{4+} in UCl_4 should make it possible to say something about covalent bonding in this compound. The reasoning involved here is described by L. E. Orgel.[1] The end result of this approach is that the F_k and ζ parameters of U^{4+} in the compound should be smaller than in the field-free ion if covalent bonding is present. Unfortunately the values of these parameters for the field-free ion are not known. However, we can look to other compounds and consider the relative amount of covalent bonding between compounds.

The comparison which would have the greatest hope of being meaningful is that between UCl_4, and UF_4 in CaF_2.[2] It does not seem meaningful to compare F_k parameters because of the approximations made in the latter calculation. In UCl_4 ζ is approx 13% smaller than in $UF_4 \cdot CaF_2$. This is the result to be expected if UCl_4 were covalently bonded to a greater extent than UF_4.

Eisenstein has suggested that f^3s or f^2ds orbitals are responsible for covalent bonding in UCl_4, with a preference for the latter.[3] If configuration f^2ds were low-lying, interaction with configuration f^2 would be expected. In veiw of the evidence for small configuration interaction found in this work a preference for f^3s orbitals or non-f orbitals is expressed.

[2] J. G. Conway, J. Chem. Phys. 31, 1002 (1959).

[3] J. C. Eisenstein, J. Chem. Phys. 25, 142-6 (1956).

$^3F_4$ $^1G_4$ +389 —— $^3F_3$ $^3P_1$

E

—— 9224

+120 —— E

—— 9794

+57 —— E —— 17801

+12 —— A_2

—— 9715   -10 —— E

-50 —— A_2 —— 14923

-162 —— E

-114 —— A_2 —— 17597

-231 —— E —— 8667

—— 8614

-329 —— A_2

-401 —— E —— 14578
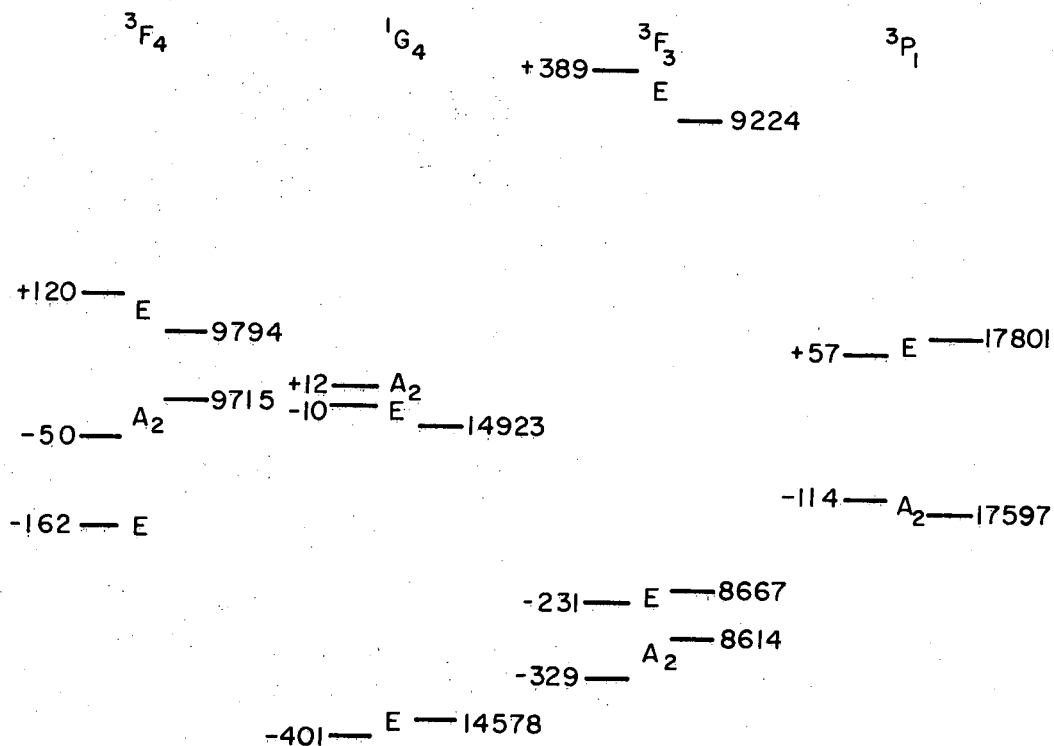
MU-25050

Fig. D.8-2. Calculated positions of the states are on the left; observed positions are on the right. Only states to which allowed electronic transitions are expected have been presented.

$^3H_6$ $^1I_6$

+701—— E —— 12045

+433—— E ——20470

+327——E ——20296

+26 ——A_2——11422

-124—— A_2

-580—— E ——19420

-628——E ——10699

-1231—— E
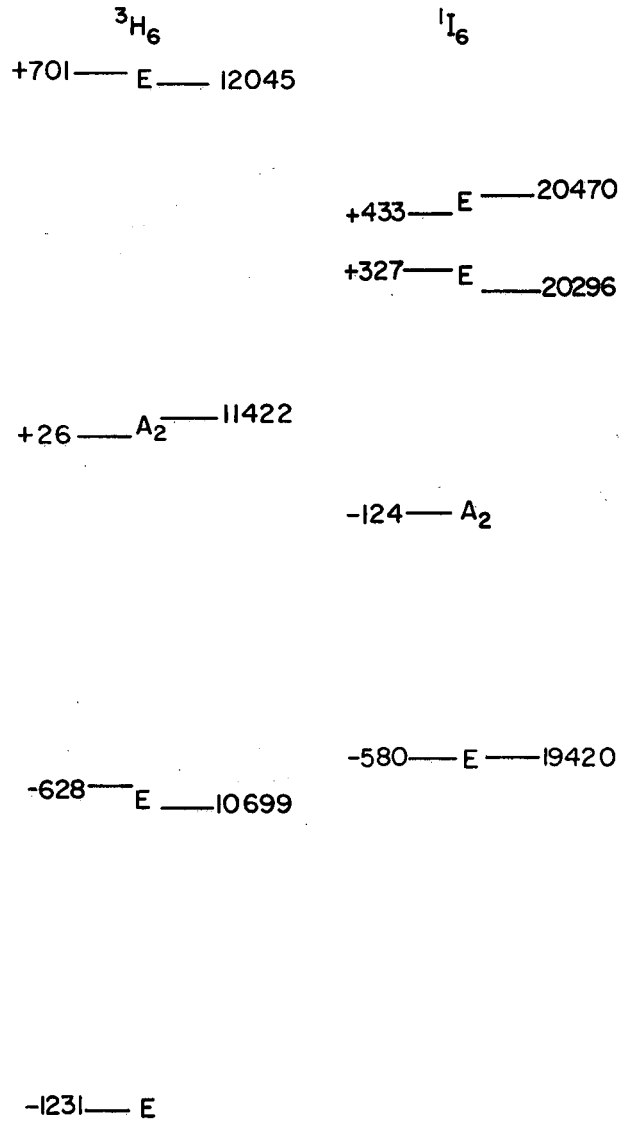
MU-25052

Fig. D.8-1. Calculated positions of the states are on the left; observed
positions are on the right. Only states to which allowed electronic
transitions are expected have been presented.

9. ABSORPTION AND SELF-LUMINESCENCE SPECTRA OF Cf^{+3} $(5\underline{f}^9)$ [*]

John G. Conway, John B. Gruber,[†] E. Kenneth Hulet,
Richard J. Morrow, and Ralph G. Gutmacher

Introduction

Since the discovery of element 98, californium, in 1950 by Thompson, Street, ghiorso, and Seaborg,[1] studies on certain physical properties of Cf^{+3} by Cunningham and Wallmann[2] indicate that the +3 ion is similar to the rare earth analog, Dy^{+3} $(4f^9)$. Cunningham has observed part of the absorption spectrum of Cf^{+3} $(5f^9)$ on a Dowex-50 ion-exchange bead[2] and in an aqueous acid solution.[3] Very weak absorption peaks are observed at 7800 and 8320 A in solution, and at 5750 A on the bead.

The results we report in this paper tend to confirm these absorption features. In addition, several sharp but very weak absorption lines are observed in the ultraviolet region of the spectrum. As a result of these studies, we believe that the molar extinction coefficients of Cf^{+3} are in general between 1 and 10 -- a range quite similar to Dy^{+3}.

Californium Purification

The major portion of californium (consisting of the isotopes Cf^{249}, approx 10%; Cf^{250}, approx 50%; and Cf^{252}, approx 40%) used in our studies was isolated from the capture and fission products produced by a series of long neutron irradiations of U^{242}. After the initial separations, curium was removed by a series of column elutions from Dowex-50 12% DVB resin at 87°C with ammonium α-hydroxy-isobutyrate.[4] Berkelium was separated either during this ion-exchange procedure or by extraction of Bk^{+4} with di-iso-octyl ortho phosphoric acid.[5] Plutonium, lanthanum, and residual rare earths were separated from the combined californium fractions by a combination of ion-exchange methods.[6] Final purification consisted of iodate,

[1] S. G. Thompson K. Street, Jr., A. Ghiorso, and G. T. Seaborg, Phys. Rev. 80, 790 (1950).

[2] B. B. Cunningham and J. C. Wallmann (Lawrence Radiation Laboratory), private communication.

[3] B. B. Cunningham, J. Chem. Ed. 36, 32 (1959).

[4] G. R. Choppin, B. G. Harvey, and S. G. Thompson, J. Inorg. Nuclear Chem. 2, 66 (1956).

[5] D. F. Peppard, S. W. Moline, and G. W. Mason, J. Inorg. Nuclear Chem. 4, 344 (1957).

[6] S. G. Thompson, B. G. Harvey, G. R. Choppin, and G. T. Seaborg, J. Am. Chem Soc. 76, 6229 (1954).

hydroxide, and oxalate precipitations followed by elution of the adsorbed californium with 6 $\underline{M}$ HCl from a 2-mm by 4-cm Dowex-50 colloidal resin bed. To provide the necessary crystal matrix, approximately 1 mg of 99.997% pure La_2O_3 (Lindsey Chemical Co.) was dissolved in approximately 0.3 ml of eluate.

Preparation of $CfCl_3$-$LaCl_3$ Crystals

The solution containing Cf^{+3} and La^{+3} in chloride form was transferred to a 6-mm quartz tube and slowly evaporated to dryness. A stream of dry hydrogen chloride was passed over the material at 400° C to produce the anhydrous chlorides. As a final step in purification, the anhydrous chlorides were sublimed under vacuum, and the sublimate collected in a portion of the quartz tube that could be sealed off and removed from the vacuum line. The evacuated quartz tube containing the $CfCl_3$-$LaCl_3$ was passed through a crystal-growing furnace.[7]

Because the total volume of the sample was less than 0.5 mm^3, the crystal was regrown in a 0.4-mm-diam quartz capillary tube attached to a joint having a 90-deg bend near the opening. The sample from the 6-mm tube was transferred in a dry box to the capillary tube, and the latter attached to a vacuum line. The material was contained in the 90-deg bend where complete outgassing was possible. The capillary tube was then rotated so that the sample fell to the bottom. The tube was then sealed under vacuum, and slowly lowered through a crystal-growing furnace.[7]

Observations and Conclusions

The self-luminescence and absorption spectra of Cf^{+3} in $LaCl_3$ were photographed on a Hilger $\underline{f}/4$ quartz spectrograph and a Jarrell-Ash $\underline{f}/6$ grating spectrograph. The spectra could be photographed in a matter of several hours, although exposures as long as 90 hr were necessary in order to observe several weak satellite lines associated with certain strong-resonance emission lines. A low-pressure Hg lamp provided a standard reference spectrum. With the exception of two groupings in the infrared, the luninescence spectrum was observed with both instruments.

As a result of intense radioactivity, the crystals blackened with time because of the formation of color centers. In order to recover the optical quality of a crystal, it was necessary to anneal it at 110° C for several hours.

A strong continuum is observed extending from 3000 to 5000 A. Superimposed on this continuum and extending beyond it into the infrared are the distinct peaks of Cf^{+3}. The continuum is associated with the bremsstrahlung radiation observed in the self-luminescence spectrum of various radioactive ions.[8] In addition, six features are observed in the spectrum corresponding

[7] D. M. Gruen, J. G. Conway, and R. D. McLaughlin, J. Chem. Phys. 25, 1102 (1956).

[8] J. G. Conway and J. B. Gruber, J. Chem. Phys. 32, 1586 (1960).

to absorption groupings. In the table we list the wave lengths of the observed groupings and note in particular that groups at 3504, 4004, and 5940 A show structure. Such structure indicates a small crystal-field splitting compared with the spin-orbit splitting.

Absorption and self-luminescence spectra of Cf^{+3}

Number	Wave length in air (A)	Wave numbers in vacuum
1	3114^a	32,100
2	3448^b	28,990
3	3504^b	28,530
4	3541^b	28,230
5	3587^b	27,870
6	$4004^{a,c}$	24,970
7	$4102^{a,b}$	24,370
8	4361^a	22,920
9	4583^a	21,810
10	5006^a	19,970
11	5320^a	18,790
12	5750^d	17,390
13	5940^a	16,830
14	6500^a	15,380
15	7200^a	13,890
16	7800^e	12,820
17	8320^e	12,020
18	8400^a	11,900

[a] Luminescence spectrum of Cf^{+3} in $LaCl_3$.

[b] Absorption spectrum of Cf^{+3} in $LaCl_3$.

[c] This is close to a Cm^{+3} fluorescence peak, but the separation chemistry should have removed Cm^{+3}. For that reason we believe this peak is due to Cf^{+3}.

[d] Observed on ion-exchange bead.[2] We believe this peak corresponds to the 590 A peak of Cf^{+3} in $LaCl_3$.

[e] Observed in solution absorption spectra.[3]

As the basis for a tentative assignment of the reported energy spectrum, a perturbation calculation was made that considers the effect of the ^4G_J, ^4H_J, and ^4I_J levels upon the ground multiplet, ^6H_J. The general treatment is based on the method of evaluating the spin-orbit matrix elements given by Judd.[9] If we assume $\zeta = 4000 \text{ cm}^{-1}$ and $F_2 = 300 \text{ cm}^{-1}$ for Cf^{+3} $(5f^9)$, and assume further that the observed absorption spectrum in the visible and ultraviolet corresponds to several of the previously mentioned excited multiplets, we obtain a calculated energy spectrum for the lowest levels of the ground multiplet, ^6H_J, that is in reasonable agreement with the observed energy spectrum reported in Fig. D.9-1. Assignments are based on the parent LSJ levels. There is no question that intermediate coupling effects are important in the ground multiplet. However, the actual composition of the states is not known at present.

Because of the small quantity of material used and the low molar extinction coefficients, much of the expected absorption spectrum of Cf^{+3} has not yet been observed. More definitive assignments must await polarization and Zeeman studies on larger crystals containing larger quantities of the less radioactive isotope, Cf^{249}.

[9] B. R. Judd, Proc. Phys. Soc. (London) A **69**, 157 (1956).

10. THE EMISSION SPECTRUM OF CALIFORNIUM [*]

John G. Conway, E. Kenneth Hulet, and Richard J. Morrow

Californium, element number 98, was discovered in 1950 by Thompson, Street, Ghiorso, and Seaborg.[1] Since then many nuclear properties[2] of its various isotopes have been studied, whereas the chemical and physical properties have only been briefly investigated.

Present spectroscopic research indicates that Cf^{+3} should be similar to Dy^{+3}, the rare earth homolog.[3] It is very likely that CfI and CfII will have similar electronic configurations to DyI and DyII, namely $5f^9 7s^2$ for CfI and $5f^9 7s$ for CfII. Further interest in the optical spectrum of Cf arises from the suggestion by Burbridge et al.[4] that spontaneous fission of Cf^{254} may release the predominant energy during the decay of Type I supernovae.

[*] J. Opt. Soc. Am. **52**, 222 (1962).

[1] S. G. Thompson, K. Street, Jr., A. Ghiorso, and G. T. Seaborg, Phys. Rev. **80**, 790 (1950).

[2] D. Strominger, J. M. Hollander, and G. T. Seaborg, Revs. Modern Phys. **30**, 585 (1958).

[3] B. B. Cunningham, J. Chem. Ed. **36**, 32 (1959); B. B. Cunningham and J. C. Wallman (Lawrence Radiation Laboratory), private communications; and J. G. Conway, J. B. Gruber, E. K. Hulet, R. J. Morrow, and R. G. Gutmacher J. Chem. Phys. **36**, 189 (1962) (see Paper D.9).

[4] G. R. Burbidge, F. Hoyle, E. M. Burbidge, R. F. Christy, and W. A. Fowler, Phys. Rev. **103**, 1145 (1956).

<u>Experiment</u>   <u>Theory</u>

32,100

30,000

28,990   28,530

Excited
multiplets,
^4H_J ,
^4G_J ,
and
^4I_J

25,000

24,370

Energy (cm^{-1})

20,000

16,830

15,000

$^6F_{1/2,5/2}$

$^6F_{3/2,7/2}$

$^6H_{5/2}, ^6F_{9/2}$

13,890
11,900

$^6F_{11/2}$

$^6H_{7/2}$

10,000   1 6   2 8 10   3 9   7 11 14   13   15   18

$^6H_{9/2}$

$^6H_{11/2}$

5,000

$^6H_{13/2}$

0

$^6H_{15/2}$
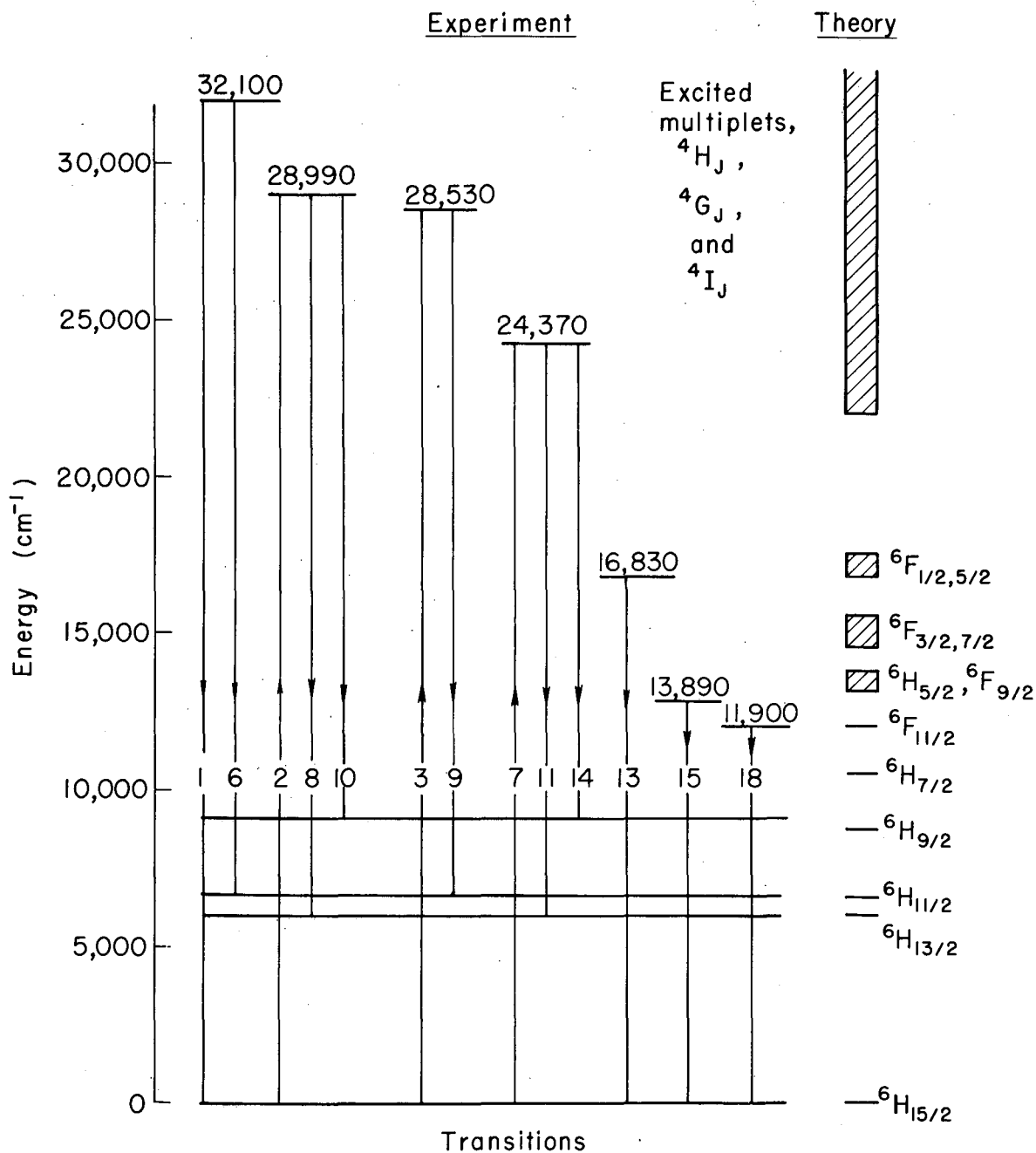
Transitions

MUB-652

Fig. D.9-1. Suggested energy -level scheme for $Cf^{+3}(5f^9)$ in $LaCl_3$.
On the left is the observed energy spectrum, and on the right, the
results from perturbation theory, where $F_2 (5f^9) = 300$ cm^{-1} and
$\zeta = 4000$ cm^{-1}. The numbered transitions correspond to the ob-
served absorption and luminescence features reported in the table.

Since spectral observations of supernovae are available,[5] curiosity impelled a comparison with a measured emission spectrum of californium.

For this work 0.4 μg of Cf was used, since only limited quantities of Cf are available. The material was produced by neutron irradiation of Pu^{242} and was isolated from capture and fission products by ion-exchange and precipitation procedures. As a final step to remove residual impurities, Cf was eluted from a very small Dowex-50 collodial resin bed with 6 M HCl. The fraction containing Cf was then evaporated onto 1/4-in. copper electrodes and sparked[6] in an enclosed chamber.[7] The column eluant immediately preceding the Cf was used as a blank, and any emission lines that appeared in this blank were removed from the Cf line list.

The spectra were taken on a 3-meter Eagle grating mount having a dispersion of 5.57 A/min. The wave-length region was first order from 3640 to 5040 A. A portion of the slit was covered with glass while the remaining portion was left uncovered; thus, the uncovered portion had the second order superimposed on the first order. There were no lines in the region of 2000 to 25000 A due to Cf. To determine the presence of impurities, reference spectra taken on the same instrument were compared with the Cf spectra. Only Ca and Sr appeared in appreciable quantities in the Cf sample; however, Ba, Fe, and Mg were detected. Forty-four other elements whose strong lines would have appeared in this region were not detectable. A search was made for the weak lines (in this wave-length region) of fourteen other elements, and none were found. A final list of wave-lengths, accurate to ±0.1A, of the residual lines credited to Cf are given in the table.

A comparison between the spectral features of the supernovae IC 4182 and NGC 1003[5] and those of Cf proved fruitless regardless of any red or violet shift. Because the source environments are drastically different (on the order of $10^9 \ K^o$) it is unlikely that any similarity would occur.

[5] R. Minkowski, Astrophys. J. 89, 143 (1939).

[6] M. Fred, N. H. Nachtrieb, and F. S. Tomkins, J. Opt. Soc. Am. 37, 279 (1947).

[7] J. G. Conway, Spectroscopy of Radioactive Materials, in Symposium on Spectroscopy (Special Technical Publication No 269) (published by American Society for Testing Materials, Philadelphia, Pa., 1959).

Wave lengths and relative intensities of Cf line

Wave length (A)	Relative intensity
3706.4	3
3722.2	8
3724.5	4
3743.4	4
3785.6	9
3789.1	10
3844.5	2[b]
3851.6	2[b]
3893.1	9
4266.7	4
4283.8	5
4302.6	2
4307.7	3[b]
4335.2	5

[b] broad

11. THE ABSORPTION SPECTRUM AND ZEEMAN EFFECT OF Am^{+3} IN LaCl$_3$ [*]

John B. Gruber[†] and John G. Conway

Introduction

Although many investigaters[1-3] have reported the solution spectra of Am^{+3}, relatively few papers have appeared in the literature on the solid-

[*] J. Chem. Phys. 36, 191 (1962).

[†] Present address: Inst. fur Technische Physik, Technische Hochschule, Darmstadt, W. Germany.

[1] D. C. Stewart, Absorption Spectra of Lanthanide and Actinide Rare Earths. II. Transition Probabilities for +3 Ions in the Two Series, Argonne National Laboratory Report ANL-4812, Feb. 1952.

[2] L. B. Asprey and T. K. Keenan, J. Inorg. Nuclear Chem. 7, 27 (1958).

[3] J. J. Katz and G. T. Seaborg, The Chemistry of the Actinide Elements (Methuen and Company Ltd., New York, 1957).

state sharp line spectra of Am^{+3}. Stover and Conway in 1952 published part of the absorption spectrum of hydrated americium trichloride,[4] and Iakovlev, Gorkenko-Germanov, Zenkova, Razbitnoi, and Kazanskii have reported a study of the absorption spectra of Am^{+3} in the double sulfates of potassium, thallium, rubidium, and cesium.[5] In addition, Gruen, Conway, McLaughlin, and Cunningham have observed the fluorescence spectrum of Am^{+3} in $LaCl_3$.[6] Gruber has recently interpreted the infrared absorption spectrum from 0.79 μ to 16 μ as arising from transitions within the ^7F multiplet.[7]

A detailed analysis of the energy spectrum is very much needed, since it would reveal the multipolarity of the transitions observed and yield information on the quantum nature of the states of the free ion. In addition, a knowledge of the symmetry character, and the relative position of the crystal quantum sublevels of a crystal-field split J level, would give us some indication of the degree to which the field-free levels of Am^{+3} are split by the crystal field.

Preparation of Single Crystals

Single crystals of $AmCl_3$-$LaCl_3$, containing Am^{+3} in amounts from 0.1 to 10% by weight, were prepared in the following manner. A known volume of Am^{+3} (americium-241; half life: 458 yr) in 2.0 M HCl was added to a quartz sublimation tube. The ion-exchange-purified Am^{+3} was found to be spectroscopically pure, and an α assay of the solution gave a reliable value for the concentration of americium. The solution was slowly evaporated on a vacuum line and anhydrous $AmCl_3$ formed by heating the hydrate slowly in the presence of dry HCl. After the tube was flushed repeatedly with dry argon, a known quantity of spectroscopically pure anhydrous $LaCl_3$ was added. The mixture was then thoroughly degassed and melted to form a solution. The sublimation and single-crystal-growing techniques employed were quite similar to those reported by Sayre, Sancier, and Freed[8] and Gruen, Conway, and McLaughlin.[9] The intense radioactivity of americium-241, as well as the hygroscopic nature of anhydrous $LaCl_3$, requires that the crystal be mounted in a dry-nitrogen-atmosphere box suitably prepared for radioactive work.

In order to determine whether the $AmCl_3$-$LaCl_3$ mixed crystal system preserved C_{3h} symmetry about the cation sites, anhydrous $PrCl_3$ was added to the mixture before the single crystals were grown. When the absorption spectrum of the single crystal was taken, the Pr^{+3} lines were found to have the same polarization and energy positions as reported by Sayre, Sancier,

[4] B. J. Stover and J. G. Conway, J. Chem. Phys. 20, 1490 (1952).

[5] G. N. Iakovlev, D. S. Gorkenko-Germanov, R. A. Zenkova, V. M. Razbitnoi, and K. S. Kazanskii, J. Gen. Chem. U.S.S.R. 28, 2653 (1958) (English translation).

[6] D. M. Gruen, J. G. Conway, R. D. McLaughlin, and B. B. Cunningham, J. Chem. Phys. 24, 1115 (1956).

[7] J. B. Gruber, J. Chem. Phys. 35, 2186 (1961).

[8] E. V. Sayre, K. M. Sancier, and S. Freed, J. Chem. Phys. 23, 2060 (1955).

[9] D. M. Gruen, J. G. Conway, and R. D. McLaughlin, J. Chem. Phys. 25, 1102 (1956).

and Freed.[8] We conclude, therefore, that the symmetry about Pr^{+3} ion is similar to that reported by Sayre, Sancier, and Freed, who had no Am^{+3} in their crystals, and that the symmetry about the americium ions very probably is C_{3h}. Also the observed polarization spectrum of $AmCl_3$-$LaCl_3$ is consistent with the selection rules for C_{3h}.

Spectrographic Equipment

The absorption spectrum of the single crystals was taken with a Wadsworth-mount 3.4-m spectrograph. Two gratings were used in this instrument--one with 7,500 lines per inch and another with 14,400 lines per inch. In the first order, the reciprocal linear dispersion was 10.1 A/mm and 5.3 A/mm, respectively. Crystals were maintained at selected temperatures of 77° K (liquid nitrogen) and 4° K (liquid helium) in quartz and pyrex Dewars.

The Zeeman experiments were at fields of 28,750 and 37,000 gauss at temperatures of liquid nitrogen (77° K) and a dispersion of 5.3 A/mm. A single experiment at 4° K and 28,750 gauss was performed, but no sharpening of lines was observed.

The Polarized Absorption Spectrum

The polarized absorption spectrum of Am^{+3} in $LaCl_3$ was studied from 2000 A to 8000 A. In almost every instance, spectral lines observed are sharp and completely polarized. Definite groupings of lines appear in every portion of the spectrum.

For the particular point symmetry, C_{3h}, which is consistent with experiment, the polarized transverse and the axial spectra indicate forced electric-dipole transitions. Magnetic-dipole transitions are observed from $^7F_0$ (the ground level) to excited $J = 1$ levels, and forced electric-dipole transitions are observed from $^7F_0$ to the excited crystal-field-split components $\mu = \pm 2$ and $\mu = \pm 3$ of J levels greater than one. The quantum numbers, μ, have been defined by K. H. Hellwege,[10] and the selection rules have been worked out by K. H. Hellwege[10] and Sayre, Sancier, and Freed.[8]

Many of the sharp lines in the visible and near-ultraviolet spectra split into two components in a Zeeman field. Thus, from the g values and the total number of allowed transitions to a gvien J Manifold, we can establish a value for the field-free J level. The sublevels split in a magnetic field are indicated in the table. Complications in the analysis of the Am^{+3} spectrum result from the intermediate coupling effects and the intermixing of crystal-field components of a given J level with those of J levels having nearly the same energy.

10
K. H. Hellwege, Nachr. Akad. Wiss. Götingen, Math.-physik. Kl. 37, 1947; Ann. Physik (6) 4, 95 (1948); idem. (6) 4, 127 (1948); idem. (6) 4, 136 (1948).; idem. (6) 4, 143 (1948); idem. (6) 4, 357 (1949).

An additional handicap to interpretation, pointed out by Sayre and Freed, is that of working with a crystal of C_{3h} symmetry and an ion of $J = 0$ ground state.[11] All these complications combine to make a positive assignment of L and S very difficult. The only sure assignments for Eu^{+3}, the rare earth analog, are for the $^5D_{0,1,2}$. These levels are of very low intensity and, in the case of Am^{+3}, shifted to the infrared.[12] In the dilute crystals studied no levels were identified which could be assigned to the ^5D multiplet. It would appear that pure crystals of Am salts would be needed to identify these levels. The levels observed probably belong to the ^5L, ^5G, ^5H, ^5I, ^5F multiplets, but strong intermediate coupling prevents a simple direct correlation with the theoretical LSJ values.

Visible and ultraviolet absorption spectra, polarization, and intensities of Am^{+3} in Cl_3

Wave length (A) (in air) 77° K	Wave numbers (in vacuum) 77° K	$g = \dfrac{\Delta \nu}{2\beta H}$ $\Delta \nu$=splitting between two Zeeman components	P Polarization	I Relative Intensity
5119.1	19,529	b	σ	7[a]
5093.0	19,630	b	σ	10[c]
5089.6	19,642	b	σ	4[d]
5083.2	19,667		π	8[d]
5075.0	19,699		π	10[c]
4623.1	21,624	b	σ	5[e]
4561.5	21,916	1.45	σ	8[a,f]
4432.4	22,555		π	6[a,g]
4305.0	23,222	b	σ	6[a]
4298.7	23,256		π	4[a,g]
4262.5	23,454		π	3[d]
4260.0	23,468		π	3[h]
4257.3	23,482		π	3[e]
4245.2	23,549		π	7[h]
4245.2	23,549		π	7[h]
4242.5	23,564		π	7[h]
4239.9	23,579		π	7[h]

(next page)

[11] E. V. Sayre and S. Freed, J. Chem. Phys. 24, 1211 (1956).

[12] J. B Gruber and J. G. Conway, J. Chem. Phys. 34 632 (1961).

(continued)

Wave length (A) (in air) 77° K	Wave numbers (in vacuum) 77° K	$g = \dfrac{\Delta \nu}{2\beta H}$ $\Delta \nu$ = splitting between two Zeeman components	P Polarization	I Relative Intensity
4232.2	23,622	b	σ	7[d]
4216.0	23,713	b	σ	6[i]
4163.5	24,012	1.22	σ	4[a,f]
4041.9	24,734		π	5[g,j]
4041.1	24,739		π	2[g,j]
4038.8	24,753	3.35	σ	6[f,j]
3968.2	25,193	2.30	σ	4[g,j]
3963.8	25,221		π	4[f,j]
3795.3	26,344	0.69	σ	9[d]
3775.4	26,480		π	10[i]
3773.0	26,497		π	4[d]
3771.8	26,505		π	4[d]
3765.0	26,553	2.58	σ	8[h]
3759.5	26,592		σ	3[h]
3754.3	26,629	5.07	σ	5[a,f]
3745.7	26,690		π	3[d]
3740.5	26,727		π	3[h]
3732.6	26,783		σ	4[b,i]
3658.2	27,328	2.68	σ	8[a,f]
3632.7	27,520		σ	5[a,f]
3629.8	27,542		π	7[a]
3627.9	27,556	3.71	σ	6[a,f]
3574.6	27,967		π	2[i]
3418.5	29,244		π	4[e]
3410.3	29,315		σ	4[e]
3388.2	29,506		σ	4[e]
3380.9	29,569		σ	4[e]
3377.3	29,601		π	6[e]
3155.0	31,687		σ	6[j]

(continued)

Wave length (A) (in air) 77° K	Wave numbers (in vacuum) 77° K	$f = \dfrac{\Delta\nu}{2\beta H}$ $\Delta\nu$ = splitting between two Zeeman components	P Polarization	I Relative Intensity
3153.2	31,705		π	6[j]
3077.8	32,481		π	4[d]
3067.7	32,588		σ	4[a]
3060.1	32,669		π	4[d]
2994.4	33,386		π	3[j]
2993.6	33,395		σ	3[a]
2986.4	33,475		σ	3[j]
2939.2	34,013		σ	6[a]
2934.0	34,073		π	10[d]
2916.4	34,279		σ	7[a]
2914.0	34,307		π	7[a]

[a]Line width: 0.3 to 0.5 A.

[b]Line broadened in magnetic field.

[c]Unresolved band structure.

[d]Line width: 0.5 to 1.0 A.

[e]Line width: 2.0 to 5.0 A; possible unresolved doublet.

[f]Absorption line split into two observable components in applied magnetic field.

[g]Line not broadened in magnetic field.

[h]Line width: 1.0 to 1.5 A.

[i]Line width: 1.5 to 2.0 A.

[j]Line width: 0.1 to 0.3 A.

12. LOW-LYING LEVELS IN CERTAIN ACTINIDE ATOMS [*]

B. R. Judd

It is now well established that the ground configurations of PaI, UI, NpI, PuI, AmI, and CmI are $5f^2 6d$, $5f^3 6d$, $5f^4 6d$, $5f^6$, $5f^7$, and $5f^7 6d$ respectively. The problem of calculating the ordering and properties of low-lying levels in configurations of the type $5f^n$ is well understood; for those of the type $5f^n 6d$, the problem falls into four parts: (a) the choice of a coupling scheme to define the basic eigenfunctions; (b) the evaluation of the matrix elements of the spin-orbit interaction and of the Coulomb interaction in the form of linear combinations of certain radial integrals; (c) the estimation of the radial integrals; (d) the diagonalization of the energy matrices. With regard to (a), evidence from g values points to the J_j coupling scheme as being the most appropriate; this implies that the Coulomb interaction between the core (comprising the equivalent f electrons) and the d electron (to whose levels the respective symbols J and j refer) is weak compared with the interactions within the two systems. Part (b) can be carried out by applying the tensor operator and group theoretical methods of Racah. For (c), values of the Slater integrals $F_k(5f, 6d)$ and $G_k(5f, 6d)$ can be estimated for various atoms by assuming that they maintain the ratios one to another as they do in Th III, and that their variation along the actinide series parallels the variation of $G^3(5f, 7s)$. The last parameter is known for Th III, and analyses of U II, Pu II and Am II show that it decreases as one advances along the actinide series. This decline is interpreted as being due to the collapse of the 5f shell, and the internal nature of the 5f electrons allows some general statements to be made about the spin-orbit coupling constants. Additional information on the parameters is provided by an analysis of the properties of the four lowest levels of CmI. Part (d) is accomplished for the very lowest levels of $f^2 d$, $f^3 d$, $f^4 d$, $f^8 d$ and $f^{10} d$ by the simple expedient of neglecting all off-diagonal elements; for UI $f^3 d$, for which extensive spectroscopic information is available, the interaction of the levels deriving from the J_j coupling of $^4 I_{9/2}$ to $^2 D_{5/2}$ with those deriving from the J_j coupling of $^4 I_{11/2}$ to $^2 D_{3/2}$ is included. Where experimental data are available, agreement with the theory, both in respect to the positions of the levels and to their Landé g values, is good --- often surprisingly so in view of the approximations made.

13. DOUBLE-TENSOR OPERATORS FOR CONFIGURATIONS OF EQUIVALENT ELECTRONS [*]

B. R. Judd

In calculating the splittings induced in the levels of an ion when it is embedded in a crystal lattice, reduced matrix elements of the unit tensors $U^{(k)}$ are required, where k is even. On the other hand, the calculation of the

hyperfine structures of the levels, whether for a free ion or one in a crystal, requires the evaluation of reduced matrix elements of the double tensor $U^{(12)}$. For a given level, the reduced matrix elements of $U^{(k)}$ and $U^{(1k)}$ are not simply related. However, it is possible to find pairs of levels drawn from different electronic configurations ℓ^n that are connected by a simple formula. As is shown in the report that bears the same title as this note, the connection, expressed in its most general form, is

$$\frac{(\ell^n \, v_1 \, W \, \xi \, S_1 \, L \, \| \, W^{(\kappa \, k)} \, \| \, \ell^n \, v_1' \, W' \, \xi' \, S_1' \, L')}{(\ell^m \, v_2 \, W \, \xi \, S_2 \, L \, \| \, W^{(\kappa' k)} \, \| \, \ell^m \, v_2' \, W' \xi' \, S_2' \, L')}$$

$$= (-1)^{x + \frac{1}{2}(n+v_1-m-v_2)} \begin{pmatrix} \frac{1}{2}(2\ell+1-v_1) & \kappa' & \frac{1}{2}(2\ell+1-v_1') \\ \frac{1}{2}(2\ell+1-n) & 0 & -\frac{1}{2}(2\ell+1-n) \end{pmatrix}$$

$$\times \begin{pmatrix} \frac{1}{2}(2\ell+1-v_2) & \kappa & \frac{1}{2}(2\ell+1-v_2') \\ \frac{1}{2}(2\ell+1-m) & 0 & -\frac{1}{2}(2\ell+1-m) \end{pmatrix}^{-1} , \qquad (1)$$

where the seniority and spin couples (v_1, S_1) and (v_2, S_2) corresponding to the same irreducible representation W of the rotation group in $2\ell+1$ dimensions are dissimilar where ξ is a symbol that serves to define the corresponding state uniquely; where L is the quantum number of the total orbital angular momentum; where $W^{(\kappa \, k)}$ is a tensor related to the unit tensors by the equation

$$W^{(\kappa \, k)} = U^{(\kappa \, k)} (2\kappa + 1)^{\frac{1}{2}} (2k + 1)^{\frac{1}{2}};$$

where the sum $\kappa + \kappa' + k$ is odd; where x is a phase angle independent of ξ, ξ', L and L', and which for f electrons gives the conventional phase if we insist

$$x = v_1 \, \delta(v_1, \, v_1') + v_2 \, \delta(v_2, \, v_2') + 1;$$

and where the primed quantities have analogous definitions.

     Use of Eq. (1) enables us, for example, to calculate the contribution to the hyperfine structure of PuI $5f^6 \; {}^7F_J$ coming from admixtures of quintet states from the crystal splitting calculations of the levels of NdIV $4f^3$, thereby saving much labor.

14. ATOMIC-BEAM INVESTIGATIONS OF ELECTRONIC AND NUCLEAR GROUND STATES IN THE RARE-EARTH REGION[*]

Amado Y. Cabezas,[†] Ingvar Lindgren, [‡] and Richard Marrus

A number of radioactive isotopes in the rare-earth region have been investigated by using the atomic-beam magnetic-resonance technique. The total electronic angular momentum (J) and the atomic g value (g_j) have been determined for some low-lying levels in, Pm, Dy, Ho, and Er. These observations are consistent with the following ground-state assignments: PmI—$(4f)^5 (6s)^2$, $^6H_{5/2}$; DyI—$(4f)^{10} (6s)^2$, $^5I_8$; HoI—$(4f)^{11}(6s)^2$, $^4I_{15/2}$; and ErI—$(4f)^{12} (6s)^2$, $^3H_6$. The ground-level assignments agree with the Hund's-rule predictions, and the g values approximate the Landé values well. Our present experimental knowledge concerning electronic ground states in the rare-earth region is summarized. The following nuclear spin values have been obtained: Pm^{149}, I=7/2; Pm^{151}, I=5/2; Gd^{159}, I=3/2; Tb^{160}, I=3; Dy^{165}, I=7/2; Dy^{166}, I=0 27-hr Ho^{166}, I=0; Er^{169}, I=1/2; Er^{171}, I=5/2; and Tm^{171}, I=1/2. These values are compared with available beta-decay results. Most of these isotopes have large nuclear deformations, and the spin values are discussed in relation to the single-particle energy-level diagrams given by Nilsson. A few results are explained with the shell model.

---

15. HYPERFINE STRUCTURE AND NUCLEAR MOMENTS OF PRASEODYMIUM-142 [*]

Richard Marrus, Amado Y. Cabezas Ingvar Lindgren, and William A. Nierenberg

Measurements made by the atomic-beam method on the J = 9/2 electronic ground state of Pr^{142} have yielded values for the magnetic-dipole (A) and electric-quadrupole (B) hyperfine-structure coupling constatns. They are A = ±67.5(5) Mc and B = ±7.0(2.0) Mc. From these values and assumptions made concerning the electronic fields at the nucleus, the nuclear moments are inferred to be μ_I= ±0.30(3) nm and Q = ±0.035(15) b. The error in μ_I is the estimated error arising from the calculated magnetic field; the error in Q is due to experimental uncertainties. The value of μ_I is substantially larger than the value obtained by Grace et al.,[1] but is surprisingly smaller then the shell-model value. A value obtained for the electronic splitting factor of the J = 9/2 state, g_J = -0.7311(3), is found to be in good agreement with a theoretical prediction based on the breakdown of Russell-Saunders coupling

---

[1]M. A. Grace, C. E. Johnson, R. G. Scurlock, and R. T. Taylor, Phil. Mag. 3, 456 (1958).

by the spin-orbit interaction , and the inclusion of relativistic and diamagnetic effects.[2]

_____

[2] B. R. Judd and I. Lindgren, Phys. Rev. 122, 1802 (1961).

16. HYPERFINE STRUCTURE OF PROMETHIUM-147 [*]

Burton Budick[†] and Richard Marrus.

The magnetic dipole interaction constant, A, and the electric quad-
rupole constant, B, for Pm^{147} have been measured by the method of atomic
beams and found to be A = ±447 ± 9 Mc, B = ∓ 267 ± 70 Mc. Pm in the form of
the chloride was purchased as a fission product from Oak Ridge. Beams
were produced via a lanthanum reduction of the oxide. Hfs investigations
were made in the J = 7/2 electronic state. The spin is already known to be
7/2.[1] All four observable flop-in transitions were found. A value of
$g_J = 8281 \pm .005$ was obtained. This is close to the Russell-Saunders value
and consistent with the theoretical result of Judd and Lindgren.[2] Inferred
values of the nuclear moments are $| \mu_I | = 3.2 \pm .3$ nm, $| Q | = 0.95 \pm .35$ b, with
μ and Q of the same sign. A strict single-particle shell model predicts
$\mu = 1.7$ nm, while on the collective model with a value of the deformation im-
plied by the quadrupole moment one finds $\mu = 1.6$ nm.

_____

[*] Abstract for the American Physical Society New York meeting, Jan. 24-27,
1962.

[1] A. Y. Cabezas, I. Lindgren, and others, Nuclear Phys. 20, 509 (1960).

[2] B. R. Judd and I. Lindgren, Phys. Rev. 122, 1802 (1961).

17. NUCLEAR SPIN OF HOLMIUM-161 [*]

Burton Budick[†] and Richard Marrus

The nuclear spin of holmium-161 has been measured as 7/2 by the
method of atomic beams. In addition, the ground-state electronic angular
momentum (J) is established as 15/2, which very probably arises from the
Hund"s Rule term ^4I of the configuration $(4f)^{11} (6s)^2$. Production of the
holmium is by a p-n reaction on dysprosium at the Berkeley 60-inch cyclotron.
Beams are produced by direct vaporization from the dysprosium metal. The
holmium is detected by counting electrons from the radioactive decay. The
isotope is unambiguously identified as holmium-161 on the basis of the method
of production, the measured g_J and J values, and the measured half life of
2.5 hr.

_____

[*] Abstract for the American Physical Society Los Angeles meeting, Dec.
27-29, 1961.

[†] Abraham Rosenberg Research fellow.

18. PROPOSED METHOD FOR THE ENHANCEMENT OF OPTICAL-PUMPING
DOUBLE-RESONANCE SIGNALS [*]

E. Lipworth

Optical-pumping double-resonance experiments are usually performed
by illuminating a bulb, containing a vapor of the substance under investiga-
tion, with linearly polarized light, and observing changes in the intensity
and polarization of the scattered light when magnetic resonance is induced in
the excited state. The first experiment of this type was that of Brossel and
Bitter[1] in the $^3P_1$ state of mercury, and their method has been used to meas-
ure the hyperfine splittings in the first excited $^2P_{3/2}$ states of many of the
alkali metals; a typical experiment in the alkali metal vapor is that by Althoff,[2]
who measured the hyperfine splittings in the $7^2P_{3/2}$ state of cesium.

All experiments of this general type have been carried out in bulbs with-
out wall coatings, where a collision of an alkali atom with the wall would re-
sult in the immediate destruction of any ground-state polarization or alignment,
should it exist. It is the purpose of this note to point out that a considerable
enhancement of the effects of certain excited-state transitions should be ob-
tained under the following conditions: (a) that the experiment be performed in
an evacuated bulb where the inside walls are coated with a nonrelaxing mate-
rial (e.g., Paraflint Wax or Dri-Film) and (b) that the pumping light be cir-
cularly polarized.

Consider, for example, a coated bulb containing cesium vapor pumped
by right-circularly polarized D_2 radiation (see Fig. d.18-1) directed along a
weak applied magnetic field. In a manner very similar to the method of single
D_1 line pumping proposed by Franzen and Emslie,[3] and independently by
Dehmelt, all atoms are pumped by the D_2 light (which induces transitions with
$\Delta M = + 1$) to the state of highest M_F in the $^2S_{1/2}$ ground state; for cesium this
is the level (44). In contrast, however, to the case in which D_1 light alone
is used for pumping, this level is still highly absorbing for the D_2 radiation,
so that, for instance, in the presence of a buffer gas, no ground-state pop-
ulation differential would be obtained because of mixing by collision among
the $^2P_{3/2}$ excited levels. In the present circumstances, however (neglecting
any collisions among cesium atoms themselves, or with the walls while an
atom is excited), the selection rules for decay force any atom in the ground-
state level (44) excited by D_2 light to return to the same level. The equilib-
rium ground-state population inequality is thus unaffected by this absorption
if effects due to multiple scattering of the D_2 radiation, within the bulb, are
ignored. It is this ground-state population inequality that should allow one
to enhance the effect of certain excited-state transitions.

An analysis has been made of the situation in which a fraction a of the
atoms excited from the level (44) of the ground state by right-circularly
polarized D_2 radiation are transferred, by a radio-frequency field, from the

[*] Abstract for Conference on Quantum Electronics, Berkeley, March 23-25, 1961.

[1] J. Brossel and F. Bitter, Phys. Rev. 86, 308 (1952).

[2] K. Althoff, z Physik 141, 33 (1955).

[3] W. Franzen and A. G. Emslie, Phys. Rev. 108, 1453 (1957).
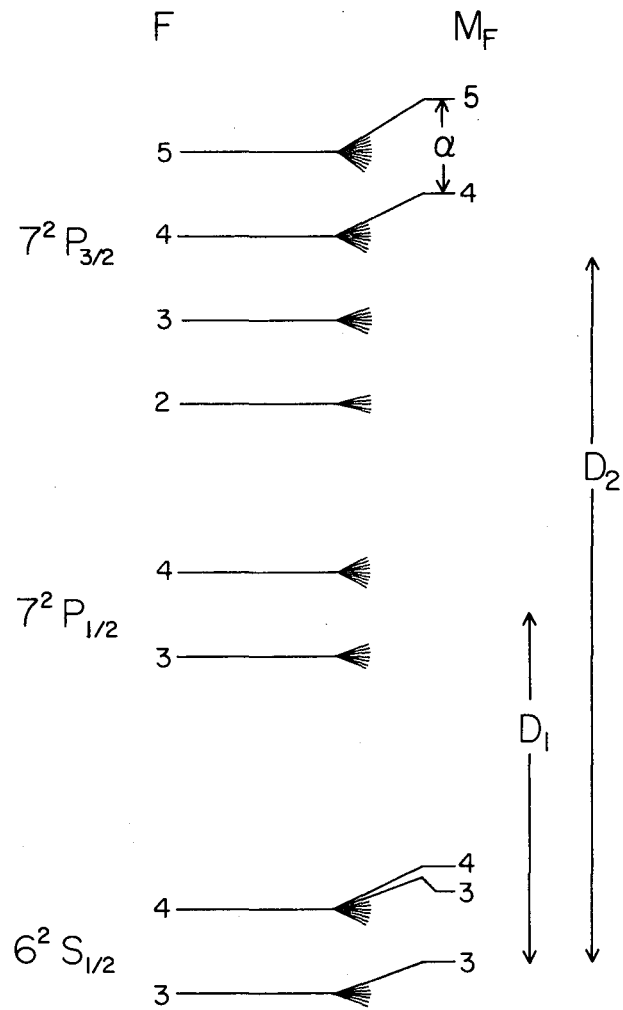
Fig. D. 18-1.

level (55) to the level (44) in the $7^2P_{3/2}$ excited state, and in which the ground-state relaxation time is assumed infinite; depolarizing effects due to multiple scattering of D_2 light are neglected. At equilibrium the populations in the levels (44), (43), and (33) of the ground state stand in the ratio

$$\frac{116\,a + 133}{3a} : 35 : 83, \tag{1}$$

and the population of all other ground-state levels is zero. The ratio of the change in the equilibrium absorption of D_2 light, with and without an applied rf field, to the change in absorption that would result if the populations of the levels of the $F = 4$ state of the ground state were equalized by a strong rf field is

$$R = \frac{16632\,a}{43\,(470\,a + 133)} . \tag{2}$$

For $a = 0.5$, $R = 0.53$. Thus a resonance in the excited state should, in principle, be observable in transmission with a signal-to-noise ratio approximating that of the ground-state resonance. In practice, the conditions that this statement be true are simply that the pumping time be short compared with the ground-state relaxation time and that no appreciable relaxation effects occur in the excited state in the pumping time.

Ground-state resonances in cesium with D_2 line pumping have been observed with good signal-to-noise ratio in wall-coated vacuum bulbs.[4] Pumping times in alkali vapors as short as 1 msec have been reported,[5] and ground-state relaxation times as long as 0.1 sec are easily obtainable;[6] so the method appears to be feasible.

Transitions in the $7^2P_{3/2}$ state other than that discussed here could be observed by multiple quantum effects or by the application of multiple rf fields. A possible application of the method would perhaps be to enhance signals in experiments in which the scattered light is observed. One obvious point to notice is that large excited-state resonances should be observable with no filter at all, i.e., with both D_1 and D_2 pumping radiation present. It is hoped that this technique will permit strong resonances to be observed in higher excited states than the first.

---

[4] By D. Buchla and E. Lipworth, (Lawrence Radiation Laboratory).

[5] A. L. Bloom (Varian Associates), private communication.

[6] W. Franzen, Phys. Rev. 115, 850 (1959).

19. THE RADIOLYSIS OF BIACETYL VAPOR [*]

Gilbert J. Mains, Amos S. Newton, and Aldo F. Sciamanna

The study of the vapor-phase radiolysis of simple systems which have been studied extensively by photochemical methods leads to information regarding mechanisms by observing the differences between the photolysis and the radiolysis. An important question still unanswered is the role of ions in the radiolysis process, and studies comparing photolysis where no ionization is possible with radiolysis should be useful in clarifying the situation. Ausloos and Paulson[1] have estimated that 85% of the methane formed in the liquid-phase radiolysis of acetone could be explained by normal abstraction reactions of methyl radicals, hence ketones appear attractive for such comparative studies.

The radiolysis of biacetyl vapor has been studied in the pressure range 5 to 30 mm and the temperature range 25 to 200° using the pulsed electron beam from a 4.2-Mev microwave linear accelerator. Runs were also made with a continuous electron beam from a Van de Graaff accelerator for comparison of pulsed versus continuous beams on the system.

Analyses were made by separating product fractions volatile at -160°, -119°, and -80°. These were analyzed by use of a mass spectrometer. In experiments in which I_2 was added, the excess I_2 was determined by titration with sodium arsenite after separation of the gaseous products. The yields of products from the irradiation of biacetyl vapor at 20 mm pressure with and without added I_2 are shown in the table.

In all cases with added I_2, the yield of CH_3I is about equal to the CO yield. The iodine uptake equals the CH_3I yield except at 200°, where almost twice as much iodine was used as CH_3I found. At room temperature, iodine reduces the yield of H_2, CO, C_2H_2 and CO_2 by about 25 to 30%. Methane is reduced by about 85% and ethane by 99%. The methane result was variable, however, and in some cases more methane was found in the presence of I_2 than in its absence. The system is apparently sensitive to traces of unidentified impurities. It is possible that no methane would be found in the presence of iodine in an ideal experiment.

The effect of pressure, temperature, geometry of cell, total dose, dose rate, and continuous vs pulsed radiation were also investigated. The results may be summarized as follows:

1. At any given temperature, the effects of varying the other parameters on the system are small; the yields of C_2H_6/CO, H_2/CO, and CO_2/CO are almost constant. The ratio CH_4/C_2H_6 increases slightly with increasing pressure and total dose. In a 12-liter spherical cell where dead space exists, the ratio of CH_4/C_2H_6 was higher than in the normal cells, which were

_____

[*] Brief version of paper published in J. Phys. Chem. 65, 1286 (1961).

[1] P. Ausloos and J. F. Paulson, J. Am. Chem. Soc. 80, 5117 (1958).

Yields, of products from the irradiation of biacetyl vapor with electrons[a]

	G (product)					
	Temperature					
	25°		120°		200°	
	No I_2	I_2 added[b]	No I_2	I_2 added[b]	No I_2	I_2 added[b]
Product						
H_2[c]	0.55	0.38	0.55	0.35	0.55	0.49
CH_4[d]	0.22	0.03	1.4	0.07	5.9	0.22
C_2H_2	0.15	0.1	0.15	0.09	0.15	0.14
C_2H_4	0.06	0.03	0.1	0.02	0.2	0.05
C_2H_6	2.0	.02	2.2	0.02	1.8	0.01
CO	7.4	6.3	9.2	5.5	16.0	8.4
C_3H_6	0.03	0.013	-	-	-	-
C_3H_8	0.06	0.006	-	-	-	-
CO_2	0.1	0.07	0.4	0.07	0.6	0.16
CH_2CO[d,f]	0.5	-	0.7	-	2.0	-
CH_3CHO	0.3	-	0.4	-	0.3	-
CH_3COCH_3[d]	1.1	-	1.1	-	2.4	-
$C_2H_5COCOCH_3$	0.3	-	0.5	-	0.7	-
CH_3I	-	5.9	-	5.2	-	7.7
I (atoms reacted)	-	6.4	-	5.3	-	14.8

[a] Values are for 20 mm biacetyl, 30 pulses/sec, 50 ma/pulse, 5-μsec pulse length; 90 min irradiation.

[b] Represents average from 7 experiments. Values at 120° and 200° single experiments.

[c] G. values normalized on H_2 yields. Probable error in absolute values is ± 20%.

[d] Value depends on irradiation parameters.

[e] Results variable. Values listed are lowest found.

[f] Not found in all irradiations at 25° and 120°; behavior erratic.

cylinders 5.4 cm in diameter and 60 cm long and were irradiated through a thin end window. These contained essentially no dead space.

In addition, at 25°, the effect of pulse rate on the system was measured. Assuming methyl radicals to be the precursors of methane and ethane, then a single pulse of 5 μsec duration at 50 ma current will yield an initial methyl radical concentration of 0.7×10^{12} radicals/ml. (equal to the CO yield). Assuming a rate constant for methyl radical recombination of $10^{13.6}$ cc sec^{-1},[2] the calculated time to reduce the methyl radical concentration to half its initial value is 22 msec. This probably represents a maximum value.

In Fig. D.19-1, $R_{CH_4}/R^{1/2}(C_2H_6)$ for each respective pulse rate is plotted against the time between pulses. If each pulse is an individual event, then the points should follow a line proportional to $t^{-1/2}$, whereas if the pulses are overlapping there should be a deviation from this line. This deviation appears at about 30 msec, and the mean life of the radicals must be less than this. The agreement is sufficient for one to conclude that the bulk of the methane and ethane are formed by thermal radical reactions.

Only two ion molecule reactions are observed in the mass spectrum biacetyl. One at mass 129 presumably arises from the reaction

$$CH_3CO^+ + (CH_3CO)_2 \longrightarrow (CH_3CO)_3^+, \tag{1}$$
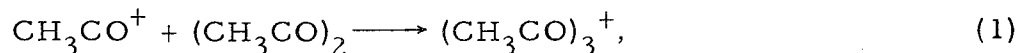
whereas the other is at mass 59 and may arise from the reaction

$$CH_3^+ (CH_3CO)_2 \longrightarrow CH_3 (CH_3CO)_2^+ \longrightarrow CH_2CO + (CH_3)_2 CHO^+. \tag{2}$$
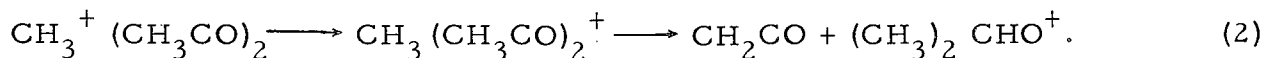
These reactions cannot contribute to ethane or methane production, though Reaction (2) might contribute to the formation of ketene and acetone.

Mechanism

Except for H_2 and possibly a small fraction of the methane, the results are indicative of a thermal radical mechanism. Such a mechanism has been suggested to account for the photolysis and pyrolysis experiments on biacetyl.[3-8] Stief and Ausloos[9] have applied a thermal radical mechanism to the radiolysis of azomethane vapor.

[3] P. Ausloos and E. W. R. Steacie, Can. J. Chem. 33, 39 (1955).

[4] F. E. Blacet and W. E. Bell, Disc. Faraday Soc. 14, 70 (1953).

[5] E. W. R. Steacie, Atomic and Free Radical Reactions (Reinhold Publ. Corp., New York, 1954), p. 354.

[6] G. F. Sheats and W. A. Noyes, Jr., J. Am. Chem. Soc. 77, 1421 (1955).

[7] G. F. Sheats and W. A. Noyes, Jr., ibid. 77, 4532 (1955).

[8] J. H. Heicklen and W. A. Noyes, Jr., ibid. 81, 3858 (1959).

[9] L. J. Stief and P. Ausloos, Paper presented at 138th meeting of the American Chemical Society, New York, Sept. 1960.
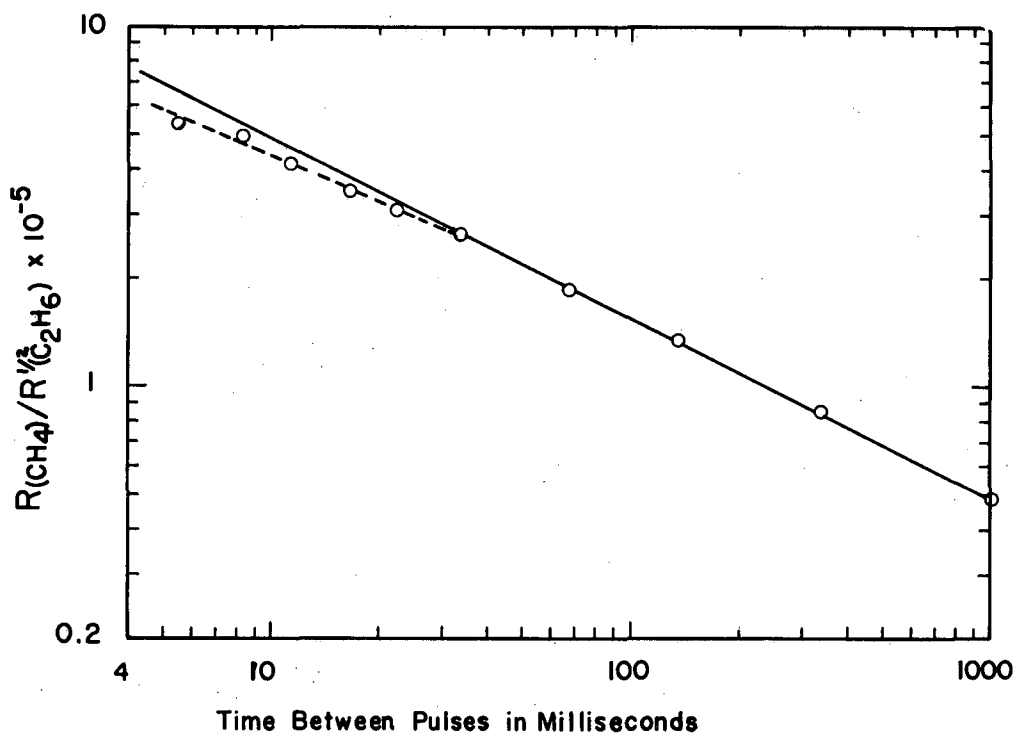
Fig. D.19-1. Plot of $R_{CH_4}/R_{C_2H_6}^{1/2}$ vs time between pulses for the irradiation of biacetyl vapor at 25°, 20 mm pressure, 50 ma pulse current, and selected repetition rates. Points at high repetition rates have been corrected for falloff in pulse current by normalization to a constant CO yield/pulse. Points at 16.7 and 33.3 nsec are averages of several close points. Solid line is of slope $t^{-1/2}$.

MU-22721

Radical Formation

$$(CH_3CO)_2 \leadsto CH_3 + CO + CH_3CO \tag{3}$$

$$\leadsto CH_3CO + CH_3CO^* \tag{4}$$

$$\leadsto H^* + CH_2COCOCH_3, \tag{5}$$

$$CH_3CO^* \longrightarrow CH_3 + CO, \tag{6}$$

$$CH_3CO \longrightarrow CH_3 + CO, \tag{7}$$

$$H^* + M \longrightarrow H + M. \tag{8}$$
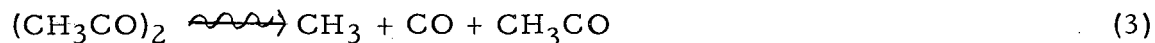
Reactions (3), (4), and (5) may not be primary steps, since these species could arise from ion neutralization as well as direct energy absorption. There is no evidence of Reaction (8) in this investigation, and Reaction (7) is of importance only at elevated temperatures. Sheats and Noyes[6] have shown their photolysis data to be consistent with a fragmentation according to Reaction 3 rather than Reaction 4.

Hydrogen Formation

$$H^* + (CH_3CO)_2 \longrightarrow H_2 + CH_2COCOCH_3, \tag{9}$$

$$H + H + M \longrightarrow H_2 + M \tag{10}$$
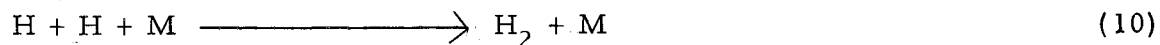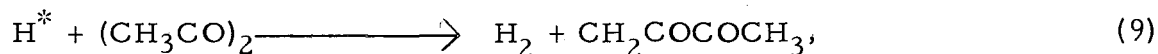
The bulk of the hydrogen must be formed by Reaction (9) and its thermal analog. No evidence for Reaction (10) was seen in this investigation. Further, carbonyl compounds are known to be good scavengers of H atoms,[10] so that addition reactions by thermal hydrogens should effectively scavenge such radicals from the system. The products of such a reaction are not known.

$$H + (CH_3CO)_2 \longrightarrow CH_3COCOHCH_3 \ (?) \tag{11}$$

Methane

$$CH_3^* + (CH_3CO)_2 \longrightarrow CH_4 + CH_2COCOCH_3 \tag{12}$$

$$CH_3 + (CH_3CO)_2 \longrightarrow CH_4 + CH_2COCOCH_3 \tag{13}$$

$$CH_3 + CH_3CO \longrightarrow CH_4 + CH_2CO \tag{14}$$

Ethane

$$CH_3 + CH_3 \longrightarrow C_2H_6 \tag{15}$$
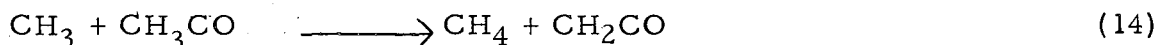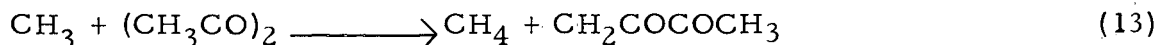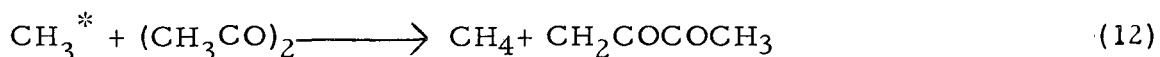
Carbon Monoxide

Reactions (3), (6), and (7).

---

[10] J. D. Strong and J. G. Burr, J. Am. Chem. Soc. **80**, 5117 (1958).

Acetone

$$CH_3 + CH_3CO \longrightarrow CH_3COCH_3 \tag{16}$$

$$CH_3 + (CH_3CO)_2 \longrightarrow CH_3COCH_3 + CH_3CO \tag{17}$$
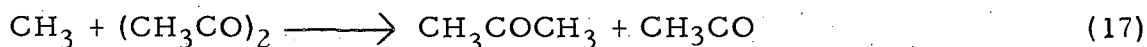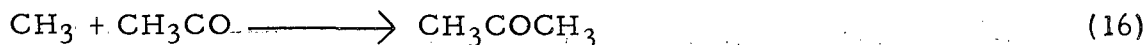
Ketene and Acetaldehyde

$$2CH_3CO \longrightarrow CH_2CO + CH_3CHO \tag{18}$$

$$CH_2COCOCH_3 \longrightarrow CH_2CO + CH_3CO \tag{19}$$

Acetyl propionyl

$$CH_3 + CH_2COCOCH_3 \longrightarrow CH_3CH_2COCOCH_3 \tag{20}$$
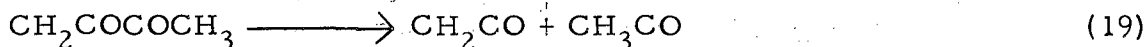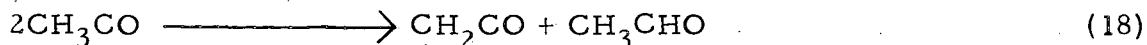
Except for the formation of H_2 and the hot methyl reaction (12), all these reactions have been proposed in photolysis studies. Reaction (12) can contriubte less than 30% of the methane at room temperature.

The observed activation energy for methane formation was 4.7 kcal between 25° and 120°, and 7.0 kcal between 120° and 200°. The latter figure agrees with the photolysis results of Blacet and Bell,[4] but is lower than those of Ausloos and Steacie.[3]

The material balance accounts for about 80% of the methyl radicals produced. The mechanism given does not account for the unsaturated hydrocarbons or for CO_2. Qualitatively, however, it is sufficient to explain the formation of the major products and the effects of changes of experimental parameters on the yields of these products.

Acknowledgments

20. THE RADIOLYSIS OF LIQUID ISOBUTANE WITH PULSED ELECTRONS[(*)]

B. Y. Yamamoto, A. F. Sciamanna, and Amos S. Newton

Isobutane is the simplest hydrocarbon in which specificity in radiolytic behavior owing to structural configuration should be apparent. The hydrogen atom bonded to the tertiary carbon should, on the basis of bond strength

---

[*]Brief version of a note submitted to J. Phys. Chem.

alone, be several times as reactive as other hydrogen atoms in the system.

Keenan, Lincoln, Rogers, and Burwasser have irradiated liquid iso-
butane at -30° and reported C_1 to C_8 hydrocarbons to be formed.[1] Kivel and
Voigt have recently irradiated isobutane labeled with C^{14} and discussed the
formation of products through the pentanes.[2]

Liquid isobutane was irradiated at 25° in a stainless steel target vessel
with 4.2-Mev electrons from a microwave linear accelerator to a dose of
5.4×10^{21} ev/g. This resulted in approximately 2.5% decomposition. The low-
boiling products were removed by refluxing under vacuum (condenser temp
of -140°) and samples volatile at -196 and -140° collected. The liquid was
separated and analyzed by a combination of distillation, gas chromatography,
and mass spectrometry. The main products are listed in Table I. Some
runs were made on liquid isobutane at 25° with Co^{60} γ-ray irradiation. These
results are also listed in Table I.

The γ-ray values shown are in substantial agreement with the results
of Kivel and Voigt except that they report more propane than is reported
here.

Discussion

The present data are not sufficient to justify proposing any complete
kinetic mechanism for the radiolysis of isobutane, but certain regularities
can be pointed out which are indicative of a free-radical mechanism for the
formation of the higher products. First, the pentanes, heptanes, and octanes
in highest yield are those formed by methyl, isopropyl, isobutyl, and tertiary
butyl radicals. Isomerization of these groups, if it occurs, must be less
than a tenth of the total yield of these radicals.

If one assumes that the products ethane, isopentane, neopentane,
2,3-dimethyl butane, 2,4-dimethyl pentane, 2,2,3-trimethyl butane,
2,2,4-trimethyl pentane, 2,5-dimethyl hexane, and 2,2,3,3-tetramethyl
butane are formed by combination of methyl, isopropyl, isobutyl, and tertiary
butyl radicals, then from the yields of radical dimers one can calculate the
expected yield of mixed radical products, assuming combination occurs
according to the binomial expansion for any two types of radicals. This
assumes no activation energy or steric effects in the combination. The re-
sults of such a calculation are shown in Table II. The agreement between
calculated and observed yields in the heptanes and octanes is satisfactory.
The lack of agreement in neopentane and isopentane may indicate that some
of the ethane is formed by nonradical processes. A similar suggestion had
been made by Taylor, Mori, and Burton in the radiolysis of neopentane.[3]

---

[1] V. J. Keenan, R. M. Lincoln, R. L. Rogers, and H. Burwasser, J. Am.
Chem Soc. 79, 5125 (1957).

[2] J. Kivel and A. F. Voight, J. Appl. Radiation and Isotopes 10, 181 (1961).

[3] W. H. Taylor, S. Mori, and M. Burton, J. Am. Chem. Soc. 82, 5817
(1960).

Table I. Products from the radiolysis of liquid isobutane at 25°

Product	Pulsed electrons	Co^{60} γ rays
H_2	2.9	4.4
CH_4	1.4	2.2
C_2H_2	0.04	0.04
C_2H_4	0.07	0.08
C_2H_6	0.22	0.2
C_3H_6	1.1	0.6
C_3H_8	0.5	0.3
$n-C_4H_{10}$	0.10	
$i-C_4H_8$	1.1	
Butene-1	0.01	
Butene-2 (cis + trans)	0.05	
Methyl cyclopropane	0.04	
Neopentane	0.16	
Isopentane	0.20	
2, 3-Dimethyl butane	0.030	
2, 2, 3-Trimethyl butane	0.10	
2, 4-Dimethyl pentane	0.12	
2, 5-Dimethyl hexane	0.13	
2, 2,4 -Trimethyl pentane	0.19	
2, 2, 3, 3-Tetramethyl butane	0.08	

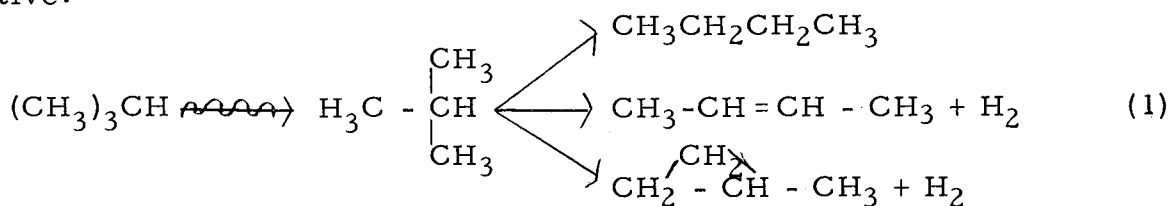Table II. Calculated and observed yields of mixed products from radicals

R_1	R_2	Mixed product	$G_{R_1R_2}$ Observed	$G_{R_1R_2}$ Calculated[a]
CH_3	$(CH_3)_2CHCH_2$	isopentane	$\geqslant 0.20$	0.34
CH_3	$(CH_3)_3C$	neopentane	0.16	0.26
$(CH_2)_2CH$	$(CH_3)_2CHCH_2$	2,4-dimethyl pentane	0.12	0.118
$(CH_3)_2CH$	$(CH_3)_3C$	2,2,3-trimethyl butane	0.10	0.098
$(CH_3)_2CHCH_2$	$(CH_3)_3C$	2,2,4-trimethyl pentane	0.19	0.194

[a] Calculated by the equation

$$G_{R_1R_2} = 2(G_{R_1R_1}^{1/2} \cdot G_{R_2R_2}^{1/2}) .$$

The distribution of heptanes and octanes is consistent with a ratio of isobutyl to tertiary butyl radicals of about 1.25:1. This distribution implies that tertiary bonded H atoms are at least seven times as reactive as primary H atoms in isobutane. It is a higher difference in reactivity than would be calculated from the results of Keenan et al.,[1] but lower than would be calculated from the results of Kivel and Voigt,[2] who found 2.5 to 3.6 times as much neopentane as isopentane to be formed in the γ radiolysis of isobutane, suggesting a reactivity difference of a factor of 22 to 32.

An unexpected observation was the occurrence of methyl cyclopropane among the radiolysis products. It appears that about 3% of the C_4H_8 yield is formed as methyl cyclopropane. This is the first time a high-energy isomer has been observed to be formed in a radiolysis process. The identity of the methyl cyclopropane was established by comparison of both its mass spectrometer ionization pattern and gas chromatographic elution time with the mass spectrometer pattern and elution time of an authentic synthetic sample of methyl cyclopropane.[4] Methyl cyclopropane may be formed via a cyclic intermediate in a highly excited state of isobutane. The existence of such a state could also be used to explain the formation of n-butane and the linear butenes in the radiolysis. It may also explain the temperature sensitivity of the n-butane yield found by Kivel and Voight.[2] The competitive modes of decay of such a state as shown in Reaction (1) should be temperature-sensitive.

$$(CH_3)_3CH \rightsquigarrow H_3C-\underset{\overset{|}{CH_3}}{\overset{\overset{|}{CH_3}}{C}}H
\begin{cases}
\nearrow CH_3CH_2CH_2CH_3 \\
\longleftrightarrow CH_3-CH=CH-CH_3 + H_2 \\
\searrow CH_2\overset{CH_2}{\diagup\diagdown}CH-CH_3 + H_2
\end{cases} \qquad (1)$$

[4] Synthesized by method of J. T. Gragson, K. W. Greenlee, J. M. Diefer, and C. E. Board, J. Am. Chem. Soc. 75, 3344 (1953).

Unfortunately the yields are low, and the experimental difficulties inherent in a meaningful investigation of the effect of temperature on this system preclude further work on this system at present.

Acknowledgments

The authors wish to thank Mr. William L. Everette for the electron irradiations, Mr. John Olmsted for the Co^{60} results, Mrs. Mary Pong for reading the mass spectrometer records, Mr. Phillip Wadsworth of the Shell Development Company for an authentic sample of 2,2,3,3-tetremethyl butane, and Dr. K. L. Hall of the California Research Corporation for authentic samples of 2,2,3-trimethyl butane, 2,2-dimethyl pentane, and 2,5-dimethyl hexane.

21. "HOT ATOM" CHEMISTRY OF SULFUR-35 IN GASEOUS SULFUR COMPOUNDS

Monte L. Hyder and Samuel S. Markowitz

The chemical behavior of "hot" S^{35} recoils from the $S^{34}(n, \gamma)S^{35}$ reaction has been studied in H_2S and SO_2, as part of a series of such studies on sulfur-containing gases. These recoils may possess up to 750 ev of energy, and the extent of breakup of the original molecule and the oxidation state of the resulting product are of interest.

Quartz capsules containing about 10 cc of gas at various pressures were irradiated in the thermal facility of the Livermore LPTR reactor. Typical irradiation conditions were 16 hr at an average flux of 3×10^{11} n/cm^2-sec. The capsules were broken open in a vacuum system, and the gaseous activity was counted internally in a proportional counter as previously described.[1] When it was necessary to determine the relative amounts of H_2S and SO_2, the sample was absorbed in a NaOH solution with the appropriate carrier for chemical separation. The activity remaining on the walls of the capsule was determined by crushing the capsule in an aqueous solution containing appropriate carriers. The various fractions were precipitated as CuS or $BaSO_4$ and ignited to SO_2 for counting. Sulfide and elemental sulfur, which exchange in solution, were determined together.

In all cases the sum of the activities actually observed was taken as 100% of the total. Experiments with monitor foils showed that the neutron flux might very by a factor of two or more in a few centimeters distance. This result invalidated much earlier data where total activity determinations were not made, and introduces a bothersome source of error into the present experiments.

---

[1]M. L. Hyder and Samuel S. Markowitz, in Chemistry Division Semiannual Report, UCRL-9093, Nov. 1959, p. 71-73.

H_2S

The radioactive products of H_2S included H_2S, SO_2, solid S, and SO_3. The latter two are found on the tube walls. The oxidized species presumably result from reaction with trace impurities. As shown in Table I, the proportion of SO_3 formed decreases with increasing pressure. Variation of surface area by packing the capsule with quartz wool had no great effect.

Table I. Radioactive products from pure H_2S.

P_{H_2S},	Total activity observed, (%) by chemical form					
(cm Hg)	H_2S	SO_2	Total gaseous	S	SO_3	Total solid
1.65	67	10	77	9	14	23
9.6	86	6	92	3	5	8
9.6			94			6
25.6			96	2	2	4
25.0			98	1	1	2
47.25	85	13	98	-	2	2
47.25			97			3
Capsules packed with quartz wool						
9.7	94	3	97	1	2	3
48.95	86	13	99	-	1	1
48.75			99			1

Table II. Radioactive products from 9.5 cm Hg of H_2S plus O_2

P_{O_2}	Total activity observed, (%) by chemical form					
(cm Hg)	H_2S	SO_2	Total gaseous	S	SO_3	Total solid
1.65	2	76	78	9	12	21
1.65			71			29
10.6	-	76	76	6	18	24
10.6			82	4	14	18

Table II shows the effect of adding oxygen to the H_2S capsule. Oxidized species are virtually the only products. This implies that the H_2S is completely broken up following neutron capture and de-excitation of the S^{35} nuclei, and that the resulting S species is readily oxidized, mainly to SO_2. As the simple H_2S molecule is the least likely to be disrupted by recoil, one may expect some disruption in all sulfur compounds following (n, γ) reactions.

SO_2

This is a more complex system, and the data are difficult to reproduce. The products are S, SO_2, and SO_3. Table III shows some sample results on SO_2 alone, where some pressure dependence is seen. Table IV shows how added oxygen affects the system: the S fraction disappears and the SO_2/SO_3 ratio approaches that found in $H_2S + O_2$.

Table III. Radioactive products from pure SO_2

P_{SO_2}, (cm. Hg)	SO$_2$, gas	Total activity observed (%), by chemical form			
			Adsorbed on walls		
		S	SO$_2$	SO$_3$	total
0.9	28	29	26	17	72
8.0	48	12	8	32	52
8.0	48	24	6	22	52
65	65	4	15	17	35
68	84	7	2	7	16
68	82	5	2	12	18

Table IV. Radioactive products from SO_2 with added oxygen $(P_{SO_2} = 10$ cm Hg in all cases).

P_{O_2}, (cm Hg)	Total activity (%), by chemical form.				
	SO$_2$, gas	S	SO$_2$	SO$_3$	total
0	48	18	7	27	52
1.0	57	4	1	38	43
1.0	60	2	1	37	40
10	55	1	1	43	45
	61				39
60	82	3	4	10	18
	76	8	2	14	24

Table V shows the interesting effect of adding NO to the SO_2. This result may be due to oxidation and reduction by the NO, and possible impurity NO_2, or may result from disruption of the usual mechanisms. The effect of NO in other systems is being investigated.

Work continues on these systems, SF_6, CH_3SH, and thiophene, in an effort to determine the general behavior of the "hot" S^{35}.

Table V. Radioactive products from SO_2 with added NO
$(P_{SO_2} = 19$ cm Hg in all cases$)$.

P_{NO}, (cm Hg)	Total activity observed (%), by chemical form				
	SO_2, gas	Adsorbed on walls			
		S	SO_2	SO_3	total
0 (Interpolated)	60	15	5	20	40
1.2	91	3	2	4	9
10.0	97	1	-	2	3
10.0	93				7

22. ACTIVATION ANALYSIS FOR OXYGEN AND OTHER ELEMENTS BY MEANS OF He^3-INDUCED NUCLEAR REACTIONS [*]

John D. Mahony and Samuel S. Markowitz

I. General Considerations

A. Introduction

A simple, rapid, and absolute method for detection of oxygen and other elements over the concentration range from 1 part per billion to 100% has been advanced. Only a few milligrams of total sample material is required. The key feature of this method is the use of He^3 ions accelerated to comparatively low kinetic energies to induce nuclear reactions which give radioactive products. These products, which decay mainly by emission of positrons or negatrons, can be detected by conventional nuclear techniques; the radio-activities may also be distinguished by half lives.

More than one element can be detected simultaneously in the same activation. This depends upon the half lives and decay schemes of the radio-activities induced in the given sample. Solids, liquids, and gases may be analyzed. This analysis will not per se identify the chemical form of the unknown. The method is nondestructive. Activation analysis in general has been previously described in the literature, and review articles are available.[1-3]

The He^3 ion offers distinct advantages as an incident particle for reasons based upon energetics, formation cross sections, versatility, and convenience of product detection.

The reactions $O^{16}(He^3, p)F^{18}$ and $O^{16}(He^3, n)Ne^{18} \rightarrow F^{18}$ have been used to analyze for oxygen in thorium, beryllium, and Mylar. By extension of known principles, this activation analysis may be applied for the analysis of many other elements. Relative or absolute analyses may be performed.

B. Energy of the He^3 Beam

The maximum cross section for a particular reaction depends on the He^3 energy. Greater sensitivity is obtained at higher cross sections. The cross sections, which should be experimentally determined, approximate within factors of two or three the geometric cross sections of the target nucleus for He^3 energies at the peak of the excitation function. If the He^3 energy is low, only simple reactions take place and interferences are minimized. On the other hand, the energy must be high enough to overcome any negative Q and the Coulomb barrier for the target nucleus. The Coulomb barrier restriction can, however, serve to advantage because no element heavier than calcium produces any interfering radioactivities. For O^{16} analysis, the excitation function as shown in Fig. D.22-1 indicates that the maximum cross section for F^{18} formation is at $E_{He^3} = 7.5$ Mev.

If a cyclotron were to be built specifically for He^3 activation analysis at 8 Mev, Hρ would be 350 kilogauss-cm, which for a 15-kilogauss field gives 9.2 in. for the radius. Such a small cyclotron would allow analysis only for elements up to $Z \approx 20$ (calcium) because of Coulomb barrier restrictions on the cross sections. It nevertheless would be extremely useful.

C. Depth of Penetration

An 8-Mev He^3 ion has a range of only 14 mg/cm^2 (approx 0.002 in.) in aluminum and 31 mg/cm^2 (approx 0.001 in.) in lead. Thus the depth of penetration is a few mils, depending on the host or bulk material in a given sample. It is therefore possible to analyze surfaces for impurities such as oxygen, carbon, or others by controlling the energy of the incident beam by appropriate absorbers or by varying the cyclotron probe radius. The limited depth of penetration need not confine this method to surface analysis, because

[1] W. W. Meinke, Anal. Chem. 32, 104R (1960).

[2] D. H. . Atkins and A. A. Smales, Advances in Inorg. Chem. Radiochem. 1, 315 (1959).

[3] B. A. Thompson, Anal. Chem. 33, 583 (1961).

O^{16} (He^3 ,n) Ne^{18} $Q_m = -3.0$ Mev

1.6 sec

O^{16} (He^3 ,p) F^{18} $Q_m = +2.0$ Mev
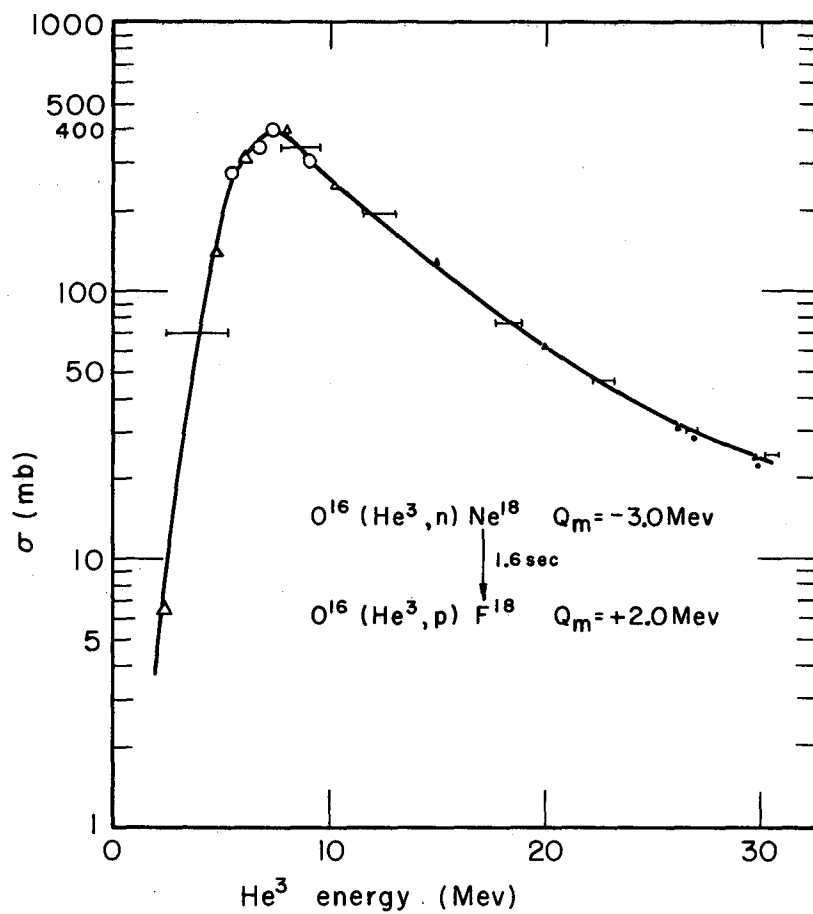
MU – 24829

Fig. D.22-1. Excitation function for the production of F^{18} from O^{16}. The ordinate represents the sum of the $O^{16}(He^3, n)$ and $O^{16}(He^3, p)$ reaction cross sections.

the sample itself can be treated (by slicing, cleaning, or etching) to bring the "interior" within range of the He^3 beam.

D. Sensitivity

The sensitivity depends on the lowest activity that can be detected above background, the beam intensity, the reaction cross section, the length of bombardment, and the half life of the detected product. If the length of bombardment is many times the half life ("saturation bombardment"), the sensitivity can be considered independent of the product half life. For most of the nuclides of $Z \leqslant 20$, the half lives are sufficiently short so that such an approximation can be met, if really necessary, in practice. If positron detection is carried out, for example, with conventional proportional-counter instrumentation, a disintegration rate D_0 of 10 dis/min can be determined. If the cross section for production of the radioactivity is 400 mb, as it is for F^{18} from O^{16} at $E_{He^3} = 7.5$ Mev, and if a beam of only $1 \mu a$ of He^3 ions is used, then $n = 1.34 \times 10^{11}$ atoms O^{16} per cm^2, and $m = 3.55 \times 10^{-12}$ g O^{16} per cm^2. Thus in a 0.0005-in. Al foil (3.55 mg/cm^2), for example, $1 \times 10^{-7}\%$ by weight of O^{16} or 1 part per billion could be detected. The sensitivity is about 1 ppb only if the beam is limited to $1 \mu a$ of He^3; at 25 μa, 0.04 ppb could be detected if the target were properly cooled.

E. Interferences

(i) Production of the observed radioactivity from extraneous sources

The cross sections for He^3 reactions vary with incident energy. It should be possible, by a proper choice of He^3 energy, to exclude some, if not all, of the unwanted contribution to the radioactivity being observed from extraneous sources. For example, it is desired to analyze for O^{16} in aluminum by $O^{16}(He^3, p)F^{18}$ reaction. The Q of the $Al^{27}(He^3, 3a)F^{18}$ reaction is -10.4 Mev. Therefore this reaction cannot take place at $E_{He^3} < 10.4$ Mev. The peak in the O^{16} cross section is at 7.5 Mev. Bombardment at this energy will not, however, exclude F^{18} production by $Na^{23}(He^3, 2a)F^{18}$ and $F^{19}(He^3, a)F^{18}$ reactions, whose Q values are -0.3 Mev and + 10.1 Mev, respectively. In order to correct for such F^{18} contributors, measurement of the above reaction cross sections may be necessary. It should be possible, in the same bombardment, to determine both the O^{16} and F^{19} content by two different reactions; the O^{16} by $(He^3, p)F^{18}$ and the F^{19} by $(He^3, n)Na^{21}$. The Na^{21} has a 23-sec half life and it could be separated by decay-curve analysis from the F^{18} (110-min) and other very short-lived activities produced from the Al^{27} by 7.5-Mev He^3 ions.

(ii) Production of radioactivities which differ from the desired product

In some cases impurities produce radioactive products, which, although not identical to the desired product, decay with similar half lives or emit similar radiations, thus complicating the detection techniques. In these cases, various detection systems may be used to enhance the overall detection coefficient of the desired radioactive product; decay-curve analysis may also be sufficient.

F. Precision and Accuracy

An estimate of the precision, based upon general experience with counting techniques, indicates that the reproducibility should approach $\pm 5\%$ or less in straightforward cases. Estimates of errors indicate that accuracies of $\pm 10\%$ should be possible, the percent errors being standard deviations.

II. Determination of Cross Sections for F^{18} Formation from $O^{16} + He^3$

A. Target and Irradiation

The cross section for formation of 110-min F^{18} from O^{16} by $(He^3, p)F^{18}$ plus $(He^3, n)Ne^{18} \longrightarrow F^{18}$ reactions was determined by bombardment of 0.00025-in.)0.93 mg/cm^2) stacked foils of Mylar with 1- to 31-Mev He^3 ions at the heavy-ion linear accelerator (Hilac).[4] Four hours after bombardment the 110-min F^{18} was the only nuclide detected, the 20-min C^{11} formed by the $C^{12}(He^3, a)C^{11}$ reaction having decayed to a very low level. The length of the bombardments varied between 10 and 25 min and the average beam currents were about 0.010 to 0.100 μa of $He^{3(++)}$. These irradiation conditions produced convenient amounts of F^{18} for detection. The total charge received by a Faraday cup was measured by a calibrated integrating electrometer.

### B. Radioactivity Detection and Overall Detection Coefficient

After the bombarment, the positron-emission rate of the Mylar foils was measured with calibrated end-window gas-flow proportional counters.

III. Oxygen Analysis in Thorium, Beryllium, and Mylar

Thin foils of thorium (0.001 in.) of thickness 35 mg/cm^2 and 1-in. diameter were cleaned and washed in a nitrogen atmosphere. They were then irradiated, and counted in a 0.001-in. polystyrene envelope so that oxygen was excluded from the surroundings. The results of absolute analysis by He^3 reactions to give F^{18} were $0.61 \pm .06\%$.[5] Determination of 110-min F^{18} was accomplished by means of (a) a calibrated proportional counter, (b) a 3×3-in. NaI(Tl) scintillation counter and 100-channel pulse-height analyzer which were calibrated for annihilation radiation. The pulse-height spectrum is displayed in Fig. D.22-2. This indicates the 0.511-Mev full-energy peak from F^{18} positron annihilation in the source is greater in intensity than the γ-ray "background" from the thorium daughters at about 0.51 Mev by a factor

---

[4] E. L. Hubbard, W. R. Baker, K. W. Ehlers, et al., Rev. Sci. Instr. 32, 621 (1961).

[5] The thorium samples were analyzed for oxygen by Mr. J. Fraser of the Lawrence Radiation Laboratory at Livermore by vacuum-fusion technique; the thorium was fused in a graphite crucible and CO and CO_2 gas were measured. Their results (0.35% oxygen by weight) differ from our own (0.61.) by more than the estimated experimental uncertainties.
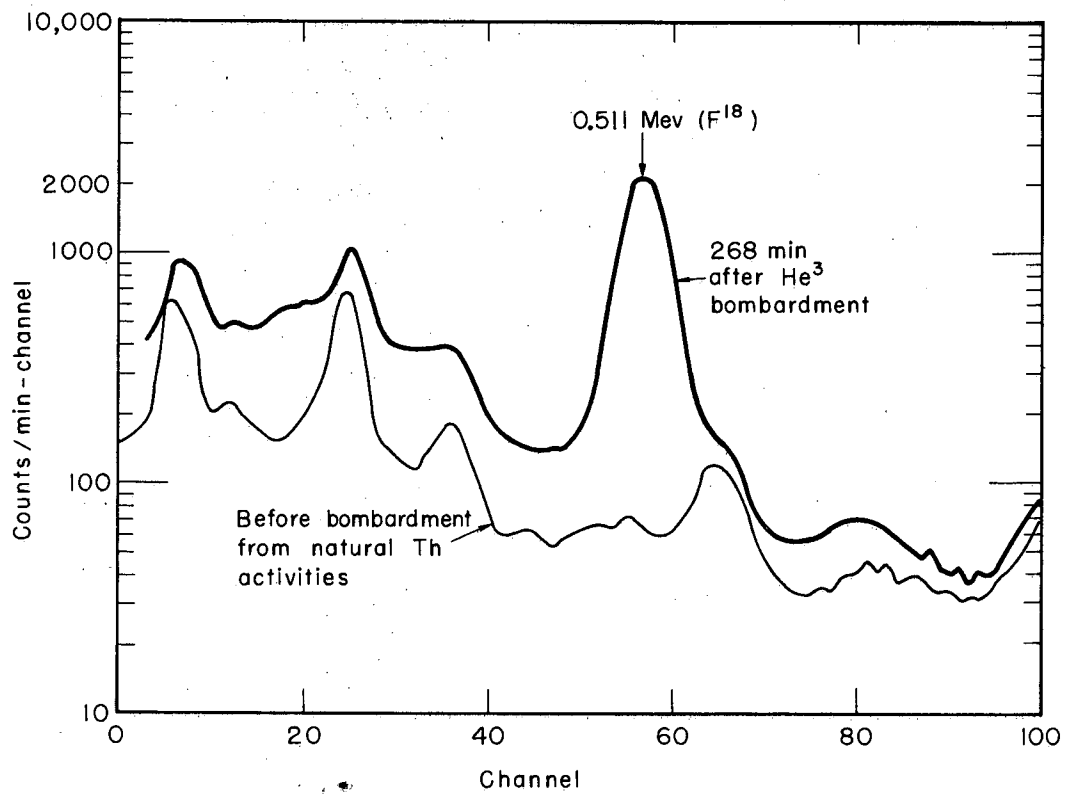
Fig. D.22-2. Gamma-ray spectrum from thorium foil before and after He³ activation. The peak at 0.51 Mev results from the annihilation of positrons from F¹⁸ in the source, which is a sandwich of the thorium foil between two pieces of copper 577 mg/cm² thick. The duration of bombardment was 14 min and the beam current was only 0.010 μa.

of about 30, and the sample shown has decayed through 2.4 F^{18} half lives (268 minutes after bombardment). The decay of the full-energy peak, which shows that the β^+ are from F^{18}, is given in Fig. E.22-3.

The oxygen content of 0.001-in. beryllium foil was found to be about 3%. (This analysis has not yet been checked by the vacuum-fusion technique[5] because of present experimental difficulties with that method.) After the F^{18} excitation function had been established, a sample of Mylar was treated as and "unknown." Absolute analysis gave a result of 33% oxygen, which agreed with the known composition of Mylar within experimental error.

23. MASS SPECTROSCOPY SURFACE IONIZATION STUDIES

F. L. Reynolds

This study has to do with the possible improvement of surface ionization sources in conjunction with high-sensitivity mass spectrometers. Any advancement in the understanding of this method of producing ions will have use in mass spectroscopy and other fields where the formation or detection of ions employs surface ionization.

The approach to this problem has centered around the use of single-crystal tungsten filaments. Much effort has gone into the methods of making suitable single-crystal filaments, the ascertaining of their crystallographic orientation, and determination of their ion thermionic characteristics.

Two methods of making single-crystal ribbon filaments of tungsten have been employed. One involved strain-annealing techniques[1] on prerolled multicrystalline ribbon filaments; the second, that of cutting-single crystal ribbon filaments from large tungsten single crystals. The first method suffers from the fact that there is little control over the orientation of the finished product. The drawing of the ribbon filament in most cases affects the crystal orientation in such a way that the multicrystal structure is aligned (110) parallel to the rolled direction. This orientation remains after strain annealing, but the grown crystals may have surface planes such as 112, 113, 115, or 310, or others.

The strain-annealed method consists of supporting the commercial tungsten ribbon filament at the top end, attaching a weight at the other, and then bombarding this ribbon with electrons by slowly moving a single loop filament along the ribbon filament. Rate of travel varied, from 1 in./hr to 1 in./24 hr, but the temperature of the moving zone was about 2500° K. Large crystals several inches long and at times the width of the ribbon filament were produced. When more than one crystal appears the surfaces are oriented the same within 1 or 2 deg.

The plane most desired on the surface is (110), and this did not occur with filaments treated as above. The second method, while tedious, resulted

----

[1]UCRL-9093, Feb. 1960, p. 68.
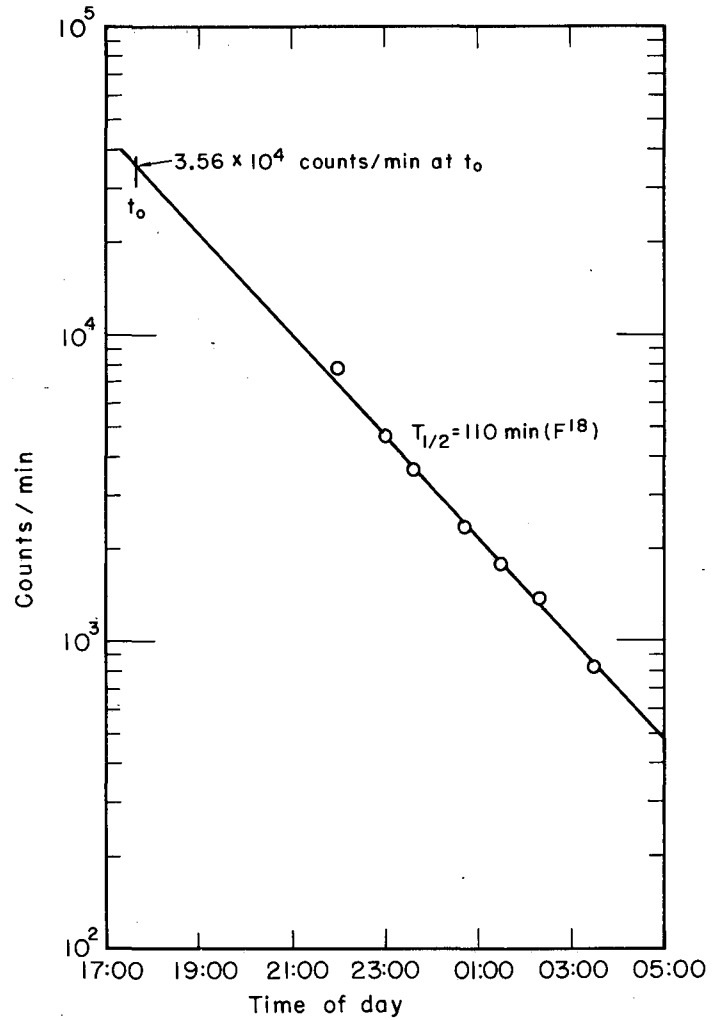
Fig. D.22-3. Decay of the full-energy peak (0.51 Mev). The area of
    that part of the γ-ray spectrum, corrected for Compton background
    from the γ-radiation emitted by the thorium daughters, was deter-
    mined as a function of time. The half-life corresponds to that of
    110-min F^{18}.

in filaments with the preferred (110) plane as the surface plane. Figure D.23-1 is a stereographic projection of this filament material, showing the orientation of the single crystal relative to the filament structure.

The bulk crystal was first cut by a slicing saw into 0.020-in.-thick wafers. The wafers were then slit into 0.030-in.-wide strips by cutting with a miniature sandblast cutter. The strips finally were ground to 0.002 in. thick and then electropolished to approximately 0.001 in. thickness. An electropolished filament can be shaped into a haripin filament at room temperature without breaking. Electropolishing also removes surface damage due to the mechanical treatment.

There is considerable spread in the published literature on the value of the work function of the (110) plane of tungsten. Most of the determinations have used the field-emission method,[2,3] which has given maximum values up to about 6 electron volts. These results are far from consistent; some workers report values as low as 4.6 ev for this plane.[4,5] The evidence that the (110) plane could be considerably higher than other crystal faces or the "bulk" work function of tungsten led to the present study, since the efficiency for the conversion of a given atom to ion is an exponential function of the difference between the work function of the metal surface and the ionization potential of the impinging atom.

To study the experimental factors closely, strontium was effused from a small oven, and the collimated neutral beam of Sr atoms impinged upon a hot polycrystalline tungsten filament. By plotting the natural logarithm of the Sr^{88} ion current against the reciprocal of the filament temperature the value of the work function of "bulk" tungsten could be ascertained. A value of 5.67 ev was taken[6] as the first ionization potential of stronitum. After a number of instrumental difficulties with the mass spectrometer a value of $4.59 \pm .03$ ev was obtained for this filament. This result is an average of 16 separate determinations. Figure D.23-2 is a graph of the data on one determination.

That this number did not come out to be 4.52 ev, the accepted value for tungsten, is not surprising. It agrees quite well with the value obtained by Werning,[7] who obtained $4.58 \pm .01$ ev for barium on tungsten by similiar methods. In addition, back-reflected Laue x-ray pictures of this filament indicated that this tungsten ribbon was no longer multicrystalline, but consisted of a few crystals of a preferred orientation with the (310) plane the

[2] E. Mueller, J. Appl. Phys. 26, 732 (1955).

[3] W. Dyke, J. Trolen, W. Dolan, and F. Grundhauser, J. Appl. Phys. 25, 106 (1954).

[4] I. S. Andreyev, Zhur. Tekh. Fiz. 22, 1428 (1952).

[5] M. Wilkinson, J. Appl. Phys. 24, 1203 (1953).

[6] R. S. Shankland Table 9 p.74 Atomic and Nuclear Physics (1960).

[7] Joseph R. Werning, Thermal Ionization at Hot Metal Surfaces, (Thesis), UCRL-8455, Sept. 1958.
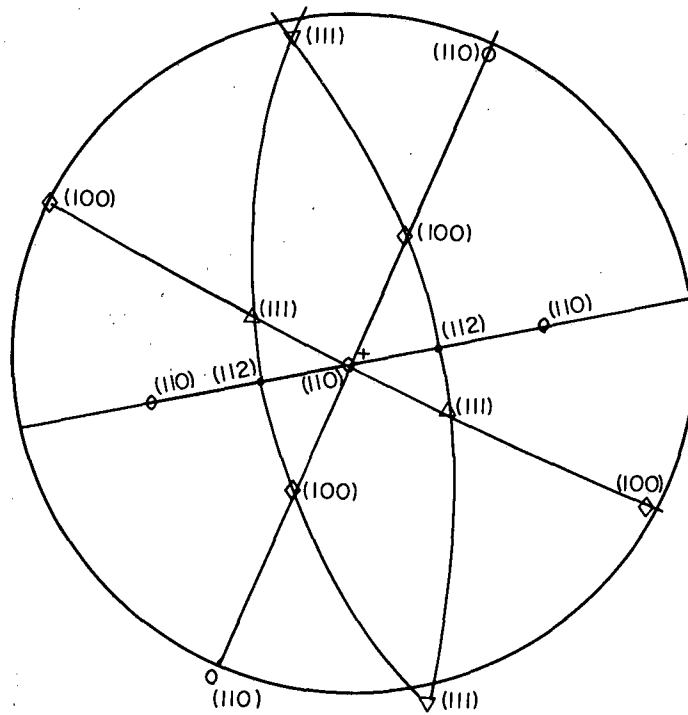
MU-25989

Fig. D.23-1. A stereographic projection of a cut single-crystal filament oriented with a (110) plane a surface normal to the long axis of the filament.
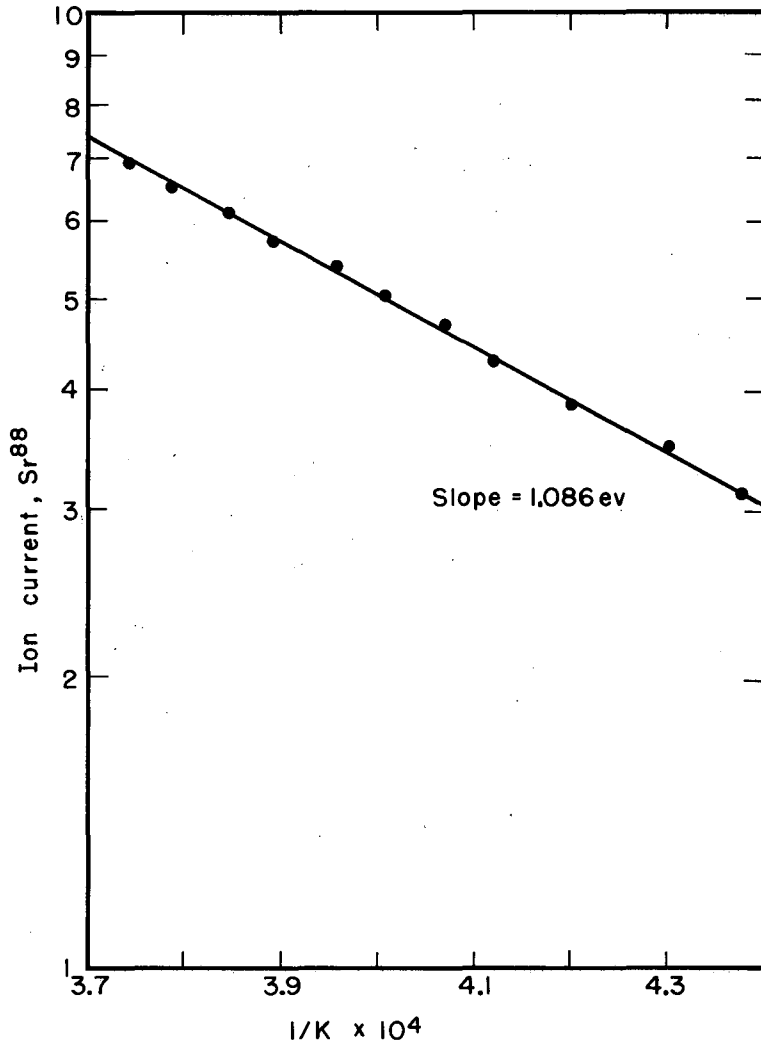
MU-25990

Fig. D.23-2. Typical Saha-Langmuir plot of the ion current against
   reciprocal filament temperatures for strontium on "bulk" tungsten.

most likely surface plane. The filament was therefore not a single crystal but several large ones all oriented the same within a degree or two. Figure D.23-3 shows a stereographic projection plot of this orientation.

A single-crystal tungsten filament having a surface structure oriented (110) was then submitted to a neutral strontium beam. Although extensive runs have not been completed, sufficient data indicate that this filament gives essentially no slope when the logarithm of the Sr^{88} ion current is plotted against $\frac{1}{T}$, the filament temperature (Fig. d.23-4). This independence of temperature can mean that the work function of the (110) plane of tungsten is equal to or greater than 5.67 ev. In the case of tungsten this represents a net gain of approximately 1 ev over the "bulk" work function.

As an example of how such a filament could be of value, let us assume a few numbers and substitute them in the Saha-Langmuir equation.[8] In its simplest form the ratio ions/neutral atoms is

$$\frac{N^+}{N_0} = \exp \left[\frac{F(\phi - IP)}{R_0 T} \right], \tag{1}$$

where ϕ is the work function of the filament, IP the ionization potential of the neutral atom, and R, F and T the gas constant, Faraday number, and absolute temperature respectively. We can say that the efficiency E_f of this process is

$$E_f = 100 \left(\frac{N^+}{N^+ + N_0} \right) \% = 100 \frac{1}{\left(1 + \frac{N_0}{N^+} \right)} \% . \tag{2}$$

$$\text{From (1), } \frac{N^+}{N_0} = \exp \left[\frac{F(\phi - IP)}{R_0 T} \right] \text{ or } \frac{N_0}{N_+} = \exp \left[\frac{1}{\frac{F(\phi - IP)}{R_0 T}} \right] . \tag{3}$$

$$\text{Therefore } E_f = \frac{100}{1 + \exp \frac{1}{\left[\frac{F(\phi - IP)}{R_0 T} \right]}} \% . \tag{4}$$

Let IP = 6 ev, ϕ = 4.52 ev, T = 1800° K; then $E_f = 7 \times 10^{-3}\%$, or 1 ion in 14,300 atoms, approximately. If ϕ is now 5.67 ev, the efficiency changes to nearly 1 ion for every 10 atoms. The absolute intensity of the emitted ion beam will of course depend on the rate of sample evaporation and arrival as well as the surface ionizing efficiency.

---

[8] I. Langmuir, Proc. Roy. Soc. (London) 107A, 61 (1925).
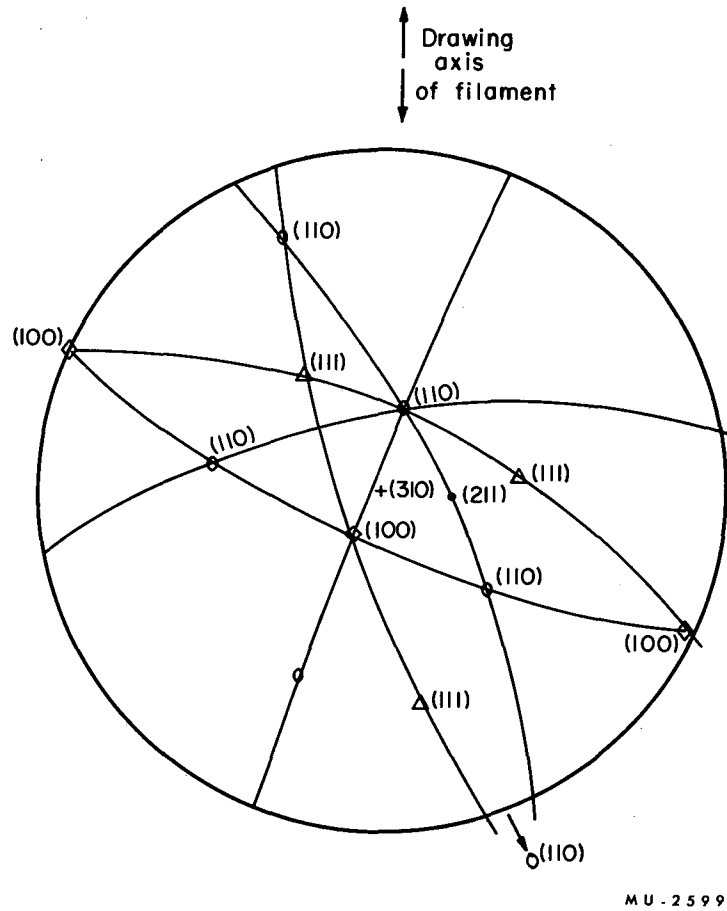
Fig. D.23-3. A stereographic projection of a "bulk" tungsten ribbon filament after heating for extended periods above 2100° K. This is sufficient proof that these filaments are not random oriented and that they would not be likely to exhibit a composite-crystal or average work function.
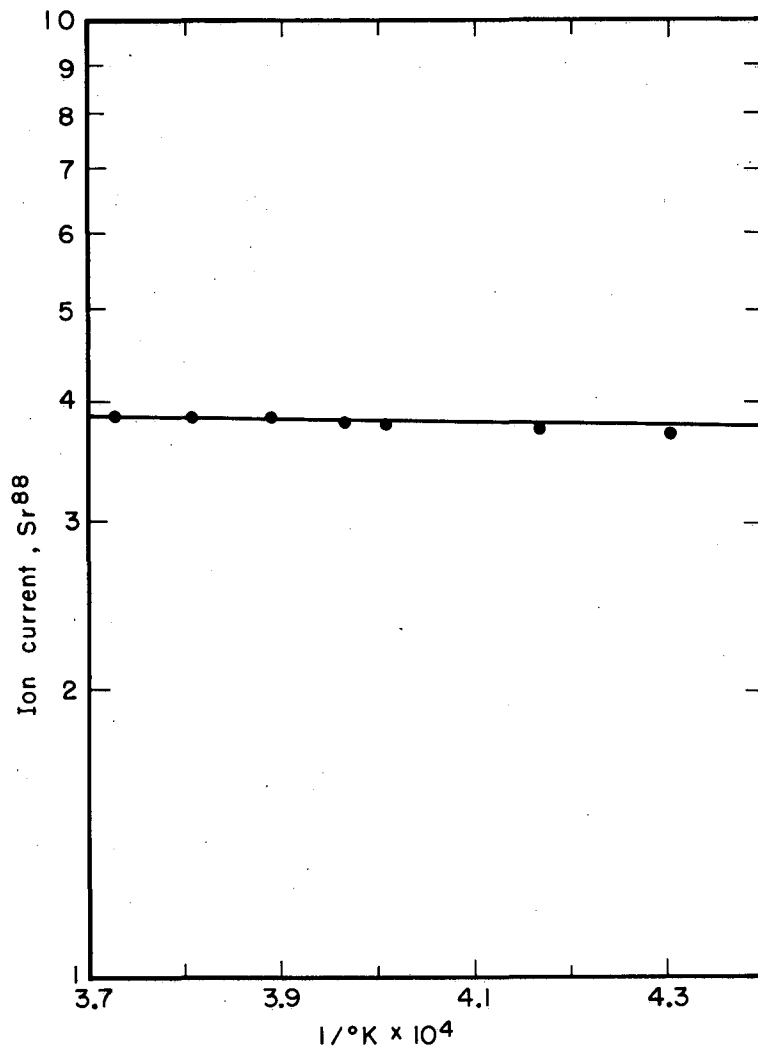
MU-25992

Fig. D.23-4. A Saha-Langmuir plot of Sr on single-crystal tungsten,
the (110) plane oriented as in Fig. D.23-1. The slight slope is due
most likely to adsorbed residual gases from the spectrometer.
This disappears with running time and with improved vacuum conditions.

E. INSTRUMENTATION

1. AN ALPHA-GAMMA COINCIDENCE RECORDING SYSTEM

D. Mosier

A system for analyzing and recording alpha-gamma coincidence information has been developed. It employs an array of ten semiconductor detectors (Fig. E.1-1) in conjunction with a double-focusing magnetic spectrometer to provide a-particle energy analysis. Gamma energies are obtained from pulse-height analysis of a NaI scintillation detector output.

Physical arrangement of the detectors is also shown in Fig. E.1-1. The system uses ten glow-transfer tube and Sodeco register scalers to record an alpha spectrum with high resolution (approx 0.1% over 1% energy range).

Amplified outputs of the alpha and gamma detectors are fed to appropriate delays and gates (see Fig. E.1-2). When an alpha-gamma coincidence occurs gates are provided to allow analysis of the gamma pulse by 100-channel "Echo" pulse-height analyzer.[1] The "Tens" and "Units" outputs of the "Echo" and the gated output of the alpha amplifiers set thirty flip-flop circuits which in turn activate thirty mercury relays. These relays provide signals to operate a Hewlett-Packard type 561A printer. This provides a record of the a-particle and γ-ray energies involved in the coincident event. Additional gates are provided on the relay outputs to allow simultaneous accumulation of the gamma spectrum in coincidence with one or more selected alpha channels. This spectrum is displayed on a 10-by-10 matrix of Sodeco registers.

Since the coincidence counting rate is limited by the printer operation, a block gate is generated which allows the printer to operate and the data circuits to be reset before acceptance of additional coincidence information.

Variation in the alpha amplifiers limit the coincidence resolving time of the system to about 3/4 μsec. Considering an alpha geometry of 0.05% and a gamma geometry of 20%, a coincidence rate of 1 per sec represents a minimum source of 6×10^5 dis/min. Under these most favorable circumstances the accidental rate is 0.75% of the true rate and the system speed of 3 coincidences per second becomes a limiting factor. In many cases shorter resolving times would be required to utilize a higher counting speed.

Using an Am^{241} a-γ (60-kev) coincidence as a standard, the coincidence efficiency of the system was found to be 100%.

Further development will include expansion to 100 alpha channels, improved resolving time, and paper tape punch output.

---

[1] R. G. Leres, Echo Pulse-Height Analyzer, UCRL-9847, Sept. 1961.
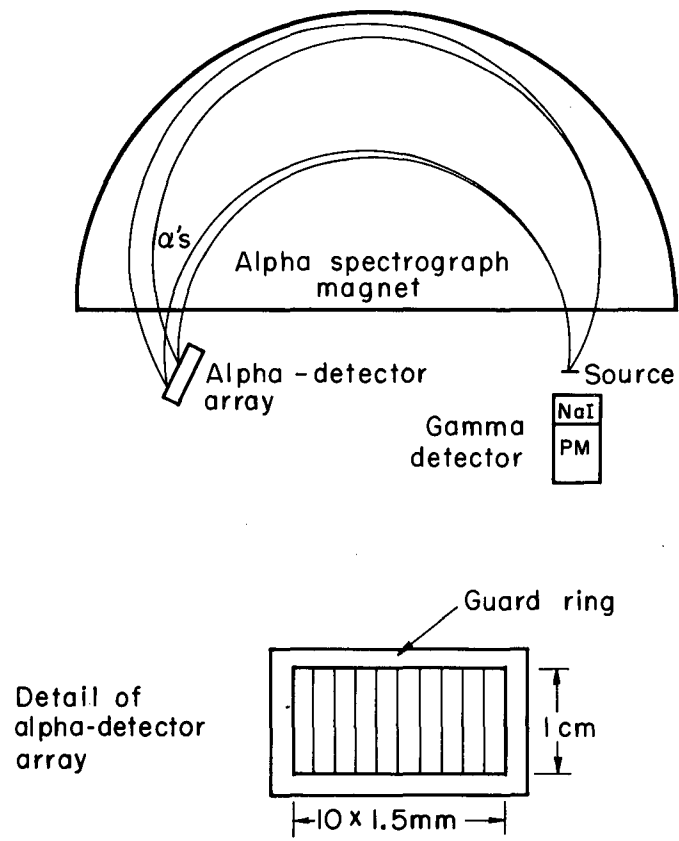
Fig. E.1-1. Arrangement of alpha-gamma coincidence system.
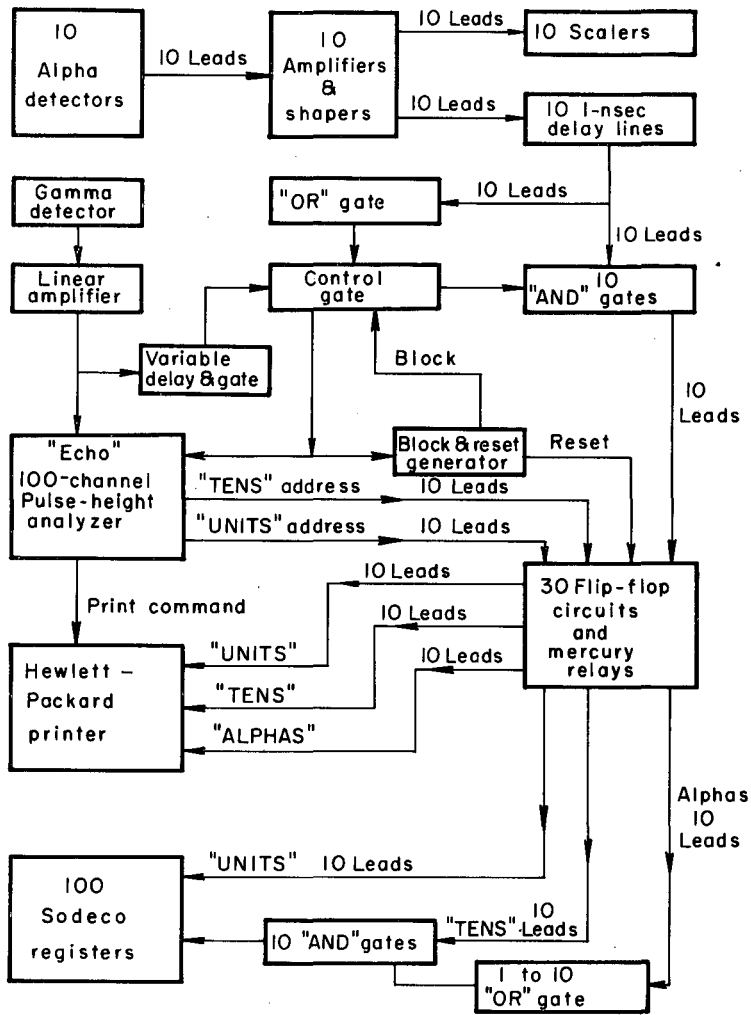
Fig. E.1-2. Block diagram of system.

Acknowledgments

2. A THIN SEMICONDUCTOR TRANSMISSION COUNTER SYSTEM FOR NUCLEAR PARTICLE DETECTION

J. H. Elliott and R. H. Pehl

The advantages of semiconductor dE/dx transmission and E counters for nuclear particle detection and identification have been shown by H. E. Wegner.[1]

Planar silicon surface barrier transmission counters as thin as 50 microns have been prepared elsewhere by lapping and etching methods.[1,2] Silicon slices are brittle and break readily when made so thin. To cope with this difficulty we lapped a hole in the center back of a 10- to 14-mil diffused-junction silicon counter to the desired thickness. This gave us a thin central region supported by a thicker outer ring where contacts could safely be made (Fig. E.2-1). Counters as thin as 30 microns have been made.

The uniformity of thickness obtained by hole lapping has not yet matched that of the lapped planar counters. The loss of resolution in the E counter due to a nonuniform-transmission counter was compensated by adding the pulses from both the dE/dx and the E counters after adjusting the ratio of the pulse heights to correspond to the ratio of energy lost in each. The passive pulse adder circuit is shown in Fig. E.2-2.

Experiments using elastically scattered α particles from the Crocker 60-inch cyclotron show that when the pulse adder is used the improvement obtained corresponds to the energy spread which was contriubted by the transmission counter.

---

[1] H. E. Wegner, Semiconductor Nuclear Particle Detectors Natl. Acad. Sci. U. S. Nuclear Sci. Sers. 32, (1961) p. 74.

[2] P. F. Andrews, Thin Silicon Surface Barrier Counters, University of Liverpool, Department of Physics Report.
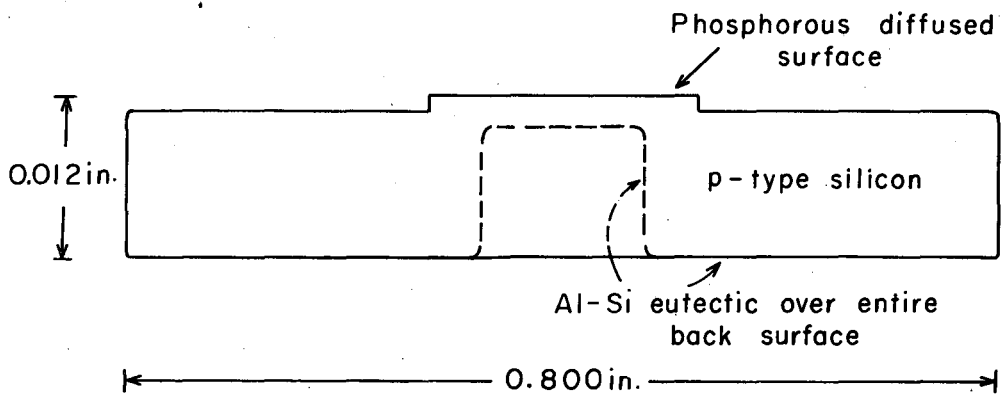
Fig. E.2-1.   Diagram of transmission counter.
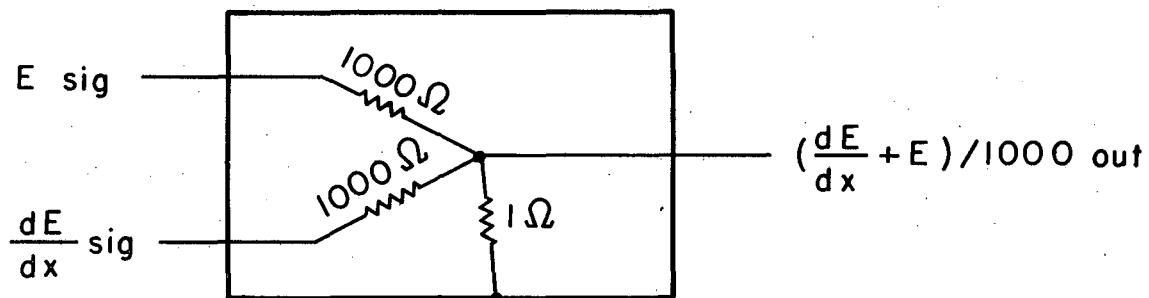
MU-25672

Fig. E.2-2. The passive pulse adder circuit.

3. THICK-JUNCTION RADIATION DETECTORS MADE BY ION DRIFT [(*)]

Jack H. Elliott

Lithium-drifted detectors with depletion thicknesses up to 3.38 mm, capable of stopping 24-Mev protons and 96-Mev α particles, have been produced. To the degree of accuracy of the experiment, the output pulse amplitude was linearly proportional to the energy absorbed in the detector, showing that the charge produced was collected with 100% efficiency. 47.6-Mev cyclotron-produced α particles were resolved to 0.9% full width at half maximum. Most if not all of this width is attributed to beam energy spread.

---

4. A FAST, SENSITIVE RADIOAUTOGRAPHIC TECHNIQUE

### R. M. Latimer, A. E. Larsh, and C. A. Corum

A fast, sensitive alpha radiographic technique has been developed by coupling a scintillation process with a high-speed photographic film process. The basic components are a ZnS screen and a Polaroid Land Camera. Individual α particles may be seen by this method.

The scintillating ZnS screen used with this technique was produced by spraying RCA 33-Z-20D ZnS phosphor on 1/3-mil pinhole-free Al. One gram of ZnS, 20 ml of Duco cement, and 80 ml of acetone were mixed in a spray gun. The ZnS is slowly sprayed on the Al until the Al is completely covered. Since the ZnS settles out rapidly, the spray gun must be shaken as it is used.

The photographic film used was Polaroid Land type 57. This film was chosen because of its high sensitivity--ASA 3000--and the ease of processing it.

The device (camera) for producing the radioautograph is shown in Fig. E.4-1. It consists of a Polaroid Land No. 500 4×5 film holder mounted in a carrier, a frame for holding the ZnS screen, and a block on which the activity can be mounted. Both the ZnS screen and the active plate are held to their respective parts with double-sided adhesive tape. When the ZnS screen is attached to its frame, it forms a lighttight shield for the film, permitting the camera to be used without a darkroom. When the camera is loaded with film, both the ZnS screen and the activity block are held away from the film by springs. During exposure, the activity and the ZnS screen are clamped tightly against the film. Accurate fiducial marks may be obtained by placing small points of activity in the corners of the activity block. To get a smoother surface on the phosphor screen, for better optical coupling to the film, the phosphor screen may be stripped from the aluminum foil. The foil and screen are then attached to the frame separately, with double-sided adhesive tape, with the smooth surface of the screen facing outward. This self-supporting scintillating screen is useful in other mounting and detecting arrangements.
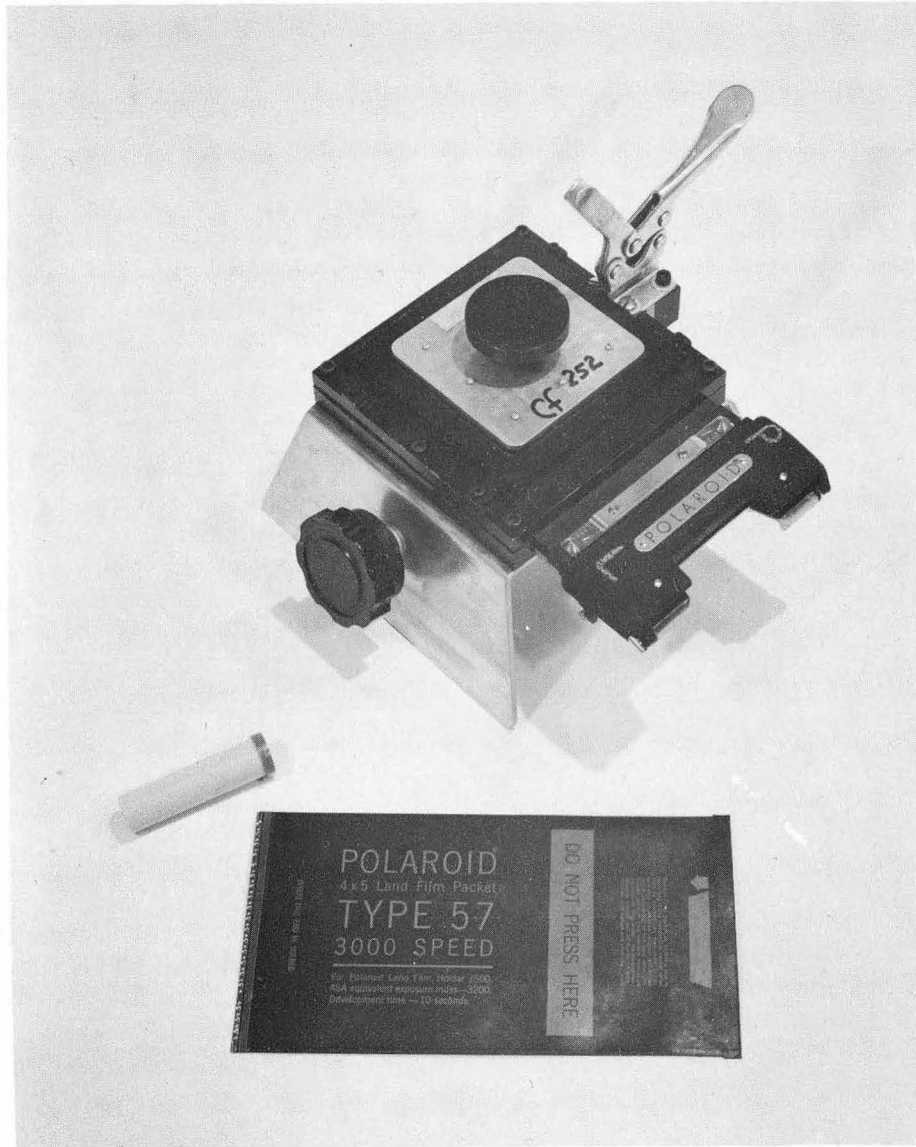
ZN-3039

Fig. E.4-1. Radioautograph camera.

A device such as ours is not necessary to use this technique. In a darkroom a Polaroid Land camera using type 47 film can be used if the activity, covered with ZnS screen, is placed at the plane of focus of the camera. In this method, the sensitivity will be lower because of the small solid angle subtended by the camera lens, and the image size may be reduced. Because the film need not be in direct contact with the scintillator, a vacuum seal may be placed between them, allowing radioautographs to be made in darkened vacuum tanks.

Another darkroom method makes use of a regular Polaroid Land camera back. The ZnS and the activity are placed directly on the film in the camera back for exposure and removed during development.

The sensitivity of the technique for α particles is high enough that individual α particles can produce images. The number (about 2/3 from a thin source) that do produce images is dependent on the thickness of the Al and the thickness and uniformity of the ZnS. The film itself is sensitive to radiation, but the use of ZnS increases its sensitivity for α particles by a factor of about 270.

Beta radiation is to a much lower extent detected directly by the film. A 2-min exposure of film against a 40-mr/hr Na^{22} source produces a barely detectable spot on the positive print. Interposing an Al-ZnS screen increases the sensitivity for beta detection by a factor of three. Plastic scintillators of the type used with photomultipliers for beta detection have a lower sensitivity increase.

Although this technique does not give the accurate energy definition of nuclear emulsions, it is to be preferred in many cases because of its ease and speed of handling.

5. AN IRON-FREE DOUBLE-FOCUSING β SPECTROMETER

K. Siegbahn, C. L. Nordling, and J. M. Hollander

An air-cored double-focusing β spectrometer for high-resolution and high-precision nuclear spectroscopy has been constructed and put into operation. Two coaxial cylindrical coils generate the magnetic field. (A cutaway view is shown in Fig. E.5-1, and data on the coils are given in the table.) The ampere-turn ratio of the coils and the geometrical dimensions have been calculated to give a two-directional focusing field of the $r^{-1/2}$ form. The deviations from the "current sheet" approximation have been taken into account in the calculations.

Calculated values of the series expansion coefficients in the vicinity of the optic circle (ρ_0 = 50 cm) are α = -0.4999, β = +0.3752, which is very close to those of an optimum field (α = -0.5000, β = +0.3750). The calculated field approximates the optimum field to within 0.01% over a distance of 3 cm on each side of the optic circle and to within 0.1% over a distance of 7 cm on each side of the optic circle. During the winding process of the coils great care was taken to achieve the coil parameters determined by the calculations,
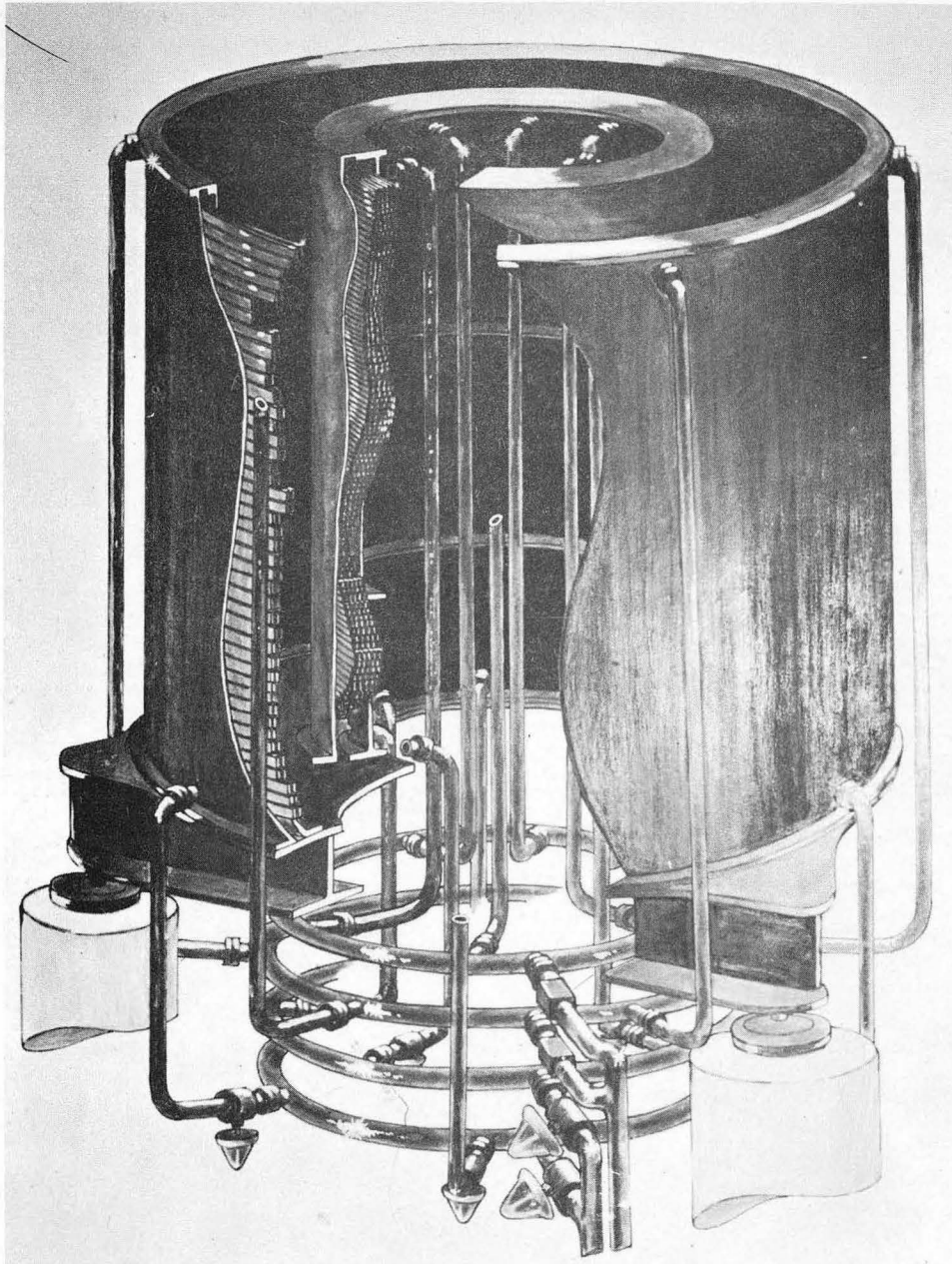
ZN-3040

Fig. E.5-1. Cutaway view of iron-free double-focusing spectrometer. The vacuum tank with source and detector arrangements is not shown. The cooling manifold has been modified.

and the height and the mean radius of each coil is within a few tenths of a millimeter from the requested values. In the preliminary tests made without any adjustments of focusing angle, etc., a resolution of 0.02% was obtained on the I line in the ThB spectrum. The maximum transmission of the spectrometer is 2%. Good access to source and detector positions has been provided. The free space between the coils is 25 cm, and the vacuum tank occupies only the active sector of $\pi \sqrt{2}$ radians, which means that the baffle, source and detector arrangements can be mounted externally. Arrangements for electron-gamma, electron-alpha, or electron-fission-fragment coincidence experiments, as well as an array of solid-state electron counters, are now being designed.

Some data for the spectrometer coils

	Outer	Inner
Number of layers	2	6
Number of turns per layer	43	103
Total number of turns	86	618
Dimensions of copper bar (mm)	20.21×3.00	7.41×4.00
Cross section area of copper bar (mm^2)	60.2	29.2
Distance between turns (mm)	1.5	1.5
" " layers (mm)	3.0	3.0
Height of coil windings (mm)	943	943
Weight of coil windings (kg)	175	355
Resistance of coil windings (Ω)	0.1	0.8
Radii of layers (mm)	647.0, 653.0	332.5, 339.5, 346.5, 353.5, 360.5, 367.5

Spectrometer current at

0.1 Mev electron energy (amp)	14	(same as for outer coil)
1.0	60	
2.0	104	
4.0	190	

A temperature change of 1°C in one of the coils (or the vacuum tank) introduces an error in the calibration of about 1 part in 10^5. Effective cooling of the coils is therefore vital to the operation of the spectrometer as a high-precision instrument. To meet the requirement for constant coil temperature each coil is enclosed in a cylindrical tank through which a coolant (Freon-11) is pumped. The coils are wound with uninsulated copper bar in direct contact with the coolant to achieve the highest possible heat transfer. In this way the mean coil temperature can be kept constant to within a few

tenths of a degree C over the whole energy range up to 4 Mev, and the temperature rise of the coolant can be kept lower than 1°C for energiesup to 2.5 Mev. At the maximum energy (4 Mev) the power consumption is 35kw. The external cooling system was designed by Eugene Miner and Luther Lucas of LRL Mechanical Engineering.

A series of 18 platinum resistor thermomenters is placed inside the coil windings to measure the temperature distribution in the coils. The ambient temperature of the instrument is kept constant by an air-conditioning system in the spectrometer room.

Electrical power to the spectrometer coils is delivered by a semiconductor rectifier system which gives a current stable to 1 part in 10^5. The electron spectrum can be scanned automatically from a preset starting current in steps ranging from 0.1 ma to 1 a and with counting times ranging from 10 sec to 32 min for each current setting. Precision shunts give seven current ranges from 1 to 170 amp, and the shunts are immersed in the coolant of the spectrometer coils for temperature constancy. The actual current setting is read to seven figures (0.1 ma) on a display panel. An IBM typewriter prints the data: spectrometer current, time of day, counting time, registered counts. The system can easily be adapted for further automation with punch-card readout for data processing, etc.

The automatic current control and printout system was designed by Ivan Lutz and Paul Slaz of LRL Electronics.

Because of the iron-free construction of the spectrometer and the high precision aimed at, it is necessary to eliminate all external magnetic fields and keep the environment free from ferromagnetic materials. Therefore a special laboratory building has been constructed to house the spectrometer. This building has been located far away (about half a mile) from the big accelerators which produce high magnetic stray fields. No ferromagnetic materials are used in the building construction, and all iron-containing equipment, such as rotary vacuum pumps, air-conditioning equipment, transformers, compressors, etc., are located in a specially built utility shelter at a distance of some 100 feet. The external field that remains to be eliminated is mainly the earth's magnetic field, which is essentially homogeneous over the volume occupied by the spectrometer. A system of eight circular coils diameter 20 feet) surrounding the instrument gives a "degaussing" field which is nearly homogeneous over the required volume. Over a radial distance of 10 cm around the central electron orbit the residual magnetic field is kept below 10^{-4} gauss, which is well within tolerable limits.

F. CHEMICAL ENGINEERING

1. DIFFUSION IN THREE-COMPONENT GASES

Richard W. Getzinger and C. R. Wilke

In ideal gases diffusion is usually described by the Stefan-Maxwell equations,[1,2] which may be written, for unidirectional diffusion, in the form

$$\frac{dy_i}{dz} = \sum_{\substack{j=1 \\ j \neq i}}^{n} \frac{1}{cD_{ij}} (y_i N_j - y_j N_i) , \qquad (1)$$

where y = mol fraction of a component,

z = distance in direction of diffusion (cm),

c = total concentration of species in the mixture (mols/cc),

N = flux of a component (mols/cc^2-sec),

D_{ij} = binary diffusion coefficient for components i and j (cm^2/sec).

A number of methods have been proposed for numerical solution of the Stefan-Maxwell equations. Gilliland[3] and Toor[4] have integrated the equations for some cases of three-component diffusion. Empirical methods covering more general situations have been proposed by Wilke,[5] Toor,[4] and Shain.[6]

Since the Stefan-Maxwell equations readily can be solved numerically with computers or by empirical methods when applicable, further experimental verification of their validity is of considerable interest. The experiments presented here were concerned with a case that had not heretofore been tested experimentally--namely, simultaneous diffusion of two components through a third stagnant component under conditions such that the diffusion of one component has an appreciable effect on the diffusion of the other. Measurements were made by evaporation of liquids from a tube into an air stream, using the technique of Stefan.[7] The apparatus is illustrated in Fig. F. 1-1. In this method the two components of the liquid exert their respective equilibrium partial pressures at the gas-liquid interface located at some depth inside the tube. The air stream passing over the tube contains none of the vapors, so

[1] J. Stefan, Sitzber. Akad. Wiss. Wien 63 (II), 63 (1871).

[2] J. C. Maxwell, Scientific Papers, Vol. 2 (Cambridge University Press, Cambridge, England, 1890), p. 57.

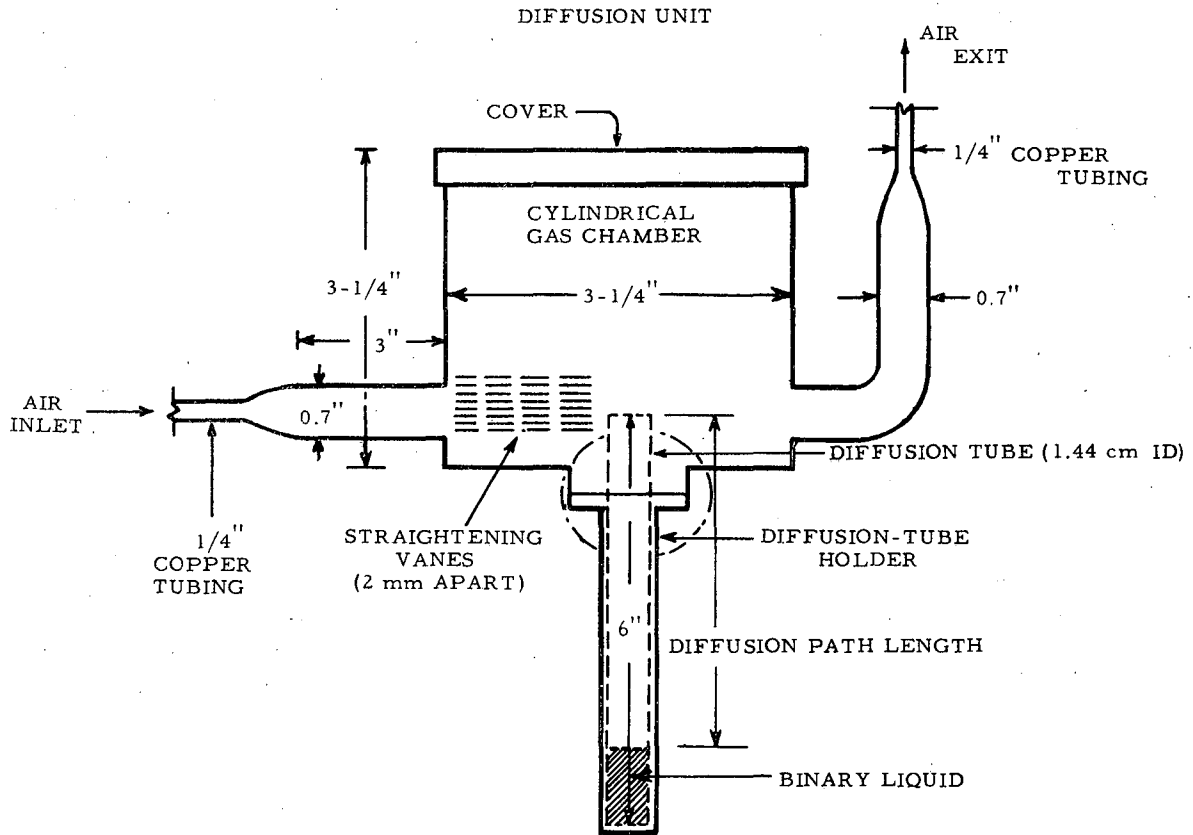[3] T. K. Sherwood, Absorption and Extraction (McGraw-Hill Book Co., Inc., New York, 1937), p. 11.

[4] H. L. Toor, A. I. Ch. E. Journal 3, 198 (1957).

[5] C. R. Wilke, Chem. Eng. Progr. 46, 95 (1950).

[6] Stephen A. Shain, A. I. Ch. E. Journal 7, 17 (1961).

[7] C. Y. Lee and C. R. Wilke, Ind. Eng. Chem. 46, 2381 (1954).

Fig. F.1-1. Diffusion tube apparatus.

MUB-701

that the partial pressures of the diffusing components are effectively zero at the open upper end of the tube. Concentration gradients are therefore established over the vapor space in the tube, and diffusion proceeds in a quasi-steady-state manner. The two components of the liquid diffuse in parallel at rates which depend on their concentration gradients, diffusion coefficients, and length of the diffusion path. To eliminate any mass-transfer resistance in the liquid phase, mixture compositions were selected for which the relative diffusion rates of the vapors corresponded to their concentrations in the liquid. From evaporation measurements on the pure liquid components, the binary diffusion coefficients of the vapors into air were determined, and the end-effect corrections to the diffusion path length in the tube were established.[7] The total weight of liquid evaporated during the experiment was obtained by weighing the diffusion tube. The amount of each component that evaporated was determined by analysis of the liquid.

From knowledge of the various binary diffusion coefficients and vapor pressures, the diffusion rates of the components could be calculated by various solutions to the Stefan-Maxwell equations and compared with the measured values. Results are given in Tables I and II for diffusion of methanol-benzene and ethanol-chloroform mixtures into air. Agreement between experimental quantities of the components evaporated and corresponding values predicted by Gilliland's exact solution[3] of the Stefan-Maxwell equations for these cases is considered satisfactory and within limits of experimental errors. It is believed that these results constitute experimental verification of the correctness of the Stefan-Maxwell equations under more stringent conditions than have been employed previously. These results in addition to earlier results for diffusion in stagnant gas mixtures[8] lend support to the general application of the equations to more complex cases of gas diffusion.

---

[8] D. F. Fairbanks and C. R. Wilke, Ind. Eng. Chem. **42**, 471 (1950).

Table I. Experimental conditions for diffusion of two vapors through air

	Ethanol (A) - chloroform (B)	Mathanol (A)- benzene (B)
Temperature ($^\circ$C)	35	35
Evaporation period (min)	985	921
Length of diffusion path (cm)	12.19	13.62
Diameter of diffusion tube (cm)	1.44	1.44
Total pressure (mm)	756	756
Average mol fraction of A in liquid	0.121	0.648
Vapor pressure of A over the liquid (mm)	32.2	170.1
Vapor pressure of B over the liquid (mm)	272.5	122.4
D for A in B (cm^2/sec)	0.0661	0.0904
D for A in air (cm^2/sec)	0.152	0.198
D for B in air (cm^2/sec)	0.106	0.110

Table II. Comparison of experimental and calculated evaporation results

Source (and reference)	Ethanol (A) -chloroform (B)			Methanol (A) - benzene (B)		
	Mols A evap. $\times 10^2$	Mols B evap. $\times 10^2$	Total mols evap. $\times 10^2$	Mols A evap. $\times 10^2$	Mols B evap. $\times 10^2$	Total mols evap. $\times 10^2$
Experimental	0.202	1.47	1.67	1.19	0.65	1.84
Exact solution of Stefan-Maxwell equations (3)	0.216	1.47	1.68	1.28	0.62	1.90
Method 2 of Wilke (5)	0.222	1.51	1.73	1.29	0.62	1.91
Method of Toor (4)	0.249	1.45	1.70	1.39	0.56	1.95
Method of Shain (6)	0.222	1.47	1.69	1.29	0.62	1.91

2. LONGITUDINAL DISPERSION IN PACKED GAS-ABSORPTION COLUMNS

T. T. Word, W. E. Dunn, C. R. Wilke, and T. Vermeulen

When a fluid of changing concentration passes through a packed bed, longitudinal dispersion or mixing tends to reduce the concentration gradient in the axial direction. This effect becomes more pronounced in two-phase countercurrent systems, where the driving force for mass transfer may be decreased considerably. Miyauchi and co-workers, in reports from this Laboratory,[1] have shown how HTU and NTU may vary with the Peclet number for longitudinal dispersion, in countercurrent systems such as extraction and adsorption columns.

In order to study longitudinal mixing on both phases in representative gas-liquid absorption conditions, apparatus developed by R. S. Brown was modified by the construction of a cylindrical column 2 feet in inside diameter, with a packed section 6 feet high.[2] The design and construction of this column have been given in a separate report.[3]

---

[1] Terukatsu Miyauchi, Longitudinal Dispersion in Solvent-Extraction Columns, UCRL-3911, Aug. 1957; Alice K. McMullen, Terukatzu Miyauchi and Theodore Vermeulen, Numerical Tables. UCRL-3911 Suppl., Jan. 1958.

[2] Robert S. Brown, Bubbling from Perforated Plates (Ph. D. Thesis), UCRL-8558, Dec. 1958.

[3] Tracy T. Word, Longitudinal Dispersion in Packed Gas-Adsorption Columns (M. S. Thesis), UCRL-9844, Sept. 1961.

The flow arrangement used is shown in Fig. F. 2-1. The column con-
struction makes it possible to change the packing material easily. To avoid
end effects, the tracer components (sodium nitrate solution and helium) are
injected within the bed, and also sampled within the bed. Design and con-
struction of column fittings and instrumentation to provide for injection into
and sampling of the two phases have been given major attention.

All runs to date have been made with 1-inch Raschig-rings. Prelim-
inary experimental results indicate that gas-phase axial dispersion is not
affected much by the liquid flow and consequently that the dispersion coef-
ficient has relatively low values. For the liquid phase, however, dispersion
rates are large and may prove to be an important factor in absorber design;
the data taken to date are scattered owing perhaps to the erraticness of
liquid flow through an absorber, and may require statistical analysis in the
course of their interpretation and correlation.

3. DISPERSION BEHAVIOR IN AGITATED LIQUID-LIQUID SYSTEMS [*]

L. H. Weiss and T. Vermeulen

The need to keep two phases rather completely intersuspended, and to
avoid regions of dead space in the regions of a mixing vessel most distant
from the impeller, is often a crucial objective of agitation. The most common
method of measuring bulk homogeneity is to draw samples from several
points in a vessel, and to compare their compositions with the overall prop-
ortions known to be present. For such data, a "mixing index" can be calcu-
lated for each measurement and then averaged to define empirically the
vessel as a whole. In this study, it has proved desirable to replace a single
mixing-index criterion by two separate characterization factors; first, the
distribution of dispersed phase within the continuous phase; and, second, the
size of the "stagnant layer" of dispersible phase that remains undispersed.

In baffled tanks, the volume fraction of dispersed phase at any one
height is sufficiently constant so that an average value for that height can be
used, which is designated by ϕ_s. A factor $\underline{\kappa}$ can then be used in an ex-
ponential distribution function of the form

$$\phi_s = \phi_B \cdot \exp\left[-\kappa(h-h_B)\right] .$$

Here ϕ_B is the volume fraction of dispersed phase in the mixture that is en-
countered at the boundary between the mixture and the undispersed part of
the dispersible phase; h is the height in the tank measured from the dispers-
ible-phase end, divided by total liquid height (that is, a fractional height);
h_B is the value of this fractional height at the boundary between unmixed and
mixed phases; and κ is an inhomogeneity factor varying between zero and
infinity.
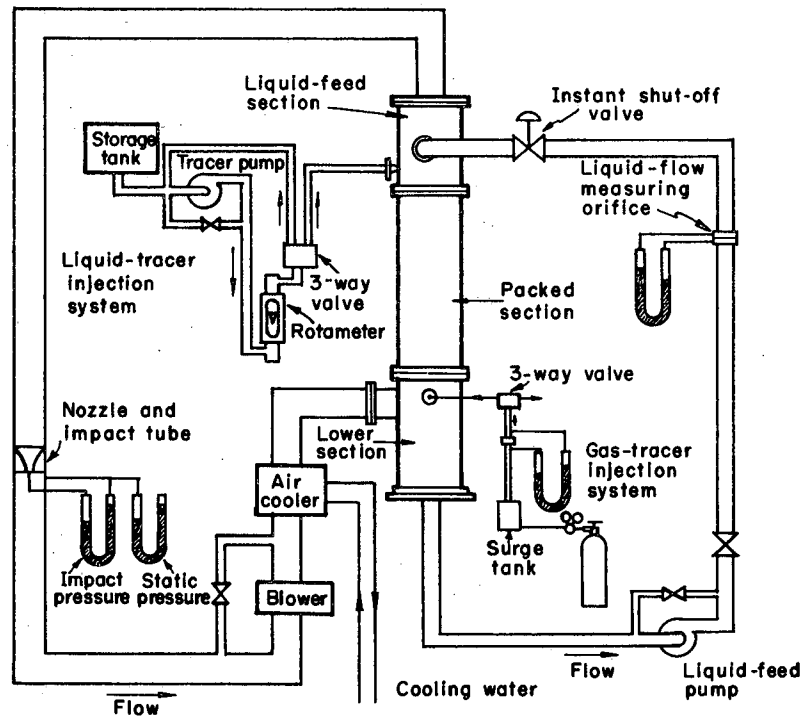
MU — 24348

Fig. F.2-1. Flow diagram for absorption system, incorporating the test column.

Experiments have been made to measure the variation in ϕ_s as a function of h, for various systems, overall volume fractions, and mixing conditions. The resulting values of κ have been correlated by

$$\kappa = 48 \left[\left(\frac{N^2 L^3 \rho_c}{d_p \, g \, (1-\phi) \, \Delta\mu} \right)^3 \left(\frac{N \, L \, d_p \rho_c}{\mu_c} \right) \left(\frac{LW}{TH} \right)^{3/2} \right]^{-1/4} .$$

Figure F.3-1. is a plot of this relation, showing experimental points. The geometrical factor LW/TH is the ratio of cross-sectional area swept out by the impeller to the total cross-sectional area of the vessel.

The fractional height for the boundary between unmixed and mixed phases has been correlated separately by Fig. F.3-2, which corresponds to the relation

$$h_B = -0.34 \, \log_{10} \left\{ \left(\frac{N^2 L^2 \rho_c}{g \, (1-\phi) \, \Delta\rho} \right) \left(\frac{LW}{TH} \right)^2 (\overline{\phi})^{-4/3} \right\} - 0.58,$$

with the obvious limitation of $\overline{\phi} \geqslant h_B \geqslant 0$. A criterion for complete bulk dispersion is therefore obtained by setting the argument of the logarithm (that is, the abscissa in Fig. F.3-2) equal to 0.020.

4. DEVELOPMENT OF DESIGN METHODS
FOR PACKED-COLUMN SOLVENT EXTRACTION

T. Vermeulen, N. N. Li, J. S. Moon, and T. Miyauchi

Five recorrelated design factors for liquid-liquid extraction columns provide an improved basis for design and scale-up. These factors are holdup of dispersed phase, flooding limits, mass-transfer coefficients, effective interfacial area, and longitudinal dispersion.

The new relations are expressed in terms of those dimensionless groups whose use is indicated by theoretical analysis, coupled with the existing experimental data and dimensional correlations. Several distinct design conditions are encountered, depending upon whether the continuous or the dispersed phase wets the pakcing, and whether or not the mass transfer is accompanied by interfacial turbulence. The study has dealt particularly with continuous-phase behavior, when this phase is wetting, in the absence of interfacial turbulence.

total holdup (X_t) is found to follow the relation

$$X_t = \frac{A \, \sigma}{d_p^2 \, g \, \Delta\rho} + \frac{B \, U_d}{d_p} \left(\frac{\mu_c \, \rho_c}{(g \, \Delta\rho)^2} \right)^{1/3} \left[1 + \frac{C U_c^2 \, \rho_c}{d_p \, g \Delta\rho} \right] . \qquad (1)$$
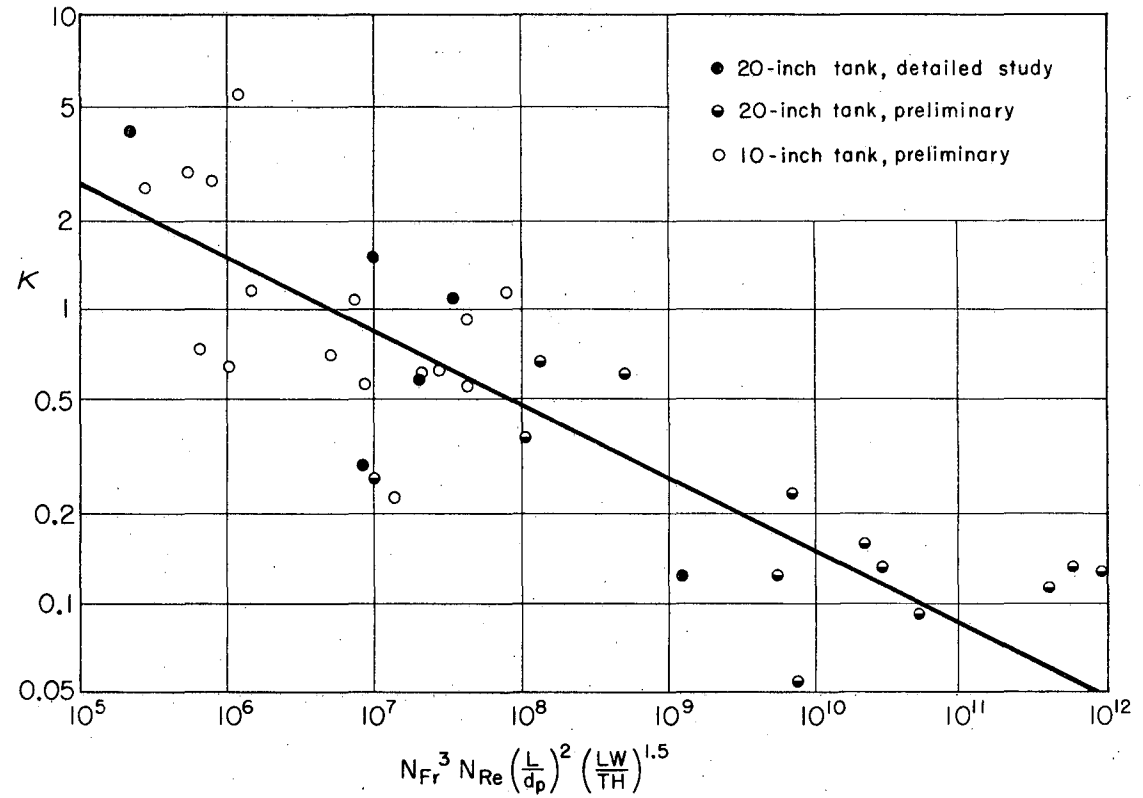
Fig. F.3-1. Dependence of inhomogeneity parameter κ upon mixing conditions.

$$N_{Fr} \left(\frac{LW}{TH}\right)^2 \left(\frac{}{P}\right)^{-4/3}$$

MU-23977
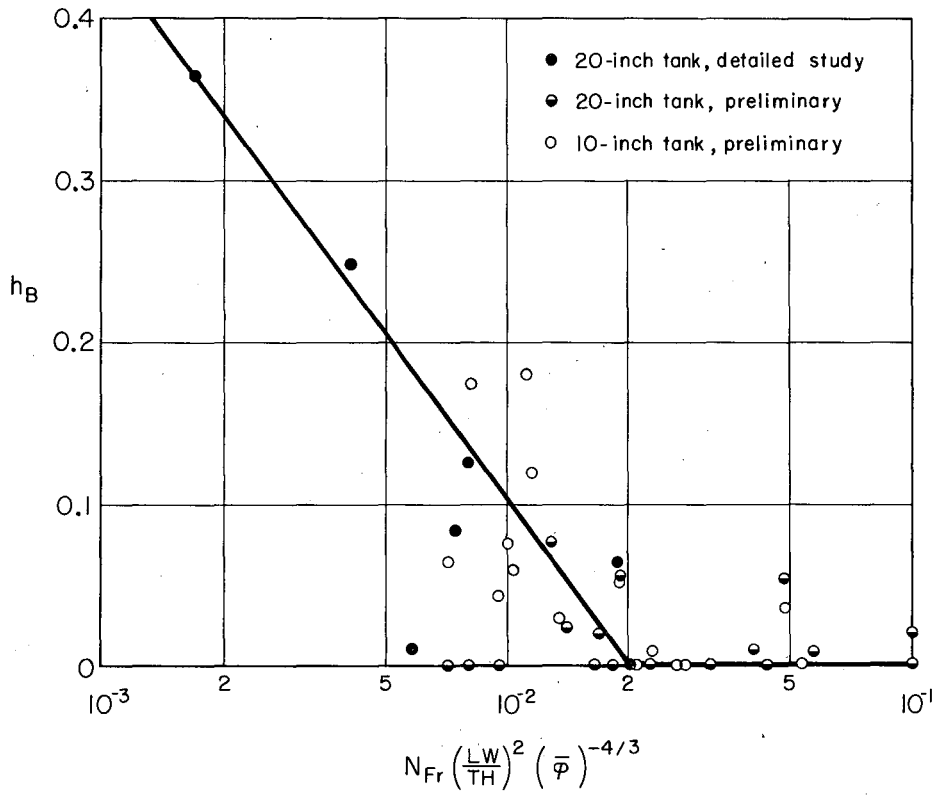
Fig. F.3-2. Dependence of height of undispersed second phase upon mixing conditions.

Here d_p is effective packing diameters; σ, interfacial tension; g, gravitational acceleration; ρ, denisty; μ, viscosity; and U, superficial velcocity. Subscripts c and d indicate respectively the continuous and dispersed phases. For Raschig rings, the constants are A = 1.14, B = 0.0040, C = 0.0012.

Flooding velocity can be correlated in terms of an effective total velocity, used, for example by Wilke, Breckenfeld, and Crawford,[1,2]

$$U_{eff} = (U_c^{0.5} + U_d^{0.5})^2 .$$ (2)

The correlation then takes the form

$$\left(\frac{U_{eff}\, a_v^{0.5}}{g^{0.5}}\right)\left(\frac{\mu^2\, a_v^3}{g\, \rho_c}\right)^{0.1} \left(\frac{\sigma\, a_v^2}{g\, \rho_c}\right)^{0.2} \left(\frac{\rho_c}{\Delta\rho}\right)^{01.6} \left(\frac{\rho_d}{\Delta\rho}\right)^{0.3} \frac{1}{\epsilon^{1.5}} = \text{const},$$ (3)

where a_v is particle surface area per unit packed volume, or $6(1-\epsilon/d_p)$; and ϵ is the void fraction.

The continuous-phase mass-transfer coefficient can be predicted from the experimental correlation of Gaffney and Drew.[3] In this correlation, the mean diameter of the dispersed-phase droplets is estimated from Gayler and Pratt's results,[4]

$$d_{drop} = 1.00 \left(\frac{\sigma}{\Delta\rho \cdot g}\right)^{1/2} (1.0 + 700\, \frac{U_c\, \mu_c}{\sigma} .$$ (4)

The continuous-phase HTU ($= H_c$), calculated in terms of the superficial velocity of this phase referred to the packing, must be corrected to reflect the relative linear velocity of the two liquids, through a factor suggested by Gayler and co-workers[5] for correlations of holdup; here, then,

$$H_c \propto \left(\frac{1}{1-X_t} + \frac{U_d}{X_f\, U_c}\right)^{0.42} ,$$ (5)

where the free holdup, X_f, is given by the second of the two terms on the right-hand side of Eq. (1).

[1] R.R. Breckenfeld, and C.R. Wilke, Chem. Eng. Prog. 46, 187 (1950).

[2] J.W. Crawford, and C.R. Wilke, ibid. 47, 423 (1951).

[3] B.J. Gaffney, and T.B. Drew, Ind. Eng. Chem. 42, 1120 (1950).

[4] R. Gayler, and H.R.C. Pratt, Trans. Inst. Chem. Engrs. (London) 31, 69 (1953).

[5] R. Gayler, N.W. Roberts, and H.R.C. Pratt, ibid. 31, 57 (1953).

Correction for the effects of longitudinal dispersion should be made by the methods of Miyauchi et al.,[6] using data of the type obtained by Jacques and co-workers.[7] In two representative numerical cases so far examined, encouraging agreement has been obtained between these predictions and the actual performance of the columns.

The results presented above were the subject of an invitational paper at the New Orleans meeting of the American Institute of Chemical Engineers in February 1961. Study of these methods is being continued, with a view to preparation of a comprehensive report.

---

[6]Terukatsu Miyauchi, Longitudinal Dispersion in Solvent-Extraction Columns, UCRL-3911, Aug. 1957; Alice K. McMullen, Terukatzu Miyauchi, and Theodore Vermuelen,Numerical Tables, UCRL-3911 Suppl., Jan. 1958.

[7]G. L. Jacques, J. E. Cotter, and T. Vermeulen, Longitudinal Dispersion in Packed Extraction Columns, UCRL-8658, April 1959.

5. DOWNFLOW FORCED-CONVECTION BOILING OF WATER IN A SINGLE UNIFORMLY HEATED TUBE [*]

Roger M. Wright, Robert L. Sani,
Graham Somerville, and LeRoy A. Bromley

There has been very little work published on the mechanisms and methods for the prediction of heat-transfer performance in the field of forced-convection boiling. Despite the large amount of experimental data obtained the complexity of the fluid-dynamic phenomena and the many ways in which boiling can occur has prohibited obtaining a general correlation for the prediction of boiling heat transfer coefficients. This work is an attempt to experimentally measure heat transfer coefficients and pressure drops in a down-flow single-tube evaporator and to correlate them with the flow variables of the system and the physical properties of the fluid.

Earlier experimenters,[1,2,3] the majority using water as a fluid, have attempted to correlate their results for forced-convection boiling to those obtained for nonboiling heat transfer, and have expressed their results in the form

---

[*]Work summarized by Roger M. Wright,Downflow Forced Convection Boiling of Water in Uniformly Heated Tubes (Thesis), UCRL-9744, Aug. 1961.

[1]C. E. Dengler and J. N. Addoms, Chem Eng. Progr. Symposium Ser. 52, No. 18, 95 (1956).

[2]S. A. Guerriere and R. D. Taity, Chem. Eng. Progr. Symposium Ser. 52, No. 18, 69 (1956).

[3]V. E. Schrock and L. M. Grossman, Univ. of California Inst. of Engr. Research (Berkeley), Series No. 73308-UCX 2082, Issue No. 2, November 1, 1959.

$$\frac{h_B}{h_0} = A\, x_{tt}^{-B},\qquad(1)$$

where h_B = heat transfer coefficient for boiling,

h_0 = heat transfer coefficient for nonboiling heat transfer,

x_{tt} = Lockhart-Martinelli parameter, [4]

$$x_{tt} = \left[\frac{\rho_g}{\rho_f}\right]^{0.5}\left[\frac{\mu_f}{\mu_g}\right]^{0.1}\left[\frac{1-x}{x}\right]^{0.9},$$

x = vapor quality,

and A and B are constants whose experimental values are suggested as

$$2.5 < A < 3.5,$$
$$0.45 < B < 0.75.$$

Mumm[5] has suggested a correlation of the form

$$Nu_B = \left[4.3 + 5\times10^{-4}\left(\frac{V_g - V_1}{V_1}\right)^{1.64}\times\right]\left[B_0\right]^{0.464}\left[Re_1\right]^{0.808},\qquad(2)$$

while Schrock and Grossman[3] have used

$$Nu_B = \left[Re_1\right]^{0.8}\left[Pr\right]^{0.33}\left[1.7\times10^{+2}\,(B_0 + 1.5\times10^{-4}\left\{x_{tt}\right\}^{-0.67})\right],\qquad(3)$$

where Nu_B = Nussult number for boiling heat transfer,

V = specific volume,

B_0 = boiling number $\dfrac{q}{G(H_g - h_1)}$,

and H, h = enthalpies.

The standard deviation in the correlated experiments of the former was ±10%, while that of the latter was ±35%.

The experimental system in the investigation presented here consisted of a semiclosed loop. Distilled water was pumped through two preheaters and flashed prior to entering the test section. This provided a range of entering vapor fractions. The test sections, made of thin-walled stainless steel

---

[4] R. W. Lockhart and R. C. Martinelli, Chem. Eng. Progr. 45, 39 (1949).

[5] J. F. Mumm, Heat Transfer to Boiling Water Forced Through a Uniformly Heated Tube, Argonne National Laboratory Report ANL-5276, Nov. 1954.

tubes, were electrically heated and fitted with pressure taps and thermo-
couples. The two-phase mixture was separated in a cyclone and the products
cooled and returned to storage. Pressures were measured with a pressure
transducer sensitive to pressure of 0.4 psia. The test sections used were
0.710 and 0.472 in. i.d. with lengths of 5.67 and 4.69 ft respectively. The
flow variables covered the ranges

mass flux	(G)	110 to 700	lb m/ft^2-sec,
heat flux	(q)	13800 to 88000	BTU/hr-ft^2,
vapor quality	(x)	0 to 19%,	
pressures		15.8 to 68.2 psia.	

The mass-vapor fraction at any location in the test section was evaluat-
ed from an overall energy balance between a reference point (before the flash
valve) and the location in question. From a knowledge of quality, wall temp-
erature, saturated liquid pressure, and heat flux the local heat transfer co-
efficients were evaluated for the entire length of the test section. All runs
indicated the following general behavior: local heat-transfer coefficients at
the inlet are large, decrease to a minimum, and finally rise steadily to the
tube outlet, thus showing the presence of thermal entrance effects.

The present data compare favorably with the initial Schrock and Grossman
correlation (Eq. 1).

Experimental values of constants A and B in Equation (1):

	A	B
Dengler and Addoms	2.5	0.5
Schrock and Grossman	2.5	0.75
This investigation	2.75	0.581

When the boiling data were compared with the correlation of Mumm[5] (Eq.2),
a definite trend was indicated but the overall scatter was very large.

Our data are correlated well by Schrock and Grossmans most recent
correlation (Eq. 3),[3] except that the numerical coefficient found by us is 320
instead of the 170 reported by them. This discrepancy may reflect the fact
that their data were taken at high pressures (up to 500 psia) whereas our data
were taken at moderate pressures. The boiling number, which can be con-
sidered to be the ratio of the mass flux normal to the wall due to boiling
$\left(\dfrac{q}{H_g - h_e}\right)$ to the total mass flow flux (G), does not appear to adequately de-
scribe the pressure dependence. A modified boiling number based on the
ratio of the volumetric flux rates appear to account for some of the observed
pressure dependence.

It has been observed that the heat flux (q) is a significant parameter, and simple calculations have shown a dependence of $q^{0.3}$. A study was made to examine the dependency of the heat-transfer coefficient on flow variables, and the dependence of G, q, and x has been determined adequately for the range covered by these experiments. Correlations of the form

$$h_B \approx G^{0.6} q^{0.3} x^{0.4}$$

have been found successful in correlating the data. However the range over which these variables were investigated limits the advancing of a general correlation for design. Also, because of the small change in the physical properties of the fluid investigated, no dependency on physical properties of the fluid has been introduced.

6. SIMULTANEOUS SOLUTION OF VOLTAGE AND MASS BALANCES IN ELECTROLYTIC CELLS [*]

Edward A. Grens, II, and Charles W. Tobias

Rational design and operation of electrolytic cells require the ability to predict the performance of the cell from a knowledge of parameters characterizing cell operation. These operating parameters are independent variables whose levels are established by the cell operator or fixed by cell environment. Frequently conditions of electrolysis vary from point to point within the cell owing to the effect of electrode reactions on the properties of the electrolyte and on the electrodes themselves. In situations of this nautre the performance of the cell is related to operating parameters by a group of interacting phenomena described mathematically by a set of simultaneous differential expressions, which in general are nonlinear. Usually no explicit relationships for variables describing cell performance in terms of cell operating parameters can be obtained.

For many electrolytic processes, theoretical or empirical relationships are available expressing various aspects of performance at some point in the cell in terms of the conditions existing at that point. These relations, together with a description of the effects of local performance throughout the cell on conditions existing at various points in the cell, permit over-all cell performance to be determined for any given values of the operating parameters.

Example of Application

To illustrate the application of this technique an idealized electrolytic cell based on a Krebs-type caustic-chlorine cell with flowing mercury cathode was considered. This model is described in detail in an earlier report.[1] The following basic assumptions are incorporated in the definition of this model:

[*] Based on article of same title, J. Electrochem. Soc. **108**, 1063 (1961).

[1] E. A. Grens, Analysis of Current Distribution in Electrolytic Cells with Flowing Mercury Cathodes (M.S. Thesis), UCRL-9187, July 1960.

a.   The amalgam flow is turbulent, with complete cross mixing and a negligible diffusion boundary layer (see Ref. 1, p. 14).

b.   The brine flow is turbulent, with a diffusion boundary layer at the cathode (see Ref. 2).

c.   The cell is isothermal at $65^\circ C$.

d.   Distribution of evolved gas is independent of flow rates.

e.   No appreciable ClO_3 is formed.

f.   Current loss is 4% owing to recombination of dissolved Cl_2 with sodium amalgam at the cathode.[1]

g.   There is no significant overvoltage for the primary cathode reaction.

h.   Electrolyte pH is 4.

i.   Current flow is independent of position in the direction normal to the electrode surfaces.

Although this model does not represent any actual cell, it incorporates certain salient features of industrial mercury cells.

In the analysis of this model the operating parameters are (a) anode type, (b) applied cell potential, (c) brine flow rate, (d) amalgam velocity, (e) inlet concentration of Na in amalgam, and (g) distance between the electrodes. These variables may be established arbitrarily by the designer or operator of the cell.

The variables describing cell performance which are determined by the values of the operating parameters are (a) current density (local and average), (b) concentration of NaCl in brine at any point, (c) concentration of Na in amalgam at any point, (d) anode potential, cathode potential, and ohmic potential drop in brine (local and average).

Voltage Balance

The total potential of the cell is composed of the anode potential ($-E_A$), the cathode potential (E_C), and the ohmic potential drop in the electrolyte (E_R):

$$E_T = -E_A + E_R + E_C . \tag{1}$$

Based on theoretical and empirical relationships, values of these component potentials are expressed in terms of local conditions at any point along the length of the cell. Empirical data are derived from Okada et al.,[3,4] and are represented in the form of second-order power series expansions by regression analysis. Thus, for anode potential,

[2] C. W. Tobias, M. Eisenberg, and C.R. Wilke, J. Electrochem. Soc. 99, 359 (1952).

[3] S. Okada, S. Yoshiyawa, F. Hine, and Z. Takehara, J. Electrochem. Soc. Japan (O.E), 26, (4-6), E 66 (1958).

[4] S. Okada, So. Yoshiyawa, F. Hine, and Z. Takehara, ibid. 26, (4-6), E 66 (1958).

$$-E_A = -E_A^O + \frac{RT}{F} \ln \frac{a_{Cl}}{a_\pm} + \omega = -\frac{RT}{F} \ln \frac{a_\pm}{a_{\pm\,sat}} + a + \beta I + \gamma I^2 \; ; \tag{2}$$

for cathode potential,

$$E_C = E_C^O - \frac{RT}{F} \ln \frac{a_\pm}{a_{NaHg}} \; ; \tag{3}$$

and for the ohmic potential drop in the electrolyte,

$$E_R = \frac{Id}{k_m} = \frac{Id}{k_e \left[\lambda + \mu \, (\ln I) + \xi \, (\ln I)^2 \right]} \; . \tag{4}$$

The activities are represented in terms of concentration as

$$a_\pm = 1.84 - 0.281m + 0.152m^2 \tag{5}$$

           (see Ref. 1)

and

$$\ln a_{NaHg} = 1.26 \ln N - 1.31 \quad \text{for } 0 \leqslant N \leqslant 0.25\%, \tag{6}$$

           (see Ref. 1)

and the pure brine conductivity is related to concentration by

$$k_e = -0.093 + 0.161m - 0.0114m^2 \quad \text{for } 4.5 \leqslant m \leqslant 6.43. \tag{7}$$

Combining Eqs. (1), (2), (3), and (4), the voltage balance for the cell becomes (with values of $a_{\pm(sat)}$)

$$\gamma I^2 + \beta + \left\{ \frac{d}{k_e \left[\lambda + \mu \, (\ln I) + \xi \, (\ln I)^2 \right]} \right\} \; I$$

$$+ \; 0.0537 + a + E_C^O - E_T + \frac{RT}{F} \ln \frac{a_{NaHg}}{a_\pm^2} = 0. \tag{8}$$

For given concentrations of brine and amalgam, current density may thus be found.

Material Balances

In order to determine concentrations at any point in the cell, an increment of length of cell Δx in the direction of brine and amalgam flow is considered. Then the changes in brine and amalgam concentration over Δx are (for Δx small)

$$-\Delta m = \frac{1000 \eta I}{QF} \Delta x \quad , \tag{9}$$

$$\Delta N = \frac{100 M_{Na} \eta I}{U \delta \rho_{Hg} F} \Delta x \quad . \tag{10}$$

Given concentrations at the upstream end of such an increment of cell length one can compute the corresponding concentrations at the downstream end.

Numerical Solution.

By use of Eqs. (5) through (10), the variables describing cell performance at all points of the cell can be determined for any desired operating condition as specified by the values of the operating parameters. This is accomplished by stepwise numerical calculations proceeding from the inlet end of the cell, carried out on a digital computer.

In order to utilize calculations of this type to examine the effects of variations in operating parameters upon cell performance, a base example, analogous for the model to normal operation in an industrial cell, was selected. This example is described in the listing below. Other examples were then chosen in order to investigate the effects of varying each of the operating parameters individually. It should be noted that in each case the values of all parameters except the one being investigated were maintained at the level used in the base example.

Operating parameters for base example	
Anode type	drilled
E_T	3.80 v
Q	5.60 g Hg per sec
U	6.25 cm/sec
m_0	6.00 M
N_0	0.010 wt%
d	0.500 cm

Representation of Cell Performance

From these calculations, the effect of individual variations of the operating parameters on variables representing cell performance can be expressed graphically. Thus, in Figs. 1 and 2 the effects on average current density due, respectively, to changes in brine flow rate and electrode spacing are shown. The effect on cell current for each of the operating parameters may be evaluated similarly. More results for this model are given in Ref. 1.
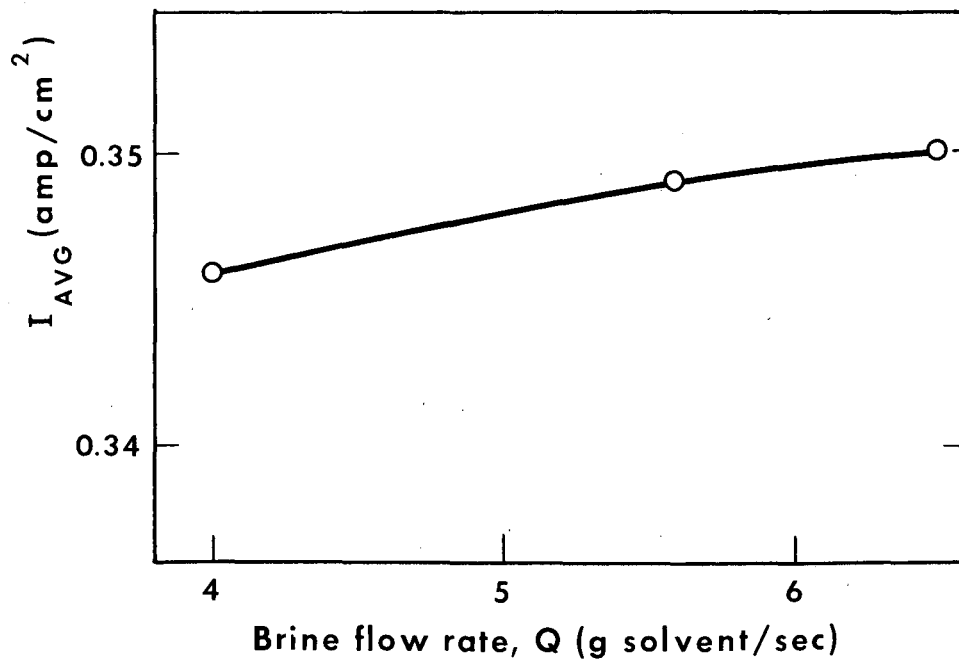
MU-26000

Fig. F.6-1. Effect of brine flow rate on average current density.
(All other operating parameters are at base example values.)
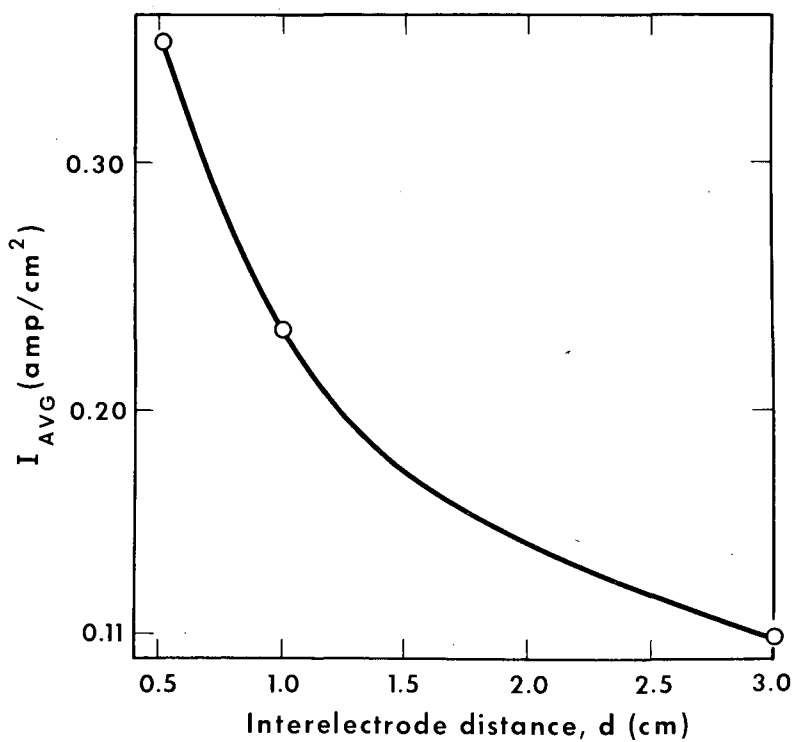
MU-26001

Fig. F.6-2. Effect of distance between electrodes on average current
density. (All other operating parameters are at base example
values.)

Nomenclature

English Letters

a,   Activity (refers to bulk of solution unless otherwise indicated).

d,   Distance between electrodes (cm)

$-E_A$, Anode potential (v)

E_C, Cathode potential (v)

E_R, Ohmic potential drop in electrolyte (v)

E_T, Total applied cell potential (v)

F,   Faraday constant

I,   Current density (amp/cm^2)

k,   Conductivity (ohm^{-1} cm^{-1})

M,   Molecular weight

m,   NaCl concentration in brine (mole/1000 g H_2O)

N,   Na concentration in amalgam (wt %)

Q,   Brine flow rate (g H_2O/sec)

R,   Gas constant

T,   Temperature, $^\circ$C or $^\circ$K

U,   Velocity of flowing mercury cathode (cm/sec)

x,   Distance along length of cell from inlet (cm)

Greek Letters

α, β, γ, λ, μ, ξ, regression constants

δ,   Mercury layer thickness (cm)

η,   Current efficiency

ρHG, Density of amalgam (g/cm^3)

ω,   Total electrode overvoltage (v)

Subscripts

avg, Average over cell

Cl,   Pertaining to chlorine

e,   Pure electrolyte

m,   Electrolyte with entrained gas

0,   Conditions at inlet end of cell

NaHg, Pertaining to sodium in amalgam

sat,   Saturated

±,   Mean ionic value

Superscript

0,   Standard electrode potential

7. NEW DEVELOPMENTS IN THE MEASUREMENT
OF MASS-TRANSFER POLARIZATION AND LIMITING CURRENTS

Charles W. Tobias

The simple techniques usually employed in connection with measurements of limiting currents[1] frequently do not yield meaningful data. Mass transport rates to and from electrode surfaces under various hydrodynamic conditions and in various cell geometries are typically functions of position and time. For this reason, it is necessary to distinguish between local limiting current density, I_L, and average limiting current density, I_{Lav}. The latter is obtained when all of the electrode surface is under limiting current: $I_{Lav} = i_L/(\text{electrode area})$, where i_L is the limiting current. When the thickness of the mass-transfer boundary layer varies over the surface, or if the primary current distribution is very nonuniform, frequently one is not able to obtain the usual "plateau" in the I-vs-E plot. In such cases it may be impossible to assign a meaningful value to I_L. It has been shown[2] that, for instance, in laminar flow past a flat plate electrode, the local limiting current density decreases with distance x from the leading edge: I_L is proportional to $x^{-1/2}$, while i_L is proportional to the square root of the length of the plate.

Under natural convection control it has been shown[3] that on vertical electrodes the local limiting current density varies as $x^{-1/4}$, where x is the distance from the leading edge. On horizontal cathodes facing upward, laminar secondary flows cause the limiting current density to be higher near the edges than over the rest of the electrode.[1] To facilitate studies of convection effects and calculations of concentration polarization for various situations, therefore, it is necessary to obtain local limiting rates.

The circuit and cell scheme shown in Fig.7-1 represents an improvement over Mantzell's "sectioned electrode" idea.[4] Instead of attempting to adjust the external resistances leading to each electrode segment (so as to eliminate any difference of potential between metal segments) small differences of potential are allowed to exist. (In typical cases these differences are on the order of < 0.1 mv.) Using a large number of segments, this circuit allows a good approximation of a continuous electrode. In its present

[1] E.J. Fenech, C.W. Tobias, Electrochimica Acta 2, 311 (1960).

[2] V.G. Levich, Discussions Faraday Soc. 1, 40 (1947).

[3] C.R. Wilke, M. Eisenberg, C.W. Tobias, J. Electrochem. Soc. 100, 513 (1953).

[4] E. Mantzell, Z. Elektrochem. 39, 10 (1935).
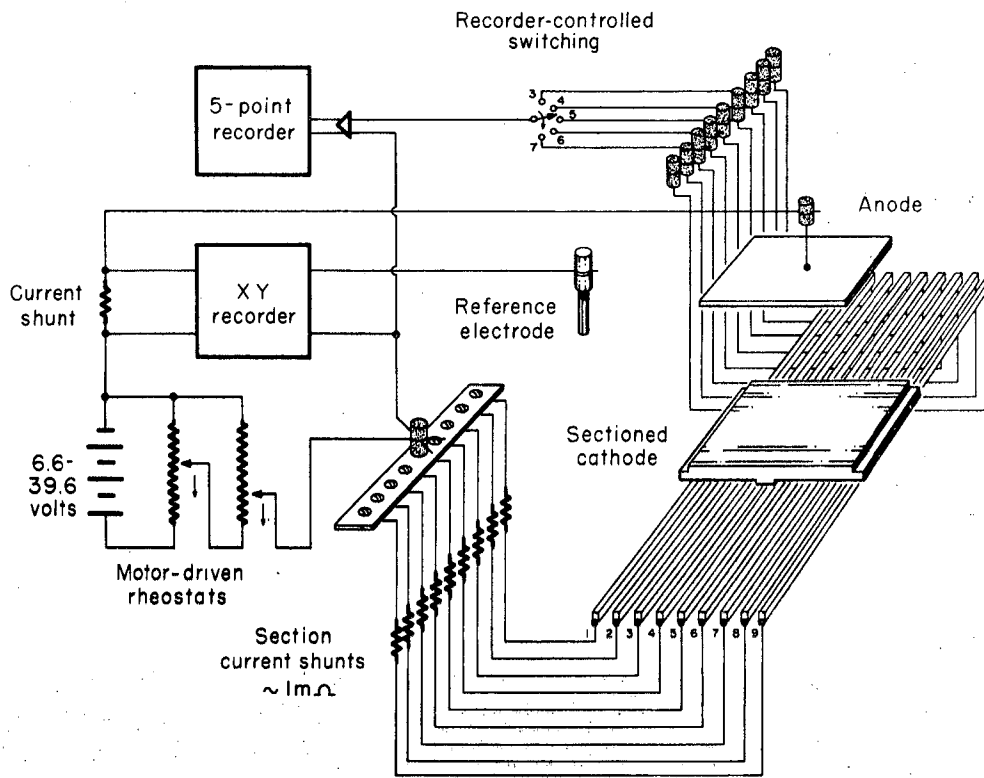
Fig. F.7-1. Circuit and cell.

MU-20034

form the apparatus is capable of automatically recording the polarization curves for nine segments (only one of which is represented in Fig. F.7-1).

Figure F.7-2 shows data obtained on a horizontal cathode facing upward, on which copper was deposited from a $0.25 \underline{M}$ $CuSO_4 + 1.5 \underline{M}$ H_2SO_4 solution. (Note the significant differences between local and average current densities.)

Using continuous records of total polarization as functions of time and applied current, one may study the unsteady-state portion of mass transfer, provided of course that the activation polarization is accurately known.

Another related problem concerns the rate of increase of current applies through the cell. Usually the current is increased continuously by a manually adjusted or moter-driven rheostat.[1] Reproducibility of applied current characteristics is important if one wishes to study unsteady-state mass transport. To achieve this, a "Programmed Current Source" has been developed which delivers a current that increases linearly with time. (Rate may be varied from 80 μa/sec to 250 ma/sec, up to 15 amp for a cell voltage < 12 v. Time to reach maximum current: 1 to 20 min. Recovery time for abrupt 10-fold increase in load: 3 m/sec. Linearity: within 0.3%. Ripple: < 0.1%.)

In the absence of external stirring, depending on the density differences arising from depletion or enrichment of solution adjacent to the electrode, steady-state convection develops slowly (in the case of dilute electrolytes) or rapidly (when ions are removed from concentrated solutions). A rapid externally forced increase of current may result in reaching a pseudo-limiting conditions, in which convection has had no time to fully develop before the potential has been reached at which a consecutive process becomes possible. In such cases one may obtain "camel back"-type polarization curves (Fig. F.7-3). Neither the top nor the bottom peak corresponds to a true steady-state limiting current. In order to assert that steady-state convection is established by the time a consecutive process begins, it is necessary to conduct a series of measurements, in which the rate of increase of current is varied. If a true steady state is reached, further increase of time for reaching the limiting condition will not cause the plateau to shift. The Programmed Current Source not only allows selection of optimal rate of increase for a set of experimental conditions, but also--since the current changes in a linear manner with time throughout the period of measurement--makes it possible to calculate the unsteady-state diffusional contribution (by solving the diffusion equation with the appropriate boundary conditions).

The use of the Segmented Electrode and the Programmed Current Source has made possible interpretation of mechanisms of mass transport phenomena near electrodes. Such refinements in experimental techniques facilitate the application of exact methods of hydrodynamics to the analysis of electrode processes.
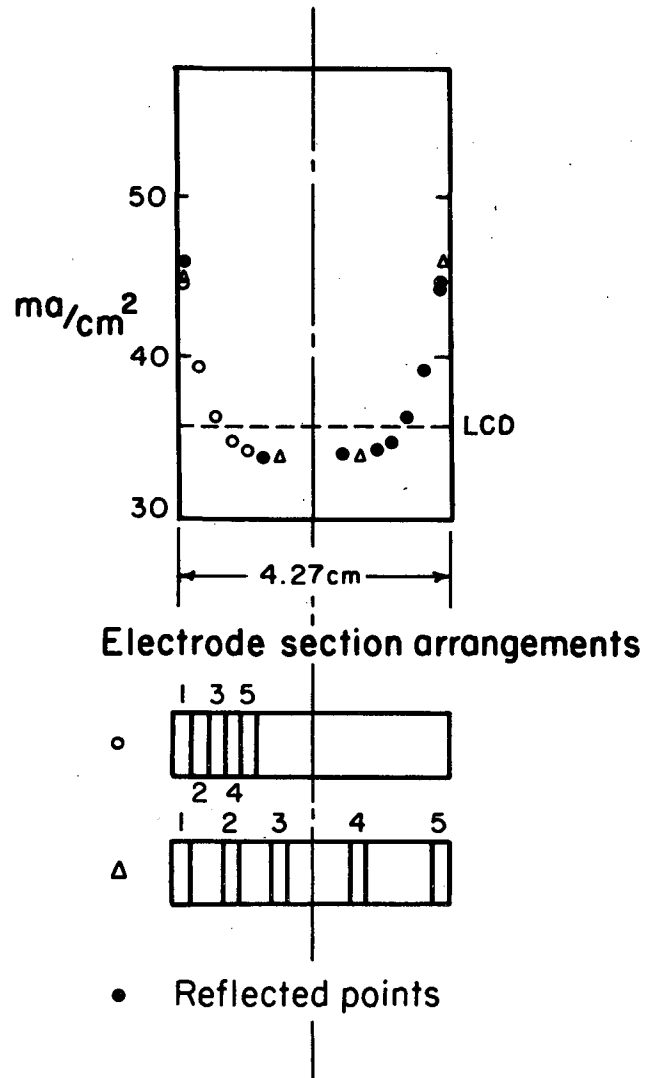
Fig. F.7-2. Results with horizontal cathode facing upward.
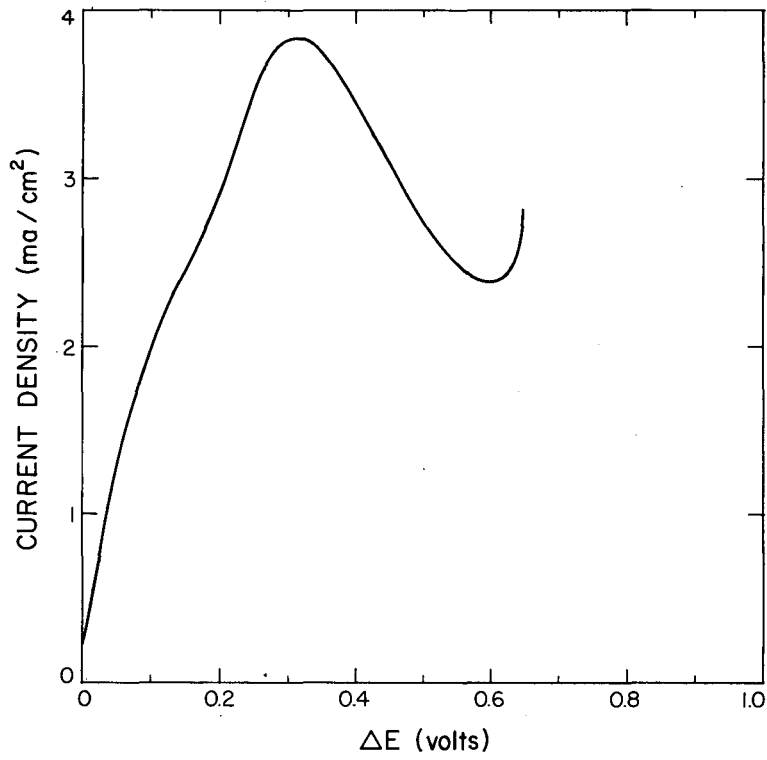
MU-12213

Fig. F.7-3. Results from run with 0.01 $\underline{M}$ AuSO$_4$, separation
8 cm, electrode 5 cm, 6 min.

G. THESIS ABSTRACTS

On the following pages the abstracts of theses issued in 1961 are reproduced from the original documents.

Paper elsewhere in this report cover work described in theses by

Denis B. Mc Whan	(Paper D.5),
Victor E. Viola, Jr.	(Paper B.7),
Tracy T. Word (ms)	(Paper F.2) and
Roger M. Wright	(Paper F.5).

1. HEAVY-ION ELASTIC SCATTERING

Jonas Alster

Lawrence Radiation Laboratory
University of California
Berkeley, California

April 17, 1961

ABSTRACT

The elastic scattering of C^{12} ions from A, Fe, Ni, Ag^{107}, In and Ta has been measured as a function of angle, at a laboratory-system energy of 124.5 Mev with the Berkeley heavy-ion linear accelerator. The experimental equipment and techniques are discussed. The angular distributions show the same general behavior as previous heavy-ion elastic scattering experiments. The experimental data were analyzed with the semiclassical Blair model as modified by McIntyre. Very good agreement with experiment was obtained. The measurements were taken with 1% statistics in order to study the structure of the angular distributions in greater detail, because only by fitting the details in the structure was it possible to obtain unambiguous sets of parameters. These parameters indicated a nuclear radius of $1.45A^{1/3} \times 10^{-13}$ cm, and a nearly constant surface thickness of 1.6×10^{-13} cm. Also, total reaction cross sections were obtained. A rainbow-model analysis by Goldman of the present data is given. Existing α- and heavy-ion scattering data have been analyzed with the McIntyre model and compared with previous optical-model analyses of the same data. It was found that, by independent analysis, the two models give the same imaginary phase shifts for all partial waves. The real phase shifts are identical above a certain ℓth partial wave, but differ widely below this ℓ value. It is shown that in the region of disagreement the real part of the phase shifts is irrelevant to the calculation of the cross section.

2. TWO-NUCLEON TRANSFER REACTIONS IN THE LIGHT ELEMENTS

Joseph Cerny III

Lawrence Radiation Laboratory
University of California
Berkeley, California

May 23, 1961

ABSTRACT

α, d reactions in the light elements have been investigated in an
attempt to determine their usefulness as spectroscopic probes. Deuter-
on energy spectra from the $Li^6(\alpha,d)Be^8$, $Li^7(\alpha,d)Be^9$, $C^{12}(\alpha,d)N^{14}$,
$N^{14}(\alpha,d)O^{16}$, and $N^{15}(\alpha,d)O^{17}$ reactions were measured and angular
distributions are given for deuteron groups arising from the formation
of resolvable final states.

Selection rules for two-nucleon transfer reactions are discussed.
Direct-reaction α, d or d, α transitions between $0+$, $T=0$ and $0+$, $T=1$
states are shown to involve difficulties with angular momentum and
parity conservation in addition to requiring nonconservation of isotopic
spin. The unobserved $C^{12}(\alpha,d)N^{14*}$ (2.31-Mev) transition is interpreted
from this point of view.

Marked variation in the relative cross sections of final states
was observed in most of the deuteron spectra. Some evidence was
obtained that the captured nucleons prefer to enter equivalent shell-
model levels and, lacking that, adjacent levels. No final states defi-
nitely known to involve more than two excited nucleons were observably
populated; however, very few states of this nature have been theoret-
ically established.

Glendenning's two-nucleon stripping theory was applied to the
deuteron angular distributions, and several excellent fits were obtained.
The fits, in general, showed little dependence on the nature of the final
nuclear configuration when several were reasonable, so that no spectro-
scopic identification of final states appears to be possible at these high-
momentum transfers. Angular distribution fits using Butler theory are
shown for comparison.

3.   THE MAGNETIC PROPERTIES OF DEFORMED NUCLEI

Lung-wen Chiao

Lawrence Radiation Laboratory
University of California
Berkeley, California

April 1961

ABSTRACT

It is shown that the magnetic moments of odd-A deformed nuclei
can be interpreted in terms of the independent-particle model with
interconfigurational mixing due to the very-short-range residual forces.
The latter are implied by using the empirically reduced spin gyromagnetic
ratios. The effects of these residual forces on the collective gyro-
magnetic ratios g_R are discussed in terms of pair correlation. The
effect of particle-rotation interaction on the magnetic moment and the
collective gyromagnetic ratio are shown. The g_R values are obtained
from the magnetic moments and the matrix elements for M1 transitions in
this band. It is found that these mechanisms give a satisfactory account
of the collective gyromagnetic ratio of Dy^{161}, Ho^{165}, Er^{167}, and Hf^{179}.

4.   EJECTION OF LARGE FRAGMENTS IN HIGH-ENERGY NUCLEAR REACTIONS

Vitor Pereira Crespo

Lawrence Radiation Laboratory
University of California
Berkeley, California

September 6, 1961

ABSTRACT

Several features of the production of Na^{24} and Mg^{28} fragments produced in the interaction of protons and He ions with Cu, Ag, Au, and U have been investigated. Formation cross sections were determined for He ions of different energies between 320 and 880 Mev and for protons of 700 Mev. Thick-target recoil experiments were performed at bombarding energies of 0.7 and 3 Bev for protons, and 880 Mev for He ions. Also given are some recoil measurements of Na^{24} from Al.

Analysis of data obtained with target materials heavier than Al shows that for the bombarding energies used in this work Na^{24} and Mg^{28} are probably produced by the cleavage of the target nucleus into two heavy fragments. One of these fragments has a mass approximately equal to the mass of Na^{24} or Mg^{28} and the other contains most of the remaining mass of the target nucleus. However, Na^{24} and Mg^{28} are very probably not slowly evaporated particles nor products of a slow fission process.

The experimental information covering fragmentation from photographic emulsion studies and radiochemical studies is discussed. The various mechanisms proposed are considered and a new one suggested. According to this new mechanism, Na^{24}, Mg^{28}, and the more energetic fragments observed in nuclear emulsions are ejected promptly from the parent nucleus by very complex nucleon-nucleon cascades and by collective effects.

5. AN ANALYSIS OF THE ABSORPTION SPECTRA OF TmIV AND AmIV

John Balsbaugh Gruber

Department of Chemistry and Lawrence Radiation Laboratory
University of California
Berkeley, California

January 1961

ABSTRACT

An analysis of the absorption spectra of $Tm(C_2H_5SO_4)_3 \cdot 9H_2O$ and AmIV in $LaCl_3$ is presented here. For TmIV, all levels corresponding to $\underline{4f} \rightarrow \underline{4f}$ transitions except transitions from $^3H_6$ to $^1S_0$ have been observed and fitted to a theoretical model which gives $\zeta_{\underline{4f}} = 1350\,cm^{-1}$, and $F_2\,(\underline{4f}) = 450\,cm^{-1}$.

The 119 electronic energy levels for the $n\underline{f}^6$ configuration have been calculated for three different sets of Slater F_k ratios: $\underline{4f}^6$ hydrogenic--$F_4/F_2 = 0.1381$, $F_6/F_2 = 0.01511$; $\underline{5f}^6$ hydrogenic--$F_4/F_2 = 0.1422$, $F_6/F_2 = 0.0161$; and $\underline{5f}^6$ based on a Hartree-Fock calculation--$F_4/F_2 = 0.159$, $F_6/F_2 = 0.0204$. A tentative theoretical analysis of the absorption spectra of Eu IV can be made by using $\zeta = 1360\,cm^{-1}$ and $F_2\,(\underline{4f}) = 370\,cm^{-1}$.

It has been possible to carry out a crystal-field splitting analysis of all the infrared electronic energy levels of AmIV. Parameters that fit the observed data are $A_2^0 \left\langle r^2 \right\rangle = 206\,cm^{-1}$, $A_4^0 \left\langle r^4 \right\rangle = -94.1\,cm^{-1}$, $A_6^0 \left\langle r^6 \right\rangle = -93.8\,cm^{-1}$, and $A_6^6 \left\langle r^6 \right\rangle = 1100\,cm^{-1}$.

6. NUCLEAR ALIGNMENT EXPERIMENTS ON CERIUM RADIOISOTOPES

James Norman Haag

Department of Chemistry and Lawrence Radiation Laboratory
University of California, Berkeley, California

September 29, 1961

ABSTRACT

Nuclei of Ce^{137m}, Ce^{137}, Ce^{139}, Ce^{141}, and Ce^{143} were aligned in a neodymium ethylsulfate lattice at low temperatures by the magnetic hyperfine-structure method. The angular distribution and the plane polarization of the emitted gamma rays were measured as functions of temperature. The results are as follows.

For the spin sequence $11/2(Ce^{137m}) \xrightarrow[255 \text{ kev}]{M^4} 3/2(Ce^{137})$, the magnetic moment of Ce^{137m} is $|\mu_N| = 0.96 \pm .09$ nm. The spin of Ce^{137m} is established as $11/2$.

For the spin sequence $3/2(Ce^{137}) \xrightarrow{i_\beta=0} 3/2 \xrightarrow[445 \text{ kev}]{M1, E2} 5/2$, the magnetic moment of Ce^{137} is $|\mu_N| = 0.95 \pm .20$ nm and $\delta(E2/M1) = -0.17 \pm .02$. The beta transition is established as predominantly $i_\beta = 0$.

For the spin sequence $3/2(Ce^{139}) \xrightarrow{i_\beta=1} 5/2 \xrightarrow[166 \text{ kev}]{M1, E2} 7/2(La^{139})$, the magnetic moment of Ce^{139} is $|\mu_N| = 0.95 \pm .20$ nm and $\delta(E2/M1) = +0.034 \pm .034$.

For the spin sequence $7/2(Ce^{141}) \xrightarrow{i_\beta=0} 7/2 \xrightarrow[142 \text{ kev}]{M1, E2} 5/2(Pr^{141})$, the magnetic moment of Ce^{141} is $|\mu_N| = 1.30 \pm .20$ nm and $\delta(E2/M1) = +0.066 \pm .022$. The spin of the 142-kev level of Pr^{141} is established as $7/2$. The β transition is established as predominantly $i_\beta = 0$.

7.   NUCLEAR ORIENTATION OF SOME RARE-EARTH ISOTOPES

Carolyn Ann Lovejoy

Lawrence Radiation Laboratory
University of California
Berkeley, California

June 1961

ABSTRACT

Nuclear orientation experiments were performed on five isotopes, Pm^{143}, Tb^{156}, Tb^{161}, Ho^{160}, and Sm^{153}, in crystals of $Nd(C_2H_5SO_4)_3 \cdot 9H_2O$. The angular distribution of the 740-kev γ ray of Nd^{143} was found to be $W(\theta) = 1 - (0.060 \pm 0.006) P_2(\cos \theta)$ at $0.02^\circ K$. Values for the mixing ratio, δ, of the 740-kev γ ray of Nd^{143} were obtained as a function of the magnetic moment of the ground state of Pm^{143} for ground state spins of 5/2 and 7/2. The spin of the excited state of Nd^{143} was assigned as 9/2-. An absolute lower limit of $|\mu| > 1.0$ was set on the magnetic moment of Pm^{143}. The mixing ratio of the 740-kev γ ray was found to lie in the range $0.23 \leq (E2/M1) \leq 0.35$ if the ground state spin is 7/2 and in the range $0.255 \geq (E2/M1) \geq 0.217$ if the ground state spin is 5/2.

The spin of the 2042-kev level in Gd^{156} populated by the decay of Tb^{156} was assigned as 4 and the spin of the 1620-kev level was assigned as 5+. The electron capture decay to both the 2042-kev level and the 1931-kev level was found to be mainly L=1. If the ground-state spin of Tb^{156} is 3 the nuclear magnetic moment was found to be $\mu = 1.45 \pm 0.06$ and the nuclear quadrupole moment, $Q = 1.40 \pm 0.16$. Mixing ratios of the γ rays were determined. The angular distribution of the 1417-kev γ ray was found to be $W(\theta) = 1 - (0.206 \pm 0.016) P_2(\cos \theta)$ at $1/t = 58.5$.

Explanations are advanced for the failure of Tb^{161}, Ho^{160} and Sm^{153} to show a noticeable anisotropy at temperatures of around $0.02^\circ K$.

8.   EFFECTS OF ANGULAR MOMENTUM ON GAMMA-RAY PRODUCTION

IN COMPOUND-NUCLEUS REACTIONS

James F. Mollenauer

Lawrence Radiation Laboratory and Department of Chemistry
·University of California, Berkeley, California

June 1961

ABSTRACT

The yields and spectra of gamma rays produced in compound nucleus reaction were measured by a coincidence technique. Pulses from the gamma detector were required to be in coincidence with pulses indicating the removal of a charged particle from the beam. The effect of the angular momentum of the compound system was studied by using pairs of targets producing the same compound nucleus when bombarded with helium and with carbon ions.

For the carbon-ion reactions studied, the total energy appearing in gamma rays was greater than the neutron binding energy. This result disagrees with the assumption of evaporation theory that nucleon emission is preferred when possible. The increased gamma yield was shown to depend on angular momentum at constant excitation energy.

The anisotropy of the gamma radiation indicated that the transitions involved in the de-excitation were primarily quadrupole when the angular momentum brought in was approximately 10 to 15 units. A greater fraction of dipole transitions was apparent for larger angular momenta. Both the anisotropy and the average photon energy were inconsistent with predictions based on single-proton transitions. Collective modes are probably involved in the radiative processes; the average and total gamma energies are more consistent with vibrational than with rotational transitions.

9.   INVESTIGATION OF NUCLEAR REACTIONS
BY RECOIL STUDIES OF RADIOACTIVE PRODUCTS

John R. Morton III

Department of Chemistry and Lawrence Radiation Laboratory
University of California
Berkeley, California

April, 1961

ABSTRACT

The ranges and angular distributions of the recoiling residual nuclei from several nuclear reactions have been studied to obtain information about the reaction mechanisms. The observed reactions were $Ra^{226}(\alpha, 4n)Th^{226}$, $Pb^{208}(\alpha, 2n)Po^{210}$, $Pr^{141}(C^{12}, 4n)Tb^{149}$, $Te^{130}(C^{12}, 5n)Ce^{137m}$, and $Pb^{207}(\alpha, n)Po^{210}$. The experimental angular distributions were compared with distributions calculated by a Monte Carlo method based upon the compound-nucleus and statistical models. The results from the $Ra^{226}(\alpha, 4n)$ and $Pr^{141}(C^{12}, 4n)$ reactions are in agreement with the simple theory. The $Te^{130}(C^{12}, 5n)$ data can be explained by formation of a compound nucleus which de-excites with enhanced probability for gamma emission. The $Pb^{208}(\alpha, 2n)$ and $Pb^{207}(\alpha, n)$ experiments require substantial contributions from direct-interaction mechanisms.

10.   THEORY OF ODD-MASS ELLIPSOIDAL NUCLEI

Lucy Wu Person

Lawrence Radiation Laboratory
University of California
Berkeley, California

July 1961

ABSTRACT

This report consists of theoretical calculations dealing with the
low-lying vibrational and rotational spectra of deformed nuclei. In the
calculations the rotational spectrum of an odd nucleon in an ellipsoidal
well is studied for the $N=2$ and $N=4$ shells. Applying this method, we
have explained the ground spins of the light cesium isotopes. Next, an
evaluation is made of the rotational-energy spectrum, magnetic moment,
and E2 reduced transition probabilities for Cs^{131}. Good agreement is
obtained with gamma = 38 deg and beta = 0.29. As another application,
we predicted the spins and parities of two levels for four nuclei, which
probably belong to the γ-vibration band in the asymmetric limit (Lu^{175},
Ta^{181}, Re^{185}, and Re^{187}). The agreement is not complete, and the results
are discussed. Also, the ground-state magnetic moment for these nuclei
was calculated. The agreement shows that asymmetry does not have a large
effect on the magnetic moment of strongly deformed nuclei.

11. ALPHA DECAY STUDIES IN THE FAMILIES

OF THE LIGHT URANIUM ISOTOPES

Carl Phillip Ruiz

Lawrence Radiation Laboratory and Department of Chemistry
University of California, Berkeley, California

April 1961

ABSTRACT

Using a 180° double-focusing alpha-particle spectrograph, an
alpha-particle ionization chamber, and scintillation spectrometers, the
alpha and gamma radiations of the $U^{228,229}$ series, U^{233}, Pa^{229}, and
Ra^{222} were investigated. Decay schemes are presented in most cases and
analysed wherever possible in terms of the theoretical nuclear models.
For the odd mass nuclides the Bohr-Mottelson model was used to interpret
the decay schemes for $A \gtrsim 225$; for $A < 225$ there was no obvious rotational
pattern present. The spectroscopic data obtained for the even-even
nuclides are in agreement with the previously existing systematics, and
are discussed in terms of the axially asymmetric theory of Davydov, et al.
The half-lives of U^{228}, Ra^{220}, $Rn^{216,217,218}$ were measured.
Conventional counting techniques were used for the U^{228} half-life deter-
mination while delayed coincidence counting and moving tape techniques
were employed for the others. The data for the even-even nuclides are
in good agreement with the systematics.

H.   AUTHOR INDEX OF UCRL REPORTS FOR 1961

Albert, R. D. , S. D. Bloom, and N. K. Glendenning

(p, n) Angular Distributions from Mirror Nucleus Targets: C^{13}, B^{11}, and Be^9
UCRL-6199, Nov. 1960   Phys. Rev. 122, 862-869, (1961)

Albridge, R. G. , J. M. Hollander, C. J. Gallagher, and J. H. Hamilton
The Energy Levels of U^{233}
UCRL-9438-Rev. , April 1961   Nuclear Phys.

Albridge, R. G. , and J. M. Hollander

The K- and L-Auger Spectrum of Uranium
UCRL-9609, March 1961   Nuclear Phys.

Alexander, J. M. , and L. Winsberg

Ranges and Range Straggling of Tb^{149}, At, and Po
UCRL-8997, April 1960   Phys. Rev. 121, No. 2, 518-528 (1961)

Alexander, J. M. , and L. Winsberg
Recoil Studies of Nuclear Reactions Induced by Heavy Ions
UCRL-9118, Aug. 1960   Phys. Rev. 121, No. 2, 529-537 (1961)

Alpert, S. S. , E. Lipworth, M. B. White, and K. F. Smith
The Magnetic Dipole and Electric Quadrupole Interaction Constants of Bi^{210}
UCRL-9474-Abstract, Nov. 1960   Bull. APS II, 6, 74 (1961)

Alster, J.

Heavy-Ion Elastic Scattering   (Ph. D. Thesis)
UCRL-9650, April 1961

Appelman, E. H.

The Half Lives of At^{211} and Bi^{207}
(No UCRL number) Aug. 1960   Phys. Rev. 121, No. 1, 253-255 (1961).

Appelman, E. H. , and H. Evans
The Oxidation States of Astatine in Aqueous Solution
(No UCRL number)   J. Am. Chem. Soc. 83, 805 (1961)

Appelman, E. H.

Solvent Extraction Studies of Interhalogen Compounds of Astatine
(No UCRL number) Dec. 1960   J. Phys. Chem. 65, 325 (1961).

Asaro, F. (see I. Perlman, UCRL-9524)

Asaro, F., M. C. Michel, S. G. Thompson, and I. Perlman
The Alpha Decay Scheme of 152-Year Am^{242m}
UCRL-9758, June 1961   Rutherford Jubilee International Con-
                                        ference, Manchester, England.

Axel, P. (see D. A. Shirley, UCRL-9554).

Bailey, S. M.
Yield Ratios for the Isomeric Pair Sc$^{44m, 44}$ Formed in (a, an) and
  (a, n) Reactions
(No UCRL number)   Phys. Rev. 123, 579-582 (1961).

Bjørnholm, S., A. B. Knutsen, and O. B. Nielsen
Rotational and Vibrational Levels in U^{232}
UCRL-9545-Abstract   APS Meeting, Washington, D. C.,
                                        April 1961; Bull. Am. Phys. Soc.

Bjørnholm, S., and M. C. Lederer
Thin Cation-Exchange Foils
UCRL-9957, Dec. 1961   J. Nuclear Inst. & Methods

Bloom, S. D. (see R. D. Albert, UCRL-6199).

Bowman, H. R. (see M. L. Muga, UCRL-9044).

Bowman, H. R., S. G. Thompson, J. C. D. Milton, and W. J. Swiatecki
Velocity and Angular Distribution of Prompt Neutrons from Spontaneous
  Fission of Cf^{252}
UCRL-9713, Nov. 1961

Bowman, H. R., S. G. Thompson, J. C. D. Milton, and W. J. Swiatecki
Velocity and Angular Distributions of Prompt Neutrons from
  Spontaneous Fission of Cf^{252}
UCRL-9713 Rev., Dec. 1961   Phys. Rev.

Cerny, J., III, B. G. Harvey and R. A. Pehl
(a, d) Reactions on Odd-Odd Targets
UCRL-9525, Feb. 1961   Nuclear Phys.

Cerny, J., III
Two-Nucleon Transfer Reactions in the Light Elements (Ph. D. Thesis)
UCRL-9714, June 1961

Cerny, J., III., N. K. Glendenning, B. G. Harvey, R. H. Pehl, and
  E. Rivet
Analysis of the Two-Nucleon Stripping Reactions $C^{12}(He^3, p)N^{14}$
UCRL-9878-Abs., Oct. 1961   APS Meeting, Los Angeles, Dec. 1961
                                   Bull. Am. Phys. Soc.

Chanda, R. N. (see R. K. Sheline, UCRL-9888)

Chiao, L., (see P. G. Hansen, No UCRL number)

Chiao, L.
The Magnetic Properties of Deformed Nuclei (Ph. D. Thesis)
UCRL-9648, May 1961

Choppin, G. R., and T. Sikkeland
Isomeric Cross Section Ratio for the (α, pn) Reaction
UCRL-9534, Feb. 1961   J. Inorg. & Nuclear Chem.

Chu, B., D. C. Whitney and R. M. Diamond
On Anion-Exchange Resin Selectivities
UCRL-9907, Nov. 1961   J. Inorg. & Nuclear Chem.

Clements, T. P. (see L. Winsberg, UCRL-8982-Rev.)

Conway, J. G. (see J. B. Gruber, UCRL-9310)

Conway, J. G. (see J. B. Gruber, UCRL-9555)

Conway, J. G., J. B. Gruber, E. K. Hulet, R. J. Morrow, and R. C.
  Gutmacher
Absorption and Self-Luminescence Spectra of $Cf^{+3}(5f^9)$
UCRL-9654, May 1961   J. Chem. Phys. $\underline{36}$, 189 (1962).

Conway, J. G., E. K. Hulet and R. J. Morrow
The Emission Spectrum of Californium
UCRL-9776, July 1961   J. Opt. Soc. Am. $\underline{52}$, 222 (1962)

Crespo, V. P.
Ejection of Large Fragments in High-Energy Nuclear Reactions (Ph. D. Thesis)
UCRL-9683, Sept. 1961

Cunningham, B. B., (Nuclear Chemistry Group under).
Microchemistry
(No UCRL number) March 1961   1961 Annual Report of the AEC on Atomic
                                     Energy Research in the Life and Physical
                                     Sciences

Cunningham, B. B. and J. C. Wallmann

Properties of the Transplutonium Elements
(No UCRL number) Sept. 1961   Abstract of talk presented at ACS
                                   Combined Regional Meeting, New
                                   Orleans, La., Dec. 1961

Cunningham, B. B.

Submicrogram Methods Used in Studies of the Synthetic Elements
(No UCRL number)   Microchemical Journal Symposium,
                                   pp. 69-93, 1961.
                                   (From the Symposium on Experi-
                                   mentation below the Microgram Range,
                                   Arlington, Virginia, May 15-18, 1960)

Cunningham, B. B.

Thermodynamics of the Actinides
(No UCRL number)   Abstract for IAEA Symposium on the
                                   Thermodynamics of Nuclear Materials,
                                   Vienna, Austria, May 1962

Diamond, R. M., J. M. Hollander, D. J. Horen, and R. A. Naumann

Neutron-Deficient Iridium Isotopes: Ir^{182}, Ir^{183}, Ir^{184}
UCRL-9532, Jan. 1961   Nuclear Phys. <u>25</u>, 248-258 (1961)

Diamond, R. M.

Proton Solvation and the Solvent Extraction of Strong Acids
(No UCRL number)   For ACS Symposium

Diamond, R. M. (see D. G. Tuck, UCRL-8897-Rev.)

Diamond, R. M. (see B. Chu, UCRL-9907)

Dodge, R. P., D. H. Templeton, and A. Zalkin

Crystal Structure of Vanadyl Bisacetylacetonate. Geometry of
   Vanadium in Fivefold Coordination
UCRL-8225-Rev., Nov. 1960   J. Chem. Phys. <u>35</u>, 55-67 (1961)

Elliott, J. H.

Thick-Junction Radiation Detectors Made by Ion Drifts
UCRL-9538, March 1961   Nuclear Instr. & Methods <u>12</u>, 60-66
                                   (1961)

Fraser, J. S. (see J. C. D. Milton, UCRL-9754)

Gallagher, C. J. (see R. G. Albridge, UCRL-9438-Rev.)

Ghiorso, A., T. Sikkeland, A. E. Larsh, and R. M. Latimer

The New Element, Lawrencium, Atomic Number 103
UCRL-9645, April 1961   Phys. Rev. Letters $\underline{6}$, 473 (1961)

Ghiorso, A.

The Search for New Elements
(No UCRL number)   Article for "DISCOVERY" magazine
                                        (sent to editor Aug. 1961)

Ghiorso, A.

Element No. 103--Lawrencium
(No UCRL number) April, 1961   Article for Encyclopedia of Science and
                                        Technology Yearbook (sent Aug. 1961)

Glendenning, N. K. (see R. D. Albert, UCRL-6199)

Glendenning, N. K.

The Two-Nucleon Stripping Reaction
UCRL-9505, Feb. 1961   Nuclear Phys.

Glendenning, N. K. (see S. G. Nilsson, No UCRL number)

Glendenning, N. K. (see S. G. Nilsson, UCRL-9552-Abs.)

Glendenning, N. K. (see S. G. Nilsson, UCRL-9803)

Glendenning, N. K. and S. G. Nilsson

Effects of Residual Interactions in Spectra of Odd-A and Odd-Odd
   Deformed Nuclei
UCRL-9631-Abs., April 1961   APS. Meeting in Mexico City, June 1961
                                       Bull. Am. Phys. Soc.

Glendenning, N. K. (see J. Cerny, UCRL-9878-Abs.)

Glendenning, N. K., and G. Kramer

Nucleon-Nucleon Triplet-Even Potentials
UCRL-9904, Dec. 1961   Phys. Rev.

Glendenning, N. K., and G. Kramer

The Scalar Nucleon Form Factor $F_1{}^n + F_1{}^P$
UCRL-9905, Oct. 1961   Phys. Rev. Letters (revised version)

Glendenning, N. K.

(p, n) Reactions in Mirror Nuclei and the Nuclear Two-Body Force
(No UCRL number)   Rutherford Jubilee International
                                    Conference, England, Sept. 1961

Glendenning, N. K. (see S. G. Nilsson, UCRL-9975)

Golding, F. S. (see W. L. Hansen, UCRL-9529-A)

Gooding, T. J., and G. Igo

Quasi-Elastic Scattering of 920-Mev α Particles by α-Particle
   Clusters in C^{12}
UCRL-9629-Abs., April 1961   APS Meeting in Mexico City, June 1961

Gooding, T. J., and G. Igo

Scattering of 915-Mev α Particles from Carbon and Helium: Direct
   Evidence for α-Particle Clustering in Nuclei
UCRL-9710, May 1961   Phys. Rev. Letters 7, 28-30 (1961)

Gordon, G. E. (see R. M. Latimer, UCRL-9217)

Gordon, G. E. (see T. Sikkeland, UCRL-9540)

Gordon, G. E. (see T. D. Thomas, UCRL-9950)

Griffioen, R. D. and J. O. Rasmussen

Analysis of Long-Range Alpha-Emission Data
UCRL-9368, Nov. 1960   Phys. Rev. 121, 1774-1778 (1961)

Griffioen, R. D. (see R. D. Macfarlane, UCRL-9541-Abs.)

Griffioen, R. D. (see R. D. Macfarlane, UCRL-9852-Abs.)

Griffioen, R. D. and R. D. Macfarlane

Neutron-Deficient Alpha Emitters of Francium
UCRL-9851-Abs., Sept. 1961   APS Meeting, Chicago, Illinois
                                    Bull. Am. Phys. Soc.

Gruber, J. B.

An Analysis of the Absorption Spectra of TmIV and AmIV (Ph. D. Thesis)
UCRL-9203, Feb. 1961

Gruber, J. B. and J. G. Conway

Evaluation of Electrostatic Energy Levels of f^6
UCRL-9310, Aug. 1960   J. Chem. Phys. $\underline{34}$, 632-638 (1961)

Gruber, J. B. and J. G. Conway

The Polarized Absorption Spectra of Am^{+3} in $LaCl_3$
UCRL-9555, Feb. 1961   J. Chem. Phys. $\underline{36}$, 191 (1962)

Gruber, J. B. and J. G. Conway

The Absorption Spectrum and Zeeman Effect of Am^{+3} in $LaCl_3$
UCRL-9555-Rev., July 1961   J. Chem. Phys. $\underline{36}$, 191 (1962)

Gruber, J. B.

An Analysis of the Infrared Absorption Spectrum of $Am^{+3}(5f^6)$ in $LaCl_3$
UCRL-9584, March 1961   J. Chem. Phys. $\underline{35}$, $2\overline{1}86$ (1961)

Gruber, J. B. (see J. G. Conway, UCRL-9654)

Gutmacher, R. C. (see J. G. Conway, UCRL-9654)

Haag, J. N., C. E. Johnson, D. A. Shirley, and D. H. Templeton

Nuclear Moment of Ce^{137m} by Nuclear Alignment
UCRL-9299, July 1960   Phys. Rev. $\underline{121}$, 591-594 (1961)

Haag, J. N.

Nuclear Alignment Experiments on Cerium Radioisotopes (Ph. D. Thesis)
UCRL-9872, Dec. 1961

Haines, E. L. (see T. Sikkeland, UCRL-9751)

Hamilton, J. H. (see R. G. Albridge, UCRL-9438-Rev.)

Hansen, P. G., K. Wilsky, D. J. Horen, and L. Chiao

High-Energy Gamma Rays in the Decay of Ho^{166}
(No UCRL number) March 1961   Nuclear Phys.

Hansen, W. L., and F. S. Goulding

Electrical Limitations to Energy Resolution in Semiconductor Particle
  Detectors
UCRL-9529-Abs., Jan. 1961   International Atomic Energy Conference
                               on Nuclear Electronics
                               Belgrade, Yugoslavia, May 1961

Harvey, B. G. (see J. Cerny, UCRL-9525)

Harvey, B. G. (see J. Cerny, UCRL-9878-Abs.)

Hoff, R. W., J. M. Hollander, and M. C. Michel
The Neutron-Deficient Chain ^{80}Sr - ^{80}Rb$^+$
UCRL-5939-T, April 1960   J. Inorg. & Nuclear Chem. 18, 1-7 (1961)

Hollander, J. M. (see R. W. Hoff, UCRL-5939-T)

Hollander, J. M. (see R. G. Albridge, UCRL-9438-Rev.)

Hollander, J. M. (see R. M. Diamond, UCRL-9532)

Hollander, J. M. (see S. Hultberg, UCRL-9608)

Hollander, J. M. (see S. Hultberg, UCRL-9608-Rev.)

Hollander, J. M. (see R. G. Albridge, UCRL-9609)

Hollander, J. M. (see M. I. Tocher, UCRL-9699)

Hollander, J. M. (see J. Valentin, UCRL-9731)

Hollander, J. M. (see J. Valentin, UCRL-9780)

Hollander, J. M. (see Y. E. Kim, UCRL-9812)

Horen, D. J. (see P. G. Hansen, No UCRL number)

Horen, D. J. (see R. M. Diamond, UCRL-9532)

Horen, D. J. (see S. Hultberg, UCRL-9608)

Horen, D. J. (see S. Hultberg, UCRL-9608 Rev)

Horen, D. J. (see J. Valentin, UCRL-9731)

Horen, D. J. (see J. Valentin, UCRL-9780)

Horen, D. J. (see Y. E. Kim, UCRL-9812)

Hulet, E. K. (see J. G. Conway, UCRL-9654)

Hulet, E. K. (see J. G. Conway, UCRL-9776)

Hultberg, S., D. J. Horen, and J. M. Hollander
Measurements of E2 Internal Conversion Coefficients. A Discussion
  of the Internal-External Conversion Method
UCRL-9608, April 1961

Hultberg, S., D. J. Horen, and J. M. Hollander
Measurements of Internal Conversion Coefficients,
UCRL-9608-Rev., July 1961   Nuclear Phys.

Hyde, E. K.
The Radioactive Decay of the Isotopes of the Transuranium Elements
UCRL-9148, Jan. 1961   (Chapter 9 of a book).

Hyde, E. K.
The Isotopes of Thorium, Protactinium, and Uranium
UCRL-9458, Jan. 1961   (Chapter 8 of a book).

Hyde, E. K.
Some Useful Tables for Nuclear Spectroscopy in Transmercury
  Group of Elements: Electron Binding Energies, X-Ray Energies,
  Auger Electron Energies, and Fluorescent Yields
UCRL-9642, May 1961

Hyde, E. K.
Radioactivity
(No UCRL number)   Article for the Reinhold Encyclopedia
                                   of Electronics, 1961

Igo, G. and B. Wilkins
Reaction Cross Section for 160-Mev O^{16} Ions in Aluminum
  by the Attenuation Method
UCRL-9628-Abs., April 1961   APS Meeting, Mexico City, June 1961
                                    Bull. Am. Phys. Soc.

Igo, G. (see T. J. Gooding, UCRL-9629 Abs.)

Igo, G. (see T. J. Gooding, UCRL-9710)

Igo, G. and B. Wilkins
Nuclear Reaction Cross Sections for 10.3-Mev Protons on Carbon and Cu.
UCRL-9906-Abs., Oct. 1961   APS Meeting, Los Angeles, Dec. 1961

Johnson, C. E. (see J. N. Haag, UCRL-9299)

Johnson, Q. C. and D. H. Templeton
Madelung Constants for Several Structures
UCRL-9439, Nov. 1960   J. Chem. Phys. 34, 2004-2007 (1961)

Judd, B. R.
Low-Lying Levels in Several Transuranic Atoms
UCRL-9678-Abs., April 1961   Atomic Spectroscopy Symposium
                                    Argonne Natl. Lab., June 1961

Judd, B. R.
Low-Lying Levels in Certain Actinide Atoms
UCRL-9779, Dec. 1961   Phys. Rev.

Judd, B. R., and L. C. Marquet
Energy Levels of ErII
UCRL-9830, Sept. 1961   J. Opt. Soc. Am.

Judd, B. R.
Double Tensor Operators for Configurations of Equivalent Factors
UCRL-9868, Oct. 1961   J. Math. Phys.

Kaplan, M. and D. A. Shirley
Nuclear Orientation of Paramagnetic Impurity Ions
UCRL-9569, Feb. 1961   Phys. Rev. Letters 6, 361-362 (1961)

Kaplan, M. (see D. A. Shirley, UCRL-9554)

Kim, Y. E., D. J. Horen, and J. M. Hollander
Isomeric State in Y^{86}
UCRL-9812, Aug. 1961   Nuclear Phys.

Knutsen, A. B. (see S. Bjørnholm, UCRL-9545-Abs.)

Kramer, G.
Photodisintegration of the Deuteron—Present Status, Information to be
   Gained from Electrodisintegration and Polarization Experiments
(No UCRL number)   Gordon Conference, Aug. 1961,
                                 New Hampshire

Kramer, G.
Angular Distribution in the Photodisintegration of the Deuteron
UCRL-9625-Abs., April 1961   APS Meeting, Mexico City, June 1961

Kramer, G. and S. G. Nilsson
On the Penetration Effect in Electric Dipole Internal Conversion
UCRL-9877, Oct. 1961   Nuclear Phys.

Kramer, G. (see N. K. Glendenning, UCRL-9904)

Kramer, G. (see N. K. Glendenning, UCRL-9905)

Lämmerman, H.
Zeeman Effect of the Transition Pu^{+++} $^6H_{5/2}$ J = 11/2 in Hexagonal
  Single Crystals
UCRL-9618-Abst., April 1961   APS Meeting in Mexico City, June 1961
                                     Bull. Am. Phys. Soc.

Larsh, A. E. (see A. Ghiorso, UCRL-9645)

Larsh, A. E. (see T. Sikkeland, UCRL-9540)

Latimer, R. M., G. E. Gordon, and T. D. Thomas
Alpha-Particle Branching Ratios for Neutron-Deficient
  Astatine Isotopes
UCRL-9217-Rev, Aug. 1960   J. Inorg. & Nuclear Chem. 17, 1-5 (1961)

Latimer, R. M.
Discovery of Lawrencium, Element 103
(No UCRL number)   The Science Teacher 28, Nov. 1961

Latimer, R. M. (see A. Ghiorso, UCRL-9645)

Latimer, R. M. (see T. D. Thomas, UCRL-9950)

Lederer, C. M. (see S. Bjørnholm, UCRL-9957)

Light, J. H. (J. K. Lum, UCRL-9679)

Lipworth, E. (see S. S. Alpert, UCRL-9474-Abs.)

Lipworth, E.

Proposed Method for the Enhancement of Optical Pumping
  Double-Resonance Signals
UCRL-9616-Abst., March 1961   Proceedings of the Conference on
                                     Quantum Electronics, Berkeley,
                                     California, March, 1961

Lovejoy, C. A., J. O. Rasmussen, and D. A. Shirley

Nuclear Orientation of Pm^{143}
UCRL-9452, Feb. 1961   Phys. Rev.

Lovejoy, C. A.

Nuclear Orientation of Some Rare Earth Isotopes (Ph. D. Thesis)
UCRL-9747, July 1961

Lovejoy, C. A., and D. A. Shirley

Nuclear Orientation of Tb^{156}
UCRL-9788, July 1961   Nuclear Phys.

Lovejoy, C. A. (see D. A. Shirley, UCRL-9912-Abs.)

Lum, J. K., J. H. Light, and F. Asaro

Clebsch-Gordan Coefficients for Nuclear Transition Probabilities:
  I. Odd-Mass Nuclides
UCRL-9679, Aug. 1961

Macfarlane, R. D.

Dysprosium-154, A Long-Lived Alpha Emitter
UCRL-9335, Aug. 1960   J. Inorg. & Nuclear Chem. 19, 9-12
                                     (1961)

Macfarlane, R. D. and R. D. Griffioen

Neutron-Deficient Alpha Emitters of Holmium
UCRL-9541-Abs., Jan. 1961   APS Meeting, Washington, D. C.,
                                     April 1961, Bull. Am. Phys. Soc.

Macfarlane, R. D. (see R. D. Griffioen, UCRL-9851 Abs.)

Macfarlane, R. D. and R. D. Griffioen

Neutron-Deficient Alpha Emitters of Erbium
UCRL-9852-Abs., Sept. 1961   APS Meeting, Chicago, Ill., Nov. 1961

Macfarlane, R. D.

An Alpha-Emitting Isomeric State of Tb^{149}
UCRL-9870, Sept. 1961

Macfarlane, R. D.
An Alpha-Emitting Isomeric State of Tb^{149}
UCRL-9870-Rev, Nov. 1961   Phys. Rev.

Mahony, J. D. (see S. S. Markowitz, UCRL-9908-Abs.)

Mahony, J. D. (see S. S. Markowitz, UCRL-9908)

Mains, G. J., and A. S. Newton
The Mercury-Sensitized Photolysis and Radiolysis of Methane
UCRL-9045-Rev., May 1960   J. Phys. Chem. 65, 212 (1961)

Mains, G. J., A. S. Newton, and A. F. Sciamanna
The Radiolysis of Biacetyl Vapor
UCRL-9363, Sept. 1960   J. Phys. Chem. 65, 1286 (1961)

Mains, G. J., A. S. Newton, and A. F. Sciamanna
The Radiolysis of Biacetyl Vapor
UCRL-9363-Rev., June 1961   Anal. Chem.

Margulis, T. N., and D. H. Templeton
Crystal and Molecular Structure of the Compound of Triethyl
   Phosphine and Carbon Disulfide
(No UCRL number)   J. Am. Chem. Soc. 83, 995 (1961)

Margulis, T. N. (see D. H. Templeton, No UCRL number)

Margulis, T. N., and D. H. Templeton
Crystal and Molecular Structure of Triethylscarphane
UCRL-9893, Oct. 1961   J. Chem. Phys.

Markowitz, S. S. and L. C. Sah
N^{14}(p, pn)N^{13} and N^{15}(p, p2n)N^{13} Reactions Induced by Protons
   of Energy 0.4 to 6.2 Gev
UCRL-9468-Abs., Nov. 1960   Bull. Am. Phys. Soc. 6,   (1961)

Markowitz, S. S., and J. D. Mahony
Activation Analysis for Oxygen and other Elements by Means of
   He^{3}-Induced Nuclear Reactions
UCRL-9908, Nov. 1961

Markowitz, S. S., and J. D. Mahony

Activation Analysis for Oxygen and Other Elements by Means of
   He^3-Induced Reactions
UCRL-9908-Abs., Nov. 1961   APS Meeting, New York, Jan. 1962
                                       Bull. Am. Phys. Soc.

Marquet, L. C. (see B. R. Judd, UCRL-9830)

Michel, M. C. (see R. W. Hoff, UCRL-5939-T)

Michel, M. C. (see F. Asaro, UCRL-9758)

Milton, J. C. D. (see H. R. Bowman, UCRL-9713)

Milton, J. C. D. (see H. R. Bowman, UCRL-9713-Rev.)

Milton, J. C. D., and J. S. Fraser

Prompt Fission Yields and Total Kinetic Energy Behavior from
   Time-of-Flight Measurements
UCRL-9754, June 1961   Phys. Rev. Letters 7, 67-69 (1961)

Milton, J. C. D.

Fission Energy Tables
UCRL-9883, Oct. 1961

Mollenauer, J. F.

Effects of Angular Momentum on Gamma-Ray Production in Compound-
   Nucleus Reactions (Ph. D. Thesis)
UCRL-9724, June 1961

Mollenauer, J. F.

A Computer Analysis for Complex Gamma Spectra
UCRL-9748, Aug. 1961

Morrow, R. J. (see J. G. Conway, UCRL-9654)

Morrow, R. J. (see J. G. Conway, UCRL-9776)

Morton, J. R., III

Investigation of Nuclear Reactions by Recoil Studies of Radioactive
   Products (Ph. D. Thesis)
UCRL-9595, April 1961

Muga, M. L. and H. R. Bowman, and S. G. Thompson
Tripartition in the Spontaneous Fission Decay of Cf^{252}
UCRL-9044, July 1960   Phys. Rev. 121, 270-274 (1961)

McHugh, J.
Semiempirical Correlation of β^+ Annihilation Rates in Metals
UCRL-9793, July 1961   Phys. Rev.

McLaughlin, R. D.
The Spectrum of UCl_4
UCRL-9937, Nov. 1961   Chem. Phys.

McWhan, D. B.
Crystal Structure and Physical Properties of Americium Metal (Ph. D. Thesis)
UCRL-9695, May 1961

Naumann, R. A., M. C. Michel and J. L. Power
Mass Spectrometric Identification of Long-Lived Tb^{157}, Ho^{163}, Hf^{182}
(No UCRL number)   Bull. Am. Phys. Soc. 6,   (1961)

Naumann, R. A. (see R. M. Diamond, UCRL-9532)

Navarro, Q., and D. A. Shirley
Nuclear Orientation of Dy^{155} and Dy^{157}
UCRL-9508, Jan. 1961   Phys. Rev. 123, 186-189 (1961)

Newby, N. D. Jr.
Odd-Even Shifting in the K=0 Band of Odd-Odd Deformed Nuclei
UCRL-9470-Abs., Nov. 1960   Abstract for APS N. Y. Meeting, Feb. 1961
                                    Bull. Am. Phys. Soc. 6, 78 (1961)

Newby, N. D.
Scattering in the K=0 Band of Odd-Odd Deformed Nuclei
UCRL-9764, July 1961   Phys. Rev.

Newton, A. S. (see B. Y. Yamamoto, UCRL-9924)

Newton, A. S. (see G. J. Mains, UCRL-9045-Rev.)

Newton, A. S. (see G. J. Mains, UCRL-9363)

Newton, A. S. (see G. J. Mains, UCRL-9363-Rev.)

Nielsen, O. B. (see S. Bjørnholm, UCRL-9545-Abs.)

Nilsson, S. G., J. Sawicki, and N. K. Glendenning
Extended Shell-Model Calculations and the Giant E1 Resonance in
  Deformed Nuclei
UCRL-9552-Abs.   APS Meeting, Washington, D. C., April 1961

Nilsson, S. G., J. Sawicki, and N. K. Glendenning
The Giant E1 Resonance for Deformed Nuclei
(No UCRL number) June 1961   Rutherford Jubilee International Con-
                                        ference, Manchester, England, Sept. 1961

Nilsson, S. G. (see N. K. Glendenning, UCRL-9631-Abs.)

Nilsson, S. G. (see G. Kramer, UCRL-9877)

Nilsson, S. G., J. Sawicki, and N. K. Glendenning
The Giant E1 Resonance for Deformed Nuclei Treated by the Random-
  Phase Approximation
UCRL-9975, Dec. 1961   Nuclear Phys.

Olovsson, I. (see H. W. Ruben, UCRL-8977)

Olovsson, I. (see D. H. Templeton, UCRL-9703-Abs.)

Pehl, R. A. (see J. Cerny, UCRL-9525)

Pehl, R. A. (see J. Cerny, UCRL-9878-Abs.)

Perlman, I.
Particle States in Strongly Deformed Nuclei
(No UCRL number) 1960   Proc. Intern. Conf. Nuclear Structure
                                        Kingston, 1960, pp. 547-562

Perlman, I. and F. Asaro
Decay-Energy-Systematics of the Heavy Elements
UCRL-9524, Jan. 1961   Handbook of Physics (Am. Inst. of
                                        Physics and McGraw Hill, N. Y.)

Person, L. W.
Theory of Odd-Mass Ellipsoidal Nuclei (Ph. D. Thesis)
UCRL-9753, July 1961

Rasmussen, J. O. (see R. D. Griffioen, UCRL-9368)

Rasmussen, J. O. (see C. A. Lovejoy, UCRL-9452)

Rasmussen, J. O.

A Refinement of Alpha-Decay Branching Relations for Odd-Mass
  Spheroidal Nuclei
UCRL-9542-Abs., Jan. 1961   APS Meeting, Washington D. C., April
                                     1961
                                   Bull. Am. Phys. Soc.

Reynolds, F. L.

Single-Crystal Tungsten Ribbon
UCRL-9502, Jan. 1961   Chem. Phys. (Letter to Editor)

Rivet, E. (see J. Cerny, UCRL-9878-Abs.)

Rosenstein, R. D. (see H. Ruben, UCRL-8977)

Ruben, H., D. H. Templeton, R. D. Rosenstein, and I. Olovsson

Crystal Structure and Entropy of Sodium Sulfate Decahydrate
UCRL-8977, Aug. 1960   J. Am. Chem. Soc. 83, 820 (1961)

Ruben, H. (see A. Zalkin, UCRL-9702-Abs.)

Ruben, H. (see A. Zalkin, UCRL-9802)

Ruben, H. (see D. H. Templeton, UCRL-9703-Abs.)

Ruiz, C. P.

Alpha-Decay Studies in the Families of the Light Uranium Isotopes
  (Ph. D. Thesis)
UCRL-9511, April 1961

Sah, L. C. (see S. S. Markowitz, UCRL-9468-Abs.)

Sawicki, J. (see S. G. Nilsson, No UCRL number)

Sawicki, J. (see S. G. Nilsson, UCRL-9552-Abs.)

Sawicki, J. (see S. G. Nilsson, UCRL-9803)

Sawicki, J. (see S. G. Nilsson, UCRL-9975)

Sciamanna, A. F. (see G. J. Mains, UCRL-9363)

Sciamanna, A. F. (see G. J. Mains, UCRL-9363-Rev.)

Sciamanna, A. F. (see B. Y. Yamamoto, UCRL-9924)

Seaborg, G. T.

The Transuranium Elements
(No UCRL number)   Nuclear Sci. and Eng. 9,475-487 (1961)

Seaborg, G. T.

The Actinide Elements
(No UCRL number) Sept. 1961   Encyclopedia of Chemical Technology

Seaborg, G. T. (see D. T. Thomas, UCRL-9950)

Sheline, R. K., T. Sikkeland, and R. N. Chanda

Experimental Observation of a New Region of Nuclear Deformation
UCRL-9888, Nov. 1961   Phys. Rev. Letters

Shirley, D. A.

Isomeric Chemical Shifts in Odd-Proton Nuclei
UCRL-9530-Abs., Jan. 1961   APS Meeting, Monterey, Calif.
                                        Bull. Am. Phys. Soc.

Shirley, D. A. (see J. N. Haag, UCRL-9299)

Shirley, D. A. (see C. A. Lovejoy, UCRL-9452)

Shirley, D. A. (see Q. Navarro, UCRL-9508)

Shirley, D. A., M. Kaplan, and P. Axel

Recoil-Free Resonant Absorption in Au^{197}
UCRL-9554, Feb. 1961   Phys. Rev.

Shirley, D. A. (see G. A. Westenbarger, UCRL-9562)

Shirley, D. A. (see M. Kaplan, UCRL-9569)

Shirley, D. A.

Interpretation of the Isomeric Chemical Shifts in Au^{197}
UCRL-9700, May 1961   Phys. Rev. 124, 354-358 (1961)

Shirley, D. A. (see C. A. Lovejoy, UCRL-9788)

Shirley, D. A.

Nuclear Applications of Isomeric Shifts
(No UCRL number)   Speech given at Saclay Conference,
                                                 France, Jan. 1961

Shirley, D. A. and C. A. Lovejoy

Quadrupole Coupling in Europium Ethylsulfate
UCRL-9912-Abs., Oct. 1961   APS Meeting, Los Angeles, Calif.
                                        Dec. 1961
                                        Bull. Am. Phys. Soc.

Sikkeland, T., A. E. Larsh, and G. E. Gordon

Fission of Uranium-238 with Carbon Ions
UCRL-9540, April 1961   Phys. Rev. 123, 2112-2122, (1961)

Sikkeland, T. (see A. Ghiorso, UCRL-9645)

Sikkeland, T. (see G. R. Choppin, UCRL-9534)

Sikkeland, T., E. L. Haines, and V. E. Viola, Jr.

Momentum Transfer in Heavy-Ion-Induced Fission
UCRL-9751, July 1961   Phys. Rev.

Sikkeland, T. (see R. K. Sheline, UCRL-9888)

Smith, K. F. (see S. S. Alpert, UCRL-9474-Abs.)

Strieter, F. J., and D. H. Templeton

Crystal Structure of Butyric Acid
UCRL-9746, June 1961   Acta Cryst.

Strieter, F. J., and D. H. Templeton

Crystal Structure of Propionic Acid
UCRL-9705, May 1961   Acta Cryst.

Strieter, F. J. and D. H. Templeton

Crystal Structure of the Carbon Tetrabromide p-Xylene Complex
UCRL-9955, Nov. 1961

Swiatecki, W. J. (see H. R. Bowman, UCRL-9713)

Swiatecki, W. J. (see H. R. Bowman, UCRL-9713-Rev.)

Templeton, D. H. (see T. N. Margulis, No UCRL number)

Templeton, D. H. (see R. P. Dodge, UCRL-8225-Rev.)

Templeton, D. H. (see H. Ruben, UCRL-8977)

Templeton, D. H. (see J. N. Haag, UCRL-9299)

Templeton, D. H. (see Q. C. Johnson, UCRL-9439)

Templeton, D. H. (see A. Zalkin, UCRL-9702-Abs.)

Templeton, D. H., H. W. Ruben, and I. Olovsson
Crystal Structure and Hydrogen Bonding of Sodium Chromate Tetrahydrate
UCRL-9703-Abs., May 1961

Templeton, D. H. (see F. J. Strieter, UCRL-9705)

Templeton, D. H. (see F. J. Strieter, UCRL-9746)

Templeton, D. H. (see A. Zalkin, UCRL-9802)

Templeton, D. H. (see T. N. Margulis, UCRL-9893)

Templeton, D. H. (see F. J. Strieter, UCRL-9955)

Thomas, T. D. (see R. M. Latimer, UCRL-9217)

Thomas, T. D., G. E. Gordon, R. M. Latimer, and G. T. Seaborg
Spallation-Fission Competition in Astatine Compound Nuclei Formed
  by Heavy-Ion Bombardment
UCRL-9950, Nov. 1961   Phys. Rev.

Thompson, S. G. (see M. L. Muga, UCRL-9044)

Thompson, S. G. (see H. R. Bowman, UCRL-9713)

Tocher, M. I. and J. M. Hollander
Carrier-Free Separation of Hafnium from Rare-Earth Oxides
UCRL-9699, May 1961   Anal. Chem.

Tuck, D. G., and R. M. Diamond
The Primary Solvation of the Proton in the Solvent Extraction of
 Mineral Acid
UCRL-8897-Rev., Sept. 1960   J. Phys. Chem. $\underline{65}$, 193 (1961)

Valentin, J., D. J. Horen, and J. M. Hollander
The Decay of $_{72}Hf^{173}$
UCRL-9731, June 1961   Nuclear Phys.

Valentin, J., D. J. Horen, and J. M. Hollander
Energy Levels of $_{71}Lu_{101}^{172}$
UCRL-9780, Aug. 1961   Nuclear Phys.

Viola, V. E., Jr.
Angular Distributions from Heavy-Ion-Induced Fission (Ph. D. Thesis)
UCRL-9619, April 1961

Viola, V. E., Jr. (see T. Sikkeland, UCRL-9751)

Wallmann, J. C. (see B. B. Cunningham, No UCRL number)

Westenbarger, G. A., and D. A. Shirley
Nuclear Orientation of Nd^{147}
UCRL-9562, Feb. 1961   Phys. Rev. $\underline{123}$, 1812-1818 (1961)

White, M. B. (see S. S. Alpert, UCRL-9474-Abs.)

Whitney, D. C. (see B. Chu, UCRL-9907)

Wilcox, W. R.
Simultaneous Heat and Mass Transfer in Free Convection
UCRL-8807, Aug. 1959   Chem. Eng. Sci. $\underline{13}$, 113-119 (1961)

Wilkins, B. (see G. Igo, UCRL-9628-Abs.)

Wilkins, B. (see G. Igo, UCRL-9906-Abs.)

Wilsky, K. (see P. G. Hansen, No UCRL number)

Winsberg, L., and T. P. Clements
Direct Nucleon-Nucleon Collisions Inside the Nucleus According to
 the Impulse Approximation
UCRL-8982-Rev., Aug. 1960   Phys. Rev. $\underline{122}$, 1623-1630 (1961)

Winsberg, L. (see J. Alexander, UCRL-8997)

Winsberg, L. (see J. Alexander, UCRL-9118)

Word, T. T.

Longitudinal Dispersion in Packed Gas Absorption Columns (M. S. Thesis)
UCRL-9844, Sept. 1961

Wright, R. M.

Downflow Forced Convection Boiling of Water in Uniformly Heated
  Tubes (Ph. D. Thesis)
UCRL-9744, Aug. 1961

Wydler, A. A.

The Multiplex Pulse-Height Analyzer
UCRL-9720, June 1961

Yamamoto, B. Y., A. F. Sciamanna, and A. S. Newton

The Radiolysis of Liquid Isobutane with Pulsed Electrons
UCRL-9924, Oct. 1961   J. Phys. Chem.

Zalkin, A. (see R. P. Dodge, UCRL-8225-Rev.)

Zalkin, A., D. H. Templeton, and H. W. Ruben

Crystal Structure and Hydrogen Bonding of Cobalt Sulfate Hexahydrate
UCRL-9702-Abs., May 1961

Zalkin, A., H. W. Ruben, and D. H. Templeton

The Crystal Structure of Cobalt Sulfate Hexahydrate
UCRL-9802, Aug. 1961   Acta. Cryst.

H. AUTHOR INDEX

Moon, J. S. F.4

Morrow, R. J. D.9, D.10

Morton, J. R. III G.9

Mosier, D. E.1

Navarro, Q. O. A.1

Newton, A. S. D.19, D.20

Nierenberg, W. A. D.15

Nilsson, S. G. C.12

Nordling, C. L. E.5

Pehl, R. H. C.6, C.7, E.2

Perlman, I. A.8

Person, L. W. G.10

Phillips, L. B.4

Plasil, F. B.3

Rasmussen, J. O. A.1, A.3

Reeder, Paul L. C.10

Reynolds, F. L. D.23

Rivet, E. C.6

Ruben, H. D.7

Ruiz, C.P. G.11

Sani, R. L. F.5

Sawicki, W. J. C.12

Schumacher, H. D.4

Sciamanna, A. F. D.19, D.20

Sheline, R. K. A.12

Shirley, D. A. A.1, A.2, A.3, A.4, A.7

Siegbahn, K. E.5

Sikkeland, T. A.12, A.18, B.5, B.6

Simonoff, G. C.3

Singh, S. C.4

Sisson, D. C.1

Sommerville, G. F.5

Swiatecki, W. J. B.11

Templeton, D. H.   D.6, D.7

Thomas, T. D.   B.7

Thompson, S. G.   A.8, B.4, B.11

Tobias, C.   F.6, F.7

Trips, A. R.   B.8

Valentin, J.   A.9, A.10

Vermeulen, T.   F.2, F.3, F.4

Vidal, J. G.   C.9

Viola, V. Jr.   B.5, B.6, B.7, B.8

Wallmann, J. C.   D.5

Weiss, L. H.   F.3

Whitney, D. C.   D.1, D.2

Wilke, C. R.   F.1, F.2

Word, T. T.   F.2

Wright, R. M.   F.5

Yamamoto, B. Y.   D.20

Zalkin, A.   D.6, D.7